

UC Irvine

UC Irvine Electronic Theses and Dissertations

Title

Development of Nucleoside Analogs and Probes for the Exploration of RNA Biology

Permalink

<https://escholarship.org/uc/item/4bv3s0m8>

Author

Kubota, Miles

Publication Date

2018

Peer reviewed|Thesis/dissertation

UNIVERSITY OF CALIFORNIA,
IRVINE

Development of Nucleoside Analogs and Probes for the Exploration of RNA Biology

DISSERTATION

submitted in partial satisfaction of the requirements
for the degree of

DOCTOR OF PHILOSOPHY

in Pharmacological Sciences

by

Miles Kubota

Dissertation Committee:
Associate Professor Robert C. Spitale, Chair
Professor Richard Chamberlin
Professor Celia Goulding

2018

DEDICATION

To

my parents, Ken and Grace,
my family, friends, and the love of my life, Sabrina
for their love and support throughout this process.

“They can’t comprehend
Or even come close to understanding him
I guess if I was boring they would love me more
Guess if I was simple in the mind
Everything would be fine.”

-Kid Cudi

“we gon’ be alright”

-K.Dot

TABLE OF CONTENTS

	Page
LISTS OF SCHEMES.....	iv
LIST OF FIGURES.....	v
LIST OF TABLES.....	vii
ACKNOWLEDGMENTS.....	viii
CURRICULUM VITAE.....	ix
ABSTRACT OF THE DISSERTATION.....	xiii
INTRODUCTION.....	1
References.....	10
CHAPTER 1: Metabolic Incorporation and Application of 2'-Azidonucleosides.....	15
1.1 Introduction.....	15
1.2 Results & Discussion.....	16
1.3 Conclusion.....	23
1.4 Experimental Details.....	24
1.5 References.....	32
CHAPTER 2: Inverse-Electron Demand Diels-Alder Reactions of Vinyl-Nucleosides with Tetrazines to Study RNA.....	34
2.1 Abstract.....	34
2.2 Introduction.....	34
2.3 Results & Discussion.....	37
2.4 Conclusion.....	51
2.5 Experimental Details.....	52
2.6 References.....	153
CHAPTER 3: Conclusions and Future Perspectives.....	159
3.1 Conclusion and Future Perspectives.....	159
3.2 References.....	162
APPENDIX A: Supplemental NMR Spectra.....	163

LIST OF SCHEMES

	Page
Scheme 1-1. 2'-Azidouridine Synthetic Scheme.....	17
Scheme 1-2. 2'-Azidocytidine Synthetic Scheme.....	17
Scheme 2-1. Vinyl-Nucleoside Synthetic Scheme.....	136
Scheme 2-2. Tetrazine Synthetic Scheme.....	137
Scheme 2-3. Tetrazine Conjugate Synthetic Scheme.....	137

LIST OF FIGURES

	Page
Figure 1-1. HeLa cells treated with 1 mM analog for 5 h.....	20
Figure 1-2. 2'-Azidocytidine Incorporation Analysis by Dot Blot.....	21
Figure 1-3. Dot Blot Analysis of 2'-Azidocytidine Incorporation Inhibition with ActD ₈	22
Figure 1-4. Fluorescent Imaging of 2'-Azidocytidine Incorporation in HEK239T Cells via CuAAC with Alkyne-Alexa48.....	23
Figure 2-1. Schematic of Metabolic Labeling of RNA.....	36
Figure 2-2. Initial Analysis of Vinyl-Nucleoside Incorporation into RNA.....	39
Figure 2-3. Screening Tetrazines for IEDDA Reactions with Vinyl-Nucleosides.....	42
Figure 2-4. Establishing Reaction Conditions to Stabilize Tetrazines during IEDDA.....	46
Figure 2-5. Effects of Vinyl-Nucleosides on Cell Viability and use for RNA Imaging.....	50
Figure 2-S1. LC-MS Analysis of Nucleosides in TRIzol.....	60
Figure 2-S2. Calculated HOMO and LUMO+1 orbital energy.....	63
Figure 2-S3i. Rate plots of Tz-1 with nucleosides and nucleobases.....	64
Figure 2-S3ii. Rate plots of Tz-2 with nucleosides and nucleobases.....	65
Figure 2-S3iii. Rate plots of Tz-3 with nucleosides and nucleobases.....	66
Figure 2-S2iv. Rate plots of Tz-4 with nucleosides and nucleobases.....	68
Figure 2-S2v. Rate plots of Tz-5 with nucleosides and nucleobases.....	69
Figure 2-S2vi. Rate plots of DP-Tz with nucleosides and nucleobases.....	70
Figure 2-S2vii. Rate plots of Tz-3 with nucleosides and nucleobases.....	72
Figure 2-S2viii. Rate plots of Tz-4 with nucleosides and nucleobases.....	73

Figure 2-S3ix. Rate plots of Tz-1 with nucleosides and nucleobases.....	74
Figure 2-S4. LC-MS Analysis of Reactions.....	76
Figure S5. Structures by Calculation.....	113
Figure 2-S6. ¹ H NMR analysis of Tz-1 hydrolysis.....	128
Figure 2-S7. Trypan Blue Exclusion assay cells.....	130
Figure 2-S8. MTT Viability assay of cells.....	131
Figure 2-S9. Fluorescent imaging of 2-VA and 7-dVA in HEK293T cells.....	132
Figure 2-S10. Mutually Orthogonal Bioorthogonal Chemistries.....	134

LIST OF TABLES

	Page
Table 1-1. Optimization of the Azidation of 2,2'-Anhydrouridine.....	20
Table 2-S2. Free Energy Barrier for each Tetrazine-Vinylnucleobase Pair.....	126

ACKNOWLEDGMENTS

I am grateful to all my professors at Whittier College, especially Dr. Iimoto and Dr. Isovitsch. I am forever thankful for allowing me to take my first steps in Chemistry Research. I am also thankful for the advising during my undergraduate experience whether it was academically, professionally, or personally related. I would not be where I am today without you both.

I thank Professor Rob Spitale for giving me the opportunity to be in the lab. When I started graduate school I wanted to synthesize small molecules that could be used in some type of biological assay and I was able to do that in the Spitale lab. I would also like to thank Rob for all the professional and academic advice throughout my years at UCI.

I would like to thank my committee Dr. Richard Chamberlin and Dr. Celia Goulding. You have both seen me go through this process throughout my graduate career and I couldn't be more thankful for a great committee. I would especially like to thank Dr. Chamberlin for allowing me to participate in your group meetings where I was able to learn and explore a large set of chemistry at these meetings. I would also like to thank Dr. Chamberlin for the advice throughout the years.

I would like to thank the members of the Spitale lab for all the advice and help throughout the years. It has been a great experience working with every one of you. I am also thankful for those who helped setup the lab when we first started.

I have to acknowledge all the help I have had throughout my career at UCI from various labs at UCI. The Jarvo lab: Dr. Konev and Dr. Hanna; the Presher lab: Dr. Shih, Dr. Patterson, Dr. McCutcheon, Dr. Steinhardt, and Dr. Row; the Nowick lab: Dr. Kreutzer, Dr. Salveson, and Dr. Chen; the Weiss lab: Dr. Speciale and Dr. Fletcher; the Furche lab: Dr. Parker; and the Vanderwal lab: Dr. Karns and Dr. White.

I would like to express my gratitude for my wife Sabrina for being by my side throughout this entire adventure known as graduate school. You have been there at my proudest moments and at my darkest moments. I could not reach this step in my life without your help and guidance. I can't wait to see what the future holds for us.

I would like to thank my parents Ken and Grace for supporting me through this process and through my entire life. I always enjoyed the time I got to spend with you while in graduate school. It really allowed me to escape the pressures and stresses of graduate school and come back to my work refreshed.

To my friends at UCI and outside of UCI, thank you for being in my life and being a friend to me. I cannot express how helpful even a small coffee break, a simple phone call, or a good roll on the mats. I will always cherish these moments and I hope for more throughout my life.

Curriculum Vitae

MILES KUBOTA, M.S., Ph.D. Candidate

Irvine, CA || (206) 779-0324 || kubota.miles@gmail.com || www.linkedin.com/in/mdkubota

Education

08/2013 – Present, Ph.D. Candidate

University of California, Irvine
Department of Pharmaceutical Sciences
Advisor: Prof. Robert Spitale

08/2013 – 08/2016, M.S. Chemistry

University of California, Irvine
Department of Chemistry
Advisor: Prof. Robert Spitale

08/2009 – 05/2013, B.A. Chemistry

Whittier College
Department of Chemistry
Advisor: Prof. Ralph Isovitch

08/2004 – 05/2009, H.S. Diploma

O'Dea High School

Employment

08/2013 – Present, *Graduate Research Assistant*, University of California, Irvine, Irvine, CA

Advisor: Professor Robert Spitale

- Apply medicinal chemistry approaches to design and synthesize modified nucleosides for metabolic incorporation into RNA transcripts for the interrogation of RNA biology in cancer and neurodegenerative disease models with prospects toward sequencing methods
- Propose new synthetic strategies toward target molecules and optimize synthetic routes through creative synthetic design
- Design and synthesize small molecule probes and modified nucleosides at milligram to gram scales for structure activity relationship analysis and other biological applications
- Apply computational methods to aid design of small molecules
- Manage multiple projects through individual and team efforts toward bioorthogonal nucleoside projects
- Multidisciplinary collaboration and communication (Biology, Chemistry, Computer Science, Public Health)
- Formulate testable hypotheses through efficient and cost-effective experimental design within project scope
- Develop instrumental and operational standard operating protocols within the lab
- Utilize, troubleshoot, maintain, and calibrate both chromatography instruments and solvent system
- Perform as laboratory waste manager and chemical safety manager to ensure OSHA regulations
- Contribute to manuscript drafting, preparation, and editing resulting in various publications within lab
- Participate and contribute in weekly meetings, presentations (oral and poster), and scientific conferences

- Train and mentor undergraduate and graduate students on instruments and lab procedures

06/2011 – 09/2013, *Intern*, Los Angeles County Sanitation Districts, Whittier, CA

Supervisor: Steve Carr

- Perform analytical chemistry techniques toward the development of various methods on waste water samples.
- Method development of perchlorate extraction in waste water through use of zeolites
- Method development for pyrethroid detection in waste water samples by GC-MS
- Analysis of estrogens and fire retardants in waste water samples by LC-MS
- Organized local, state, and national evidence for prosecution for environmental pollution
- Maintain a safe and effective work environment

10/2010 – 05/2013, *Undergraduate Research Assistant*, Whittier College, Whittier, CA

Advisor: Professor Ralph Isovitsch

- Synthesis and characterization of ligands and metal complexes (Pd, Pt, Rh, Ir) for catalysis
- Formed crystals of ligands and metal complexes for X-ray crystallographic analysis
- Maintenance and care of NMR

05/2006 – 09/2008, *Intern*, Starbucks Coffee Company, Seattle, WA

Supervisor: Penni Peotter

- Performed network administration for store emails and voicemails
- Project Management for server synchronization of email and voicemail servers

Teaching Experience

2013-present, University of California, Irvine *Graduate Teaching Assistant*, Irvine, CA

Life 101 (PharmSci-42) – led discussions and monitored responses

Ecology & Evolution (Bio-94) – led discussions and created quiz questions

Pharmacotherapy (PharmSci-173) – created discussions, evaluated topics

Physical Biochemistry (PharmSci-171) – created discussions, created homework, quiz, and exam questions

Organic Chemistry Lab (Chem-51LC) – led lab experiments, led discussions, held office hours

Proficiencies

- **Lab Techniques:** column chromatography (normal phase, reverse phase, size-exclusion, affinity), recrystallization, distillation, air-free techniques, gel-electrophoresis, blotting, protein purification, RNA purification, cell culture
 - Specialization in nucleic acid chemistry and bioconjugation
- **Instrumentation:** GC-MS, LC-MS, ESI-MS, MALDI-TOF, HPLC, UHPLC, FTIR, CombiFlash Rf+, AA, Fluorometer, UV-Vis, NMR (¹H, ¹³C, ³¹P, ¹⁹F)
 - Use, troubleshooting, and repair
- **OS:** Windows 2000, XP Professional, Vista, 2003 Server, 7, 10; Apple OS 10; Linux Ubuntu
- **Software:** MS Office, Adobe Photoshop, Illustrator, ChemDraw, MestreNova, PyMol, Spartan

Publications

10. "Inverse-Electron Demand Diels-Alder Reactions of Vinyl-Nucleosides with Tetrazines to Study RNA." **Kubota, M.**; Nainar, S.; Parker, S. M.; Furche, F.; Spitale, R. C. *Manuscript in preparation.*
9. "Psoralen Crosslinking of Mitochondrial RNA." **Kubota, M.**; Nainar, S.; Sophal, K.; Tran, C.; Spitale, R. C. *Manuscript in preparation.*
8. "Interrogation of Cell-Specific RNA Labeling with 2'-Azido-pyrimidine Nucleosides." Nainar, S.; **Kubota, M.**; Cuthbert, B.; Goulding, CW.; Spitale, R. C. *Manuscript in preparation.*
7. "Identification of RNA Binding Proteins and Post-Translational Modification on Proteins." England, W. C.; Chan, D.; Nguyen, K., Aggarwal, M., Feng, C., Beasley, S.; Nainar, S.; **Kubota, M.**; Li, Y.; Fazio, M.; Spitale, R. C. *Manuscript in preparation.*
6. "Temporal Labeling of Nascent RNA Using Photoclick Chemistry in Live Cells." Nainar, S.; **Kubota, M.**; McNitt, C.; Tran, C.; Popik, V.; Spitale, R. C. *Journal of the American Chemical Society*, **2017**, *139*, 8090.
5. "Cell-Selective Bioorthogonal Metabolic Labeling of RNA." Nguyen, K.; Fazio, M.; **Kubota, M.**; Nainar, S.; Feng, C.; Li, X.; Atwood, S. X.; Bredy, T. W.; Spitale, R. C. *Journal of the American Chemical Society*, **2017**, *139*, 2148.
4. "Metabolic Incorporation of Azide Functionality into Cellular RNA." Nainar, S.; Beasley, S.; Fazio, M.; **Kubota, M.**; Dai, N.; Corrêa, I. R.; Spitale, R. C. *ChemBioChem*, **2016**, *17*, 2149.
3. "Progress and challenges for chemical probing of RNA structure inside living cells." **Kubota, M.**; Tran, C.; Spitale, R. C. *Nature Chemical Biology*, **2015**, *11*, 933.
2. "RNA structure: Merging chemistry and genomics for a holistic perspective." **Kubota M.**; Chan D.; Spitale, R. C. *BioEssays*, **2015**, *37*, 1129.
1. "Synthesis, structure, and spectroscopy of two benzil-based α -diimine ligands and their palladium(II) complexes." **Kubota, M.**; Covarrubias, D.; Pye, C.; Fronczek, F. R.; Isovitsch, R. *Journal of Coordination Chemistry*, **2013**, *66*, 1350.

Presentations

8. Poster Presentation: "Inverse Electron Demand Diels-Alder (IEDDA) Mediated Conjugation for Metabolic Labeling of RNA," *University of California Chemical Symposium*, Lake Arrowhead, CA. March 26th, **2018**.
7. Poster Presentation: "Inverse Electron Demand Diels-Alder (IEDDA) Mediated Conjugation for Metabolic Labeling of RNA," *University of California Irvine Chemistry Graduate Student Visitation*, Irvine, CA. March 9th, **2018**.
6. Oral Presentation: "Bioorthogonal Nucleosides for Studying RNA Biology," *Pharmaceutical Sciences Chemistry Meeting*, Irvine, CA. February 21st, **2018**.

5. Poster Presentation: "Inverse Electron Demand Diels-Alder (IEDDA) Mediated Conjugation for Metabolic Labeling of RNA," *University of California Irvine Pharmaceutical Sciences Graduate Student Visitation*, Irvine, CA. January 19th, **2018**.

4. Oral Presentation: "Snapshots of RNA Biology with Chemical Probing," *Whittier College Chemistry Career Presentations*, Whittier, CA. April, 21st **2017**.

3. Oral Presentation: "Assaying RNA Localization with Bioorthogonal Chemistry," *Pharmaceutical Sciences Chemistry Meeting*, Irvine, CA. October 5th, **2016**.

2. Oral Presentation: "Polyphenol Palladium Complexes for Enhanced HIV Enzyme Inhibition," *Whittier College Senior Presentations*, Whittier, CA. May 8th, **2013**.

1. Poster Presentation: "Synthesis, structure, and spectroscopy of two benzil-based α -diimine ligands and their palladium(II) complexes," *243rd ACS National Meeting*, San Diego, CA. March 25th-29th, **2012**.

Professional Career Development

5. Attendee: *University of California Irvine 4th Annual RNA Symposium*, Irvine, CA. April 6th, **2018**.

4. Attendee: *University of California Irvine 3rd Annual RNA Symposium*, Irvine, CA. April 14th, **2017**.

3. Attendee: *Seeking Resilience: A Discussion On The Future Of Southern California's Water System*, Irvine, CA. October, 4th, **2016**.

2. Attendee: *251st ACS National Meeting*, San Diego, CA. March 13th-17th, **2016**.

1. Attendee: *University of California Irvine Annual RNA Symposium*, Irvine, CA. April 24th, **2015**.

Honors and Awards

2014 – Amgen Fellowship

2013 – Undergraduate Research Award

References

Prof. Robert C. Spitale
Department of Pharmaceutical Sciences
University of California, Irvine
Phone: (949) 824-5011
Email: rspitale@uci.edu

Prof. Richard A. Chamberlin
Department of Pharmaceutical Sciences
University of California, Irvine
Phone: (949) 824-7089
Email: richard.chamberlin@uci.edu

Prof. Celia W. Goulding
Department of Pharmaceutical Sciences
University of California, Irvine
Phone: (949) 824-0337
Email: celia.goulding@uci.edu

ABSTRACT OF THE DISSERTATION

Development of Nucleoside Analogs and Probes for the Exploration of RNA Biology

By

Miles Kubota

Doctor of Philosophy in Pharmacological Sciences

University of California, Irvine, 2018

Associate Professor Robert C. Spitale, Chair

RNA is a highly regulatory biomolecule within the cell. RNA has been identified in many biological functions that involve growth and development, and dysregulation of RNA has been demonstrated to be critical in the onset of cancer and neurodegenerative diseases. Toward the goal of elucidating novel RNA functions chemical methods have been developed. These include chemical probing of RNA structures and metabolic incorporation of modified nucleosides into nascent transcripts. These approaches add precision to current methods through subcellular profiling, enzyme-substrate pairs for cell-type specific labeling, multifunctional nucleosides for profiling RNA-protein interactions, and multicomponent labeling for RNA lifetimes with determination of sites of incorporation. Combining these chemical techniques with modern sequencing methods offers a holistic view of RNA biology in real time. Here, is presented the work toward advancing chemical methods for studying RNA biology.

INTRODUCTION

Gene expression plays a crucial role in molecular biology. A model for gene expression proposed by Francis Crick, commonly known as the central dogma of molecular biology, describes the flow of genetic information from DNA, which holds information, to RNA, which translates genetic information into protein.¹⁻² This model was developed in the context of examining the intermediates needed to produce proteins.³ Further development of the model revealed the passage of information between macromolecules is much more complex in nature. Experiments on reverse transcriptase showed that the flow of information can be transferred from RNA to DNA, a reversal of the original central dogma model.⁴⁻⁵ The central dogma model was further complicated by the discovery of non-coding RNA that serves regulatory roles, e.g. siRNA and miRNA.⁶⁻⁷ These discoveries not only showed the complexity of gene expression, but also revealed the greater role of RNA in biology.

Our understanding of the role of RNA in biology has shifted away from seeing its role as purely an agent of information transfer from DNA to protein. This shift was revealed through the work of the Human Genome Project and the ENCODE Consortium. The Human Genome Project showed that only 1.5% of DNA contains protein-coding genes.⁸ From this discovery, it was determined that nucleic acids in the cell must play greater biological roles beyond coding for protein expression. The ENCODE project revealed the composition of RNA within humans. From here, it was determined that only 18% of the transcriptome is made up of mRNA, 60% made up of long non-coding RNAs, and the remaining 22% consists of small, non-coding RNAs.⁹ In the context of other molecules within the cell, RNA only makes up 4% of the dry mass of the entire cell. In comparison to protein, which makes up 59% of

the dry mass in the entire cell, RNAs make up only a small fraction of the contents of the cell.¹⁰

RNA's role in coding for protein expression represents only a small portion of RNA biology. Exploration of non-coding RNAs (ncRNAs) has revealed exotic roles in RNA biology that have a major effect on gene expression. Some RNAs that exemplify this are riboswitches and the long noncoding RNA (lncRNA) X-inactive specific transcript (XIST). Each of these examples has a unique mechanism of action, but both participate in a regulatory role.

Riboswitches were first discovered in bacteria, where they were found to be a feedback mechanism to synthesize protein needed for a specific biosynthetic pathway.¹¹⁻¹² The mechanism of action for riboswitches is dependent on their three-dimensional structures. In general, they create a three-dimensional structure that blocks a ribosome binding site when a specific metabolite is not present, thereby inhibiting translation following the riboswitch.¹³ When the metabolite is present, the three-dimensional structure of the riboswitch changes and allows the ribosome to bind to the RNA and translate the gene. Riboswitches have complex secondary and tertiary structures.¹⁴ The binding motif of the binding metabolites often interact with the heteroatoms found in RNA through electrostatic interactions, which contribute to tight binding.¹⁵ Through these interactions, riboswitches regulate gene expression; however, riboswitches are not the only RNAs that exhibit regulatory traits.

One of the largest and well-studied lncRNAs is XIST. This RNA is 17 kb in humans and plays a major role in the X inactivation process.¹⁶ Females possess two X chromosomes, while males have only a single X chromosome and a single Y chromosome. In females one of the two X chromosomes is silenced in mitotic division. This allows for dosage equivalence of X and Y chromosomes between males and females. XIST is a major factor in this process; it

participates in the nucleus, where it covers the inactive X chromosome and inhibits gene expression of the inactive X chromosome.¹⁷ This regulatory role of XIST is crucial to the cell cycle in mammals.

Many ncRNAs have been identified as participating in human diseases, specifically, cancers and neurodegenerative diseases. There is a great variety of such RNAs, but examples of micro RNAs (miRNAs) and lncRNAs contributing to these diseases will be described here. Each of these RNAs differs in size and purpose within the cell, but all have a critical role in disease.

miRNAs are one of the smallest transcripts studied. These RNAs are roughly 19–24 nucleotides in length and participate in gene silencing of mRNA into proteins.¹⁸ miRNAs regulate a wide range of process within the cell, including apoptosis, development, differentiation, and proliferation. miRNAs silence genes via a multistep process: nascent transcripts of miRNA (pri-miRNA) roughly 70 nucleotides in length are processed by RNase-III enzymes Drosha and Dicer, resulting in the mature miRNAs roughly 20 nucleotides in length, they are loaded into the Dicer complex, which forms the RNA-induced silencing complex (RISC).¹⁹ The miRNAs then hybridize with the mRNA target, shutting down initiation of translation, after which are degraded by the endonuclease activity of RISC.²⁰ These short RNAs play a major role in the regulation of genes and their dysregulation is deleterious to the cell. miRNAs in cancer are exemplified by mutations in TARBP2, DICER1, and exportin 5, genes that code for the processing machinery of miRNAs to mature miRNAs.²¹⁻²³ Such mutations inhibit the maturation of miRNAs, which has a downstream effect through the of dysregulation of oncogenes and tumor suppressors.

Beta-site amyloid precursor protein (APP)-cleaving enzyme (BACE1-AS) is an lncRNA that is transcribed from the antisense strand to BACE1, the protease that cleaves APP, resulting in the formation of amyloid- β peptides. Aggregation of amyloid- β peptides in the brain is commonly observed in Alzheimer's disease. Furthermore, concentrations of BACE1 proteins, amyloid- β , and BACE1-AS are increased in subjects with Alzheimer's disease. BACE1 activity is required for normal brain function; the expression of BACE1 is regulated by BACE1-AS, and its dysregulation results in increased production of BACE1 mRNA.²⁴ This lncRNA plays a significant role in gene expression, but its dysregulation results in disease. Many biochemical techniques are used for the study of RNA. These techniques often take advantage of the chemical properties of RNA; some examples include fluorescence *in situ* hybridization (FISH), which uses an oligomer complementary to the target RNA appended with a fluorophore; chemical probing, which uses a "turn-on" chemical probe that interacts with specific functional groups of RNA; and photoactivatable ribonucleoside-enhanced crosslinking and immunoprecipitation (PAR-CLIP), which uses an unnatural photoactivatable nucleoside that crosslinks with nearby RNA binding proteins (RBPs). Each of these techniques offers unique insights into RNA biology.

FISH offers the ability to visualize a specific transcript within the cell.²⁵ This is accomplished through creation of a complimentary oligonucleotide conjugated with a fluorophore that will hybridize with the transcript within the cell. These oligonucleotides are composed of 20 pairs and are made to cover 40–50 base pairs of the target transcript. Experiments of this type are often performed to determine the location of particular transcripts within the cell. FISH has been used to determine the localization of siRNA during cell cycle, revealing the location of MALAT1 RNA in cells and the location of β -adrenergic

receptor mRNA in disease models.²⁵⁻²⁸ While FISH experiments are useful for determining the location of RNAs within cells, they lack the ability to determine structural information of the transcript of interest.

The challenges of determining RNA structure are related to the instability of RNA, which contributes to difficulties in its crystallization. Chemical probing was developed to help determine RNA structures without crystallization. Chemical probes, in this context, are essentially chemicals that react with RNA functionalities and either form covalent adducts with the RNA or cause its cleavage of the RNA. Chemicals that form covalent adducts with RNA include dimethylsulfate (DMS), 1,1-dihydroxy-3-ethoxy-2-butanone (kethoxal), diethylpyrocarbonate (DEPC), 1-cyclohexyl-(2-morpholinoethyl)carbodiimide metho-p-toluene sulfonate (CMCT), bisulfate, and selective 2'-hydroxyl acylation analyzed by primer extension (SHAPE) reagents.²⁹ All these reagents can be used *in vitro*, however, only DMS and SHAPE can be used within living cells. Reagents that cause cleavage include hydroxyl radicals and basic solvent. Where these reagents react with the RNA is intrinsic to the chemical functionality of the RNA as well as the overall structure of the RNA of interest.

Reagents that form covalent adducts with RNA react with different residues within the RNA structure. DMS probing reacts with N7 of guanosine, N3 of cytidine and N1 of adenosine. Kethoxal reacts with guanine residues on N1 and the exocyclic amine.³⁰ DEPC reacts with N7 of adenosine. CMCT reacts with the N3 of uridine. Bisulfate undergoes sulphonation of the olefin on C5 and C6 of cytosine forming an adduct on C6. SHAPE acrylates the 2'-hydroxyl of the RNA backbone. These adducts are formed when the site of the reaction is free for the chemical to react; for example, DMS probing allows for the determination of non-base paired regions because the reactivity takes place on the Watson-Crick face of

adenosine and cytidine residues and the kethoxal adduct only forms on guanine nucleotides in single-strand regions.

Hydroxy radicals and basic solvent differ from DMS, kethoxal, DEPC, CMCT, bisulfate, and SHAPE in that they are used to cause strand cleavage. Hydroxy radicals cleave solvent-accessible 5'C of the RNA backbone, forming a 3'-phosphate and a 5'-aldehyde. Basic solvent, or in-line probing, cleaves the back bone when the phosphate is aligned with the 2'hydroxyl leaving a 2',3'-cyclic phosphate and a 5' hydroxyl at a pH of 8.3.³¹ The modified RNA is then subjected to RT-PCR to determine the site of modification; truncated products are formed when the polymerase falls off the transcript and can be visualized as bands after gel electrophoresis. These reagents offer insight into RNA structure both *in vitro* and *in vivo*.

The true power of chemical probing lies in performing the reactions *in vivo* and using libraries with sequencing, facilitating transcriptome-wide structural analysis. This has been accomplished through the use of DMS and icSHAPE.³²⁻³³ After an acylation reaction with 2-azidomethylnicotinylimidazolidide, RNA can be isolated using copper-free click chemistry between the azide installed on the acylated product and a strained cyclooctyne. This is product undergoes reverse transcription and sequencing, providing *in vivo* RNA secondary structure. Transcriptome-wide analysis using this technique has revealed differences between *in vitro* and *in vivo* RNA structures;³⁴ these structural differences offer insight into RNA biology through interaction between RNA and other biomacromolecules within the cell. PAR-CLIP (photoactivatable ribonucleoside-enhanced crosslinking and immunoprecipitation) is a RNA biochemical technique that identifies RNA-protein interactions.³⁵ This technique takes advantage of a photoreactive nucleoside to crosslink protein upon photolysis. The nucleoside of choice is 4-thiouridine (4SU). 4SU replaces the

carbonyl at the 4-position with a thione; when incubated with cells it is metabolically incorporated into nascent RNA transcripts in the cell. Upon UV irradiation, an n to π^* transition occurs, forming a thiol radical. This radical reacts with aryl rings found in proteins, forming a covalent link between the RNA and protein. Cells are then lysed, and the protein of interest is isolated with an antibody which is then precipitated with the RNA crosslinked with the protein. From here, the crosslink is treated with RNase and alkylated with ^{32}P -ATP. This radioactively labelled complex can be isolated by gel electrophoresis and visualized. The protein is then digested with proteinase K, and cDNA libraries of the RNA crosslink are prepared and amplified by PCR. The amplified product is subjected to sequencing to determine the RNA interaction with the protein near the binding site. With this technique, transcriptome-wide RNA-protein interactions have been identified, revealing unique RNA biology.

Many of the advances in the methods used to study RNA come from biochemical techniques developed to study proteins. Three different chemistries are widely used as tools in protein chemical biology: copper-catalyzed alkyne-azide cycloaddition (CuAAC), strain-promoted alkyne-azide cycloaddition (SPAAC), and inverse electron-demand Diels-Alder (iEDDA). These reactions all fall into the categories of “click” and bioorthogonal chemistry.³⁶ The requirements of these classes overlap in many areas: they include modularity of the functionality used for the reaction, excellent tolerance for other functional groups on the molecule, high chemical yields, with stereospecificity and physiological stability.³⁷ CuAAC, SPAAC, and iEDDA reactions fit these requirements.

CuAAC reactions occur between an azido group and a terminal alkyne, facilitated by a Cu(I) catalyst. This reaction is a derivative of the Huisgen 1,3-dipolar cycloaddition, which

lacks a copper catalyst and instead uses high temperatures to form the 1,2,3-triazole product. The Fokin and Sharpless groups found the use of a Cu(I) catalyst allows this reaction to proceed with high yields and great regioselectivity.³⁸ This reaction has since been widely used in drug discovery and chemical biology.³⁹⁻⁴⁰

CuAAC has been used in the study of many biomacromolecules including proteins, carbohydrates, and lipids, as well as the study of RNA. The Spitale lab has developed many nucleosides that offer an alkyne or an azide functional group that can be used as a “handle” for CuAAC.⁴¹⁻⁴⁴ The incorporation of these azido and alkynyl functionalities in RNA allows specific labelling of RNA within the cell. The challenge that accompanies CuAAC on RNA is RNA degradation promoted by the copper catalyst.⁴⁵ While there are many methods to help prevent the cytotoxic behavior of the catalyst, the problem still remains.⁴⁶⁻⁴⁷ Utilizing SPAAC reactions offer a way to allow use of this labelling technique without RNA degradation.

SPAAC reactions occur between an azido group and a strained internal alkyne. These strained alkynes are commonly found in a cyclooctyne ring, which contributes significant energy via ring strain, for example, 19.9 kcal/mol on the internal alkyne for the 3,3-difluorocyclooctyne variant.⁴⁸ This ring strain raises the ground-state energy of the bond and allows facile reactions with azide groups, forming the 1,2,3-triazole product. SPAAC has the advantage of being copper-free but the disadvantage of insolubility in aqueous conditions without addition of hydrophilic functional groups to the cyclooctyne. This reaction has been used throughout chemical biology.⁴⁹

The use of the SPAAC reaction features in various RNA biochemical techniques. The Spitale lab has used these reagents in many different ways: icSHAPE, light-activated chemical probing,⁵⁰ and photo-activated SPAAC reactions with azido-modified RNA.^{32, 50-51} While

these reactions have great utility for the ligation of RNA, they lack the favorable reaction kinetics of CuAAC. An ideal bioorthogonal reaction for RNA would be metal-free and offer fast kinetics in comparison to CuAAC.

iEDDA in bioorthogonal chemistry is a [4+2] inverse electron-demand Diels-Alder reaction between an electron-deficient tetrazine and an electron-rich olefin. Derivatives of the olefin that add strain offer faster kinetics, but also add to the water solubility problem, much like cyclooctynes in SPAAC reactions.⁵² These reactions have garnered much interest in chemical biology due to their fast kinetics, on par with those found for enzymatic labeling.⁵³

These reactions are not commonly seen in RNA chemical biology because of the large size of the tetrazine or cyclooctene. However, these reactions have found use in the fluorescent detection of mRNA,⁵⁴ and post-transcriptional functionalization of RNA *in vitro*.⁵⁵ Further development of these reactions for RNA can offer in-depth insights in RNA biology by allowing specific labeling of RNA with fast kinetics.

References

1. Cobb, M., *PLOS Biology* **2017**, *15*, e2003243.
2. Crick, F., *Nature* **1970**, *227*, 561.
3. Morange, M., *Journal of Biosciences* **2008**, *33*, 171-175.
4. Temin, H. M.; Mizutani, S., *Nature* **1970**, *226*, 1211.
5. Baltimore, D., *Nature* **1970**, *226*, 1209.
6. Fire, A.; Xu, S.; Montgomery, M. K.; Kostas, S. A.; Driver, S. E.; Mello, C. C., *Nature* **1998**, *391*, 806.
7. Bartel, D. P., *Cell* **2004**, *116*, 281-297.
8. Gregory, T. R., *Nature Reviews Genetics* **2005**, *6*, 699.
9. Pertea, M., *Genes* **2012**, *3*.
10. Alberts, B., *Molecular Biology of the Cell*. Garland Science: New York, 2002.
11. Miranda-Ríos, J.; Navarro, M.; Soberón, M., *Proceedings of the National Academy of Sciences* **2001**, *98*, 9736.
12. Kadner, X. N. a. R. J., *Journal of Bacteriology* *180*, 6719-6728.
13. Mandal, M.; Breaker, R. R., *Nature Reviews Molecular Cell Biology* **2004**, *5*, 451.
14. Batey, R. T.; Gilbert, S. D.; Montange, R. K., *Nature* **2004**, *432*, 411.
15. Peselis, A.; Serganov, A., *Nature Structural & Molecular Biology* **2012**, *19*, 1182.
16. Brown, C. J.; Hendrich, B. D.; Rupert, J. L.; Lafrenière, R. G.; Xing, Y.; Lawrence, J.; Willard, H. F., *Cell* **1992**, *71*, 527-542.
17. Clemson, C. M.; McNeil, J. A.; Willard, H. F.; Lawrence, J. B., *The Journal of Cell Biology* **1996**, *132*, 259.
18. He, L.; Hannon, G. J., *Nature Reviews Genetics* **2004**, *5*, 522.

19. Krol, J.; Loedige, I.; Filipowicz, W., *Nature Reviews Genetics* **2010**, *11*, 597.
20. Czech, B.; Hannon, G. J., *Nature Reviews Genetics* **2010**, *12*, 19.
21. Melo, S. A.; Ropero, S.; Moutinho, C.; Aaltonen, L. A.; Yamamoto, H.; Calin, G. A.; Rossi, S.; Fernandez, A. F.; Carneiro, F.; Oliveira, C.; Ferreira, B.; Liu, C.-G.; Villanueva, A.; Capella, G.; Schwartz Jr, S.; Shiekhatar, R.; Esteller, M., *Nature Genetics* **2009**, *41*, 365.
22. Hill, D. A.; Ivanovich, J.; Priest, J. R.; Gurnett, C. A.; Dehner, L. P.; Desruisseau, D.; Jarzembowski, J. A.; Wikenheiser-Brokamp, K. A.; Suarez, B. K.; Whelan, A. J.; Williams, G.; Bracamontes, D.; Messinger, Y.; Goodfellow, P. J., *Science* **2009**, *325*, 965.
23. Melo, S. A.; Moutinho, C.; Ropero, S.; Calin, G. A.; Rossi, S.; Spizzo, R.; Fernandez, A. F.; Davalos, V.; Villanueva, A.; Montoya, G.; Yamamoto, H.; Schwartz, S.; Esteller, M., *Cancer Cell* **2010**, *18*, 303-315.
24. Faghihi, M. A.; Modarresi, F.; Khalil, A. M.; Wood, D. E.; Sahagan, B. G.; Morgan, T. E.; Finch, C. E.; St. Laurent Iii, G.; Kenny, P. J.; Wahlestedt, C., *Nature Medicine* **2008**, *14*, 723.
25. Langer-Safer, P. R.; Levine, M.; Ward, D. C., *Proceedings of the National Academy of Sciences* **1982**, *79*, 4381.
26. Lécuyer, E.; Yoshida, H.; Parthasarathy, N.; Alm, C.; Babak, T.; Cerovina, T.; Hughes, T. R.; Tomancak, P.; Krause, H. M., *Cell* **2007**, *131*, 174-187.
27. Zhang, B.; Arun, G.; Mao, Yuntao S.; Lazar, Z.; Hung, G.; Bhattacharjee, G.; Xiao, X.; Booth, Carmen J.; Wu, J.; Zhang, C.; Spector, David L., *Cell Reports* **2012**, *2*, 111-123.
28. Baby G. Tholanikunnel‡, Kusumam Joseph‡§, Karthikeyan Kandasamy§, Aleksander Baldys§, John R. Raymond§, Louis M. Luttrell‡§, Paul J. McDermott§ and Daniel J. Fernandes‡, *Journal of Biological Chemistry* **2010**, *285*, 33816-33825.
29. Kubota, M.; Tran, C.; Spitale, R. C., *Nature chemical biology* **2015**, *11*, 933-941.

30. Mathews, D. H.; Disney, M. D.; Childs, J. L.; Schroeder, S. J.; Zuker, M.; Turner, D. H., *Proceedings of the National Academy of Sciences of the United States of America* **2004**, *101*, 7287.
31. Regulski, E. E.; Breaker, R. R., In-Line Probing Analysis of Riboswitches. In *Post-Transcriptional Gene Regulation*, Wilusz, J., Ed. Humana Press: Totowa, NJ, 2008; pp 53-67.
32. Spitale, R. C.; Flynn, R. A.; Zhang, Q. C.; Crisalli, P.; Lee, B.; Jung, J.-W.; Kuchelmeister, H. Y.; Batista, P. J.; Torre, E. A.; Kool, E. T.; Chang, H. Y., *Nature* **2015**, *519*, 486.
33. Zubradt, M.; Gupta, P.; Persad, S.; Lambowitz, A. M.; Weissman, J. S.; Rouskin, S., *Nature Methods* **2016**, *14*, 75.
34. Flynn, R. A.; Zhang, Q. C.; Spitale, R. C.; Lee, B.; Mumbach, M. R.; Chang, H. Y., *Nature Protocols* **2016**, *11*, 273.
35. Hafner, M.; Landthaler, M.; Burger, L.; Khorshid, M.; Hausser, J.; Berninger, P.; Rothballer, A.; Ascano, M.; Jungkamp, A.-C.; Munschauer, M.; Ulrich, A.; Wardle, G. S.; Dewell, S.; Zavolan, M.; Tuschl, T., *Cell* **2010**, *141*, 129-141.
36. Becer, C. R.; Hoogenboom, R.; Schubert, U. S., *Angewandte Chemie International Edition* **2009**, *48*, 4900-4908.
37. Kolb, H. C.; Finn, M. G.; Sharpless, K. B., *Angewandte Chemie International Edition* **2001**, *40*, 2004-2021.
38. Rostovtsev, V. V.; Green, L. G.; Fokin, V. V.; Sharpless, K. B., *Angewandte Chemie International Edition* **2002**, *41*, 2596-2599.
39. Thirumurugan, P.; Matosiuk, D.; Jozwiak, K., *Chemical Reviews* **2013**, *113*, 4905-4979.
40. Kolb, H. C.; Sharpless, K. B., *Drug Discovery Today* **2003**, *8*, 1128-1137.

41. Nainar, S.; Beasley, S.; Fazio, M.; Kubota, M.; Dai, N.; Corrêa, I. R.; Spitale, R. C., *ChemBioChem* **2016**, *17*, 2149-2152.
42. Nguyen, K.; Fazio, M.; Kubota, M.; Nainar, S.; Feng, C.; Li, X.; Atwood, S. X.; Bredy, T. W.; Spitale, R. C., *Journal of the American Chemical Society* **2017**, *139*, 2148-2151.
43. Feng, C.; Li, Y.; Spitale, R. C., *Organic & Biomolecular Chemistry* **2017**, *15*, 5117-5120.
44. Hida, N.; Aboukilila, M. Y.; Burow, D. A.; Paul, R.; Greenberg, M. M.; Fazio, M.; Beasley, S.; Spitale, R. C.; Cleary, M. D., *Nucleic Acids Research* **2017**, *45*, e138-e138.
45. Hermann, T.; Heumann, H., [3] Structure and distance determination in RNA with copper phenanthroline probing. In *Methods in Enzymology*, Academic Press: 2000; Vol. 318, pp 33-43.
46. Hong, V.; Presolski, S. I.; Ma, C.; Finn, M. G., *Angewandte Chemie International Edition* **2009**, *48*, 9879-9883.
47. Paredes, E.; Das, S. R., *ChemBioChem* **2011**, *12*, 125-131.
48. Schoenebeck, F.; Ess, D. H.; Jones, G. O.; Houk, K. N., *Journal of the American Chemical Society* **2009**, *131*, 8121-8133.
49. Jewett, J. C.; Bertozzi, C. R., *Chemical Society reviews* **2010**, *39*, 1272-1279.
50. Feng C[^], C. D., Joseph J, Muuronen M, Coldren WH, Dai N, Correa IR, Furche F, Hadad C, Spitale RC*, *Nature chemical biology* **2018**.
51. Nainar, S.; Kubota, M.; McNitt, C.; Tran, C.; Popik, V. V.; Spitale, R. C., *Journal of the American Chemical Society* **2017**, *139*, 8090-8093.
52. Darko, A.; Wallace, S.; Dmitrenko, O.; Machovina, M. M.; Mehl, R. A.; Chin, J. W.; Fox, J. M., *Chemical science (Royal Society of Chemistry : 2010)* **2014**, *5*, 3770-3776.
53. Lang, K.; Chin, J. W., *ACS Chemical Biology* **2014**, *9*, 16-20.

54. Wu, H.; Alexander, S. C.; Jin, S.; Devaraj, N. K., *Journal of the American Chemical Society* **2016**, *138*, 11429-11432.
55. George, J. T.; Srivatsan, S. G., *Bioconjugate Chemistry* **2017**, *28*, 1529-1536.

Chapter 1

Metabolic Incorporation and Application of 2'-Azidonucleosides

1.1 Introduction

The regulation and dysregulation of RNA has been depicted with development and disease.¹⁻³ A key challenge is developing methods to track RNA expression, characterize its dynamics, and utilize chemical approaches to characterize their functions. The use of modified nucleosides has offered novel methods of investigating RNA biology.

Modified nucleoside derivative development and application has advanced our understanding of RNA biology. 4-thiouridine has been used to discover RNA-protein interactions.⁴ 5-ethynyluridine gave rise to methods to track transcription and image RNA through fluorescent imaging via copper-catalyzed alkyne-azide cycloaddition (CuAAC).⁵ Combining these two nucleosides offered transcriptome-wide analysis of RNA-Protein interactions through mass spectroscopy.⁶

Our lab has previously shown a variety of chemical methods and techniques to study RNA. Cell-type specific metabolic incorporation of 5-ethynyl pyrimidine bases with the transfection of uracil phosphoribosyltransferase (UPRT).⁷ Metabolic incorporation of azidonucleosides allow for the ability to perform copper-free strain promoted alkyne-azide cycloadditions (SPAAC).⁸ This technique can be extended to obtain temporal control over bioorthogonal ligations for photo-controlled imaging and RNA tagging.⁹ While innovative, these methods of labeling RNA with a bioorthogonal functional group lack in various areas:

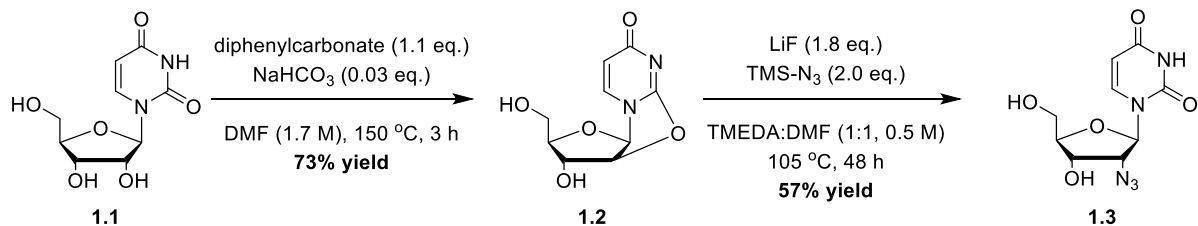
for ethynyl-nucleosides, copper-catalyzed reactions degrade RNA,¹⁰ 5-ethynyluridine is cytotoxic to cells, and cell-type specific labeling with UPRT yields background labeling in non-transfected cells after long incubation periods.

We hypothesized we could explore various positions on pyrimidine nucleosides to adapt azido functionality. In our previous work investigating azidonucleosides, we observed 2'-azidoadenosine had superior incorporation in comparison to the other modified nucleosides. Furthermore, we observed a lack of diversity in the nucleosides that were tested; only adenosine and uridine derivatives were studied. The salvage pathway for adenosine, cytidine, and uridine have a direct route from the nucleoside to incorporation into RNA. Since 2'-azidoadenosine was previously explored, we sought to explore 2'-azido-pyrimidine nucleosides. Here, we report the synthesis and application of 2'-azido-pyrimidine nucleosides.

1.2 Results & Discussion

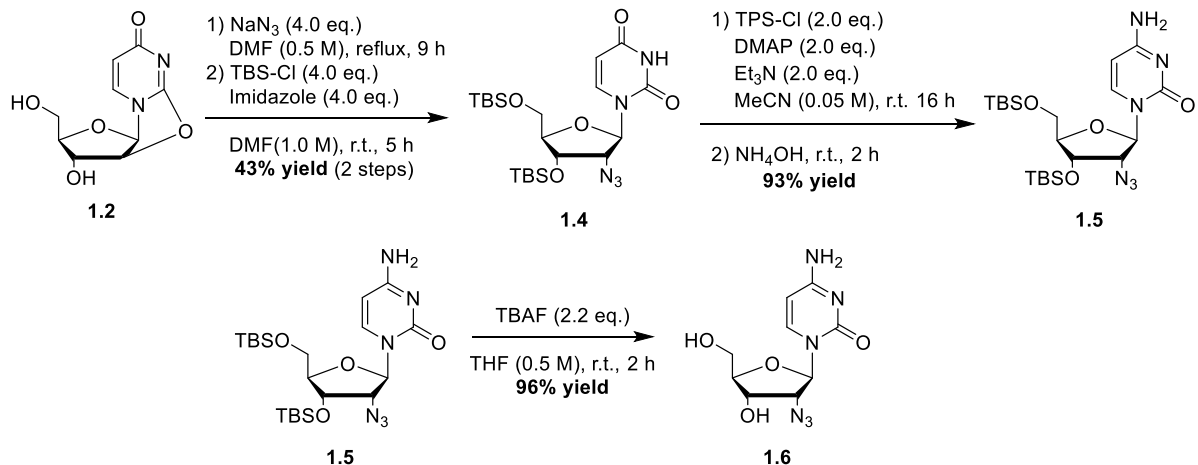
Synthesis of 2'-azidopyrimidine nucleosides.

2'-azidouridine synthesis is described in scheme 1-1. Uridine (**1.1**) was cyclized to 2,2'-anhydrouridine (**1.2**) with diphenylcarbonate with a catalytic amount of NaHCO₃. Azidation of 2,2'-anhydrouridine (**1.2**) was accomplished with TMS-Azide, Lithium Fluoride, in a mixture of TMEDA and DMF gave 2'-Azidouridine (**1.3**).



Scheme 1-1. 2'-Azidouridine Synthetic Scheme

2'-azidocytidine synthesis is described in scheme 1-2. 2,2'-anhydrouridine (**1.2**) underwent azidation with NaN_3 followed by TBS protection in the same pot to form TBS protected 2'-azidouridine (**1.4**). TPS-Cl was used to form a leaving group on the 4 position of the uracil ring followed by $\text{S}_{\text{N}}\text{Ar}$ with ammonium hydroxide to form TBA protected 2'-azidocytidine (**1.5**). Deprotection of (**1.5**) with TBAF yielded 2'-azidocytidine (**1.6**).



Scheme 1-2. 2'-Azidocytidine Synthetic Scheme

It should be noted to proceed the azidation steps with caution. Use of anhydrous materials is needed due to the possibility of formation of hydrozoic acid. Furthermore, reactions are carried out behind a blast shield due to the high nitrogen to carbon ratios.

Synthetic Optimization and Scale up

Initial synthetic schemes were used to produce milligram quantities of 2'-azidonucleosides to accomplish initial biological tests for analysis of modification of the 2' position on pyrimidine nucleosides. To accomplish these small quantities, minimal optimization was performed to meet the need of this endeavor. As the project progressed, gram quantities were needed to reach the demand for the biological tests.

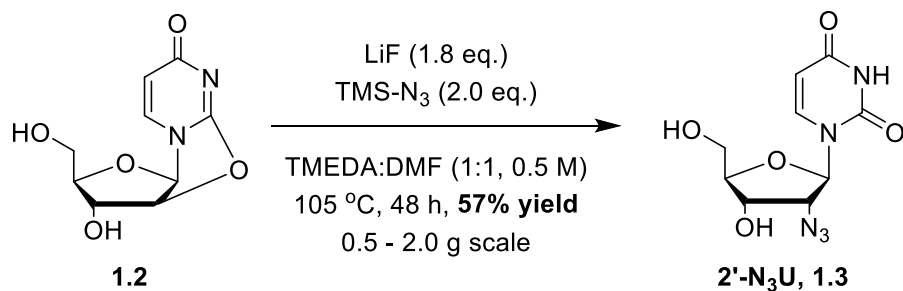
In the overall synthesis of 2'-azidonucleosides, the inefficient step is the azidation of 2,2'-anhydrouridine (**1.2**). Optimization of this azidation was explored, as shown in table 1-1. Initial trials of the synthesis of 2'-azidouridine (**1.3**) was performed with 4 equivalences of NaN_3 in DMF with escalating temperatures over 14 h. Analysis of the products formed from the reaction revealed two major products, the wanted 2'-azidouridine (**1.3**) and Uridine as a byproduct. The analysis of this uridine byproduct was determined by TLC analysis and confirmed by ESI-MS. The formation of uridine in this reaction was determined to be from water in the reaction mixture. In the second trial of this optimization, NaN_3 was dried through toluene azeotropes and used immediately. The reaction was refluxed in DMF for 9 h and resulted in a greater yield of 55%. To try to boost reactivity, DMSO was used as a solvent instead of DMF. This was due to the solubility of NaN_3 being greater in DMSO than DMF. Unfortunately, this resulted in a yield of 8% and the uridine product was observed by TLC analysis. It was concluded that the DMSO was wet and no further reactions were carried out in DMSO.

With the need to develop biological assays, co-crystallography structures, and animal models, further optimization of this synthesis needed to be performed to adjust to gram

quantity synthesis of 2'-azidonucleosides. In the analysis of the scalability of the synthesis of 2'-azidonucleosides, concerns were drawn around the azidation step. The major concern around the scalability of azidation stemmed from high nitrogen to carbon ratios that could lead to an explosion at larger quantities. To mitigate this concern, two goals needed to be met: first, lowering of the nitrogen to carbon ratio in the reaction which could be accomplished by lowering the amount of azide species in the reaction; second, lowering of the temperature of the reaction which would inherently lower the possibility of an explosion.

Both of these goals were accomplished through the use of a naked azide source. A modified procedure from Wnuk, *et al.* was used to accomplish this reaction.¹¹ This procedure uses a combination of LiF and TMS-N₃ in a TMEDA:DMF mixture to perform the azidation. This method also lowers the temperature of the reaction from 105 °C from 153 °C, but increases the reaction time to 48 h instead of 9 h. While this reaction may take longer to complete, it accomplished the aforementioned goals of lowering the azide content in the reaction, thereby lowering the overall nitrogen to carbon ratio in the reaction, and lowering the temperature of the reaction. Overall, reaction was slightly more efficient with a yield of 57% in comparison to the previous NaN₃ methods and accomplished gram scale quantities.

To possibly lower the total amount of material added to the reaction and maintain a naked azide species in the reaction, tetrabutylammonium azide (TBA-N₃) was pursued. Upon heating this reaction up to reflux, no product was formed. Analysis of the products by TLC revealed the formation of Uridine. The TBA-N₃ itself is hygroscopic and was believed to be wet. This method was no longer pursued and the TMS-N₃ with LiF was used in the overall synthesis.



Entry	Reagents	Solvent	Temp.	Time	Yield (%)	Scale
1	NaN ₃ (4.0 eq.)	DMF	40 - 100 °C	14 h	22	mg
2	NaN ₃ (4.0 eq.)	DMF	reflux	9 h	55	mg
3	NaN ₃ (4.0 eq.)	DMSO	reflux	9 h	8	mg
4	LiF (1.8 eq.), TMS-N ₃ (2.0 eq.)	TMEDA:DMF	105 °C	48 h	57	gram
5	TBA-N ₃ (1.2 eq.)	DMF	100 °C - reflux	24 h	No product	mg

Table 1-1. Optimization of the Azidation of 2,2'-Anhydrouridine (1.2)

Metabolic incorporation of 2'-modified analogs.

After successfully synthesizing 2'azidocytidine (2'N₃-C) and 2'azidouridine (2'N₃-U), we sought to test them in cell culture. Interestingly, while 2'N₃-C showed labeling comparable to that of 2'N₃-A, there was very little ostensible labeling from 2'N₃-U (Figure 1-1). Trypan blue staining indicated no cytotoxicity, and there were no notable changes in cell morphology following treatment.

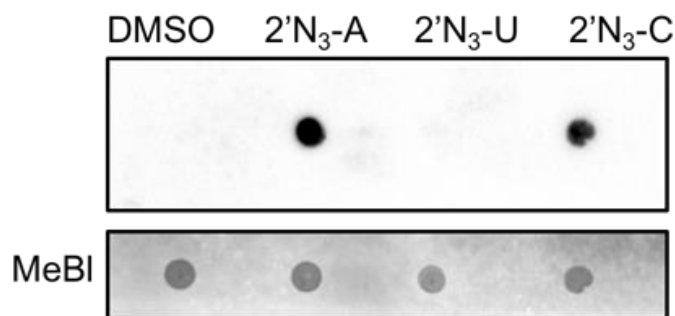


Figure 1-1. HeLa cells treated with 1 mM analog for 5 h. RNA was extracted, biotinylated and detected by streptavidin dot blot.

With 2'-Azidocytidine in hand, we assessed the incorporation of the nucleoside into nascent transcripts. A concentration titration of 2'-Azidocytidine (**1.6**) performed on HEK239T cells (Figure 1-2.). 0, 10, 100, 250, 500 μ M and 1 mM concentrations were incubated in HEK239T cells. The total RNA was extracted, reacted with biotin-alkyne via CuAAC, and visualized by dot blot analysis. At 10 μ M, incorporation of 2'-Azidocytidine (**1.6**) is seen and it was concluded that 2'-Azidocytidine (**1.6**) is robustly incorporated into nascent transcripts. Furthermore, this shows the utility of 2'-Azidocytidine (**1.6**) as a bioorthogonal nucleoside for the isolation of nascent transcripts.

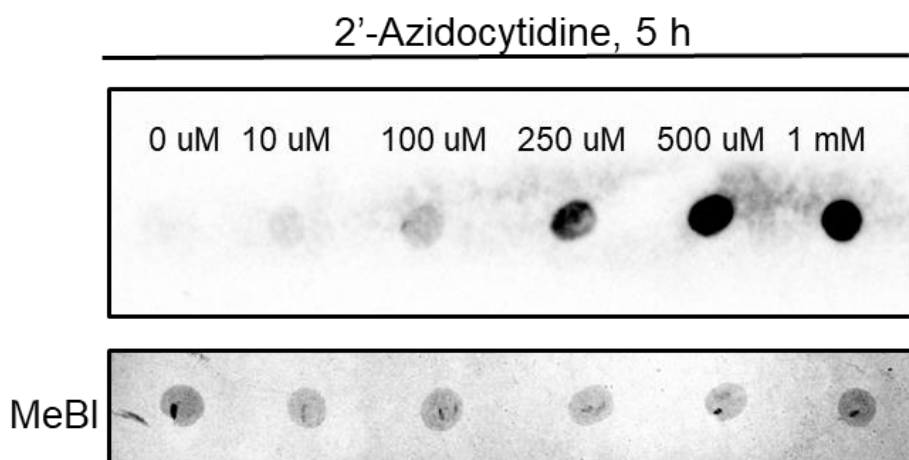


Figure 1-2. 2'-Azidocytidine Incorporation Analysis by Dot Blot

Exploration of polymerase activity for 2'-Azidocytidine (**1.6**) incorporation was assessed with actinomycin D (Act D), a polymerase I and II inhibitor at the highest concentration of 2'-Azidocytidine from above, 1 mM, to force incorporation into nascent transcripts. (Figure 1-3.). Act D concentrations varied from 0, 10, and 20 μ M. At 20 μ M. At 20 μ M of Act D, no incorporation of 2'-Azidocytidine was seen. At 0 and 10 μ M of Act D, incorporation was seen, thereby revealing that polymerase I and II are involved in the incorporation of 2'-Azidocytidine (**1.6**) into nascent transcripts.

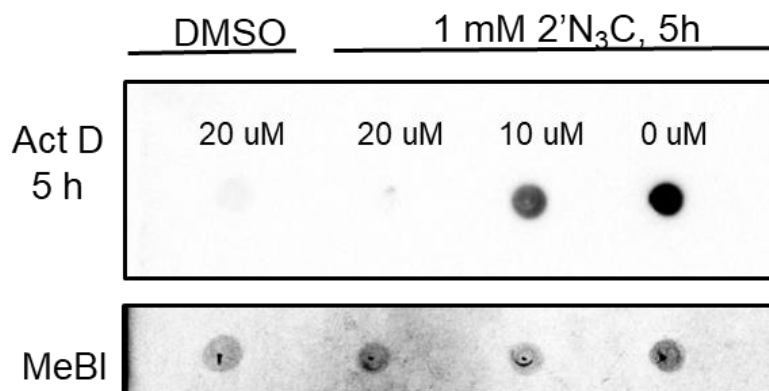


Figure 1-3. Dot Blot Analysis of 2'-Azidocytidine Incorporation Inhibition with ActD

To expand the utility of 2'-Azidocytidine (**1.6**) beyond isolation of nascent transcripts, an imaging experiment was performed (Figure 1-4.). HEK293T cells were incubated with 1 mM 2'-Azidocytidine (**1.6**) for 5 h. These cells were then fixed and reacted with alkyne-Alexa₄₈₈ via CuAAC. DAPI was used to stain the nucleus and visualized by fluorescence microscopy. Robust labeling with alkyne-Alexa₄₈₈ is seen and it can be concluded that 2'-Azidocytidine (**1.6**) is a bioorthogonal nucleoside that can be used for isolation and visualization of nascent transcripts. 2'-Azidocytidine (**1.6**) expands the bioorthogonal nucleosides available for the study of RNA. Use of cytidine analogs for bioorthogonal labeling of RNA could provide a holistic view of transcripts over adenosine analogs due to polyadenylation of mRNA and long noncoding transcripts. Adding to the holistic view of transcripts, uridine analogs could contribute to polyuridylation where cytidine analogs would not.

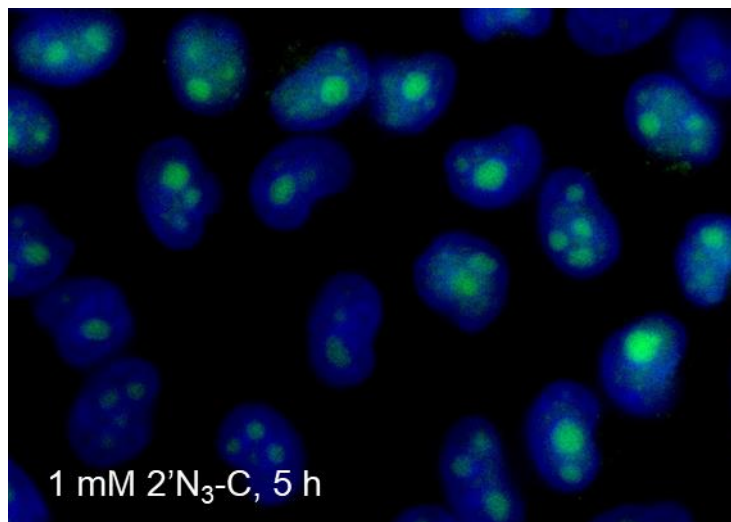


Figure 1-4 . Fluorescent Imaging of 2'-Azidocytidine (1.6) Incorporation in HEK293T Cells via CuAAC with Alkyne-Alexa₄₈₈

1.3 Conclusion

With the goal of expanding methods to study RNA biology, this study shows a facile synthesis to 2'-azidopyrimidine nucleosides and the utility of 2'-azidopyrimidine nucleosides. The use of azido-functionality offers the use of metal-free bioorthogonal reactions which prevents the degradation of RNA.

Synthetically, a gram scale synthesis of 2'-azidopyrimidine nucleosides was developed. The greatest challenge in this synthetic route was the azidation of 2,2'-anhydrouridine due to lower yields and the possibility of an explosion from high nitrogen to carbon ratios. To accomplish this, the use of TMS-N₃ and LiF allowed for the azidation to undergo more efficiently at a lower temperature, thereby, lowering the potential for an explosion and allowed for a facile scale up process.

Cytidine and uridine are both used for a variety of metabolic pathways. Specifically, cytidine is used in lipid synthesis and uridine is used in a variety of glycosylation pathways.¹⁵⁻

¹⁶ The utility of these 2'-azidopyrimidine nucleosides can offer a greater depth of study of these metabolic pathways. Overall, 2'-azidopyrimidine nucleosides are a new tool that can easily be produced and used in a variety of biological studies.

1.4 Experimental Details

Biochemical Methods

2'-azidonucleoside labeling of cellular RNA

HEK293T cells and HeLA cells (ATCC) were cultured in DMEM (Corning) supplemented with 10% FBS, 1% penicillin and streptomycin and grown at 37 °C, 5% CO₂. Analogs were added to complete culture medium from 200 mM stocks with a final concentration of <1% DMSO.

RNA isolation and biotinylation via CuAAC

After labeling, total cellular RNA was harvested using Trizol Reagent (Invitrogen) following the manufacturer's instructions or RIPA lysis buffer (150 mM NaCl, 5 mM EDTA pH 8.0, 50 mM Tris, pH 8.0, 1.0 % NP-40, 0.5 % sodium deoxycholate, 0.1% SDS) spiked with DNase Turbo and RNaseOut (Thermo Fisher). Briefly, ~20 millions cells were scraped and suspended in 2 mL of lysis buffer, and incubated on ice for 15 minutes. Lysates were mixed 1:1 with phenol/chloroform pH 5.2 (Fisher) vortexed briefly and spun down at 4 °C to separate the layers. The aqueous layer was then applied to a Zymo RNA clean and concentrator IIC column (Zymo) and total RNA was isolated according to the manufacturer's instructions, with RNA eluted in 50 µL of nuclease free water. CuAAC reactions were

prepared using 10 µg of total RNA in solutions of 6% DMSO water, and 1 mM Alkyne biotin to a final volume of 50 µL. Reactions were incubated with at 37 °C for 2 h at 400 RPM. Biotinylation reactions were purified using Zymo RNA clean and concentrator-5 spin column according to the manufacturer instructions, with RNA eluted in 10 µL of nuclease free water.

HRP-streptavidin Dot blotting

Equal amounts of column-purified RNA were spotted onto 2x SSC equilibrated Hybond-N+ membrane (GE Healthcare), allowing spots to dry in between. The membrane was crosslinked using the auto crosslink function at 254 nm on a UV Stratalinker (Stratagene). The membrane was then blocked in a 10% SDS blocking solution followed by incubation with 1:10,000 dilution of high sensitivity streptavidin-HRP (ThermoFisher Scientific) in blocking solution. The membrane was washed x2 in a 1:10 solution of blocking solution and x2 in Tris-saline buffer. It was then incubated in SuperSignal West Pico Chemiluminescent Substrate (ThermoFisher Scientific) according to manufacturer's instructions and imaged on a ChemiDoc MP imaging system (Bio-Rad) under the chemiluminescence channel. Following imaging, the blot was stained in a 0.04% methylene blue, 0.3 M sodium acetate solution to visualize all RNA as a loading control.

RNA fluorescence imaging via CuAAC

Coverslips in 6-well tissue culture plates were treated with 1x poly-D lysine solution for 3 h at 37 °C. HEK293T cells were seeded at densities of 2.5×10^5 and grown to ~50% confluency on glass cover slips. Cells were treated with 2'-azidonucleosides to final concentrations of 1 mM and incubated for 5 hours. After labeling, cells were washed twice with DPBS and fixed

for 10 min at room temperature with 3.7% paraformaldehyde. Cells were quenched with 50 mM glycine, DPBS for 5 min, and then washed twice more. Cells were permeabilized in 0.5% Triton-X DPBS for 15 min, and then washed x2 with DPBS. Cells were then treated with solutions of 5 μ M Alkyne Alexa₄₈₈ in DPBS, and incubated for 3 h at 37 °C in the dark. Cells were washed x2 with 0.25% Triton-X DPSB for 5 min, and then x5 with DPBS for 5 min each on an orbital shaker. Cells were stained with a solution of 1:3000 Hoechst 333242 for 10 min (Thermo Fisher). Coverslips were briefly washed and then mounted using VectaShield mounting medium (Vector Labs). Slides were imaged via fluorescence confocal microscopy using a 63x oil immersion objective on a Leica 700 Carl Zeiss microscope.

RNA Dot Blot with Actinomycin D

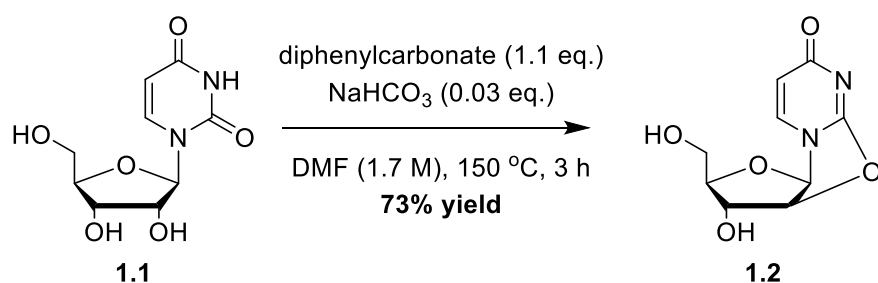
Cells were grown and treated with analog as previously described, with transcriptional inhibitor actinomycin D (Sigma) being co-administered to a final concentration of 20 μ M. Dot blot analysis was performed as previously described.

General Synthetic Methods

All reagents were purchased from commercial suppliers and were of analytical grade and used without further purification unless otherwise noted. Reaction progress was monitored by thin-layer chromatography on EMD 60 F254 plates, visualized with UV light. Compounds were purified via flash column chromatography using Sorbent Technologies 60 Å 230 x 400 mesh silica gel. Anhydrous solvents dichloromethane (DCM), methanol (MeOH), dimethylformamide (DMF), toluene (PhMe) were degassed and dried over molecular sieves. All reaction vessels were flame dried prior to use. NMR spectra were acquired with Bruker

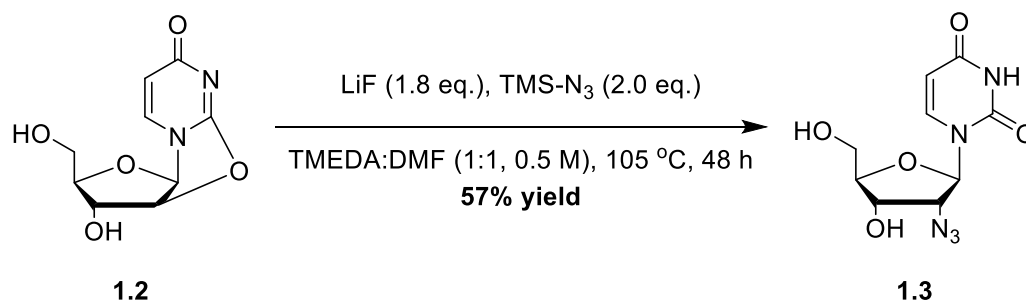
Advanced spectrometers. All reactions were carried in dark unless otherwise noted. All spectra were acquired at 298 K. ^1H -NMR spectra were acquired at 400 MHz and 500 MHz. ^{13}C -NMR spectra were acquired at 125 MHz. ^{31}P -NMR spectra were acquired at 162 MHz. Chemical shifts are reported in ppm relative to residual non-deuterated NMR solvent, and coupling constants (J) are provided in Hz. All NMR spectra was analyzed using MestreNova software. Low and high-resolution electrospray ionization (ESI) mass spectra and Gas Chromatography mass spectra were collected at the University of California-Irvine Mass Spectrometry Facility. The abbreviations used can be found in the document JOC standard Abbreviations and Acronyms, <http://pubs.acs.org/paragonplus>

Synthetic Methods



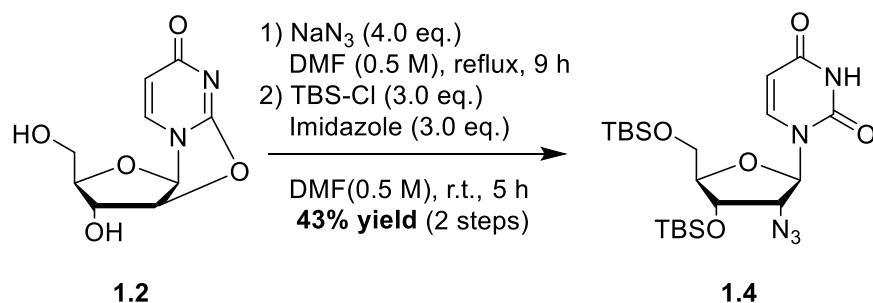
2,2'-anhydrouridine (**1.2**) was synthesized according to a modified procedure by Mahto, S. *et al.*¹⁷ Uridine (**1.1**) (10.0 g, 40.9 mmol), diphenylcarbonate (9.85 g, 45.1 mmol), and NaHCO_3 (0.10 g, 1.23 mmol) was dissolved in DMF (70 mL) and refluxed for 3 h. Upon completion, the mixture was cooled to r.t. and H_2O (200 mL) was added. The mixture was then extracted with DCM (3 x 250 mL) and the aqueous layer was concentrated *in vacuo*. Cold MeOH was added to the residue and placed on ice allowing a white precipitate to form. The precipitate was then filtered and washed with cold MeOH and dried *in vacuo* to give (2R,3R,3aR,9aR)-3-hydroxy-2-(hydroxymethyl)-2,3,3a,9a-tetrahydro-6H-furo[2',3':4,5]oxazolo[3,2-

a]pyrimidin-6-one (**1.2**) as a white solid. (6.73 g, 73%) HRMS Calcd for $C_9H_{10}N_2O_5Na$ $[M+Na^+]$ 249.05, found 249.0487 $[M+Na^+]$; 1H NMR (400 MHz, DMSO- D_6) δ 7.83 (d, $J = 7.4$ Hz, 1H), 6.30 (d, $J = 5.7$ Hz, 1H), 5.84 (d, $J = 7.4$ Hz, 1H), 5.20 (d, $J = 5.7$ Hz, 1H), 4.38 (s, 1H), 4.07 (t, $J = 5.2$ Hz, 1H), 3.23 (ddd, $J = 17.4, 11.5, 5.3$ Hz, 2H); ^{13}C NMR (101 MHz, DMSO- D_6) δ 171.13, 159.78, 136.81, 108.60, 89.99, 89.19, 88.73, 74.72, 69.37, 60.82.

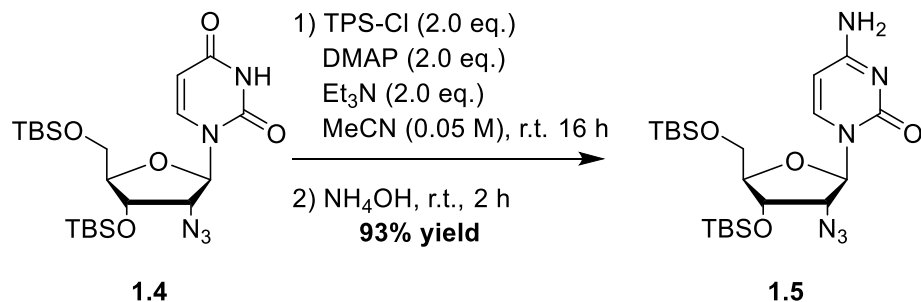


2'-azidouridine (**1.3**) was synthesized following a modified procedure from Wnuk, S. *et al.*¹¹ LiF (0.62 g, 23.9 mmol) was dissolved in $TMEDA:DMF$ (1:1, 30 mL) and heated to 105 °C. $TMS-N_3$ (3.5 mL, 26.5 mmol) was carefully added to the reaction and stirred for 30 min. 2,2'-anhydrouridine (**1.2**) (3.00 g, 13.3 mmol) was added to the reaction and stirred for 48 h. The mixture was then allowed to cool to r.t. and concentrated *in vacuo*. $MeOH$ (50 mL) was added to the viscous mixture and filtered. The filtrate was concentrated *in vacuo* and purified by silica column chromatography (0-10% $MeOH/EtOAc$). The crude product was further purified by silica column chromatography (0-10% $MeOH/DCM$) to give 2'-azidouridine (**1.3**) (2.04 g, 57%) as a white foam. HRMS Calcd for $C_9H_{10}N_5O_5$ $[M-H^-]$ 268.07, found 268.0682 $[M-H^-]$; 1H NMR (400 MHz, DMSO) δ 7.82 (d, $J = 8.1$ Hz, 1H), 5.86 (d, $J = 5.5$ Hz, 1H), 5.59 (t, $J = 8.1$ Hz, 1H), 4.29 (t, $J = 4.9$ Hz, 1H), 4.00 (t, $J = 5.4$ Hz, 1H), 3.85 (dd, $J = 7.2, 3.0$ Hz, 1H), 3.59

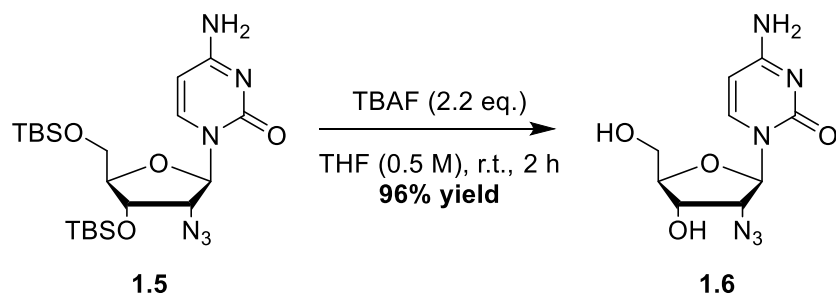
(ddd, $J = 28.7, 12.2, 3.1$ Hz, 2H); ^{13}C NMR (151 MHz, DMSO) δ 164.76, 151.73, 140.30, 102.60, 86.08, 85.71, 70.91, 65.11, 60.66.



1.2 (0.86 g, 3.79 mmol), NaN_3 (0.99 g, 15.2 mmol) was refluxed in DMF (8 mL) for 9 h. The mixture was then cooled to r.t. and TBS-Cl (1.72 g, 11.4 mmol) and imidazole (0.78 g, 11.4 mmol) was added and stirred for 5 h. The mixture was then concentrated *in vacuo* and purified by silica column flash chromatography (0-60% EtOAc/Hex) to give 1-(((2R,3R,4S,5R)-3-azido-4-((tert-butyldimethylsilyl)oxy)-5-(((tert-butyldimethylsilyl)oxy)methyl)tetrahydrofuran-2-yl)pyrimidine-2,4(1H,3H)-dione (**1.4**) (0.813 g, 43%) as a white solid. HRMS Calcd for $\text{C}_{21}\text{H}_{39}\text{N}_5\text{O}_5\text{Si}_2\text{Na}$ $[\text{M}+\text{Na}^+]$ 520.25, found 520.2388 $[\text{M}+\text{Na}^+]$; ^1H NMR (499 MHz, CDCl_3) δ 10.08 (s, 1H), 7.89 (d, $J = 8.2$ Hz, 1H), 6.10 (d, $J = 4.6$ Hz, 1H), 5.74 (d, $J = 8.2$ Hz, 1H), 4.40 (t, $J = 5.0$ Hz, 1H), 4.10 – 4.06 (m, 1H), 4.00 (dd, $J = 11.7, 2.1$ Hz, 1H), 3.78 (dd, $J = 11.7, 1.5$ Hz, 1H), 3.74 (t, $J = 4.9$ Hz, 1H), 0.95 (d, $J = 6.6$ Hz, 16H), 0.15 (dd, $J = 18.1, 9.9$ Hz, 11H); ^{13}C NMR (101 MHz, CDCl_3) δ 164.21, 150.85, 139.80, 102.92, 87.01, 85.66, 72.00, 66.53, 61.99, 26.32, 26.10, 18.77, 18.46, 18.45, 18.44, 18.43, 18.42, -4.24, -4.63, -5.11, -5.12, -5.13, -5.14, -5.15, -5.17.



The synthesis of **1.5** was accomplished following a modified procedure by Sueda, M. *et al.*¹⁸ **1.4** (100 mg, 0.20 mmol), triisopropylbenzenesulfonyl chloride (122 mg, 0.40 mmol), DMAP (49.1 mg, 0.40 mmol), and Et₃N (56 μ L, 0.40 mmol) was dissolved in MeCN (4 mL) and stirred at r.t. for 16 h. aqueous ammonia (1.0 mL) was added to the mixture and stirred for an additional 2 h. Upon completion, the mixture was concentrated *in vacuo* and purified by silica flash column chromatography (0-10% MeOH/DCM) to give 4-amino-1-((2R,3R,4S,5R)-3-azido-4-((tert-butyldimethylsilyl)oxy)-5-(((tert-butyldimethylsilyl)oxy)methyl)tetrahydrofuran-2-yl)pyrimidin-2(1H)-one (**1.5**) as an off-white solid (93.3 mg, 93%). HRMS Calcd for C₂₁H₄₀N₆O₄Si₂Na [M+Na⁺] 519.26, found 519.2548 [M+Na⁺]; ¹H NMR (400 MHz, CDCl₃) δ 7.90 (d, *J* = 7.5 Hz, 1H), 5.95 (d, *J* = 2.3 Hz, 1H), 5.84 (d, *J* = 7.5 Hz, 1H), 4.33 (t, *J* = 5.8 Hz, 1H), 4.08 – 3.94 (m, 2H), 3.83 (dd, *J* = 4.8, 2.6 Hz, 1H), 3.75 (d, *J* = 10.7 Hz, 1H), 0.92 (d, *J* = 5.1 Hz, 18H), 0.14 – 0.07 (m, 12H); ¹³C NMR (125 MHz, CDCl₃) δ 166.35, 155.97, 140.01, 95.13, 87.86, 83.91, 70.11, 66.96, 60.89, 26.02, 25.74, 18.48, 18.06, -4.51, -5.00, -5.39, -5.47.



1.5 (212 mg, 0.43 mmol) was dissolved in a 1 M solution of TBAF in THF (0.94 mL, 0.94 mmol) and stirred at r.t. for 2 h. The mixture was concentrated *in vacuo* and purified by C18 reverse phase chromatography (5-95% MeCN/H₂O) to give 4-amino-1-((2R,3R,4S,5R)-3-azido-4-hydroxy-5-(hydroxymethyl)tetrahydrofuran-2-yl)pyrimidin-2(1H)-one (**1.6**) as a white solid (110 mg, 96%). HRMS Calcd for C₉H₁₂N₆O₄Na [M+Na⁺] 291.09, found 291.0818 [M+Na⁺]; ¹H NMR (400 MHz, CD₃OD) δ 8.08 (d, *J* = 7.5 Hz, 1H), 5.94 (s, *J* = 3.7 Hz, 1H), 5.93 (d, *J* = 3.1 Hz, 1H), 4.41 (t, 1H), 4.06 (dd, *J* = 5.4, 3.8 Hz, 1H), 4.04 – 3.98 (m, 1H), 3.93 (dd, *J* = 12.4, 2.5 Hz, 1H), 3.79 (dd, *J* = 12.5, 3.0 Hz, 1H); ¹³C NMR (126 MHz, CD₃OD) δ 166.35, 156.79, 141.04, 94.75, 88.30, 84.43, 69.80, 66.75, 59.98.

1.5 References

1. Mehler, M. F.; Mattick, J. S., *Physiological Reviews* **2007**, *87*, 799-823.
2. Pek Jun, W.; Okamura, K., *Wiley Interdisciplinary Reviews: RNA* **2015**, *6*, 671-686.
3. Liu, E. Y.; Cali, C. P.; Lee, E. B., *Disease Models & Mechanisms* **2017**, *10*, 509.
4. Hafner, M.; Landthaler, M.; Burger, L.; Khorshid, M.; Hausser, J.; Berninger, P.; Rothballer, A.; Ascano, M.; Jungkamp, A.-C.; Munschauer, M.; Ulrich, A.; Wardle, G. S.; Dewell, S.; Zavolan, M.; Tuschl, T., *Cell* **2010**, *141*, 129-141.
5. Jao, C. Y.; Salic, A., *Proceedings of the National Academy of Sciences* **2008**, *105*, 15779.
6. Huang, R.; Han, M.; Meng, L.; Chen, X., *Proceedings of the National Academy of Sciences* **2018**.
7. Nguyen, K.; Fazio, M.; Kubota, M.; Nainar, S.; Feng, C.; Li, X.; Atwood, S. X.; Bredy, T. W.; Spitale, R. C., *Journal of the American Chemical Society* **2017**, *139*, 2148-2151.
8. Nainar, S.; Beasley, S.; Fazio, M.; Kubota, M.; Dai, N.; Corrêa, I. R.; Spitale, R. C., *ChemBioChem* **2016**, *17*, 2149-2152.
9. Nainar, S.; Kubota, M.; McNitt, C.; Tran, C.; Popik, V. V.; Spitale, R. C., *Journal of the American Chemical Society* **2017**, *139*, 8090-8093.
10. Hermann, T.; Heumann, H., [3] Structure and distance determination in RNA with copper phenanthroline probing. In *Methods in Enzymology*, Academic Press: 2000; Vol. 318, pp 33-43.
11. Wnuk, S. F.; Chowdhury, S. M.; Garcia, P. I.; Robins, M. J., *The Journal of Organic Chemistry* **2002**, *67*, 1816-1819.
12. van Kuilenburg, A. B. P.; Meinsma, R., *Biochimica et Biophysica Acta (BBA) - Molecular Basis of Disease* **2016**, *1862*, 1504-1512.

13. Van Rompay, A. R.; Norda, A.; Lindén, K.; Johansson, M.; Karlsson, A., *Molecular Pharmacology* **2001**, *59*, 1181.
14. Sarkisjan, D.; Julsing, J. R.; Smid, K.; de Klerk, D.; van Kuilenburg, A. B. P.; Meinsma, R.; Lee, Y. B.; Kim, D. J.; Peters, G. J., *PLOS ONE* **2016**, *11*, e0162901.
15. Urasaki, Y.; Pizzorno, G.; Le, T. T., *PLOS ONE* **2014**, *9*, e99728.
16. Liu, X.; Yin, Y.; Wu, J.; Liu, Z., *Nature Communications* **2014**, *5*, 4244.
17. Mahto, S. K.; Chow, C. S., *Bioorganic & Medicinal Chemistry* **2008**, *16*, 8795-8800.
18. Sukeda, M.; Shuto, S.; Sugimoto, I.; Ichikawa, S.; Matsuda, A., *The Journal of Organic Chemistry* **2000**, *65*, 8988-8996.

Chapter 2

Inverse-Electron Demand Diels-Alder Reactions of Vinyl-Nucleosides with Tetrazines to Study RNA

2.1 Abstract

Optimized and stringent chemical methods to profile nascent RNA expression are still in demand. Herein, we expand the toolkit for metabolic labeling of RNA through application of inverse electron demand Diels-Alder (IEDDA) chemistry. We synthesized a variety of vinyl-modified nucleosides, which we systematically tested for their ability to be installed through cellular machinery. Further, we tested these nucleosides against a panel of tetrazines to identify those which are able to react with a terminal alkene, but are stable enough for selective conjugation. The selected pairings then facilitated RNA functionalization with biotin and fluorophores. We found that this chemistry is not only amenable to preserving RNA integrity but also endows the ability to both tag and image RNA in cells. These key findings represent a significant advancement in methods to profile the nascent transcriptome using chemical approaches.

2.2 Introduction

RNA plays critical roles in the regulation of nearly all biological processes: from controlling chromatin state, to directing transcription, to regulation of cell proliferation.¹⁻² Profiling nascent RNA expression can allow researchers to identify potentially functional RNAs, and this is aided by the use of metabolic chemical reporters.³ As such, several chemical

functionalities have been adapted for RNA nucleoside analogs. 4-thiouridine is a commonly used probe, which allows for enrichment of nascent RNA through disulfide exchange chemistry.⁴ More recently, alkynyl⁵⁻⁷ and azido-containing⁸ nucleosides have been introduced into cells, wherein nascent RNA can be tracked through click chemistry. Both the Cu(I)-catalyzed azide-alkyne cycloaddition (CuAAC) and strain-promoted azide-alkyne cycloaddition (SPAAC) can be utilized for enrichment as well as imaging.⁹

Despite the utility of these analogs, their chemistries present several drawbacks. 4-thiouridine enrichment is often inefficient due to the transient nature of disulfide bonds, which further prevents RNA imaging in cells.¹⁰ Likewise, CuAAC reactions are known to dramatically compromise the integrity of RNA, where spurious fragmentation of transcripts has altered the results of downstream applications such as RNA sequencing.¹¹⁻¹² Methods that are damaging to cells or RNA integrity can confound interpretation of biologically meaningful results.¹³⁻¹⁵ Lastly, discovering novel analogs for labeling is further hindered by the selectivity of metabolic enzymes, which often have limited functional group tolerance.^{8, 16} These challenges demonstrate the need to further expand the scope of different bioorthogonal chemistries applicable for RNA metabolic labeling (**Figure 2-1A**).

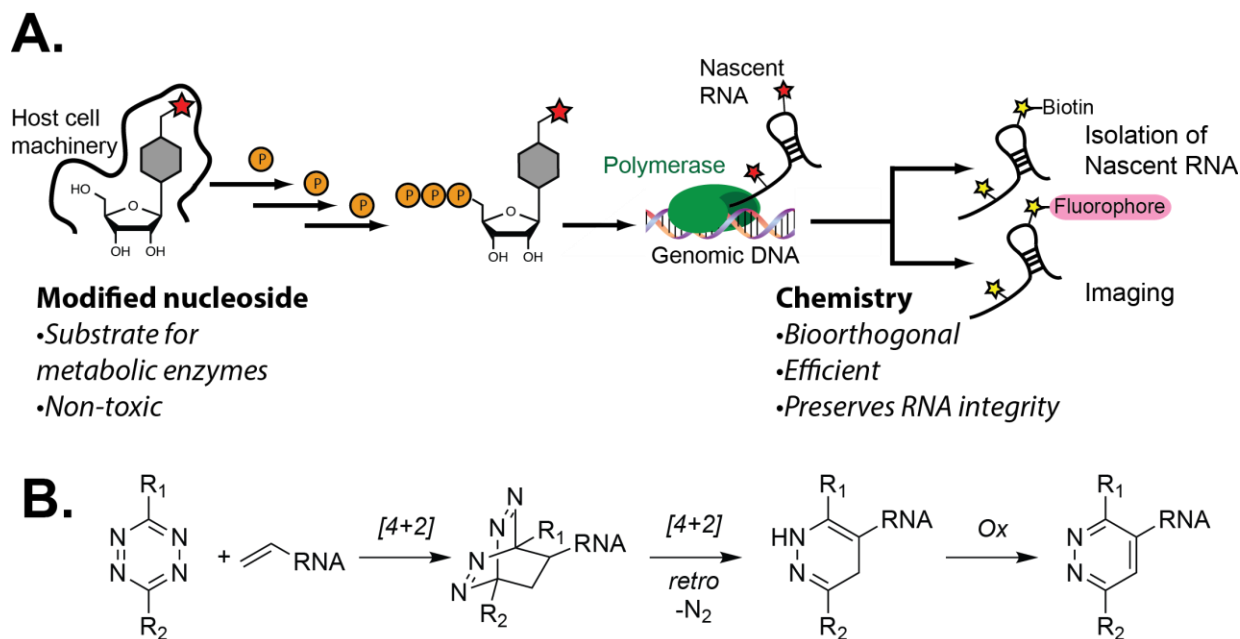


Figure 2-1. Schematic of metabolic labeling of RNA. **A.** Representative steps that are needed to be optimized in metabolic labeling of RNA. **B.** Schematic of the inverse electron-demand Diels-Alder reaction with vinyl-modified RNA.

The inverse electron-demand Diels-Alder (IEDDA) reaction represents an attractive alternative to the currently adopted chemistries. It has been widely used for labeling biomolecules due to its fast kinetics, high yields and exclusion of metal catalysts (**Figure 2-1B**).¹⁷⁻¹⁸ Traditionally, installation or genetic encoding of a strained alkene such as norbornene, *trans*-cyclooctene and cyclopropene have facilitated this rapid labeling.¹⁹⁻²¹ However, this presents a notable challenge to reporter strategies that rely solely on cellular machinery for installation, wherein the enzymes in these metabolic pathways may not accommodate large or even moderately-sized functional groups. We have observed that the size and placement of biorthogonal handles on nucleosides often dictates their utility as metabolic reporters.^{8, 16} Furthermore, there is the possibility for cross-reactivity with

nucleophiles in the cellular milieu.²² Thus, applying this chemistry requires smaller and more stable alkenes for nucleoside functionalization. These challenges present a unique opportunity to explore IEDDA reaction pairs that could be used to form cycloadducts on acceptable timescales, but at the same time are stable enough to provide selectivity.

While the application of vinyl-deoxynucleosides and vinyl-nucleotides has been explored, there has been no investigation of vinyl-nucleosides for RNA metabolic labeling in living cells.²³⁻²⁴ Furthermore, there has been no analysis of pairing vinyl-nucleosides with optimized tetrazines that balance the required reactivity with stability for labeling.

Herein, we report a holistic analysis of vinyl-nucleoside reactivity with a larger subset of tetrazines. We examine which nucleoside analogs can be incorporated into nascent RNA following addition to cellular media. We synthesized and characterized optimal tetrazine/vinyl-nucleoside pairs based on kinetics and molecular orbital analyses. Optimized pairs enable tagging and imaging of nascent RNA without compromising RNA integrity. The methods optimized herein are also orthogonal to conventional CuAAC reactions used for RNA analysis. Overall, this analysis greatly expands our understanding of IEDDA reactions with nucleoside analogs and underscores the utility of biorthogonal methods that are amenable to RNA labeling.

2.3 Results & Discussion

Metabolic Incorporation of vinyl-nucleoside analogs.

It is well-established that the mono-phosphate kinases utilized in nucleoside salvage pathways are the most selective for their substrates. These enzymes have the highest level of substrate specificity due to very specific active site structures.²⁵ Therefore, to identify

positions that could accommodate vinyl functionality, we examined the crystal structures of uridine-cytidine kinase (PDB: 1BX4)²⁶ and adenosine kinase (PDB: 1UEJ)²⁷. Uridine-cytidine kinase revealed an open space at position C5 (**Figure 2-2A**). Previous work has demonstrated that 5-ethynyluridine is well tolerated and incorporated into RNA, thus we synthesized 5-vinyluridine (**5-VU**) and 5-vinylcytidine (**5-VC**) as possible substrates.⁶ Adenosine kinase has cavernous pockets about C2, N6 and N7 of the canonical substrate. Alkyl modifications of adenosine at all three of these positions have been previously demonstrated.²⁸⁻³⁰ However, we did not wish to perturb the Watson-Crick face of the nucleoside, which is responsible for base pairing, thus we synthesized only 2-vinyladenosine (**2-VA**) and 7-deazavinyladenosine (**7-dVA**). There have been no successful reports of incorporation of C8-functionalized purine nucleosides, thus we synthesized 8-vinyladenosine (**8-VA**) and 8-vinylguanosine (**8-VG**) to test the limits of modification. This brought the final total to six vinyl-modified nucleosides, as shown in **Figure 2-2B**.

To understand the extent of nucleoside substitution, we performed LC-MS/MS to obtain quantitative analysis of percent incorporation for each analog (Table S1). RNA was isolated from cells treated with each analog, followed by digestion to mono-nucleosides. LC-MS/MS analysis showed that **2-VA** had the highest incorporation at 2.3% (**Figure 2-2C**). **5-VU** showed 0.86% incorporation, while **7-dVA** showed 0.50% incorporation. The markedly higher incorporation of **2-VA** is likely consistent with other reports that adenosine analogs with small modifications at C2 are highly incorporated into messenger RNA through polyadenylation.^{8, 28}

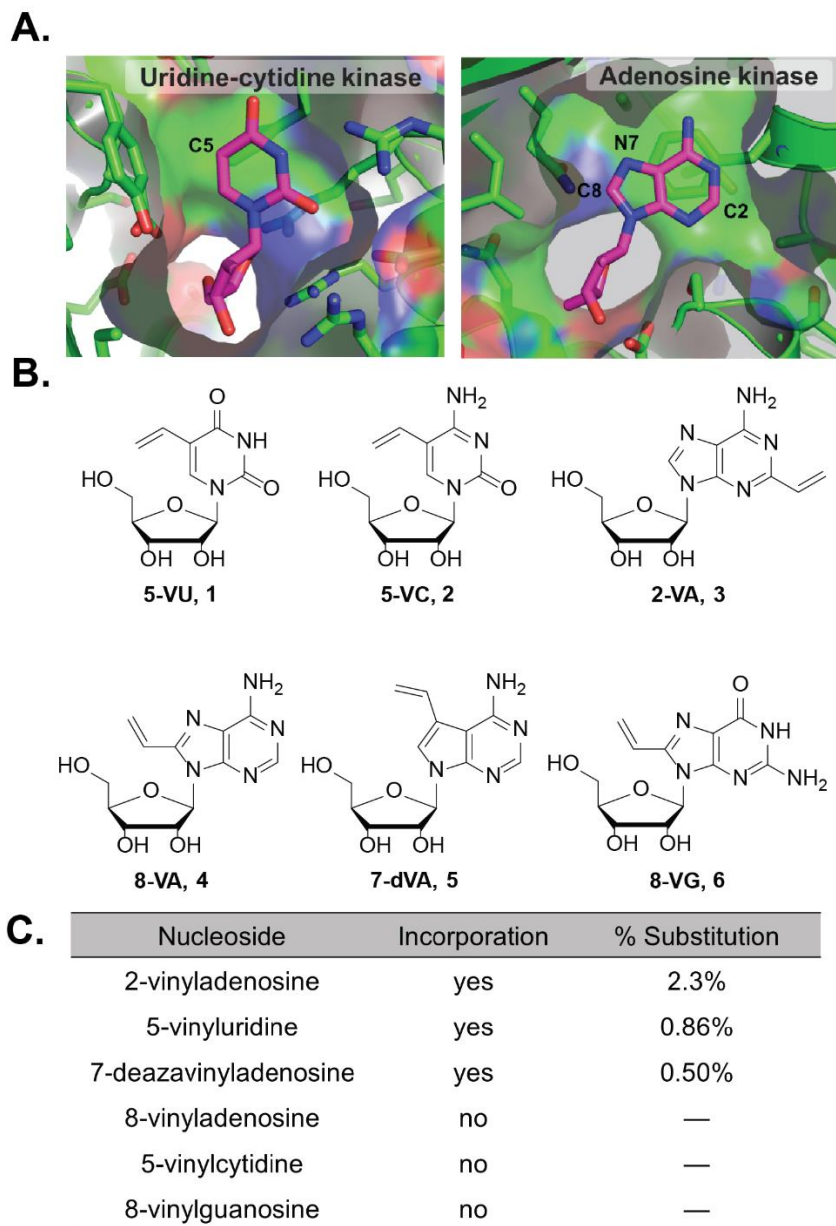


Figure 2-2. Initial analysis of vinyl nucleoside incorporation into RNA. **A.** Crystal structures of uridine-cytidine kinase and adenosine kinase bound to cytidine and adenosine, respectively. PDB: 1UEI, 1BX4 **B.** Structures of vinyl-nucleosides **C.** Incorporation rates of vinyl-nucleosides. HEK293T cells were treated for 12 h at 1 mM final concentration, after which RNA was isolated. Percent incorporation was determined through total RNA digestion and LC-MS/MS analysis of mono-nucleoside mixtures.

We were unable to detect incorporation of **8-VA**, **8-VG**, and **5-VC**. Aside from the structure of the kinases, the solution-structure of modified nucleosides could be a reason for lack of incorporation. Two of the analogs (**8-VA** and **8-VG**) may adopt a primarily *syn* conformation about their N9-C1 glycosidic bond. Analysis of other C8 modified nucleosides has demonstrated that modifications at this position can dramatically alter *syn-anti* ratios of purine nucleosides.³¹⁻³² Therefore, these analogs may not be suitable substrates for initial kinase steps. A greater surprise was the lack of **5-VC** incorporation. LC-MS analysis of the **5-VC** incubated with Trizol reagent revealed **5-VC** was completely degraded, and the Michael adduct with thiocyanate is observed (**Figure 2-S1**). Therefore, we believe **5-VC** is susceptible to other Michael donors in the cellular environment.

Our initial analysis provides an extended framework for understanding the design and successful incorporation of vinyl-modified nucleosides in cells. Furthermore, ascertaining the limitations of modification placement and size will afford greater insights into the potential design of completely orthogonal, nucleoside-enzyme systems.

Kinetic Analysis of vinyl-nucleosides and tetrazines.

Having established the structures of vinyl nucleosides tolerated by the cellular machinery, we turned our attention to identifying and characterizing paired tetrazines for IEDDA reactions. Acceptable chemical structures and functionalities of nucleoside analogs are dictated by host-cell enzymes in the metabolic pathways. As such, modifying them to achieve faster IEDDA rates through HOMO-LUMO gap narrowing can be challenging because terminal alkenes, the least reactive dienophiles, were installed. Therefore, we reasoned that

modifying the structure of tetrazines with electron withdrawing groups would lower the LUMO and thereby narrow the HOMO-LUMO energy gap. After characterization of IEDDA kinetics, we can identify nucleoside-tetrazine pairs.

We worked toward the synthesis of six tetrazine analogs (**Figure 2-3A**), each of them having unique structures that could systematically lower the LUMO+1 orbital energy. **Tz-1**, **Tz-3**, **Tz-5**, and **DP-Tz** had been used previously in IEDDA reactions with dienophile-bearing amino acids in proteins.³³⁻³⁵ **Tz-2** and **Tz-4** were pursued due to the examination of the LUMO+1 orbital energies calculated with B3LYP, 6-31+G* (**Figure 2-S2**). From these calculations, **Tz-2** showed a similar but slightly lower LUMO+1 orbital energy than **Tz-1**. Structurally, **Tz-1** and **Tz-2** differ in placement of the nitrogen of the nicotinamide ring, which is *ortho*- or *meta*- to the tetrazine, respectively. Overall, we surmised this broad range of LUMO+1 orbital energies and structures would allow us to identify tetrazine-nucleoside pairs for IEDDA reactions.

Kinetic analysis was performed by measuring the change in absorbance of tetrazine over time. The reactions exhibited a color change of red-to-yellow, which was used to determine second-order rate constants through the initial rates method.³⁶ The cycloadduct and the oxidized tetrazine products were also observed by LC-MS (**Figure 2-S3**). As expected, addition of a polar solvent (water) resulted in faster reaction kinetics. Rates of these reactions were found to be between 10^{-4} – 10^{-2} M⁻¹s⁻¹. **Tz-1** and **7-dVA** showed the fastest rate with $1.67 \pm 0.68 \times 10^{-2}$ M⁻¹s⁻¹.

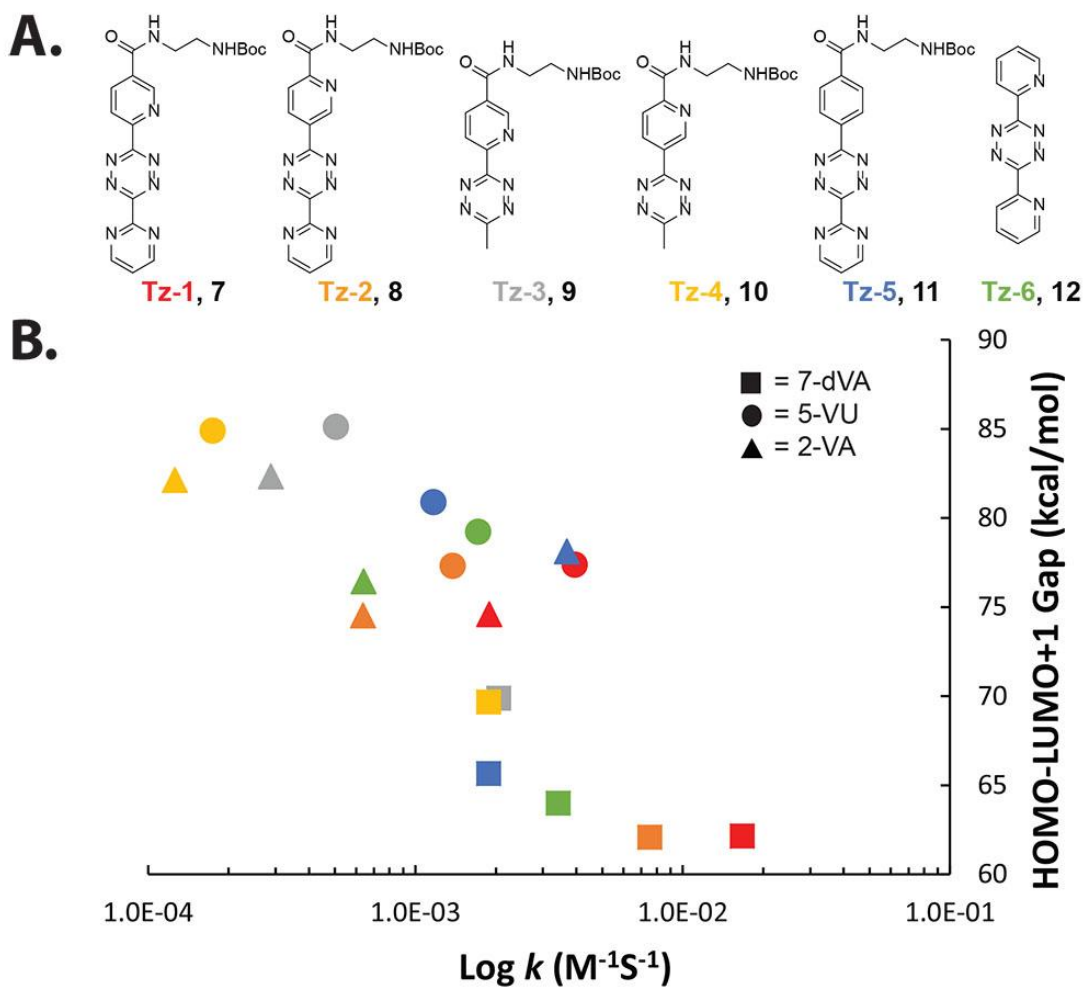


Figure 2-3. Screening tetrazines for IEDDA reactions with vinyl nucleosides A. Structures of tetrazines synthesized for this study. **B.** Comparison between HOMO-LUMO+1 energy gap and IEDDA rate constants. Second-order rate constants were determined from reactions containing 1 mM tetrazine and 10, 12.5, 15, 17.5 and 20 mM vinyl nucleoside or nucleobase.

We compared the HOMO-LUMO+1 gap and rate constants directly (**Figure 2-3B**). Overall, narrower HOMO-LUMO+1 gaps resulted in faster IEDDA reaction kinetics. Notable outliers were observed with **Tz-1** and **Tz-2** and their reaction kinetics. The rate of reactions

with each vinyl nucleoside showed that **Tz-1** were 2 to 10 factors faster than that of **Tz-2** despite having similar LUMO+1 energies. **Figure 2-S2**).

In an attempt to reconcile these differences, we modeled the transition states between **Tz-1** and **Tz-2** with **5-VUb** and **7-dVAb** (**Figure 2-S4**) using an exhaustive conformational search. The computed barrier heights closely agree with the observed trends in rate constants, predicting, for example, that for **5-VUb**, **Tz-1** is faster than **Tz-2** by a factor 10.1, compared to a measured factor of 10 (**Figure 2-S5**). The HOMO-LUMO+1 gap, on the other hand, predicts the reaction would be faster with **Tz-2**. The qualitative discrepancy between the HOMO-LUMO+1 gap results and the barrier height results indicates that the frontier orbital picture is incomplete, presumably because it ignores effects of long-range noncovalent interactions. Our calculations suggest that the tetrazine adopts a slightly bent boat conformation, which may be helping to assist in the formation of a transition state to encourage the cycloaddition reaction. Although we observed this structure with many of the tetrazines, we did not use this criterion to distinguish the differences in kinetics at this time. Future work on this topic in our lab will be more focused on distortion interaction models³⁷ and how they could explain key differences.

Overall, we have provided a comprehensive analysis of reaction rates between vinyl nucleosides and tetrazine pairs. The rates of reaction were measured to be comparable to SPAAC reactions ($\sim 10^{-2} \text{ M}^{-1}\text{s}^{-1}$). This result is especially exciting as it suggests that IEDDA reactions could be a sufficient replacement for CuAAC chemistry, and IEDDA could be orthogonal to other biorthogonal chemistry approaches for studying RNA.

Establishing reaction conditions to stabilize tetrazines during IEDDA with modified RNA.

Our kinetic analysis suggested that reactions between **Tz-1** and the vinyl-nucleosides would be the most efficient for IEDDA labeling of metabolic RNA. However, we questioned its stability in contexts where it would be used for cell imaging and RNA enrichment. A major challenge to utilizing more reactive tetrazines for IEDDA chemistry is their ability to be hydrolyzed, restricting their utility in biological applications.³⁸ We therefore tested whether each tetrazine would be amenable to conditions used for RNA labeling. Addition of water to the tetrazines resulted in a color shift of red-to-yellow, indicating disruption of the extended pi-conjugation. Hydrolysis of all tetrazines was monitored by LC-MS (**Figure 2-S3**). While there were changes noted for all tetrazines, we found that **Tz-1** was the most susceptible to hydrolysis. In light of this finding, we surmised it would not be amenable to RNA tagging reactions, despite its fast IEDDA kinetics. Further attempted syntheses of a biotinylated version failed under multiple conditions due to degradation by nucleophilic addition (data not shown).

We next sought to identify reaction conditions that could reduce hydrolysis of the tetrazines, and thus improve the efficiency. We hypothesized that the rate determining step of the hydrolysis pathway is expulsion of nitrogen after addition of water. With the addition of water being reversible, we assumed the equilibrium of the addition could be shifted through lowering the pH (**Figure 2-4A**). Hydrolysis was tested with 10% acetic acid added to reactions of **Tz-1** in a DMSO:H₂O (1:1) mixture (**Figure 2-4B**). A striking reduction of hydrolysis was observed in reactions with the addition of acetic acid (pH 5).

Kinetic analysis was then performed on reactions of **Tz-1** and vinyl-nucleosides and vinyl-nucleobases in the presence of 10% acetic acid (**Figure 2-4C and Figure 2-S2**). Interestingly, increased rates are observed in **5-VU** and **5-VC** under acidic conditions, which may be due to protonation of the nucleobase, thereby lowering the HOMO of the dienophile. These results suggest that lowered pH conditions could provide greater tetrazine stability and in turn, efficiency, while at the same time enabling robust reactivity for labeling.

We then compared RNA integrity and IEDDA biotinylation at pH 7.4 and 5.5. We observed that lowering the pH did not cause spurious RNA degradation, and may indeed be protective to RNA degradation through preventing cleavage of the phosphodiester bonds via the 2' hydroxyl (**Figure 2-4D**). We also note that at pH 5, the rate of depurination is $\sim 10^{-8} \text{ M}^{-1} \text{ s}^{-1}$,³⁹ which is far slower than the rate of IEDDA, making this a viable method for preserving RNA stability and conjugation.

After comparing reaction kinetics and tetrazine hydrolysis, we decided to pursue synthesis of **Tz-4 biotin (Supplementary Information)** due to its stability and ease of synthesis. Further, kinetic analyses in **Figure 2-3** demonstrated that this tetrazene exhibited reasonable rate constants with the all nucleosides. We then utilized our modified reaction conditions to perform dot-blot analysis of vinyl nucleoside incorporation (**Figure 2-4E**). Nucleosides were incubated in cells for 5 h, after which total RNA was extracted and reacted with **Tz-4 biotin** to enable detection of nascent transcripts through streptavidin-HRP. Notably, reactions with vinyl-modified RNA were completed in 2 h, in contrast to previous reports of IEDDA reactions taking >24 h for completion.²³⁻²⁴ Dot blot analysis confirmed that **7-dVA**, **2-VA**, and **5-VU** were robustly incorporated into nascent RNA.

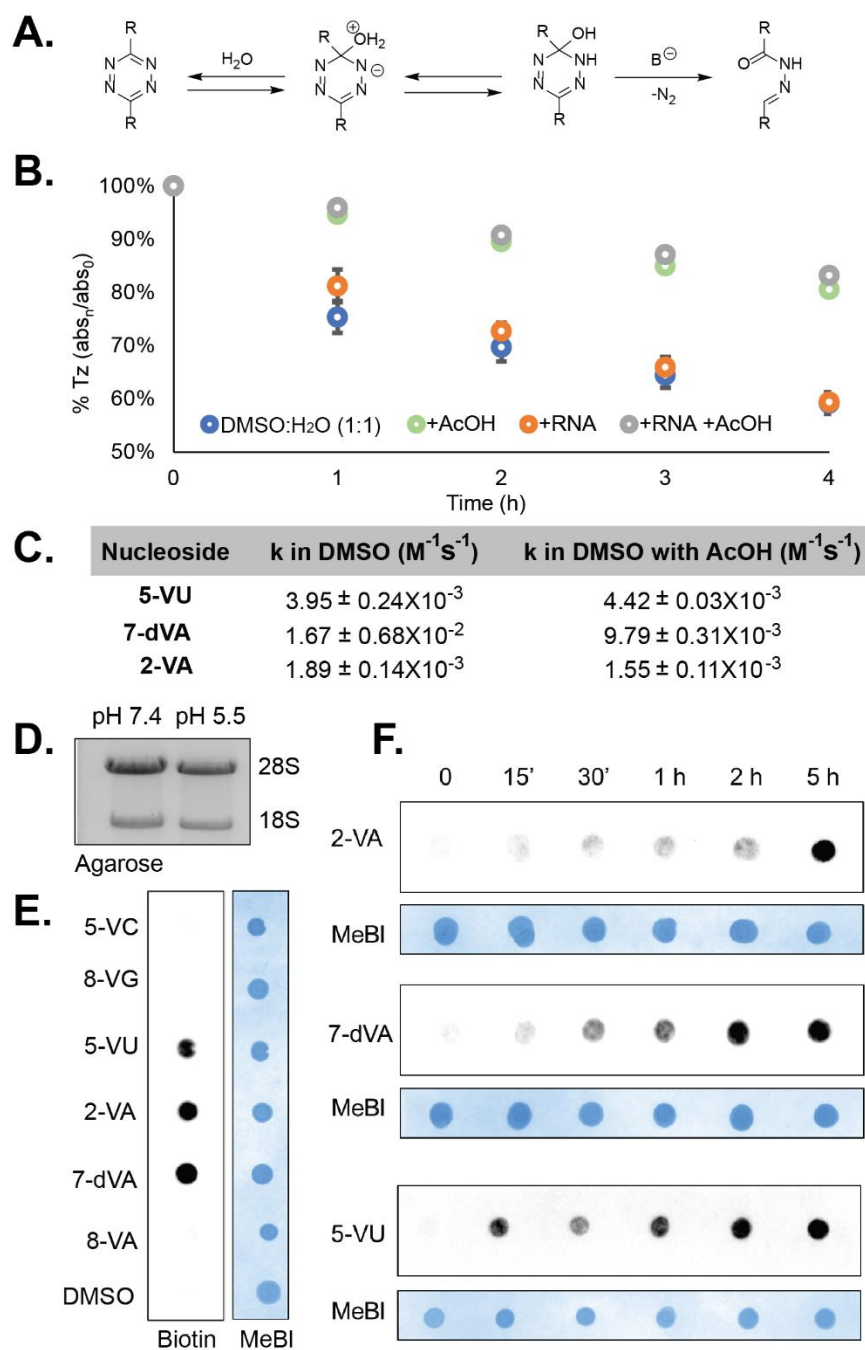


Figure 2-4. Establishing reaction conditions to stabilize tetrazines during IEDDA. A. Proposed hydrolysis reaction of tetrazines **B.** Analysis of tetrazine stability in different buffer conditions. **C.** Comparison of rate constants in DMSO and DMSO with acetic acid. **D.** Agarose gel demonstrating maintained RNA integrity post IEDDA labeling at lower pH. **E.** Streptavidin dot blot detection of analogs **2-VA**, **7-dVA** and **5-VU** demonstrates robust biotinylation

through IEDDA. HEK293T cells were treated with each analog for 5 h at 1 mM concentrations.

F. Time titration analysis of **2-VA**, **7-dVA** and **5-VU** incorporation at times 0 min, 15 min, 30 min, 1 h, 2 h and 5 h treated. At 1 mM concentrations. All IEDDA biotinylation reactions were performed with 50 μ M **Tz-4 biotin** incubated for 2 h at 37 °C.

We also analyzed the time-dependence of incorporation by dot blot analysis (**Figure 2-4F**). Notably, biotinylation signal was visible after only 15 min, and robust incorporation was noted at 5 h. While **2-VA** was the most highly incorporated according to the LC-MS/MS analysis, it is not the most reactive. We found that **5-VU**, which had second highest incorporation, also demonstrated efficient biotinylation and was more easily detected at lower time points.

The addition of acid to IEDDA markedly reduced hydrolysis of tetrazines. To the best of our knowledge, IEDDA reactions with tetrazines and olefins have typically been performed at neutral pH. As such, the possibility of augmenting IEDDA reactions through lowering the pH offers a unique improvement to contexts where the dienophile is a terminal alkene and the tetrazine is highly reactive. It is also exciting to note that reactions between modified RNA and tetrazines can be performed under conditions that preserve RNA integrity.

Utilizing vinyl nucleosides for in-cell analyses.

We have observed that many of our vinyl nucleosides can be incorporated into RNA. To further test their utility in tracking RNA synthesis, we aimed to establish: (1) vinyl analogs are non-toxic and compare them to other more widely-used analogs for RNA labeling, (2)

vinyl analogs can be imaged through IEDDA, and (3) that the IEDDA conditions developed herein are indeed orthogonal to other biorthogonal methods of labeling.

Metabolic labeling of RNA requires that the modified analogs be substrates for a wide variety of enzymes and pathways. As such, there is always the possibility that analogs could exert stress upon cells and cause cytotoxicity or inhibited growth. This is especially concerning when incubating analogs in cells for longer timescales. Furthermore, this limits their use in living animals where it can take several days for analogs to be incorporated at rates suitable for downstream analysis.

Other analogs such as 4-thiouridine⁴⁰ have been shown to induce significant amounts of toxicity in cells; however, analysis of other conventional analogs has not been extensively explored. MTT assays demonstrated that all incorporated vinyl analogs had no significant effect on cell proliferation after incubations as long as 12 h (**Figure 2-S6**). We compared this to 5-ethynyluridine (**5-EU**), a well-established, commercially available nucleoside used in metabolic labeling of RNA.⁶ Interestingly, we found that it had modest effects on cell proliferation at 12 h, but after 48 h, cell proliferation had decreased by nearly 50% (**Figure 2-5A**). Even more striking, a direct comparison with **5-VU** at these same conditions showed no significant changes in cell proliferation. Cell death assays indicated that growth inhibition, and not direct cytotoxicity was the primary effect of extended **5-EU** incubations (**Figure 2-S7**). This striking difference has also been observed with some alkynyl analogs of DNA.⁴¹ We also observed changes to cell morphology, including cell detachment and aggregation (**Figure 2-5B**), which is consistent with problems in cellular respiration and toxicity. These results demonstrate that vinyl analogs are a safer option for applications *in vivo*, which

require longer incubation times. This is an incredibly important result for researchers focused on performing RNA labeling experiments in animals.

We next investigated using vinyl-analogs for imaging of nascent transcription. We synthesized a fluorophore-conjugated tetrazine (**Tz-3 TAMRA; Supplementary Information**). As shown in **Figure 2-5C**, robust RNA labeling is observed in the nucleolus for **5-VU**, which is the location of rRNA biosynthesis. This pattern has been observed with other analogs that can be used for RNA imaging. We saw similar imaging results for **2-VA** and **7-dVA**, and treatment with actinomycin D, an RNA polymerase I/II inhibitor, significantly diminished nucleolar staining for all three analogs (**Figure 2-S8**).

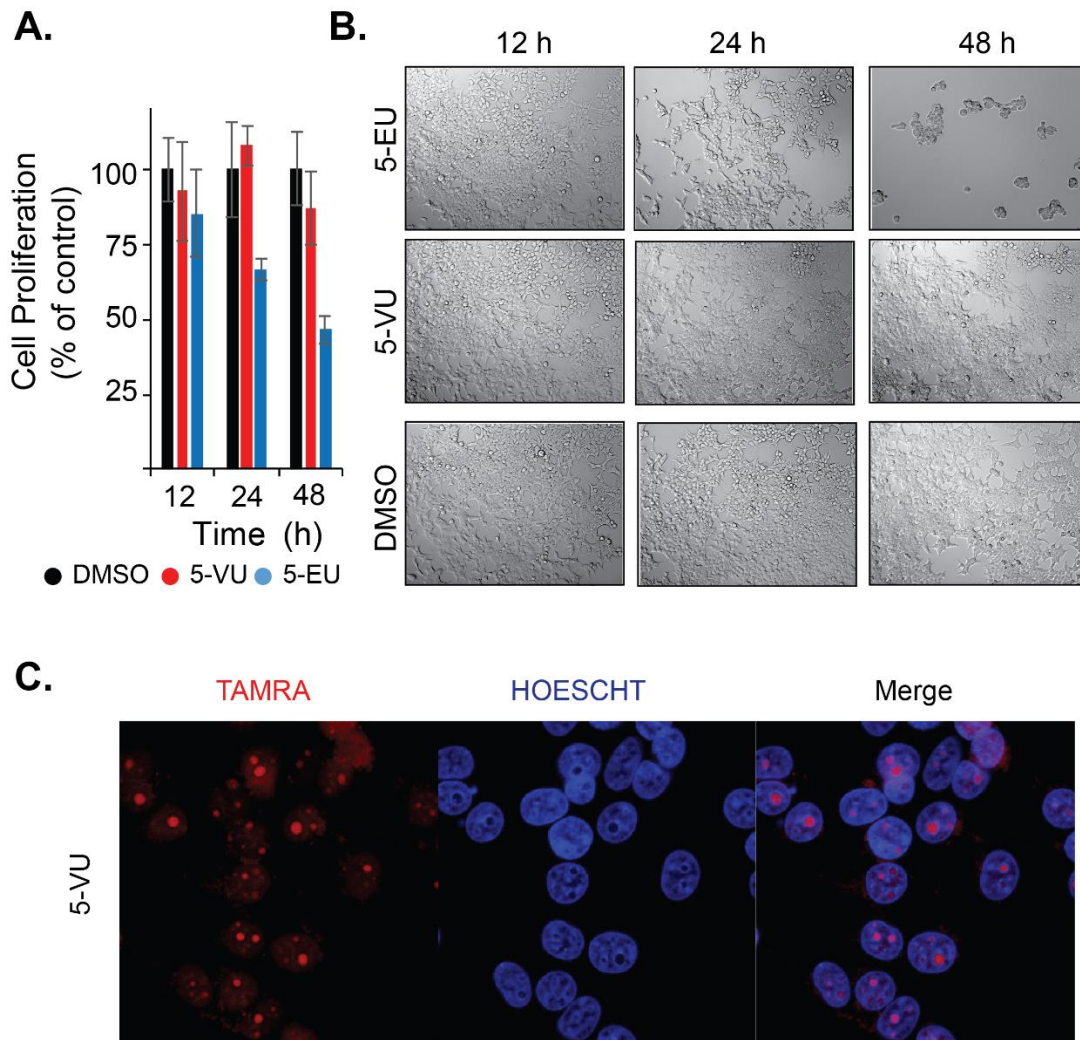


Figure 2-5. Effects of vinyl-nucleosides on cell viability and use for RNA imaging. A. MTT assays demonstrate that 5-VU does not have an effect on cell growth, whereas 5-EU produces significant growth inhibition relative to the DMSO-treated control at 1 mM for 12, 24 and 48 h. **B.** DIC imaging of cells after various incubation lengths confirms the effects on cell growth. **C.** IEDDA-based imaging demonstrates that 5-VU can be used for visualizing nascent transcription. HEK293T cells were treated with 1 mM 5-VU for 5 h, following by fixation, permeabilization and incubation with **Tz-3 TAMRA**.

Finally, we wanted to test if our IEDDA reactions would be mutually orthogonal to a CuAAC reaction with alkyne-modified RNA. That is, we wished to ascertain that the tetrazine was selective only for the alkene and the azide only for the alkyne. After incubation of **5-VU** or **5-EU** in cells and isolation of the vinyl- or alkynyl-RNA, reactions with biotin-N₃ and **Tz-4 biotin** were carried out. Dot blot analysis showed no cross talk between functional groups (**Figure 2-S9**). To our knowledge, this is the first example of mutually orthogonal reactions performed on RNA transcripts, offering the ability to perform multiple bioorthogonal reactions in the same experiment for the study of RNA. This approach may be useful on shorter time scale experiments performed *in vitro*.

2.4 Conclusion

Elucidating the utility and limitations of bioorthogonal reactions is critical to expanding their use for studying all classes of biomolecules. We have established that vinyl nucleosides can be utilized to metabolically label nascent cellular RNA. Our data indicates the successful metabolic incorporation of **2-VA**, **7-dVA**, and **5-VU**. We have also performed an exhaustive evaluation of IEDDA kinetics between all of our synthesized analogs and accompanying tetrazines. Using these comparisons, we have identified fast-acting tetrazines that could provide great utility for IEDDA reactions with vinyl analogs of any biomolecule.

Through our studies, we have also evaluated the use of acidic reaction conditions to supplant tetrazine hydrolysis, without severely compromising reaction kinetics or altering RNA integrity. Using our modified protocols, we have demonstrated that vinyl-nucleosides and tetrazines can be used to detect and image nascent transcripts. Vinyl nucleosides do not inhibit cellular proliferation like the most common nucleosides used for *in vivo* work, such

as 4-thiouridine and 5-EU. In addition, vinyl-nucleosides can be used in tandem with alkyne functionalized nucleosides and offer a multicomponent experiment for studying RNA.

We envision these vinyl nucleosides will be used extensively both *in vitro* and *in vivo*, as they are easily handled, non-toxic, are able to be functionalized through selective chemistry, and can preserve RNA integrity. Future work in our lab will be to use these exciting new tools to evaluate differences in RNA expression and biology within living systems, such as whole animals.

2.5 Experimental Details

General Procedures

Vinyl-nucleoside TRizol Reaction Analysis by LC-MS

To analyze the stability of vinyl-nucleosides in Trizol, **5-VU**, **5-VC**, **7-dVA**, and **2-VA** were placed in TRizol and analyzed by LC-MS. 20 μ L of 2 mM stock solution of Vinyl-nucleosides in DMSO were added to 80 μ L of Trizol (Life Technologies) in a HPLC vials. The mixtures were placed on a shaker at r.t. for 5 h and then analyzed by LC-MS using a C18 column and eluted with a gradient of H₂O/MeCN 5-95% with 0.1% formic acid. The mass spectrums were searched for the exact mass of each vinyl-nucleoside and the subsequent thiocyanate addition product.

HOMO-LUMO Energy Calculation

Vinyl-nucleoside HOMO energy and tetrazine LUMO+1 energies were calculated using density functional theory (DFT). Calculations were performed with Spartan 14, using the B3LYP level of theory and the basis set 6-31+G*.

Rate Studies

The reactions between vinyl-nucleosides and tetrazines were monitored by the change in the tetrazine absorbance at 530 nm. Reactions were initiated in a 96-well plate by mixing 100 μ L of 2 mM tetrazine solution in DMSO with 100 μ L of vinyl-nucleoside in the proposed solvent (DMSO, 1:1 H₂O:DMSO, and 1:5 AcOH:DMSO). The concentration of vinyl-nucleoside ranged from 10-20 mM, while tetrazine concentrations were held at 1 mM. All rate studies were performed in triplicate under pseudo-first order conditions. Absorbance measurements were recorded every min over a time period of 3 h time interval using a BioTek Epoch plate reader equipped with Gen5 software. Pseudo-first order rate constants (k_{oba}) were calculated by plotting natural log of [tetrazine] versus time (in s). Second-order rate constants were determined by plotting k_{obs} vs nucleoside concentration.

Reaction Analysis by LC-MS

To analyze the product formation from the tetrazine-nucleoside reactions were monitored by LC-MS. 50 μ L of tetrazine (1 mM) in DMSO was added to a 96 well plate. 50 μ L of nucleoside/nucleobase (1 mM) in DMSO were added to the subsequent well and reacted at r.t. for 72 h. 10 μ L of each reaction was diluted with 90 μ L and stored in a 0 $^{\circ}$ C freezer. The reactions were then analyzed by LC-MS using a cyano-column and eluted with a gradient of H₂O/MeOH 5-95%.

Structure Generation Relaxed structures for all vinylnucleotides and tetrazines were obtained through a combination of conformational search and density functional theory

(DFT) optimization. First, conformers were generated using the confab¹ tool in OpenBabel². To avoid the incorrect planarization of the tetrazine core produced by all force fields available in OpenBabel (including, for example, MMFF94³ and MMFF94s⁴), we then performed the subsequent optimization with DFT, using the TPSS⁵ density functional including D3 dispersion corrections⁶ and the def2-SVP basis set.⁷ All DFT calculations were performed using Turbomole⁸. The resolution of the identity⁹ (RI) approximation was used for the Coulomb integrals with a tight integration grid (m5) and convergence criteria (keywords scfconv = 8, denconv = 10⁻⁸). Finally, the lowest energy structure obtained from the previous step was further optimized including COSMO¹⁰ ($\epsilon = 80.1$) for solvation. Final structures for all stationary points along the reaction path were computed with identical parameters. Vibrational frequencies were computed to confirm that all structures correspond to local minima.

All stationary points (initial complexes and transition states) exhibit many low-frequency large-amplitude vibrational modes. For example, across all initial complexes computed here, the lowest frequency vibrational mode for each initial complex ranged from 6-25 cm⁻¹ and 12-15 vibrational modes had frequencies below 100 cm⁻¹. We follow the approach of Liu et al¹¹ and tame the low-frequency modes by treating all modes below 100 cm⁻¹ as 100 cm⁻¹. Relative rates were estimated using the Arrhenius equation assuming a constant prefactor such that $\frac{k_1}{k_2} = \exp\left(-\frac{\Delta G_1 - \Delta G_2}{RT}\right)$ where R is the ideal gas constant and $T = 298\text{K}$.

Reaction Generation

The reaction profiles were determined for the six cycloaddition reactions involving tetrazines **Tz-1** or **Tz-2** and nucleotides **5-VUb**, **7-dVAb**, and **2-VAb**. For each tetrazine-vinylnucleotide pair, 8-16 distinct initial complexes can be formed depending on the relative orientation of each molecule. Transition states (TSS) were computed for each such relative orientation. In total, more than 60 TSS were determined (6 reactions \times 8-16 TSS per reaction). In all cases, an asymmetric transition state was found in which the bond involving the primary vinyl carbon forms first, as seen in **Figure S5M-R**. Initial guesses for TSS were found by first optimizing the geometry while constraining the distance between the primary vinyl carbon and the tetrazine carbon (d_1 in **Figure S5S**) to be 196 pm. All structures were confirmed to be proper TSS by computation of vibrational frequencies.

Tetrazine Hydrolysis Analysis

Analysis of tetrazine hydrolysis was performed by NMR. 10 mg of Tz-1 was added to an NMR tube and dissolved in DMSO- D_6 (0.5 mL). An initial 1H NMR was performed to establish a baseline. H_2O (0.5 mL) was then added to the NMR tube and vortexed. The NMR tube was then heated to 37 °C for 24 h. 1H NMR was then performed on the sample and hydrolysis products were determined.

Tetrazine Stability with AcOH

Evaluation of the stability of Tetrazine and RNA was performed by monitoring the change of the tetrazine absorbance at 530 nm. Reactions were performed within in a 96-well plate by mixing 300 μ L of 2 mM tetrazine solution in DMSO with 300 μ L of the proposed solvent (H_2O ,

20 µg of RNA in H₂O, 20 µg of RNA in 20% AcOH in H₂O, and in 20% AcOH in H₂O). The concentration of tetrazines were held at 1 mM, AcOH concentrations were held at 10%, and RNA were held at 10 µg. All stability studies were performed in triplicate at 23 °C and absorbance measurements were recorded every hour over a time period of 4 h time interval using a BioTek Epoch plate reader equipped with Gen5 software.

Vinyl-nucleoside labeling of cellular RNA

HEK293T cells (ATCC) were cultured in DMEM (Corning) supplemented with 10% FBS, 1% penicillin and streptomycin and grown at 37 °C, 5% CO₂. Analogs were added to complete culture medium from 200 mM stocks with a final concentration of <1% DMSO.

RNA isolation and biotinylation via IEDDA

After labeling, total cellular RNA was harvested using Trizol Reagent (Invitrogen) following the manufacturer's instructions or RIPA lysis buffer (150 mM NaCl, 5 mM EDTA pH 8.0, 50 mM Tris, pH 8.0, 1.0 % NP-40, 0.5 % sodium deoxycholate, 0.1% SDS) spiked with DNase Turbo and RNaseOut (Thermo Fisher). Briefly, ~20 millions cells were scraped and suspended in 2 mL of lysis buffer, and incubated on ice for 15 min. Lysates were mixed 1:1 with phenol/chloroform pH 5.2 (Fisher) vortexed briefly and spun down at 4 °C to separate the layers. The aqueous layer was then applied to a Zymo RNA clean and concentrator IIC column (Zymo) and total RNA was isolated according to the manufacturer's instructions, with RNA eluted in 50 µL of nuclease free water. IEDDA reactions were prepared using 10 µg of total RNA in solutions of 6% DMSO water, and 1 mM Tz-4 biotin to a final volume of 50 µL. Reactions were incubated with at 37 °C for 2 h at 400 RPM. Biotinylation reactions were

purified using Zymo RNA clean and concentrator-5 spin column according to the manufacturer instructions, with RNA eluted in 10 μ L of nuclease free water.

HRP-streptavidin Dot blotting

Equal amounts of column-purified RNA were spotted onto 2x SSC equilibrated Hybond-N+ membrane (GE Healthcare), allowing spots to dry in between. The membrane was crosslinked using the auto crosslink function at 254 nm on a UV Stratalinker (Stratagene). The membrane was then blocked in a 10% SDS blocking solution followed by incubation with 1:10,000 dilution of high sensitivity streptavidin-HRP (ThermoFisher Scientific) in blocking solution. The membrane was washed x2 in a 1:10 solution of blocking solution and x2 in Tris-saline buffer. It was then incubated in SuperSignal West Pico Chemiluminescent Substrate (ThermoFisher Scientific) according to manufacturer's instructions and imaged on a ChemiDoc MP imaging system (Bio-Rad) under the chemiluminescence channel. Following imaging, the blot was stained in a 0.04% methylene blue, 0.3 M sodium acetate solution to visualize all RNA as a loading control. The blot was imaged again using the colorimetric channel.

RNA fluorescence imaging via IEDDA

Coverslips in 6-well tissue culture plates were treated with 1x poly-D lysine solution for 3 h at 37 °C. HEK293T cells were seeded at densities of 2.5×10^5 and grown to ~50% confluency on glass cover slips. Cells were treated with vinyl nucleosides to final concentrations of 1 mM and incubated for 5 h. After labeling, cells were washed twice with DPBS and fixed for 10 min at room temperature with 3.7% paraformaldehyde. Cells were quenched with 50 mM

glycine, DPBS for 5 min, and then washed twice more. Cells were permeabilized in 0.5% Triton-X DPBS for 15 min, and then washed x2 with DPBS. Cells were then treated with solutions of 5 μ M Tz-3 TAMRA in DPBS, and incubated for 3 h at 37 °C in the dark. Cells were washed x2 with 0.25% Triton-X DPSB for 5 min, and then x5 with DPBS for 5 min each on an orbital shaker. Cells were stained with a solution of 1:3000 Hoechst 333242 for 10 min (Thermo Fisher). Coverslips were briefly washed and then mounted using VectaShield mounting medium (Vector Labs). Slides were imaged via fluorescence confocal microscopy using a 63x oil immersion objective on a Leica 700 Carl Zeiss microscope.

RNA fluorescence imaging with Actinomycin D

Cells were grown and treated with analog as previously described, with transcriptional inhibitor actinomycin D (Sigma) being co-administered to a final concentration of 20 μ M. Following incubation, cells were washed x3 with DPBS and lightly fixed with 0.5% paraformaldehyde in 0.5% Triton-X DPBS. Cells were then fixed, stained, mounted and imaged as previously described.

MTT Assay

HEK293T cells were seeded at densities of 10,000 cells into a 96-well plate and grown for 1 day. Cells were then incubated for various lengths of time with compounds **2-VA**, **7-dVA**, **5-VU**, and **5-VC** at 1 mM final concentration, 0.5% DMSO or 0.5% DMSO only. Following incubation, cell viability was assessed via the cells' ability to reduce MTT (Life Technologies) to the insoluble formazan salt. Cell media was replaced with unsupplemented RPMI minus

phenol red, and cells were incubated for 3 h at 37 °C with 1 mM MTT. Formazan solid was solubilized in DMSO for 30 min at 37 °C and absorbance readings were taken at 540 nm.

Trypan Blue Assay

HEK293T cells were seeded at densities of $1.5 - 2.5 \times 10^5$ into 6 well plates and grown for 18 - 24 h. Cells were then incubated for 12, 24 and 48 h with compounds **5-VU** and **5-EU** at 1 mM final concentration. Following incubation, cells were trypsinized, removed from the plate and spun down. The supernatant was aspirated and the cells were resuspended in 1 mL of culture medium, after which 10 μ L was aliquoted for Trypan staining. To each aliquot, 10 μ L of 0.4% Trypan Blue solution (Gibco) was added and 10 μ L of this solution was applied to a hemocytometer for assessment of cell viability. Total and dead cell counts was recorded for each of the four corners of the grid, and repeated for biological duplicates of two.

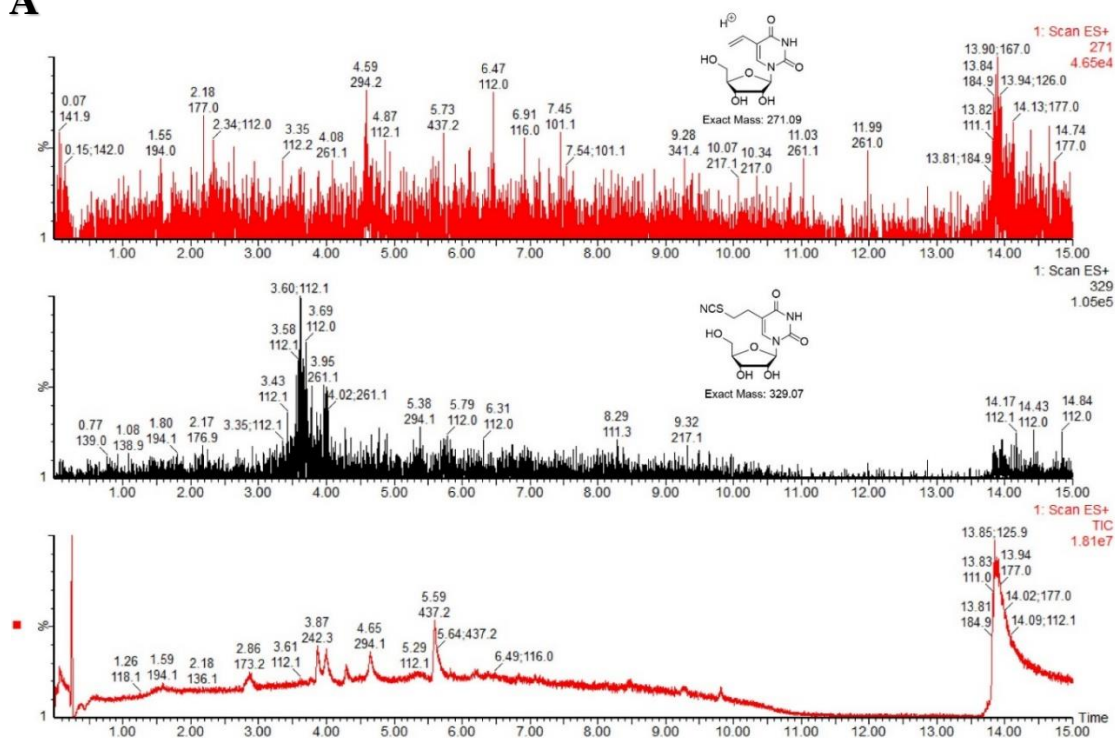
Mass spec analysis of total RNA

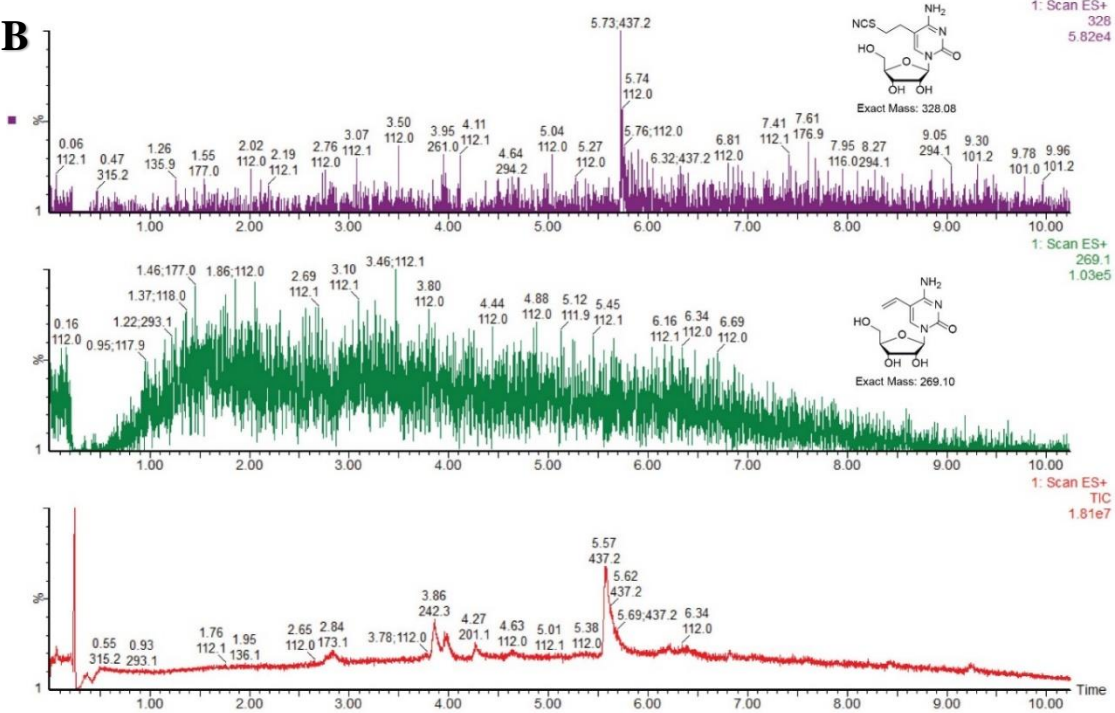
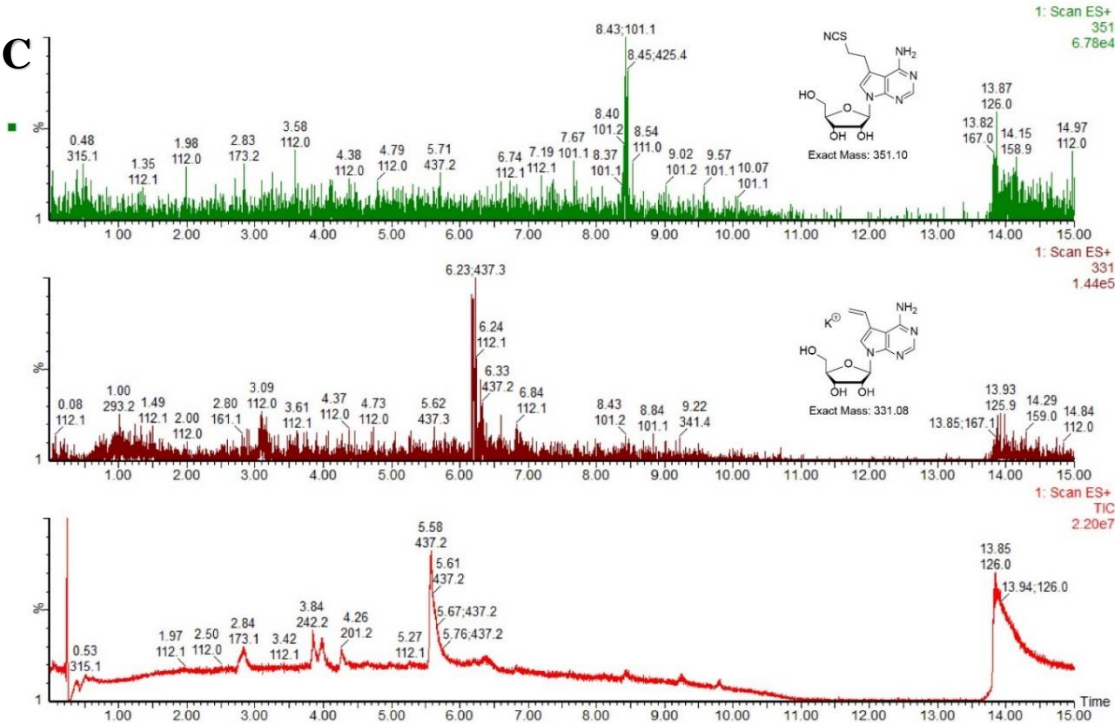
Cells were treated with 1 mM analog for 12 h as previously described. After RNA extraction with TRIzol (Thermo Fischer Scientific) and purification with RNA clean & concentrator-5 columns (Zymo), 1 μ g total RNA samples containing each analog were digested to nucleosides using a nucleoside digestion mix (New England Biolabs). A calibration curve of standard solutions containing Adenosine, Uridine, Guanosine, Uridine, vinyl-modified nucleoside analogues 5-VU, 5-VC, 7-dVA, 2-VA and 5-iodocytidine as an internal standard were injected on a Waters Micromass Quattro Premier XE LC-MS system equipped with a triple quadrupole (QQQ) mass detector operating in multiple reaction monitoring (MRM) and positive (+ESI) electrospray ionization modes. Liquid chromatography was carried out

on a Waters Acuity UPLC equipped with a C18 column (4.6 × 150 mm, 5 μm) with a gradient mobile phase consisting of water (+0.2% acetic acid) : acetonitrile. Digested RNA sample reactions were diluted 1:10 and 10 uL was directly injected. Mass spectrometry data acquisition was recorded in MRM mode and analyzed on Waters MassLynx 4.1 software. Each nucleoside was identified according to the precursor and product ions found through QuanOpt parameters. The percent substitution of each modified nucleoside was determined by dividing the spectral counts of each analog by the total spectral counts for the canonical and modified analog.

Vinyl-nucleoside TRizol Reaction Analysis by LC-MS

A



B**C**

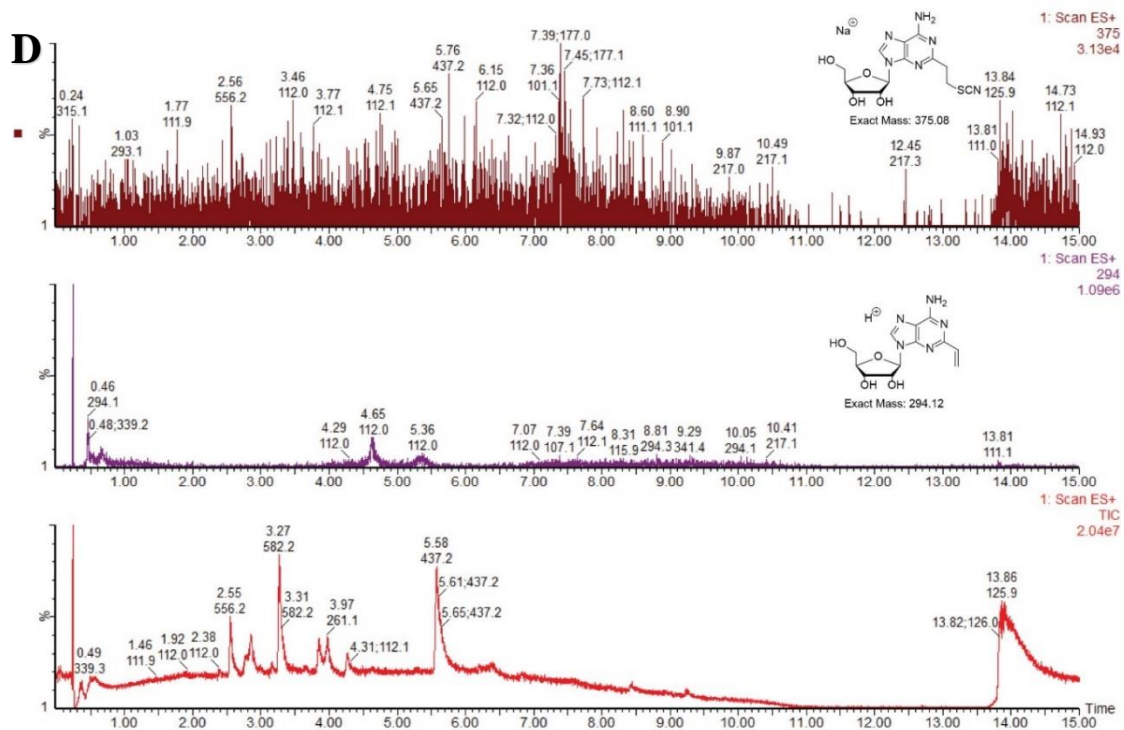


Figure 2-S1. LC-MS analysis of nucleosides in TRIzol. A) **5-VU**. B) **5-VC**. C) **7-dVA**. D) **2-VA**.

Top two panels display peaks correlated to the labeled mass. Bottom panel displays the chromatogram. **5-VC** showing little-to-no detection after TRIzol incubation and thiocyanate adduct found. **5-VC** is most susceptible to Michael addition.

HOMO-LUMO Energy Calculation and Reaction Kinetics

HOMO-LUMO Gap (kcal/mol)
 HOMO & LUMO+1 values calculated by TPSS, D3, def2-SVP (kcal/mol)
 k in 10% AcOH in DMSO ($M^{-1}s^{-1}$)
 k in DMSO ($M^{-1}s^{-1}$)
 k in 1:3 H₂O:DMSO ($M^{-1}s^{-1}$)
 * Tz-1, Tz-2 undergo hydrolysis

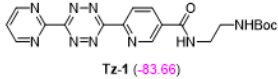
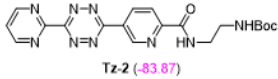
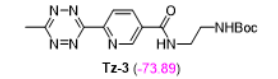
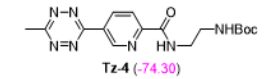
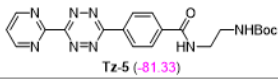
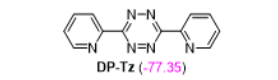
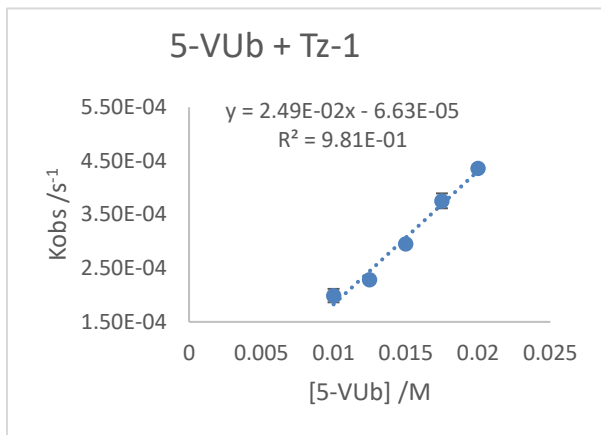
	5-VUib (-124.41)	5-VU (-124.48)	5-VC (-121.99)	7-dVA (-114.43)	7-dVAb (-111.87)	2-VA (-124.53)
 Tz-1 (-83.66)	40.75 2.49 ± 0.19X10 ⁻² 1.49 ± 0.12X10 ⁻²	40.82 3.95 ± 0.24X10 ⁻³ 4.42 ± 0.03X10 ⁻³	38.33 5.72 ± 0.44X10 ⁻³ 7.03 ± 0.25X10 ⁻³	30.76 1.67 ± 0.68X10 ⁻² 9.79 ± 0.31X10 ⁻³	28.20 5.35 ± 0.54X10 ⁻² 4.33 ± 0.08X10 ⁻³	40.87 1.89 ± 0.14X10 ⁻³ 1.55 ± 0.11X10 ⁻³
 Tz-2 (-83.87)	40.54 2.44 ± 0.20X10 ⁻³	40.61 1.38 ± 0.08X10 ⁻³	38.12 2.05 ± 0.19X10 ⁻³	30.56 7.54 ± 0.59X10 ⁻³	27.99 1.59 ± 0.15X10 ⁻²	40.66 6.37 ± 0.29X10 ⁻⁴
 Tz-3 (-73.89)	50.53 1.46 ± 0.13X10 ⁻³ 3.80 ± 0.33X10 ⁻³	50.59 5.06 ± 0.44X10 ⁻⁴ 1.08 ± 0.07X10 ⁻³	48.10 6.13 ± 0.43X10 ⁻⁴ 1.37 ± 0.03X10 ⁻³	40.54 2.05 ± 0.04X10 ⁻³ 1.48 ± 0.14X10 ⁻³	37.98 6.66 ± 0.66X10 ⁻³ 2.17 ± 0.15X10 ⁻²	50.64 2.88 ± 0.28X10 ⁻⁴ 7.44 ± 0.13X10 ⁻⁴
 Tz-4 (-74.30)	50.11 8.64 ± 0.73X10 ⁻⁴ 2.70 ± 0.15X10 ⁻³	50.18 1.75 ± 0.12X10 ⁻⁴ 6.77 ± 0.35X10 ⁻⁴	47.69 5.53 ± 0.45X10 ⁻⁴ 7.23 ± 0.36X10 ⁻⁴	40.13 1.88 ± 0.09X10 ⁻³ 7.47 ± 0.69X10 ⁻³	37.57 6.50 ± 0.22X10 ⁻³ 1.92 ± 0.08X10 ⁻²	50.23 1.26 ± 0.11X10 ⁻⁴ 4.28 ± 0.26X10 ⁻⁴
 Tz-5 (-81.33)	43.08 6.15 ± 0.62X10 ⁻³	43.15 1.17 ± 0.10X10 ⁻³	40.66 2.70 ± 0.27X10 ⁻³	33.09 1.88 ± 0.18X10 ⁻³	30.53 6.73 ± 0.54X10 ⁻³	43.19 3.69 ± 0.33X10 ⁻³
 DP-Tz (-77.35)	47.07 8.19 ± 0.24X10 ⁻³	47.14 1.72 ± 0.09X10 ⁻³	44.64 4.55 ± 0.23X10 ⁻³	37.08 3.43 ± 0.17X10 ⁻³	34.52 1.13 ± 0.08X10 ⁻²	47.18 6.41 ± 0.12X10 ⁻⁴

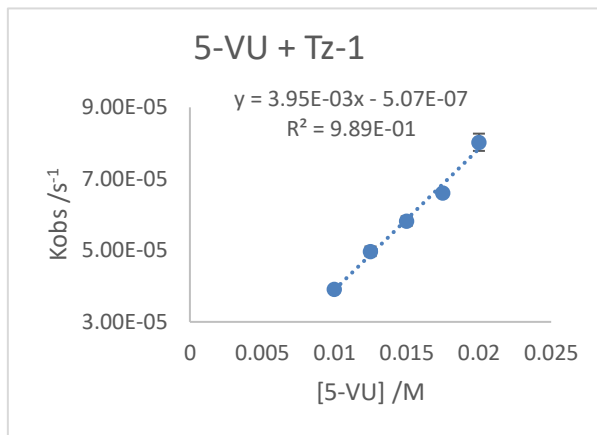
Figure 2-S2. Calculated HOMO and LUMO+1 orbital energy in kcal/mol displayed next to compounds. HOMO-LUMO+1 energy in kcal/mol displayed in green. k ($M^{-1}s^{-1}$) in DMSO displayed in black. k ($M^{-1}s^{-1}$) in 1:3 H₂O:DMSO displayed in red. k ($M^{-1}s^{-1}$) in DMSO with 10% AcOH displayed in orange.

Below are rate plots for Figure S3 Tz + Nucleoside/Nucleobase in DMSO

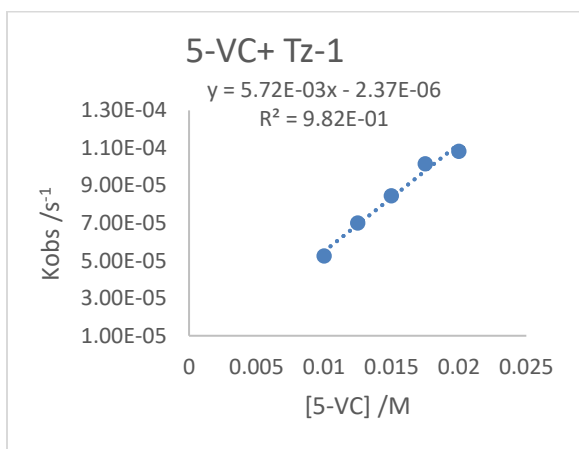
A



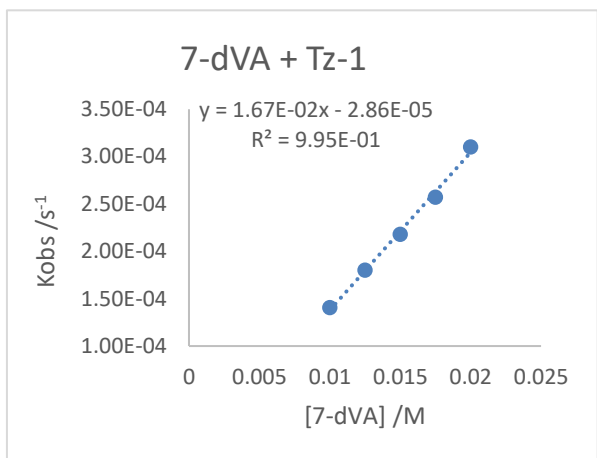
B



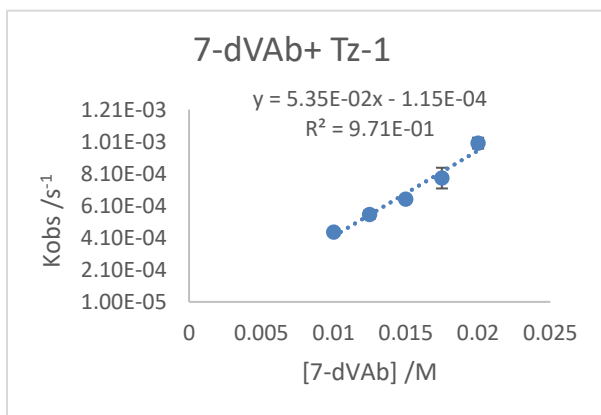
C



D



E



F

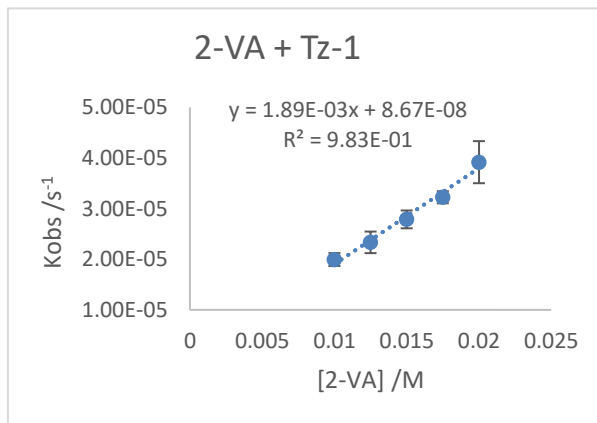
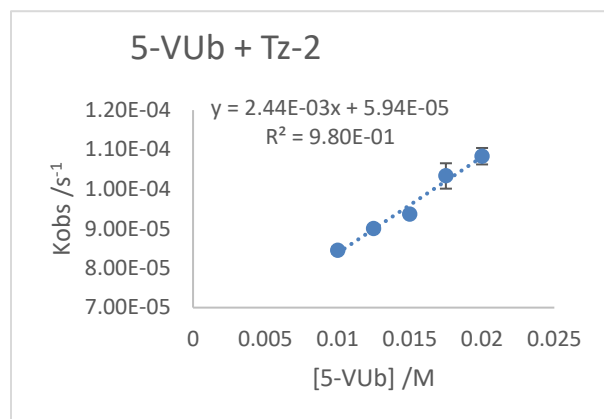
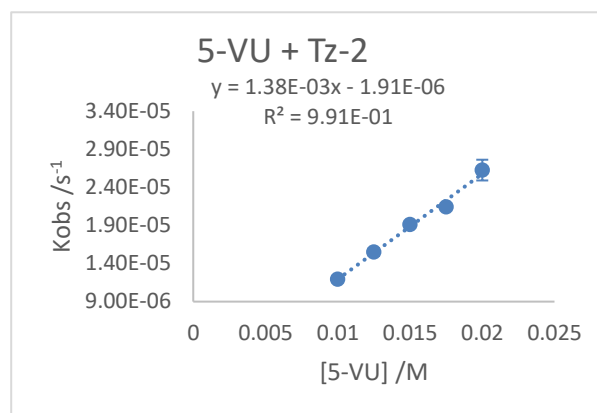


Figure 2-S3i. Rate plots used to calculate second-order rate constants of **Tz-1** with nucleosides and nucleobases: A) **5-VU_b**, B) **5-VU**, C) **5-VC**, D) **7-dVA**, E) **7-dVAb**, and F) **2-VA** in DMSO.

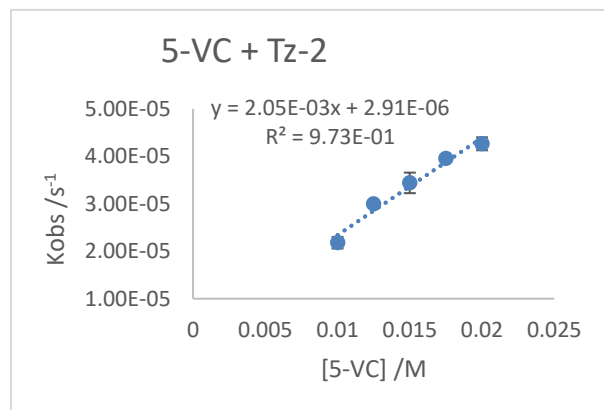
A



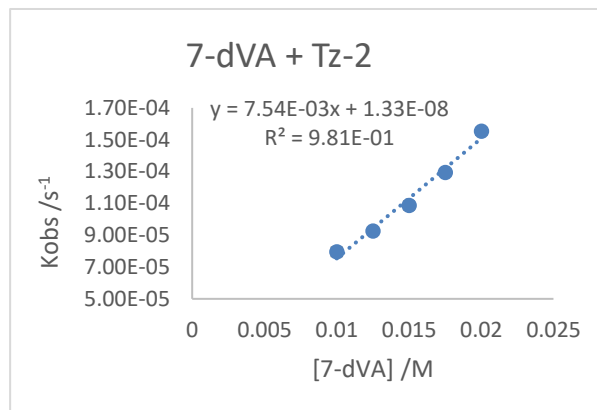
B



C



D



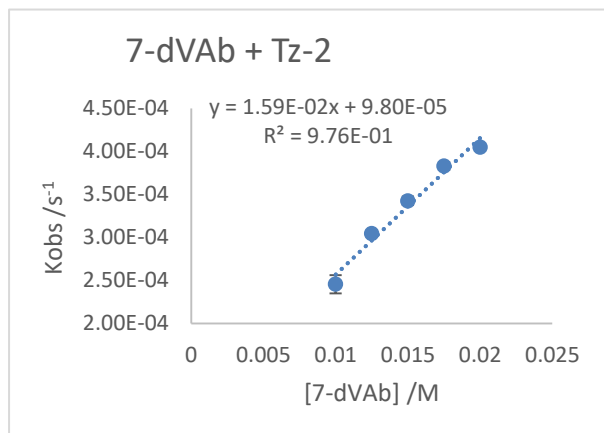
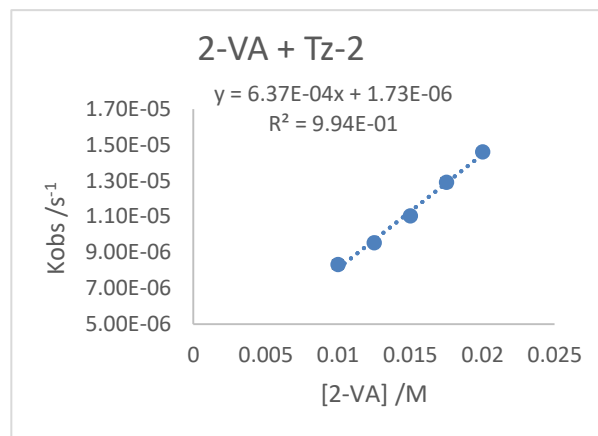
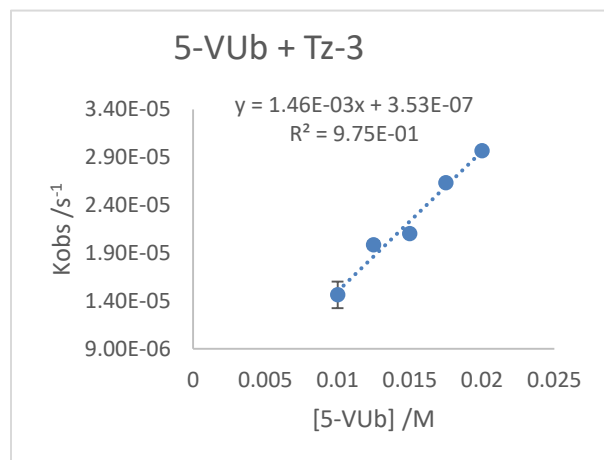
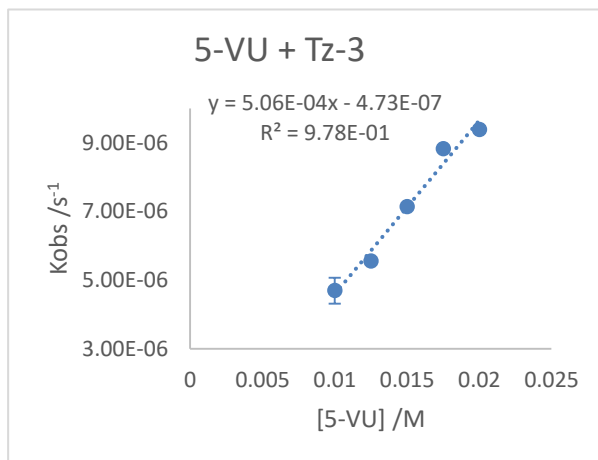
E**F**

Figure 2-S3ii. Rate plots used to calculate second-order rate constants of **Tz-2** with nucleosides and nucleobases: A) **5-VUb**, B) **5-VU**, C) **5-VC**, D) **7-dVA**, E) **7-dVAb**, and F) **2-VA** in DMSO.

A**B**

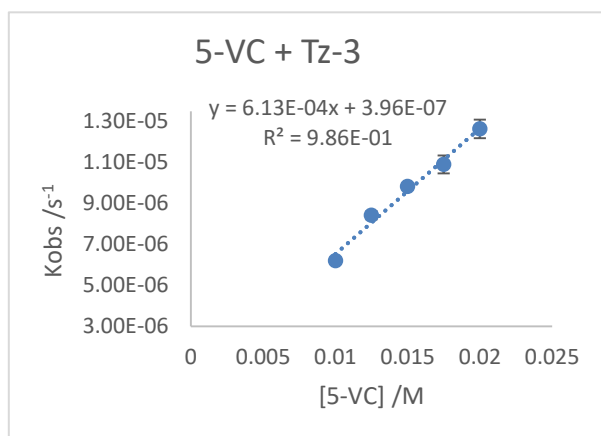
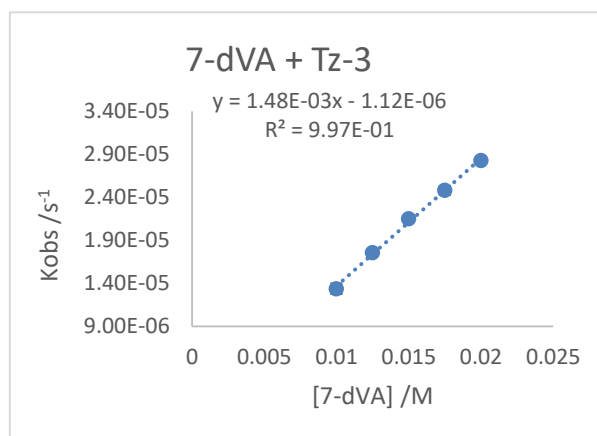
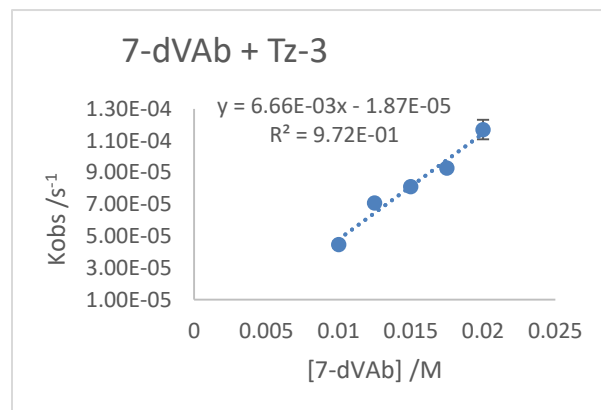
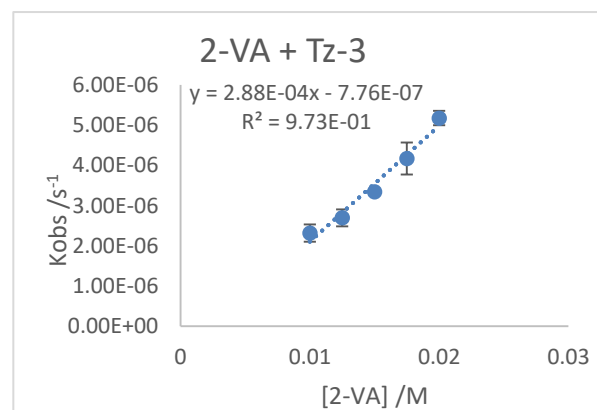
C**D****E****F**

Figure 2-S3iii. Rate plots used to calculate second-order rate constants of **Tz-3** with nucleosides and nucleobases: A) **5-VUb**, B) **5-VU**, C) **5-VC**, D) **7-dVA**, E) **7-dVAb**, and F) **2-VA** in DMSO.

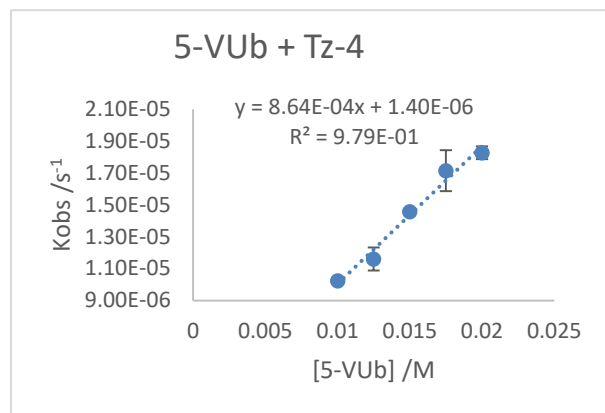
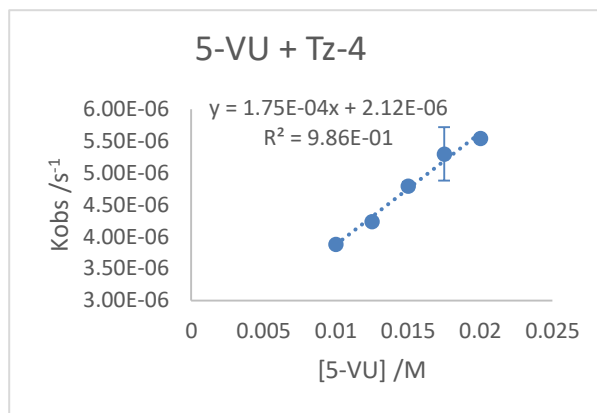
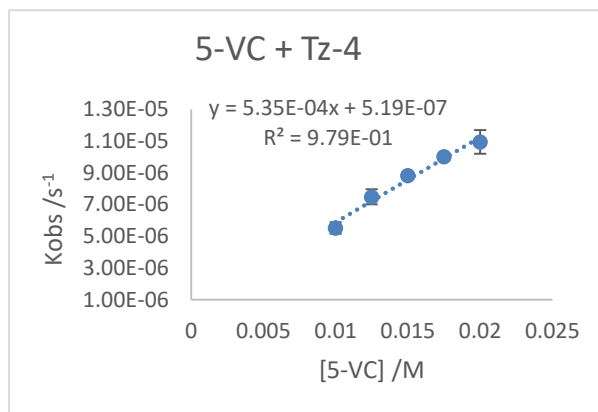
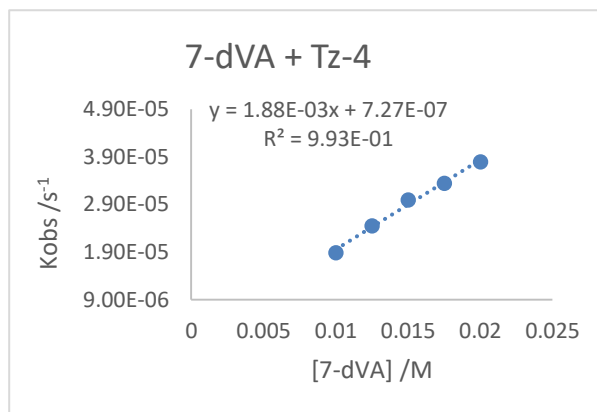
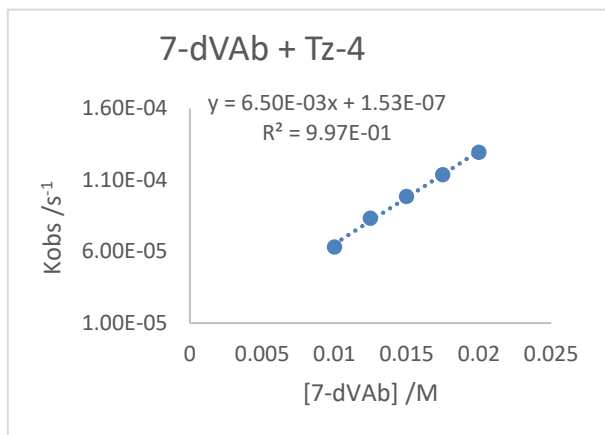
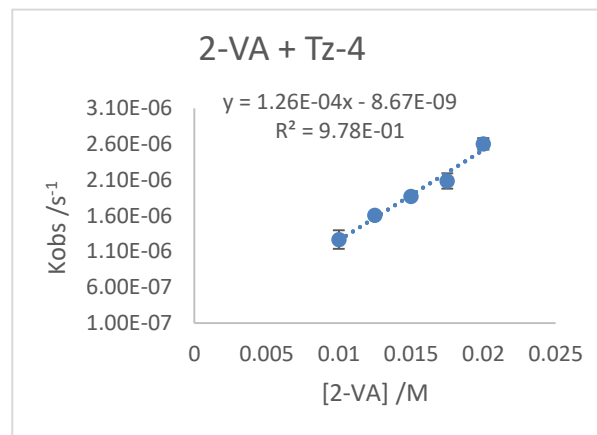
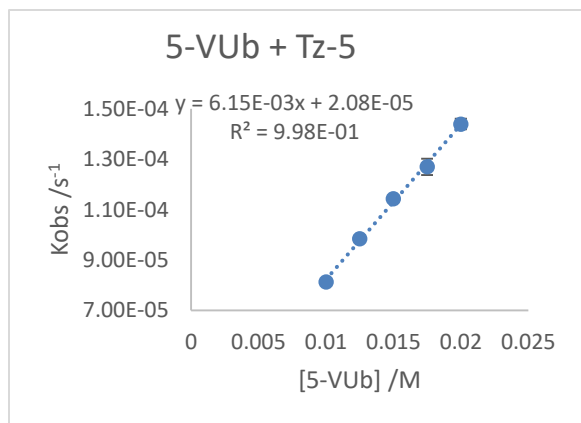
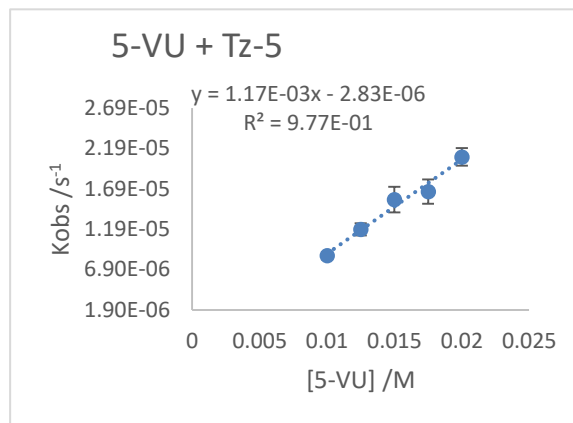
A**B****C****D****E****F**

Figure 2-S2iv. Rate plots used to calculate second-order rate constants of **Tz-4** with nucleosides and nucleobases: A) **5-VU_b**, B) **5-VU**, C) **5-VC**, D) **7-dVA**, E) **7-dVAb**, and F) **2-VA** in DMSO.

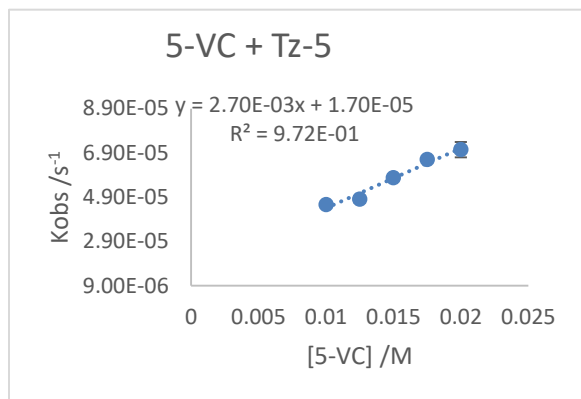
A



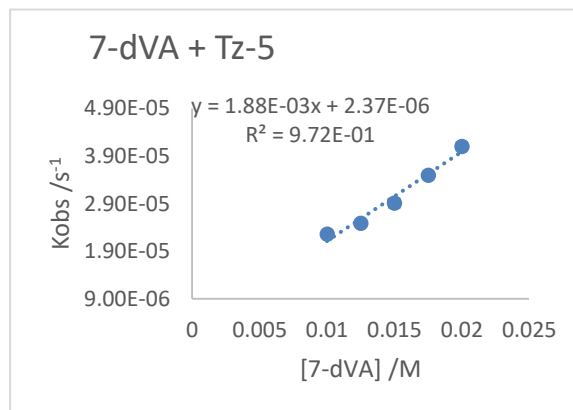
B



C



D



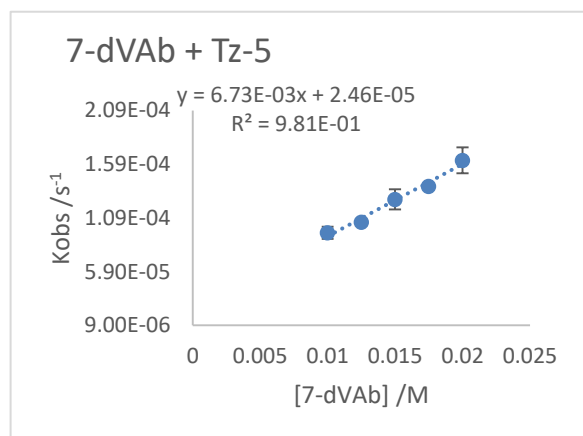
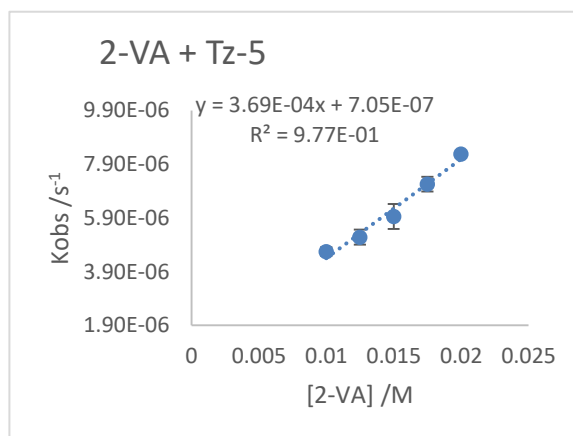
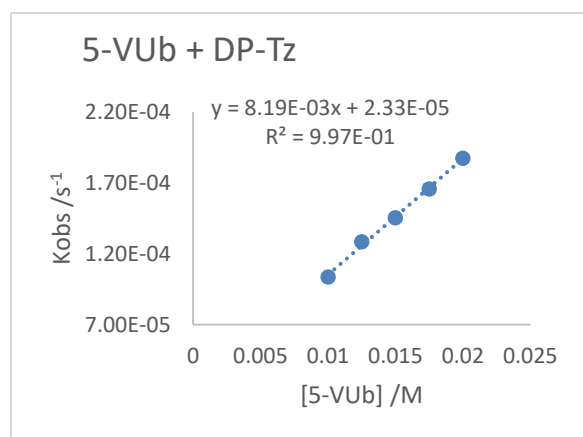
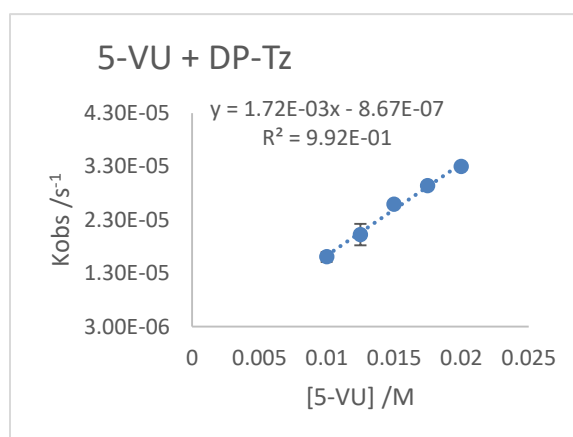
E**F**

Figure 2-S2v. Rate plots used to calculate second-order rate constants of **Tz-5** with nucleosides and nucleobases: A) **5-VUb**, B) **5-VU**, C) **5-VC**, D) **7-dVA**, E) **7-dVAb**, and F) **2-VA** in DMSO.

A**B**

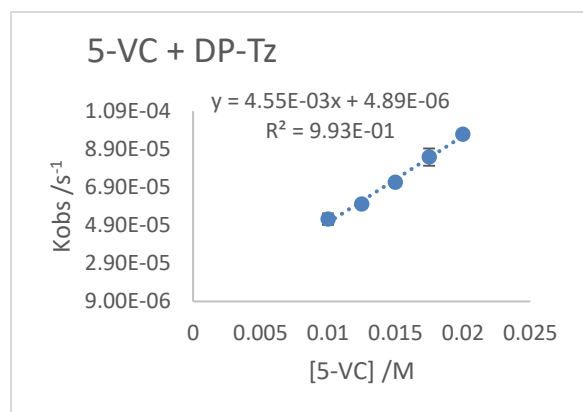
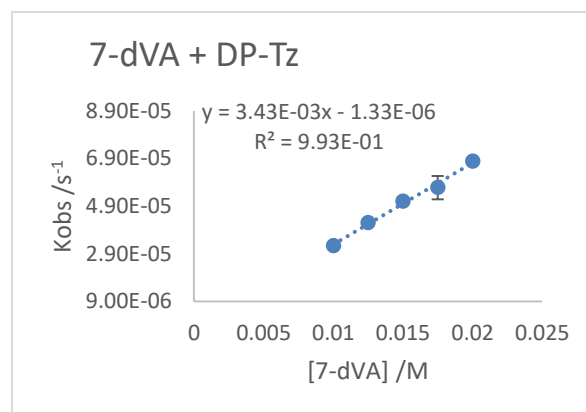
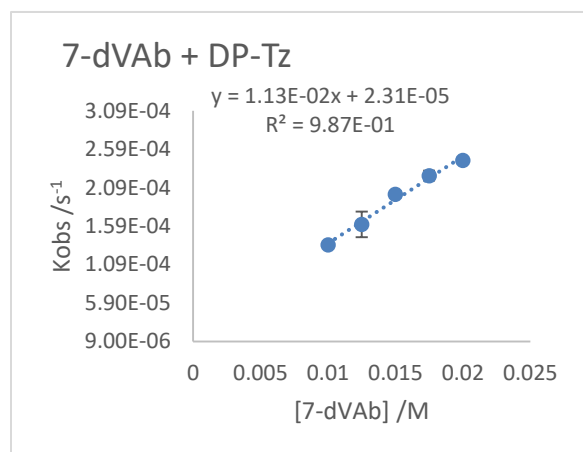
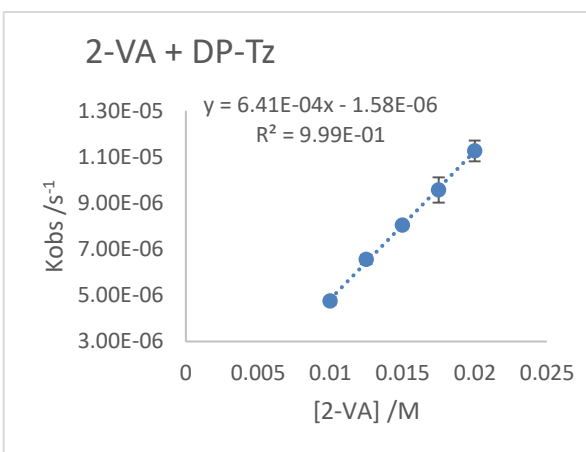
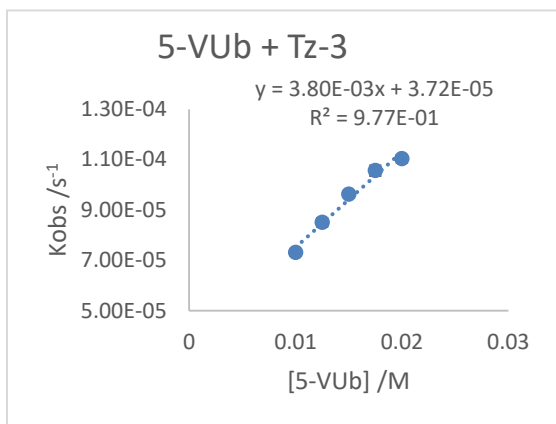
C**D****E****F**

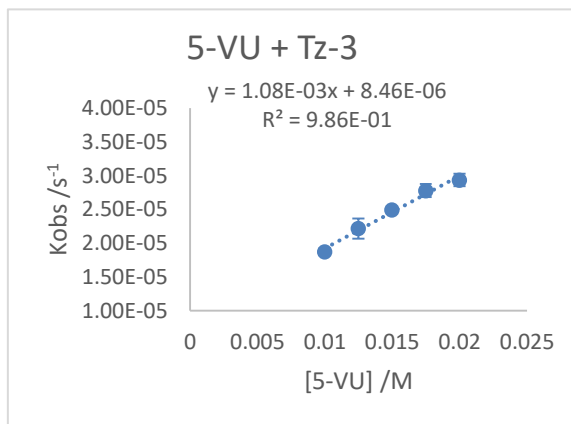
Figure 2-S2vi. Rate plots used to calculate second-order rate constants of **DP-Tz** with nucleosides and nucleobases: A) **5-VUb**, B) **5-VU**, C) **5-VC**, D) **7-dVA**, E) **7-dVAb**, and F) **2-VA** in DMSO.

Tz-3, Tz-4 + Nucleosides/Nucleobases in DMSO:H₂O (3:1)

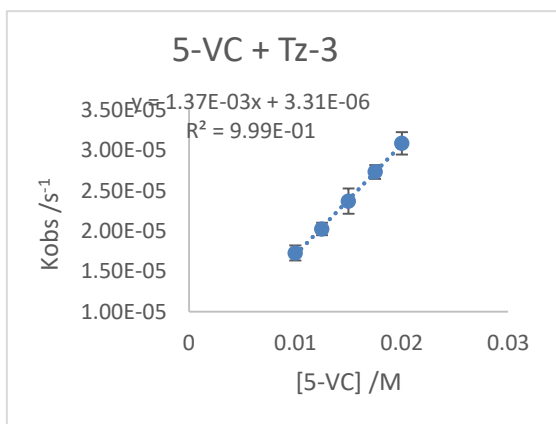
A



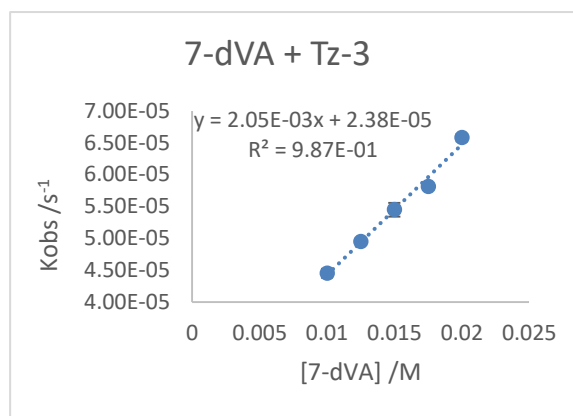
B



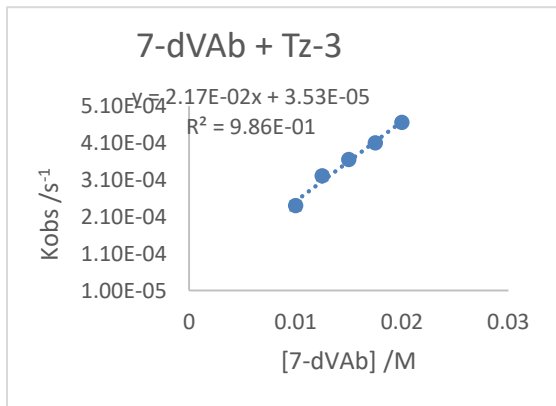
C



D



E



F

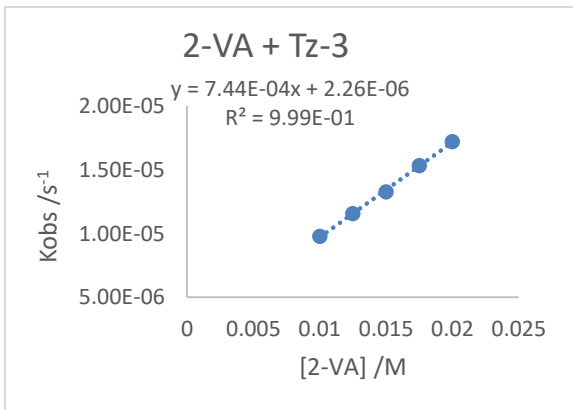
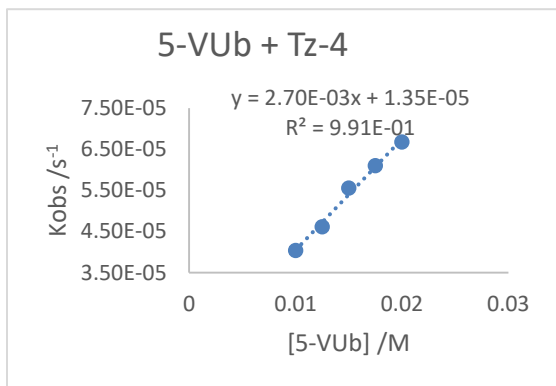
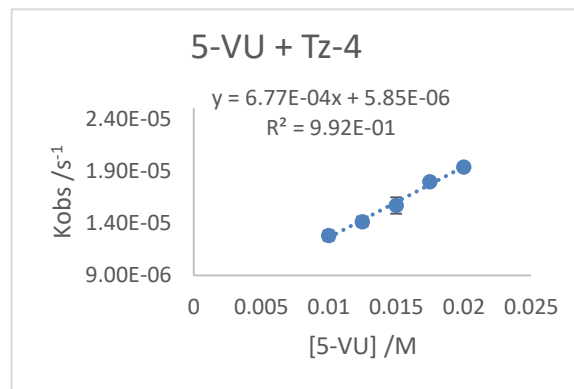


Figure 2-S2vii. Rate plots used to calculate second-order rate constants of **Tz-3** with nucleosides and nucleobases: A) **5-VUb**, B) **5-VU**, C) **5-VC**, D) **7-dVA**, E) **7-dVAb**, and F) **2-VA** in DMSO:H₂O (3:1).

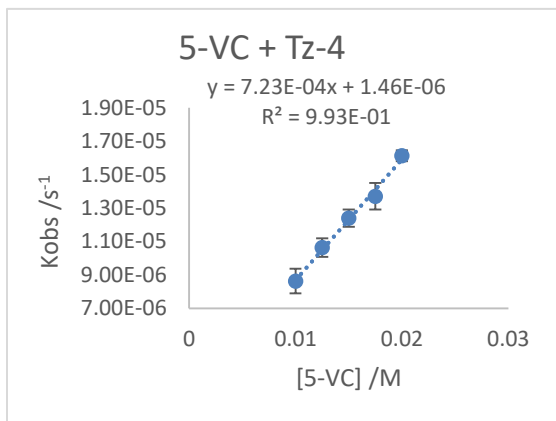
A



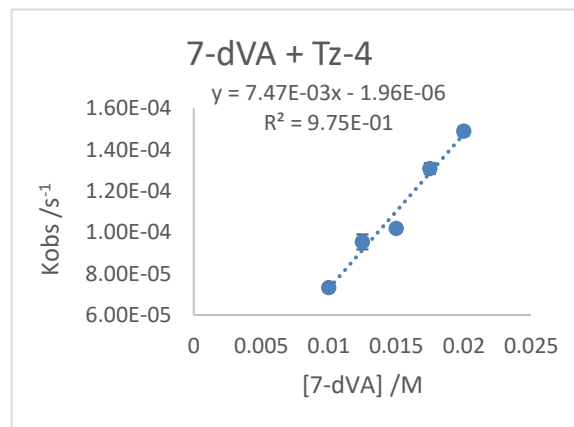
B



C



D



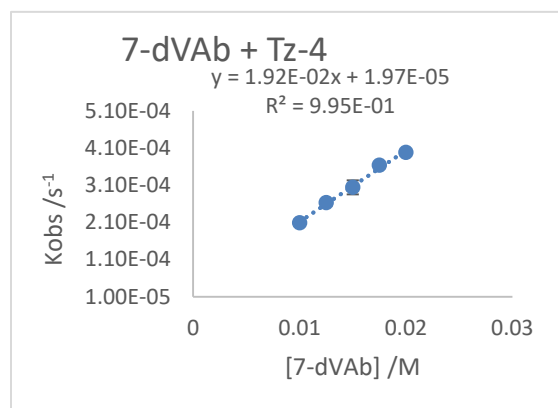
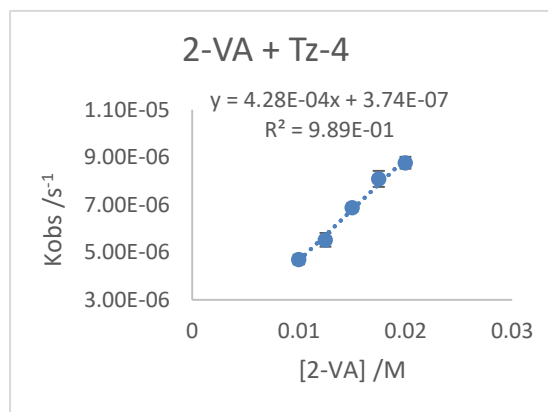
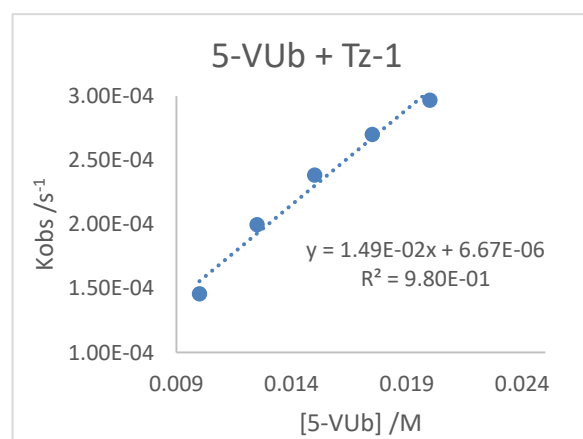
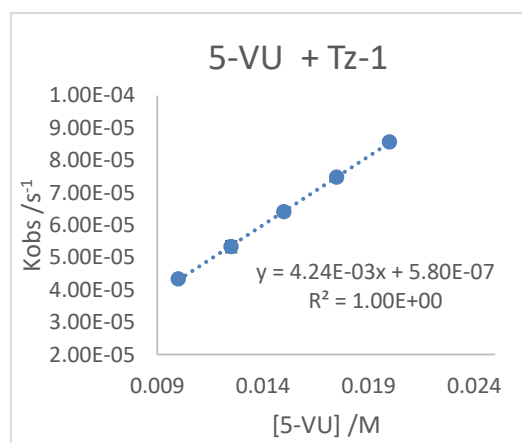
E**F**

Figure 2-S2viii. Rate plots used to calculate second-order rate constants of **Tz-4** with nucleosides and nucleobases: A) **5-VUb**, B) **5-VU**, C) **5-VC**, D) **7-dVA**, E) **7-dVAb**, and F) **2-VA** in DMSO:H₂O (3:1).

Tz-1 + Nucleoside/Nucleobase in 10% AcOH in DMSO

A**B**

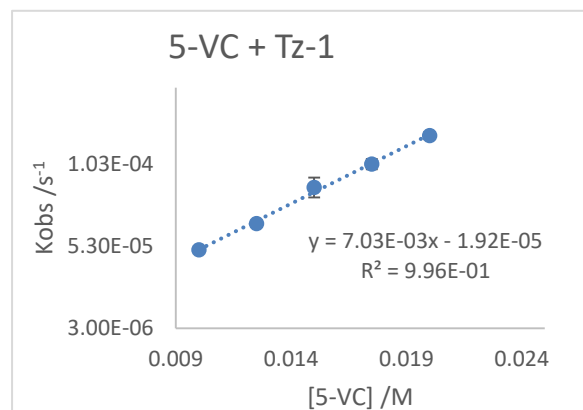
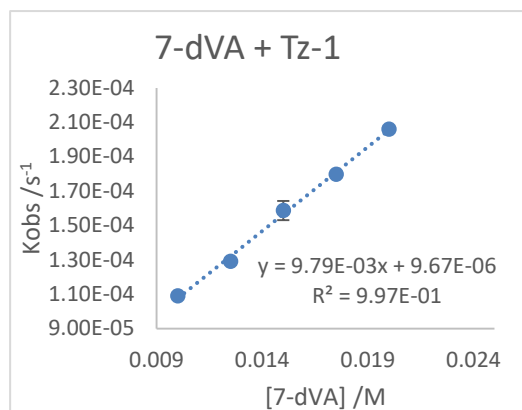
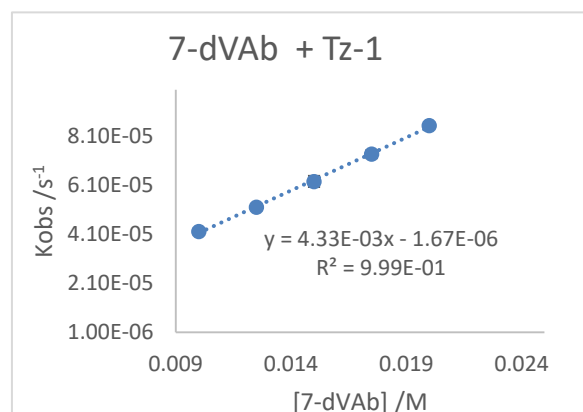
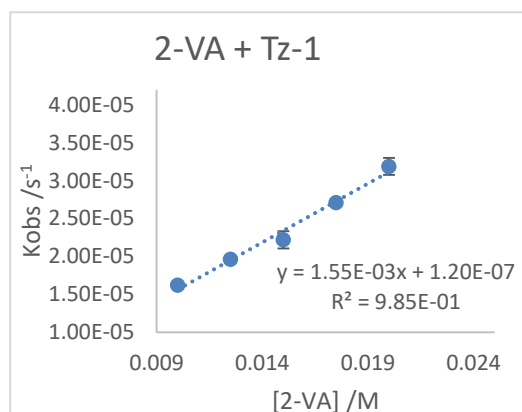
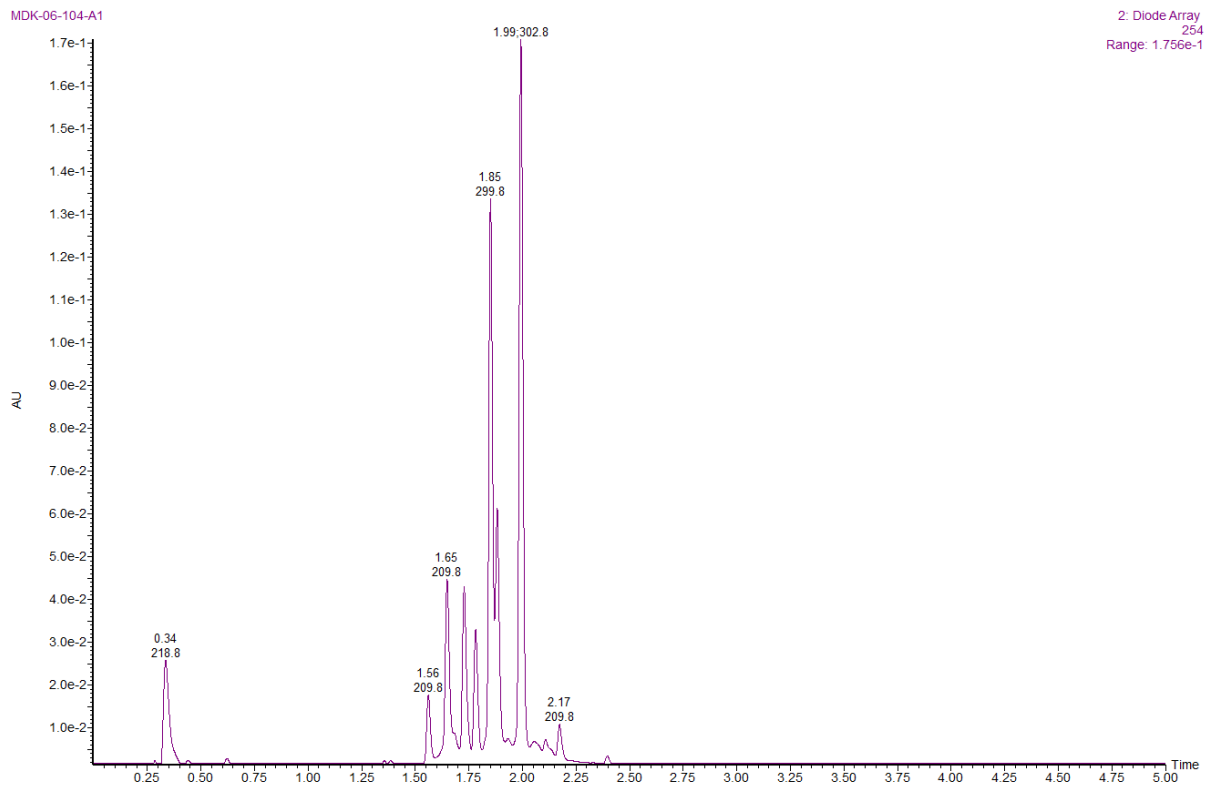
C**D****E****F**

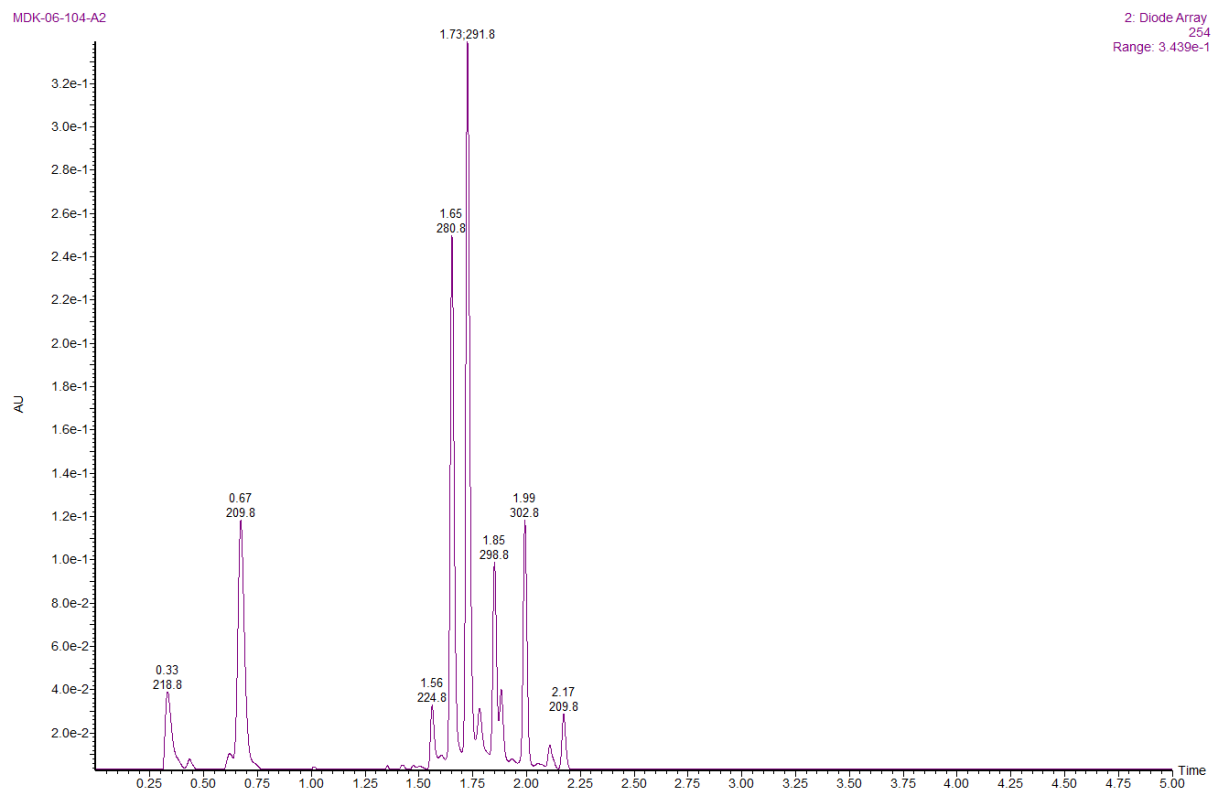
Figure 2-S3ix. Rate plots used to calculate second-order rate constants of **Tz-1** with nucleosides and nucleobases: A) **5-VUb**, B) **5-VU**, C) **5-VC**, D) **7-dVA**, E) **7-dVAb**, and F) **2-VA** in DMSO with 10% AcOH.

Below are images for Figure S4: Reaction Analysis by LC-MS



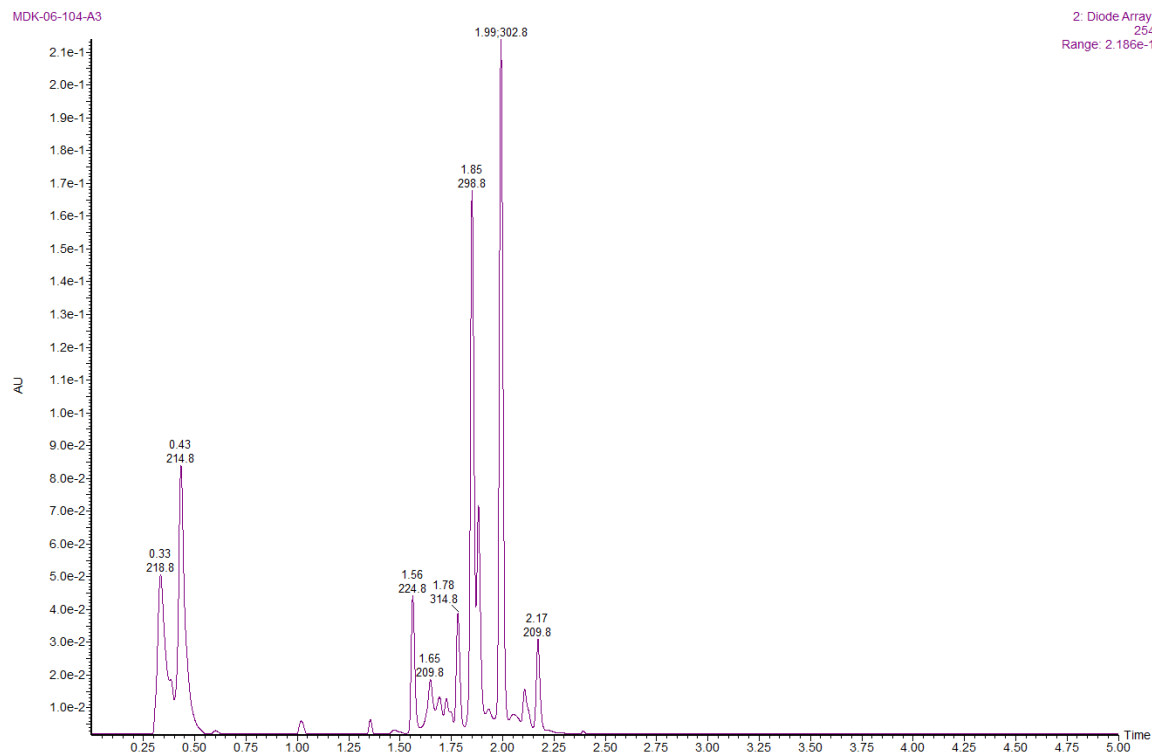
A

Tz-1 & 5-VUb				
t	mass observed	exact mass		Product
1.56	532.22, 554.17	532.21, 554.19	M+H, M+Na	Tz-1 + 5-VUb ox
1.65	532.22, 554.17	532.21, 554.19	M+H, M+Na	Tz-1 + 5-VUb ox
1.74	436.22	436.17	M+Na	Hydrolysis
1.80	436.21	436.17	M+Na	Hydrolysis
1.85	436.19	436.17	M+Na	Hydrolysis
1.99	436.20	436.17	M+Na	Hydrolysis
2.17	436.19	436.17	M+Na	Hydrolysis

B

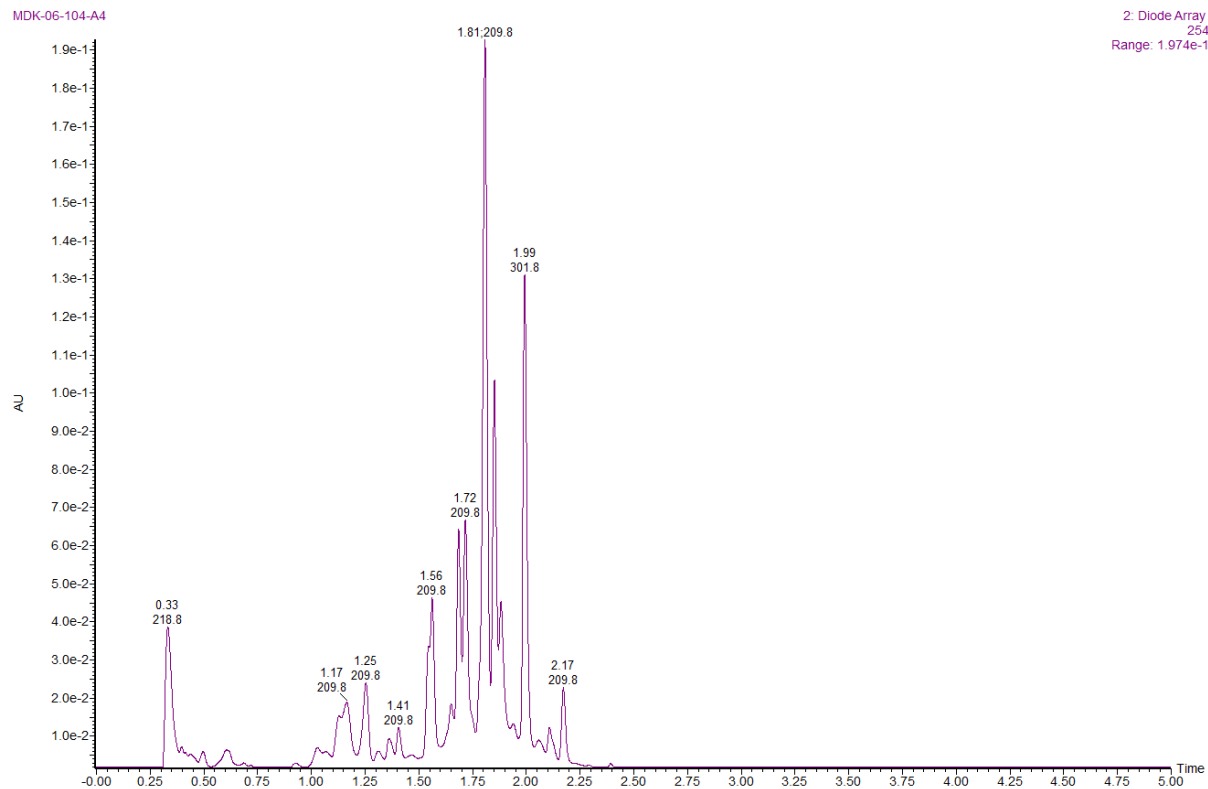
Tz-1 & 5-VU				
t	mass observed	exact mass		Product
0.67	563.13	563.14	2M+Na	5-VU
1.56	346.2	346.11	M+Na	Tz-1 - Boc
1.65	686.17	686.23	M+Na	Tz-1 + 5-VU ox
1.73	686.25	686.23	M+Na	Tz-1 + 5-VU ox
1.85	436.21	436.17	M+Na	Hydrolysis
1.99	436.2	436.17	M+Na	Hydrolysis
2.17	436.22	436.17	M+Na	Hydrolysis

C



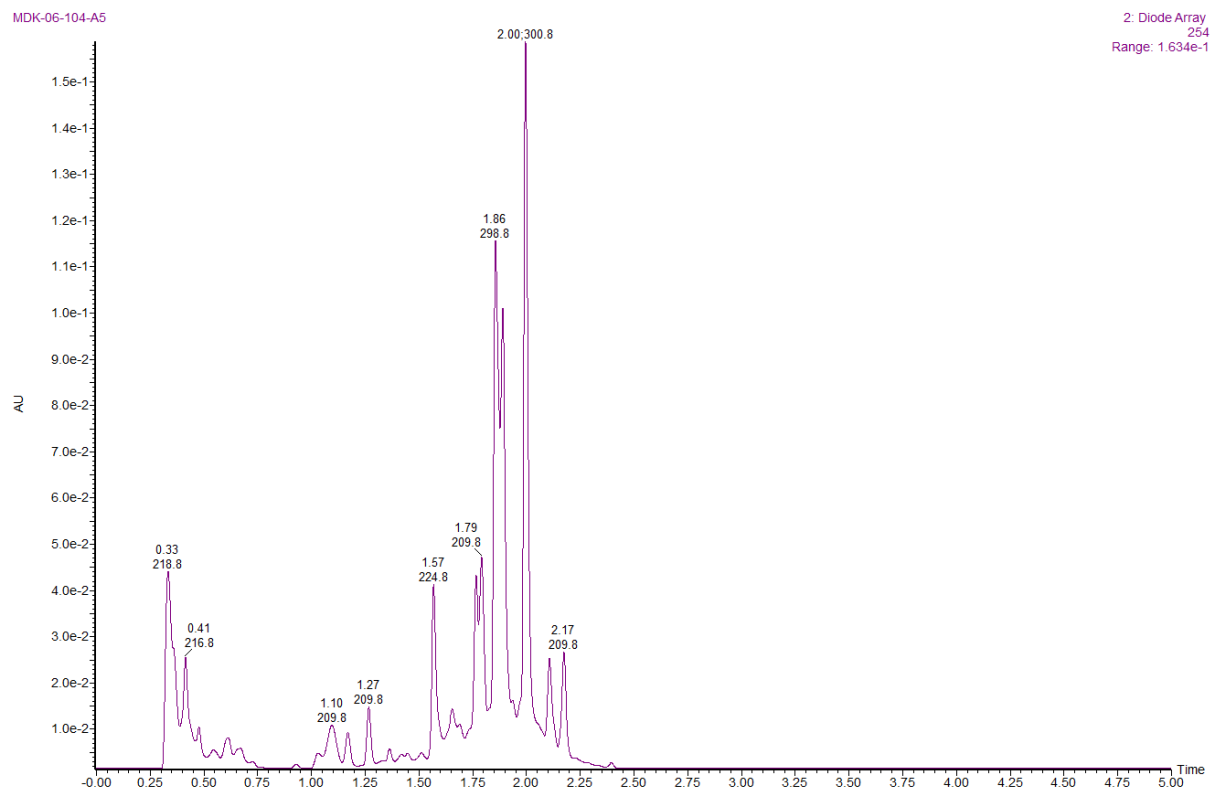
Tz-1 & 5-VC				
t	mass observed	exact mass		Product
0.43	292.09	292.09	M+Na	5-VC
1.56	346.21	346.11	M+Na	Tz-1 - Boc
1.73	665.68	665.28	M+H	Tz-1 + 5-VC
1.78	436.20	436.17	M+Na	Hydrolysis
1.83	686.69	687.26	M+Na	Tz-1 + 5-VC
1.85	436.21	436.17	M+Na	Hydrolysis
1.99	436.20	436.17	M+Na	Hydrolysis
2.17	436.22	436.17	M+Na	Hydrolysis

D

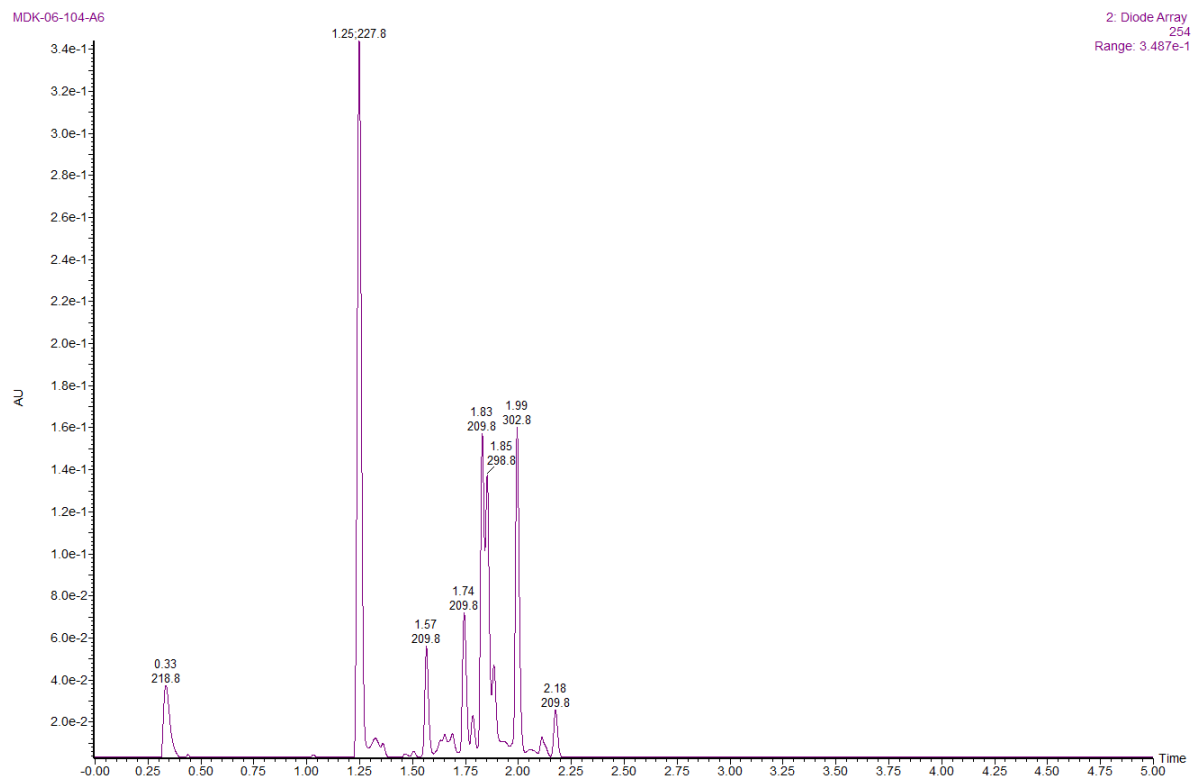


Tz-1 & 7-dVA				
t	mass observed	exact mass		Product
0.60	292.14	292312.00	M	7-dVA
1.25	293.19	293.13	M+H	7-dVA
1.56	293.02	293.13	M+H	7-dVA
1.71	708.87	708.26	M+Na	Tz-1 + 7-dVA ox
1.81	726.05	726.25	M+K	Tz-1 + 7-dVA
1.99	436.12	436.17	M+Na	Hydrolysis
2.17	436.20	436.17	M+Na	Hydrolysis

E



Tz-1 & 7-dVAb				
t	mass observed	exact mass		Product
1.77	436.20	436.17	M+Na	Hydrolysis
1.86	436.00	436.17	M+Na	Hydrolysis
1.91	436.16, 554.18	436.17, 554.24	M+Na, M+H	Hydrolysis, Tz-1 + 7-dVAb ox
2.00	436.16, 556.16	436.17, 556.26	M+Na, M+H	Hydrolysis, Tz-1 + 7-dVAb
2.17	556.33	556.26	M+H	Tz-1 + 7-dVAb

F

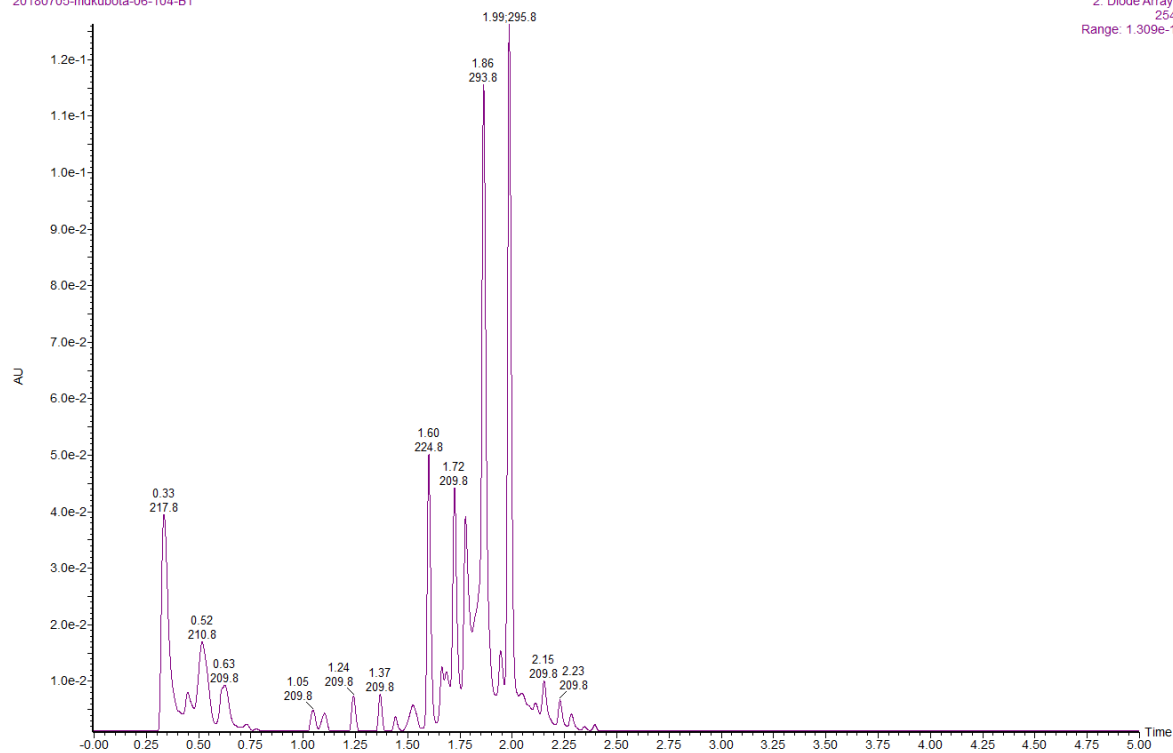
Tz-1 & 2-VA				
t	mass observed	exact mass		Product
1.25	316.10	316.10	M+Na	2-VA
1.57	346.17	346.11	M+Na	Tz-1 - Boc
1.74	709.21	709.26	M+Na	Hydrolysis, Tz-1 + 2-VA
1.83	436.20, 709.17	436.17, 709.26	M+Na, M+Na	Hydrolysis
1.99	436.28	436.17	M+Na	Hydrolysis
2.18	436.16	436.17	M+Na	Hydrolysis

G

sample

20180705-mdkubota-06-104-B1

2: Diode Array
254
Range: 1.309e-1



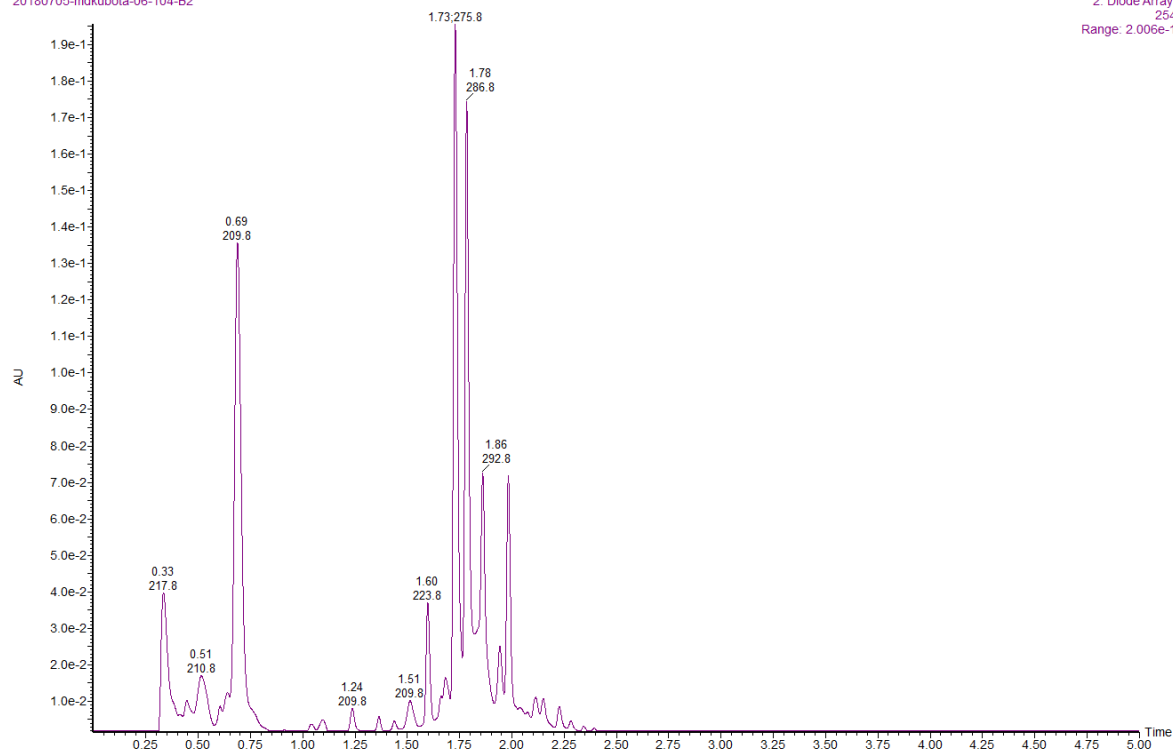
Tz-2 & 5-VUb				
t	mass observed	exact mass		Product
1.44	277.94	277.09	2M+H	5-VUb
1.72	554.27	554.19	M+Na	Tz-2 + 5-VUb ox
1.78	554.27	554.19	M+Na	Tz-2 + 5-VUb ox
1.86	436.20	436.17	M+Na	Hydrolysis
1.99	436.16	436.17	M+Na	Hydrolysis

H

sample

20180705-mdkubota-06-104-B2

2: Diode Array
254
Range: 2.006e-1



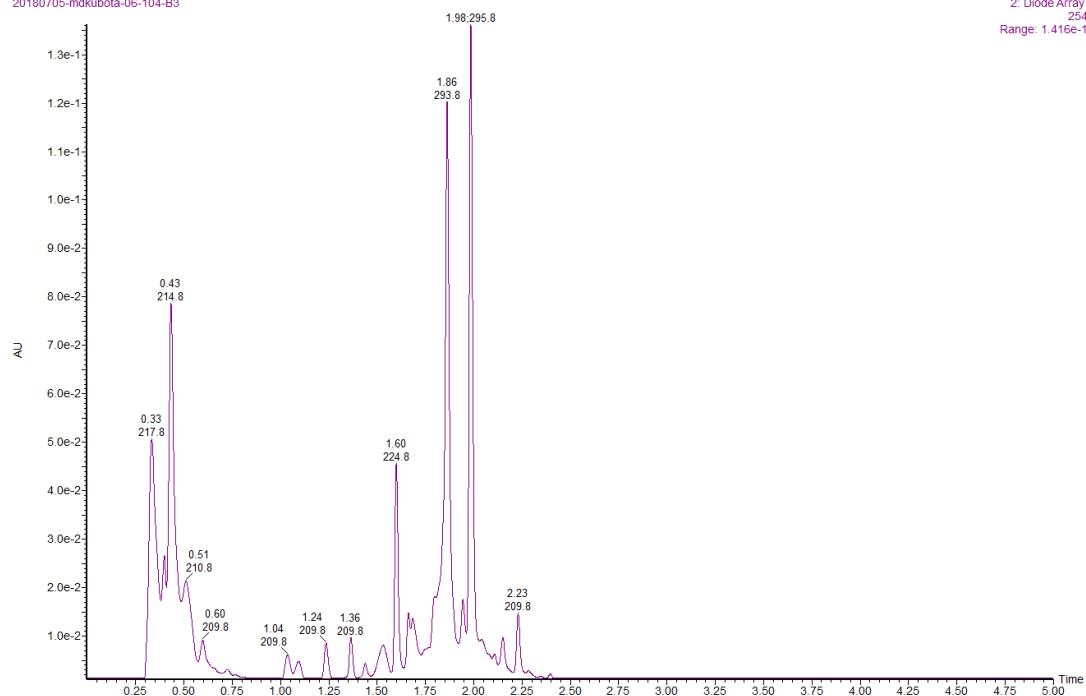
Tz-2 & 5-VU				
t	mass observed	exact mass		Product
0.69	293.15	293.07	M+Na	5-VU
1.60	346.21	346.11	M+Na	Tz-2 - Boc
1.73	686.10	686.23	M+Na	Tz-2 + 5-VU ox
1.78	686.22	686.23	M+Na	Tz-2 + 5-VU ox
1.85	686.05	686.23	M+Na	Tz-2 + 5-VU ox
1.96	435.99	436.17	M+Na	Hydrolysis

I

sample

20180705-mdkubota-06-104-B3

2: Diode Array
254
Range: 1.416e-1



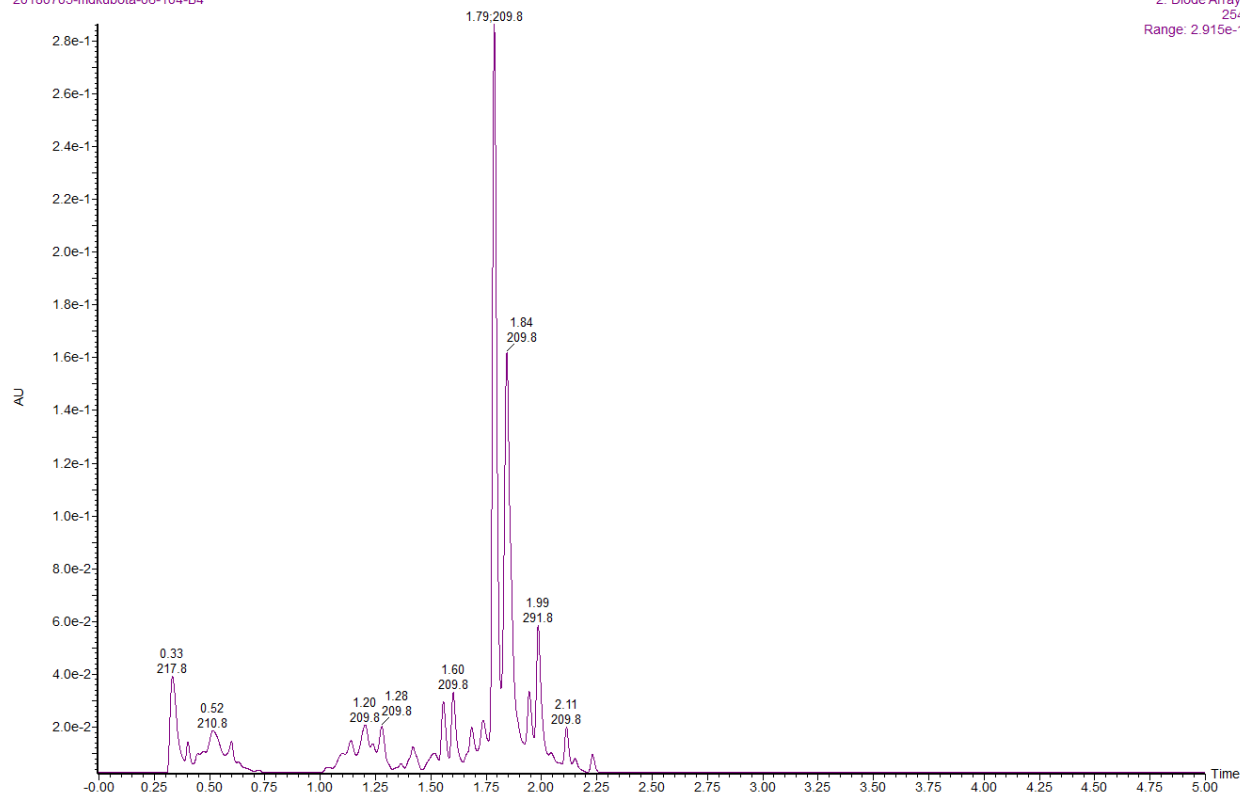
Tz-2 & 5-VC				
t	mass observed	exact mass		Product
0.43	562.10	561.18	2M+Na	5-VC
0.51	292.26	293.07	M+Na	5-VC
1.50	663.66	663.27	M+H	Tz-2 + 5-VC ox
1.60	346.21	346.11	M+Na	Tz-2 - Boc
1.69	663.57	663.27	M+H	Tz-2 + 5-VC ox
1.84	687.19	687.26	M+Na	Tz-2 + 5-VC
1.86	436.12	436.17	M+Na	Hydrolysis
1.90	685.04	685.26	M+H	Tz-2 + 5-VC ox
1.98	436.20	436.17	M+Na	Hydrolysis

J

sample

20180705-mdkubota-06-104-B4

2: Diode Array
254
Range: 2.915e-1



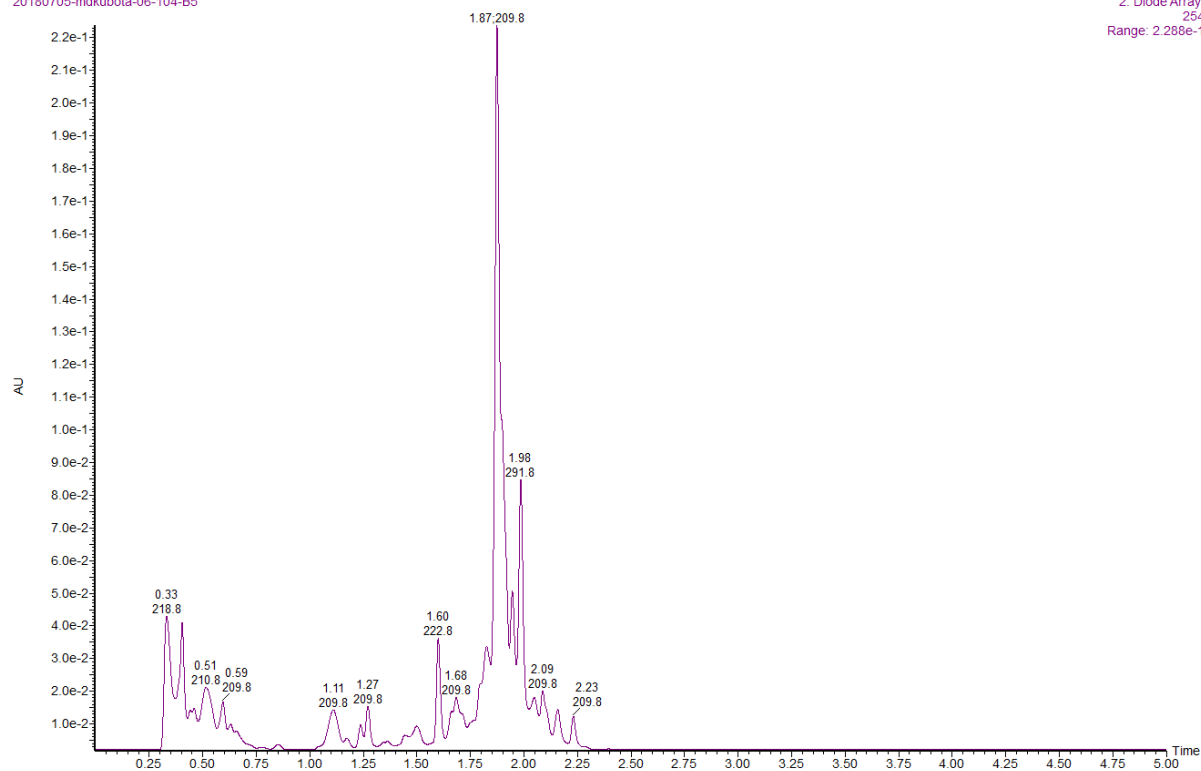
Tz-2 & 7-dVA				
t	mass observed	exact mass		Product
1.20	293.02	293.13	M+H	7-dVA
1.42	293.23	293.13	M+H	7-dVA
1.60	346.17	346.11	M+Na	Tz-2 - Boc
1.79	708.54	708.26	M+Na	Tz-2 + 7-dVA ox
1.84	726.01	726.25	M+K	Tz-2 + 7-dVA
1.99	436.20	436.17	M+Na	Hydrolysis
2.11	436.33	436.17	M+Na	Hydrolysis

K

sample

20180705-mdkubota-06-104-B5

2: Diode Array
254
Range: 2.288e-1

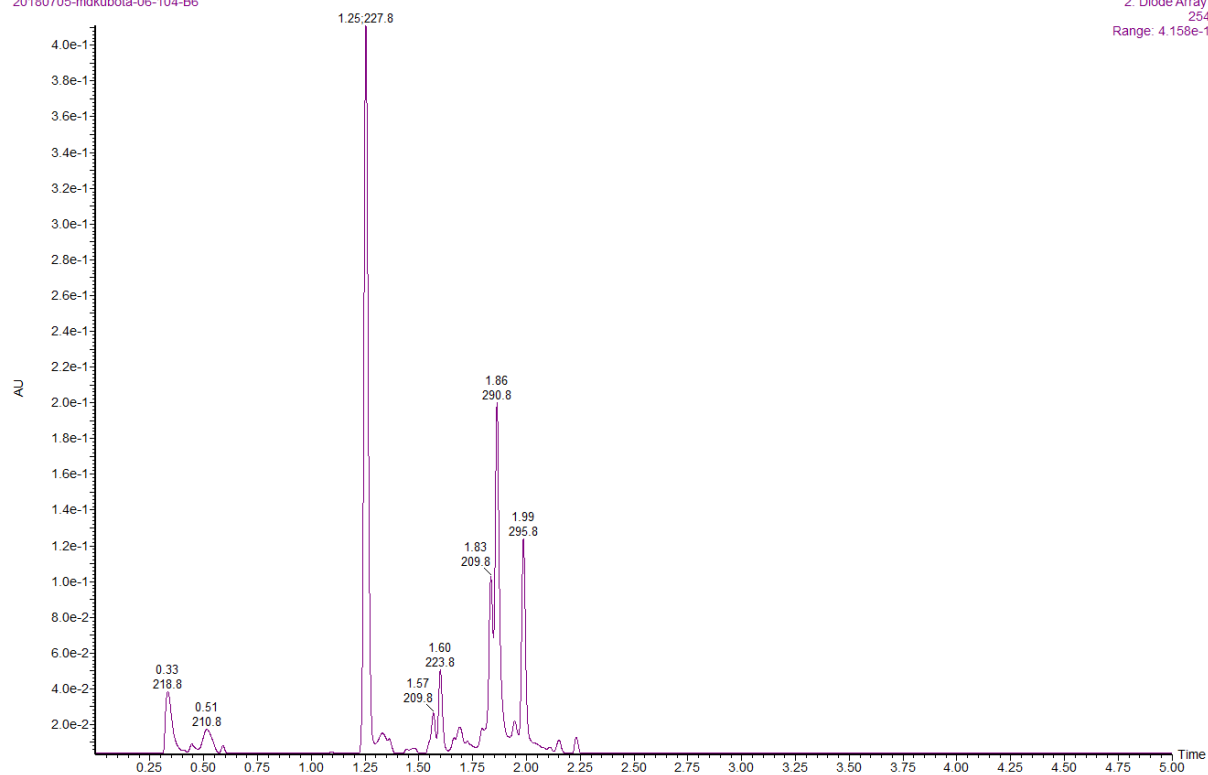


Tz-2 & 7-dVAb				
t	mass observed	exact mass		Product
1.60	346.17	346.11	M+Na	Tz-2 - Boc
1.87	436.12,	436.17,	M+Na,	Hydrolysis, Tz-2 + 7- dVAb ox
	576.21	576.22	M+Na	
1.98	436.16	436.17	M+Na	Hydrolysis
2.09	578.18	578.24	M+Na	Tz-2 + 7-dVAb

L

sample

20180705-mdkubota-06-104-B6

2: Diode Array
254
Range: 4.158e-1

Tz-2 & 2-VA				
t	mass observed	exact mass		Product
1.25	316.10	316.10	M+Na	2-VA
1.60	346.21	346.11	M+Na	Tz-2 - Boc
1.83	709.80	709.26	M+Na	Hydrolysis, Tz-2 + 2-VA
1.86	436.24	436.17	M+Na	Hydrolysis
1.99	436.24	436.17	M+Na	Hydrolysis

M

sample

20180705-mdkubota-06-104-C1

2: Diode Array
254
Range: 5.71e-1



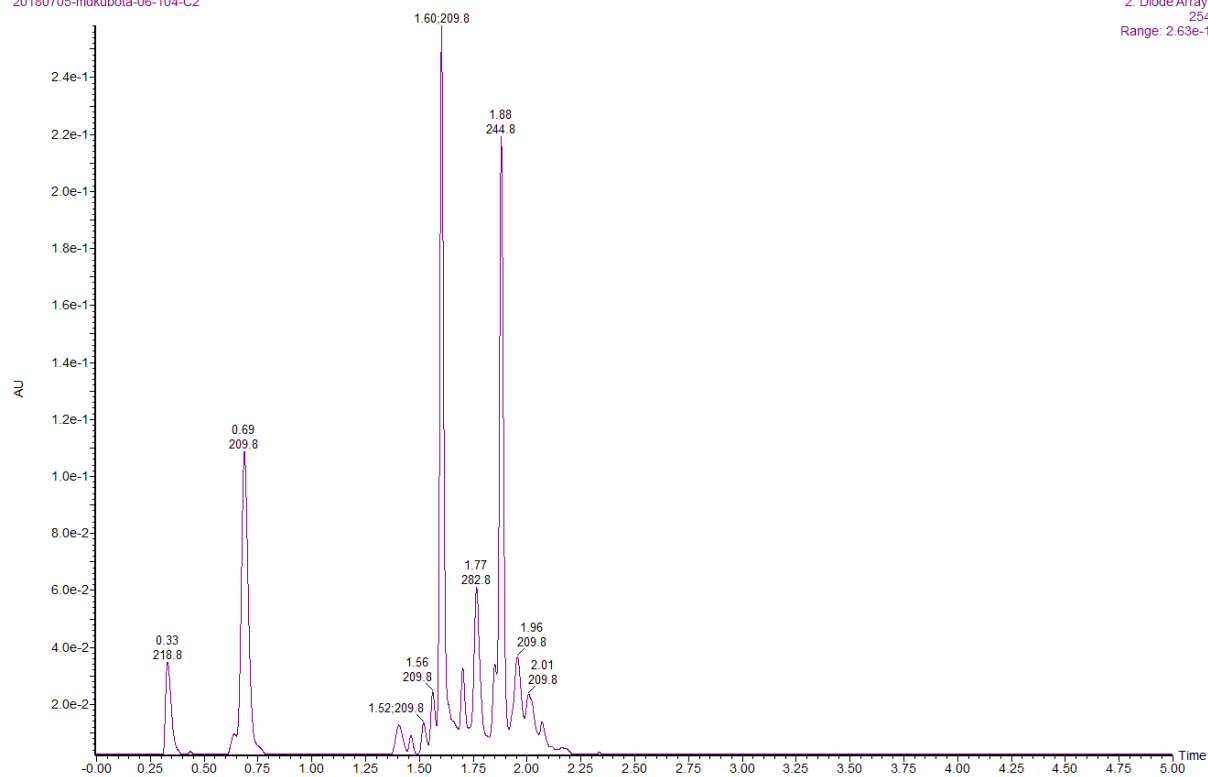
Tz-3 & 5-VUb				
t	mass observed	exact mass		Product
1.58	489.80	490.18	M+Na	Tz-3 + 5-VUb ox
1.76	372.07	372.16	M+Na	Hydrolysis
1.89	382.26	382.17	M+Na	Tz-3
1.96	382.38	382.17	M+Na	Tz-3

N

sample

20180705-mdkubota-06-104-C2

2: Diode Array
254
Range: 2.63e-1

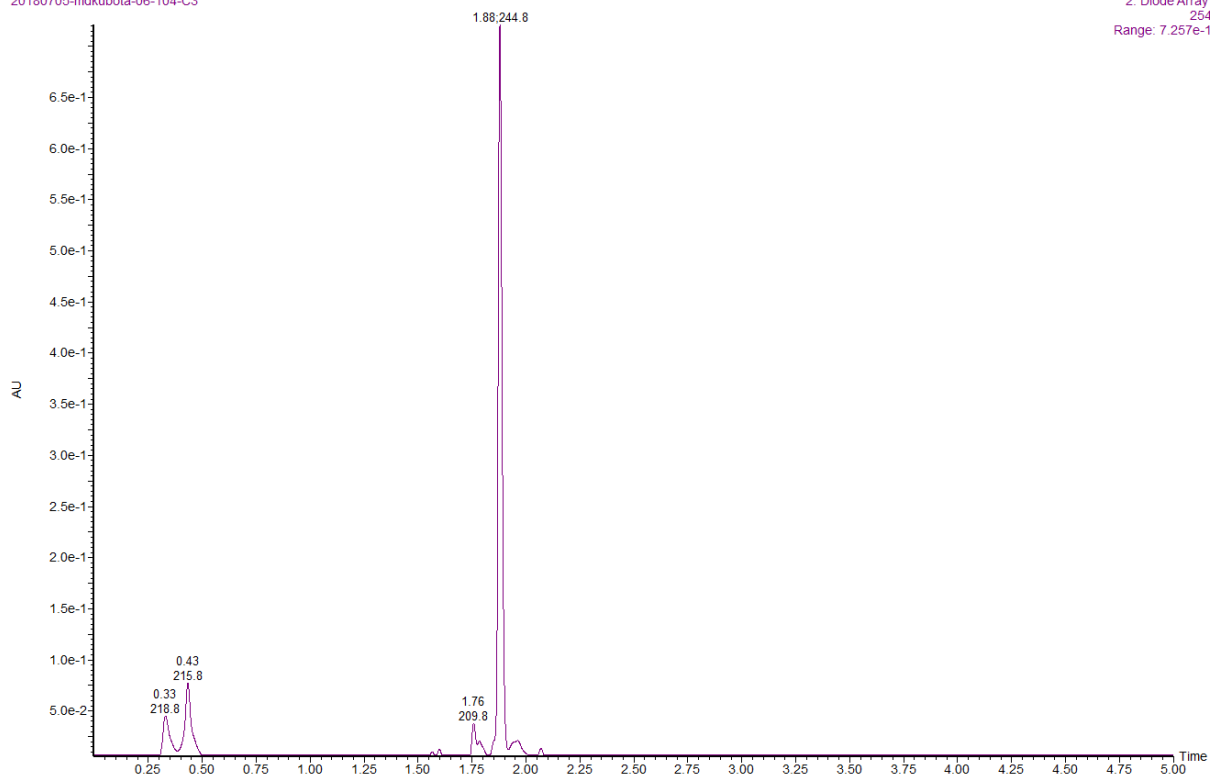


Tz-3 & 5-VU				
t	mass observed	exact mass		Product
0.69	293.19	293.07	M+Na	5-VU
1.60	622.14	622.22	M+Na	Tz-3 + 5-VU ox
1.70	624.54	624.24	M+Na	Tz-3 + 5-VU
1.77	372.02	372.16	M+Na	Hydrolysis
1.88	382.17	382.17	M+Na	Tz-3

sample

20180705-mdkubota-06-104-C3

2: Diode Array
254
Range: 7.257e-1



0

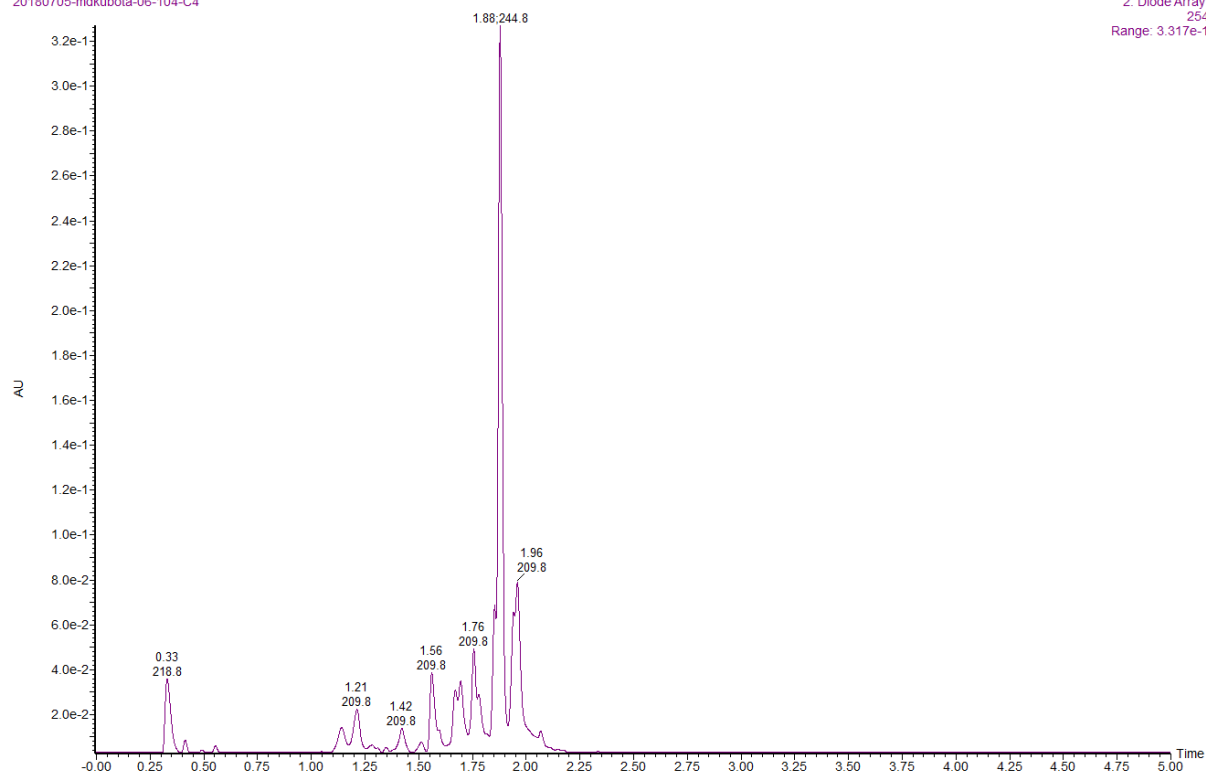
Tz-3 & 5-VC				
t	mass observed	exact mass		Product
0.43	292.15	293.07	M+Na	5-VC
1.76	372.19	372.16	M+Na	Hydrolysis
1.81	623.11	623.26	M+Na	Tz-3 + 5-VC
1.88	381.96	382.17	M+Na	Tz-3
2.18	621.26	621.24	M+Na	Tz-3 + 5-VC ox

P

sample

20180705-mdkubota-06-104-C4

2: Diode Array
254
Range: 3.317e-1



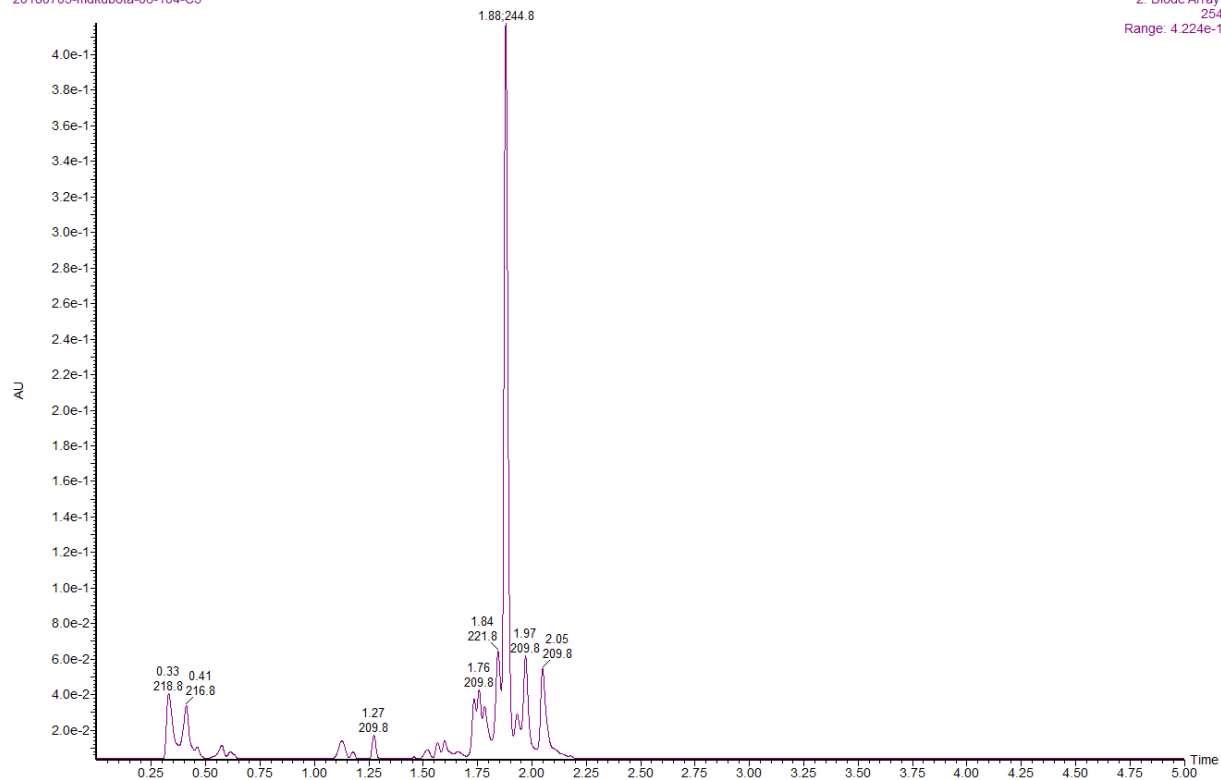
Tz-3 & 7-dVA				
t	mass observed	exact mass		Product
1.21	623.24	623.28	M	Tz-3 + 7-dVA
1.42	623.24	623.28	M	Tz-3 + 7-dVA
1.56	621.22	621.27	M	Tz-3 + 7-dVA ox
1.76	371.98	372.16	M+Na	Hydrolysis
1.88	382.13	382.17	M+Na	Tz-3
1.96	646.10	646.27	M+Na	Tz-3 + 7-dVA

Q

sample

20180705-mdkubota-06-104-C5

2: Diode Array
254
Range: 4.224e-1



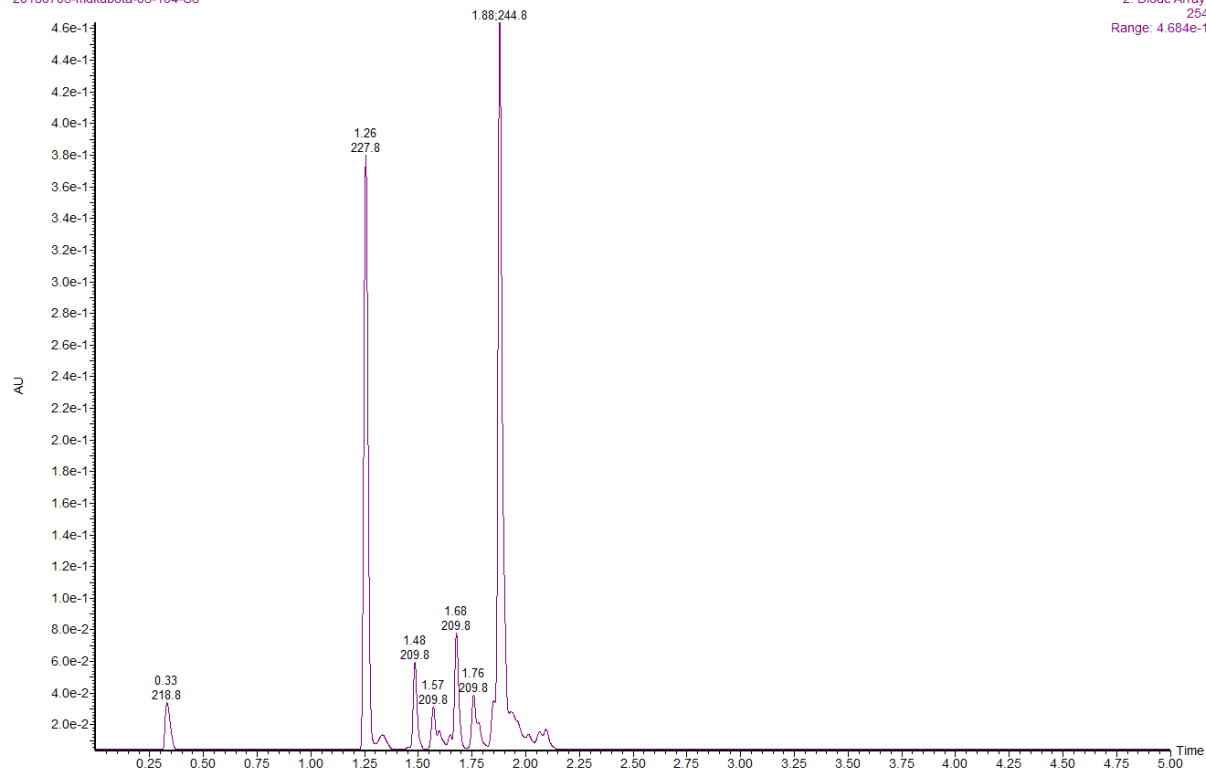
Tz-3 & 7-dVAb				
t	mass observed	exact mass		Product
1.73	513.01	512.21	M+Na	Tz-3 + 7-dVAb ox
1.88	382.13	382.17	M+Na	Tz-3
1.97	491.28	491.24	M	Tz-3 + 7-dVAb
2.05	514.23	514.23	M+Na	Tz-3 + 7-dVAb

R

sample

20180705-mdkubota-06-104-C6

2: Diode Array
254
Range: 4.684e-1

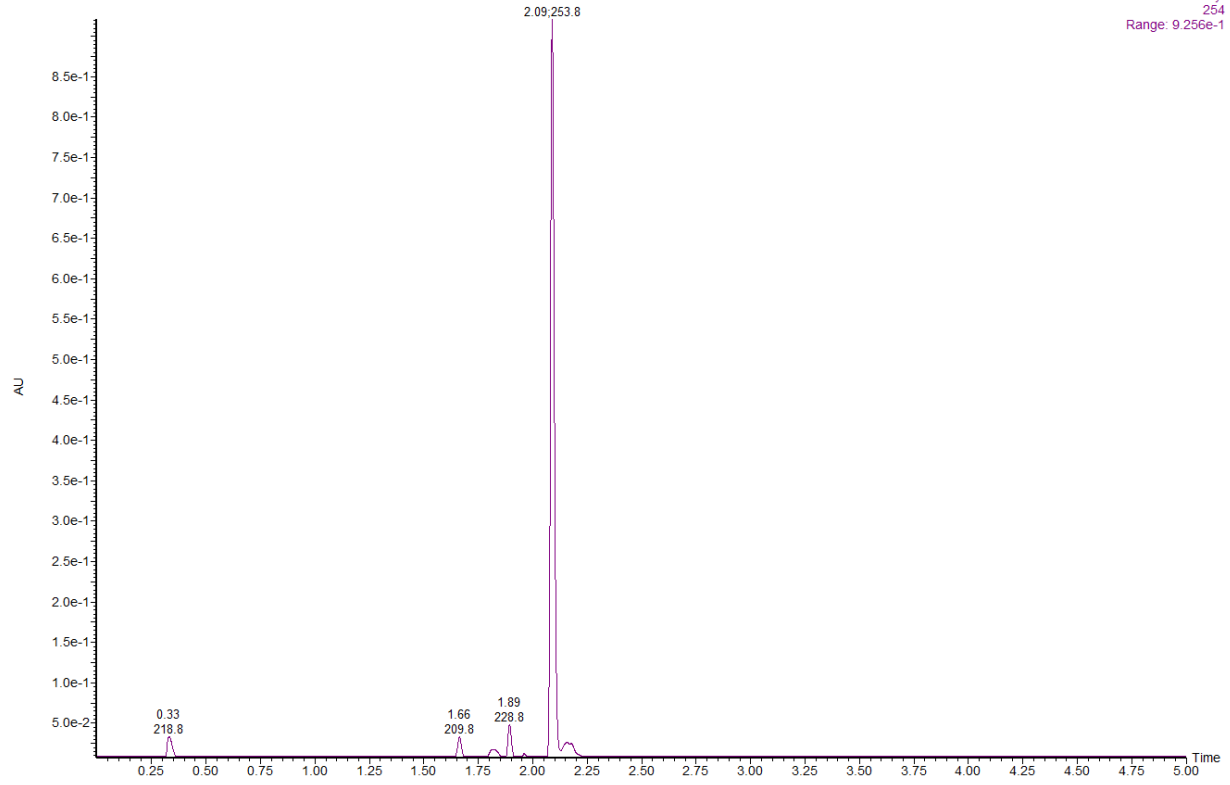


Tz-3 & 2-VA				
t	mass observed	exact mass		Product
1.25	316.10	316.10	M+Na	2-VA
1.48	661.13	661.22	M+K	Tz-3 + 2-VA ox
1.68	645.13	645.25	M+Na	Tz-3 + 2-VA
1.76	372.15	372.16	M+Na	Hydrolysis
1.88	382.13	382.17	M+Na	Tz-3

S

sample

20180705-mdkubota-06-104-D1



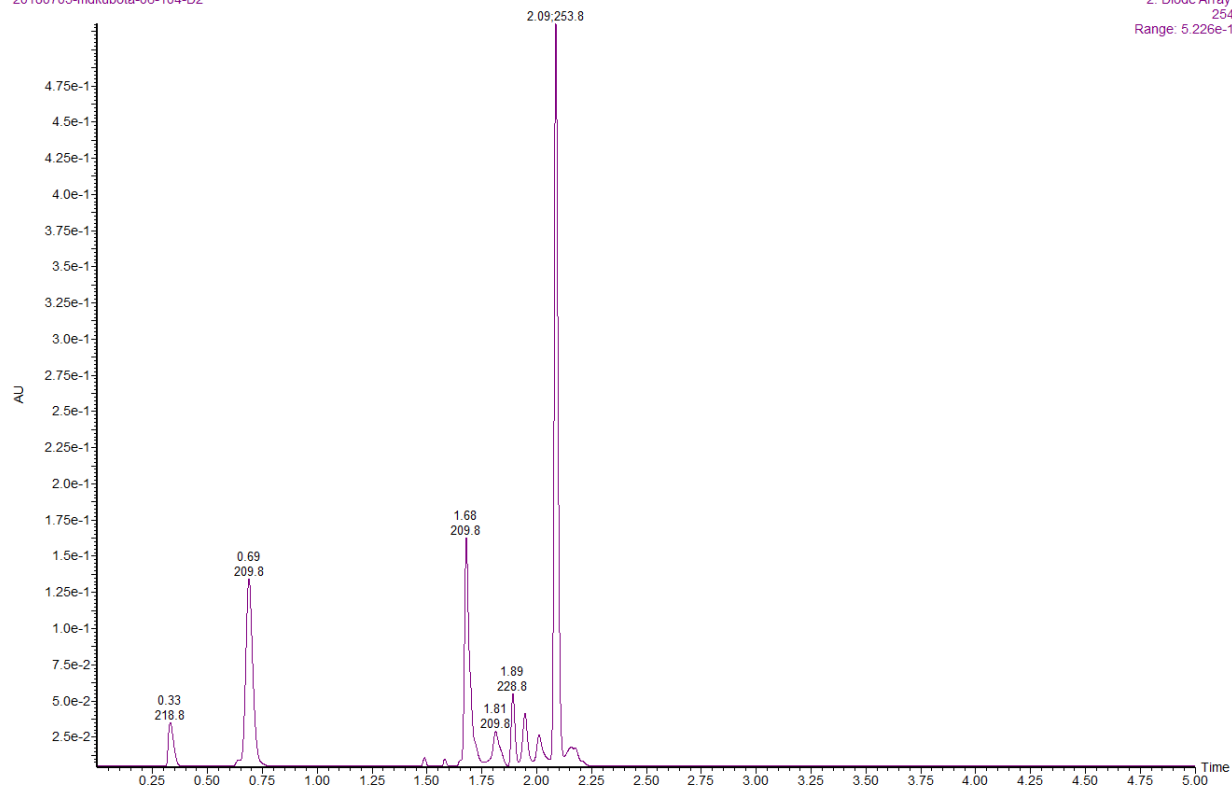
Tz-4 & 5-VUb				
t	mass observed	exact mass		Product
1.58	388.11	388.13	M+K	hydrolysis
1.66	490.48	490.18	M+Na	Tz-4 + 5-VUb ox
2.09	382.17	382.17	M+Na	Tz-4
2.16	382.17	382.17	M+Na	Tz-4

T

sample

20180705-mdkubota-06-104-D2

2: Diode Array
254
Range: 5.226e-1



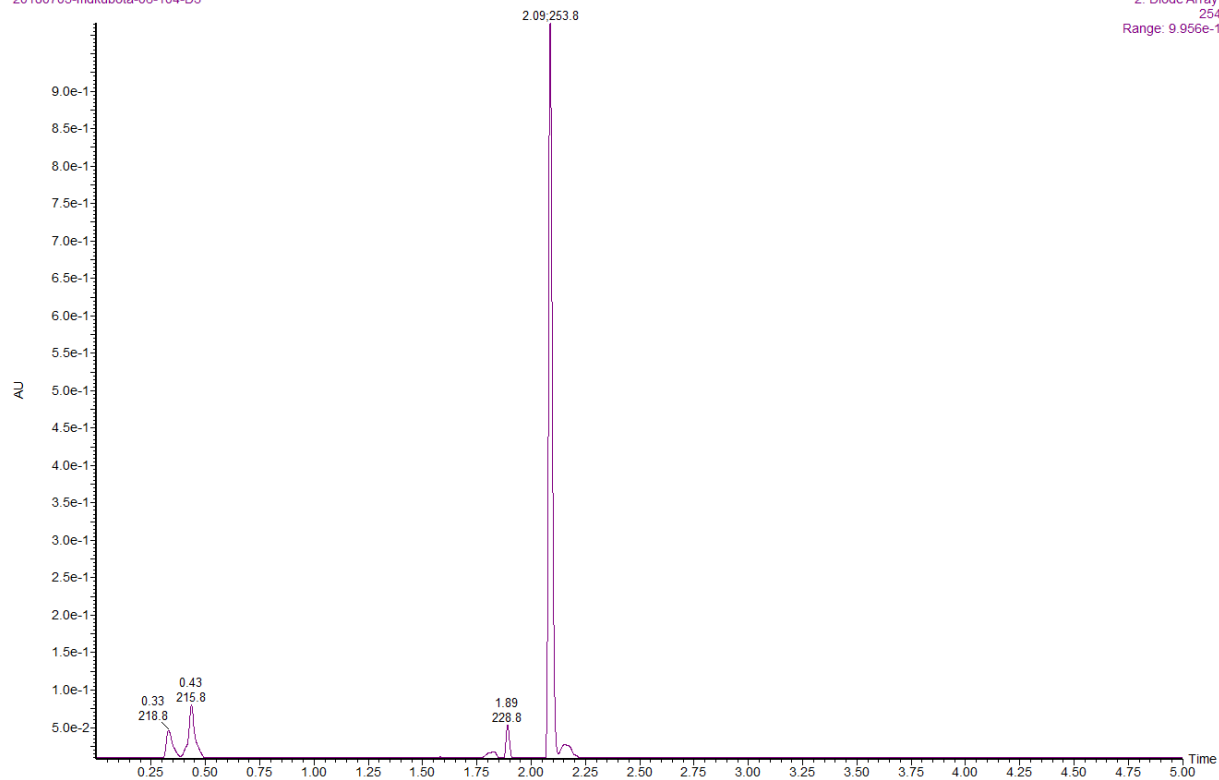
Tz-4 & 5-VU				
t	mass observed	exact mass		Product
0.69	293.07	293.07	M+Na	5-VU
1.68	622.27	622.22	M+Na	Tz-4 + 5-VU ox
2.09	382.30	382.17	M+Na	Tz-4
2.16	382.26	382.17	M+Na	Tz-4

U

sample

20180705-mdkubota-06-104-D3

2: Diode Array
254
Range: 9.956e-1



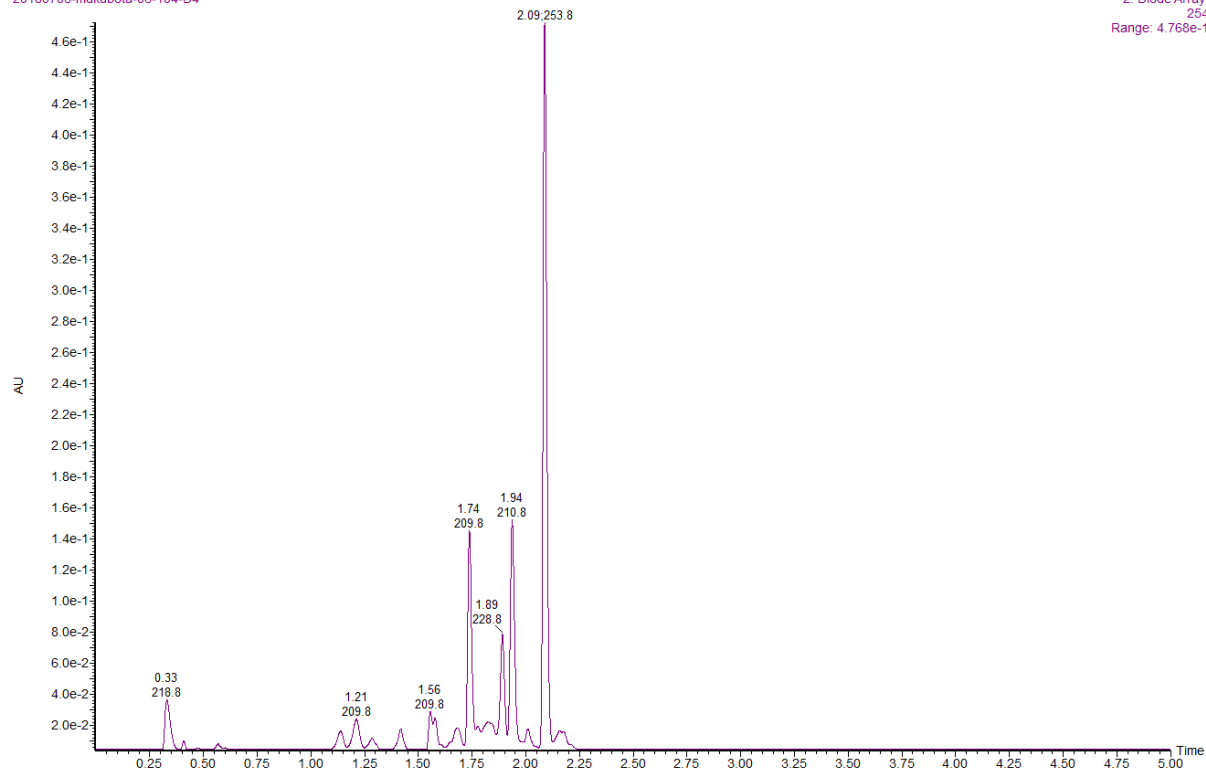
Tz-4 & 5-VC				
t	mass observed	exact mass		Product
0.43	292.81	292.09	M+Na	5-VC
1.41	598.69	598.25	M	Tz-4 + 5-VC ox
1.58	388.03	388.13	M+K	hydrolysis
1.78	623.17	623.26	M+Na	Tz-4 + 5-VC
2.08	382.17	382.17	M+Na	Tz-4
2.16	382.13	382.17	M+Na	Tz-4

V

sample

20180705-mdkubota-06-104-D4

2: Diode Array
254
Range: 4.768e-1



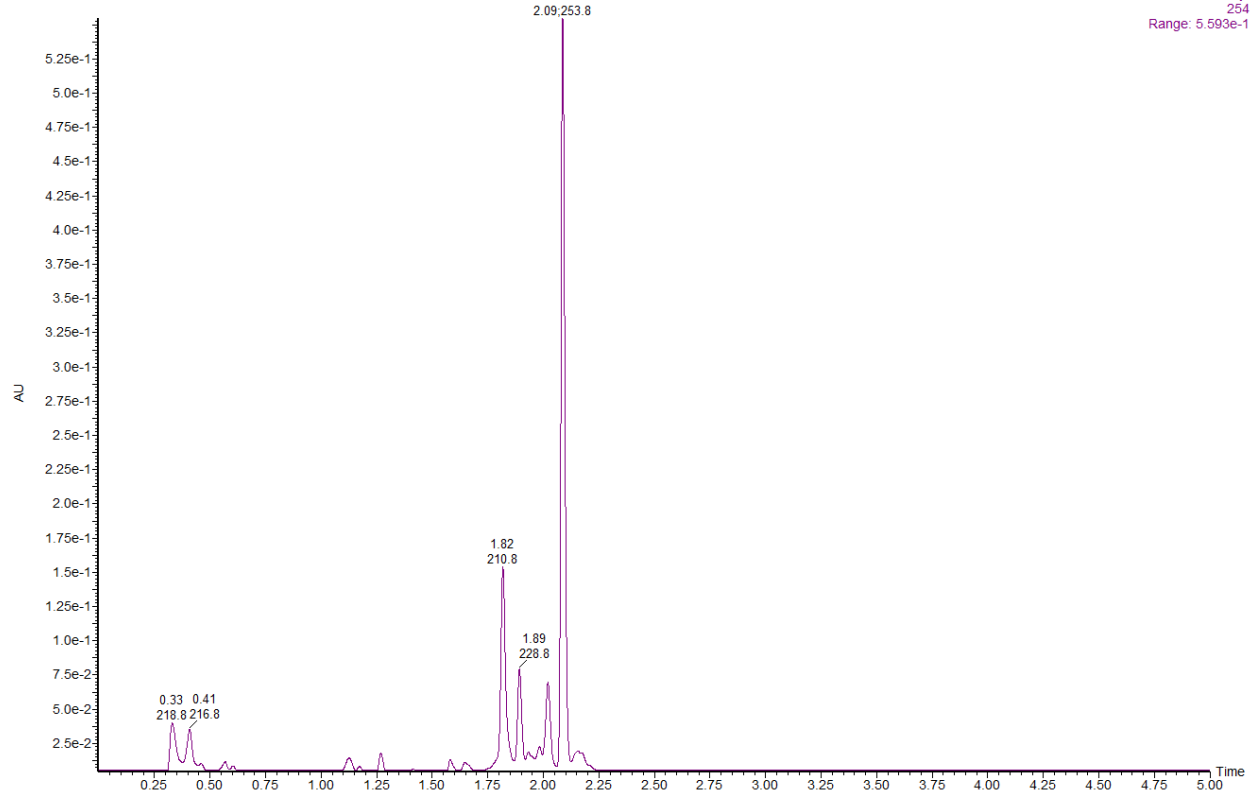
Tz-4 & 7-dVA				
t	mass observed	exact mass		Product
1.21	292.16	292.12	M	7-dVA
1.42	292.06	292.12	M	7-dVA
1.56	293.19	293.13	M+H	7-dVA
1.74	644.25	644.26	M+Na	Tz-4 + 7-dVA ox
1.82	350.51	350.18	M+H	hydrolysis
1.94	646.01	646.27	M+Na	Tz-4 + 7-dVA
2.09	382.21	382.17	M+Na	Tz-4

W

sample

20180705-mdkubota-06-104-D5

2: Diode Array
254
Range: 5.593e-1



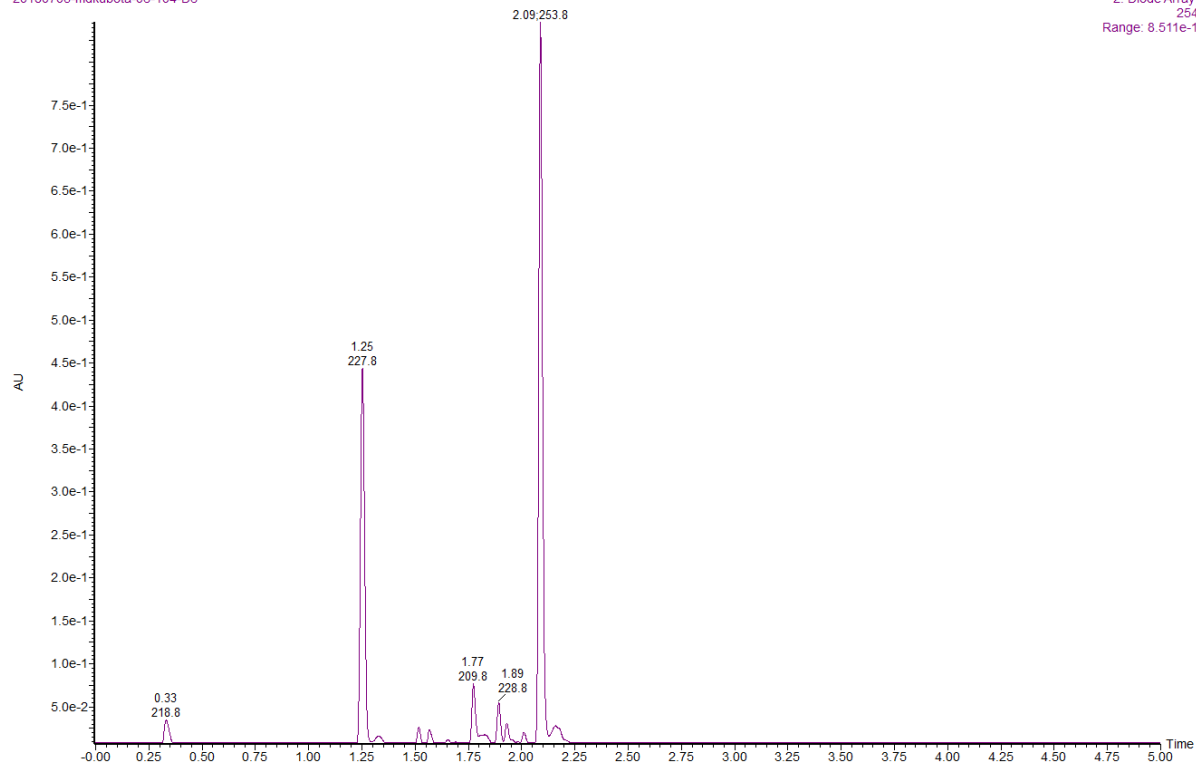
Tz-4 & 7-dVAb				
t	mass observed	exact mass		Product
1.58	388.19	388.13	M+K	hydrolysis
1.82	372.23	372.16	M+Na	Tz-4 hydrolysis
2.02	492.79	492.25	M+H	Tz-4 + 7-dVAb
2.09	382.21	382.17	M+Na	Tz-4
2.16	382.34	382.17	M+Na	Tz-4

X

sample

20180705-mdkubota-06-104-D6

2: Diode Array
254
Range: 8.511e-1

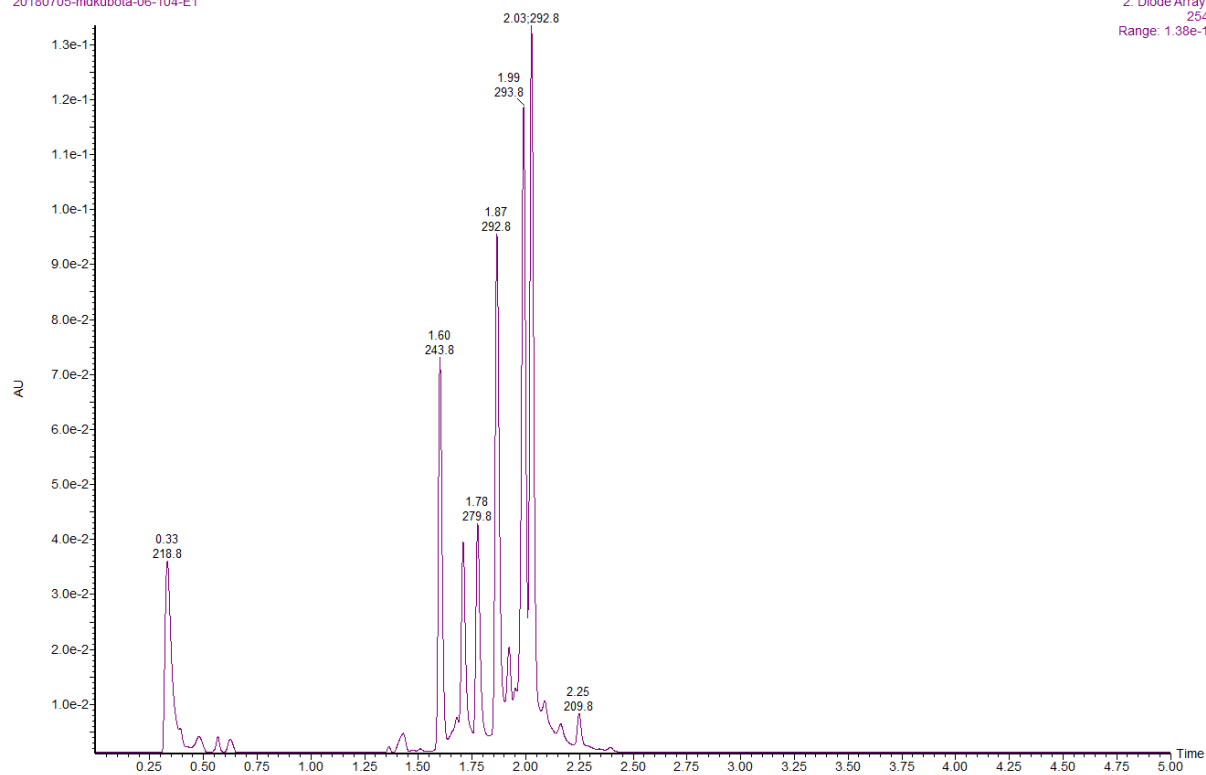


Tz-4 & 2-VA				
t	mass observed	exact mass		Product
1.25	316.12	316.10	M+Na	2-VA
1.77	645.17	645.25	M+Na	Tz-4 + 2-VA ox
1.82	349.07	549.19	M	hydrolysis
1.93	644.92	645.25	M+Na	Tz-4 + 2-VA ox
2.09	382.17	382.17	M+Na	Tz-4
2.16	382.21	382.17	M+Na	Tz-4

Y

sample
20180705-mdkubota-06-104-E1

2: Diode Array
254
Range: 1.38e-1



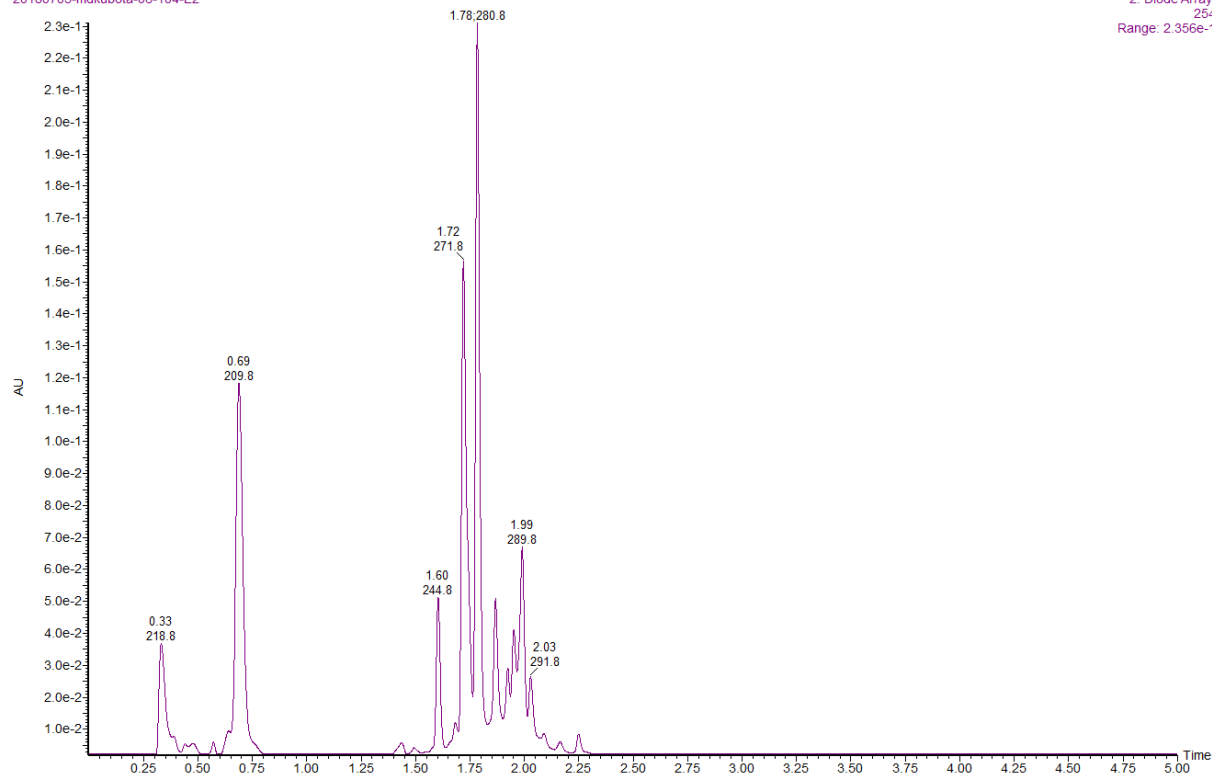
Tz-5 & 5-VUb				
t	mass observed	exact mass		Product
1.70	553.07	533.23	M+H	Tz-5 + 5-VUb
1.78	533.26	533.23	M+H	Tz-5 + 5-VUb
1.87	435.27	435.18	M+Na	hydrolysis
1.99	435.06	435.18	M+Na	hydrolysis
2.03	445.09	445.17	M+Na	Tz-5

Z

sample

20180705-mdkubota-06-104-E2

2: Diode Array
254
Range: 2.356e-1



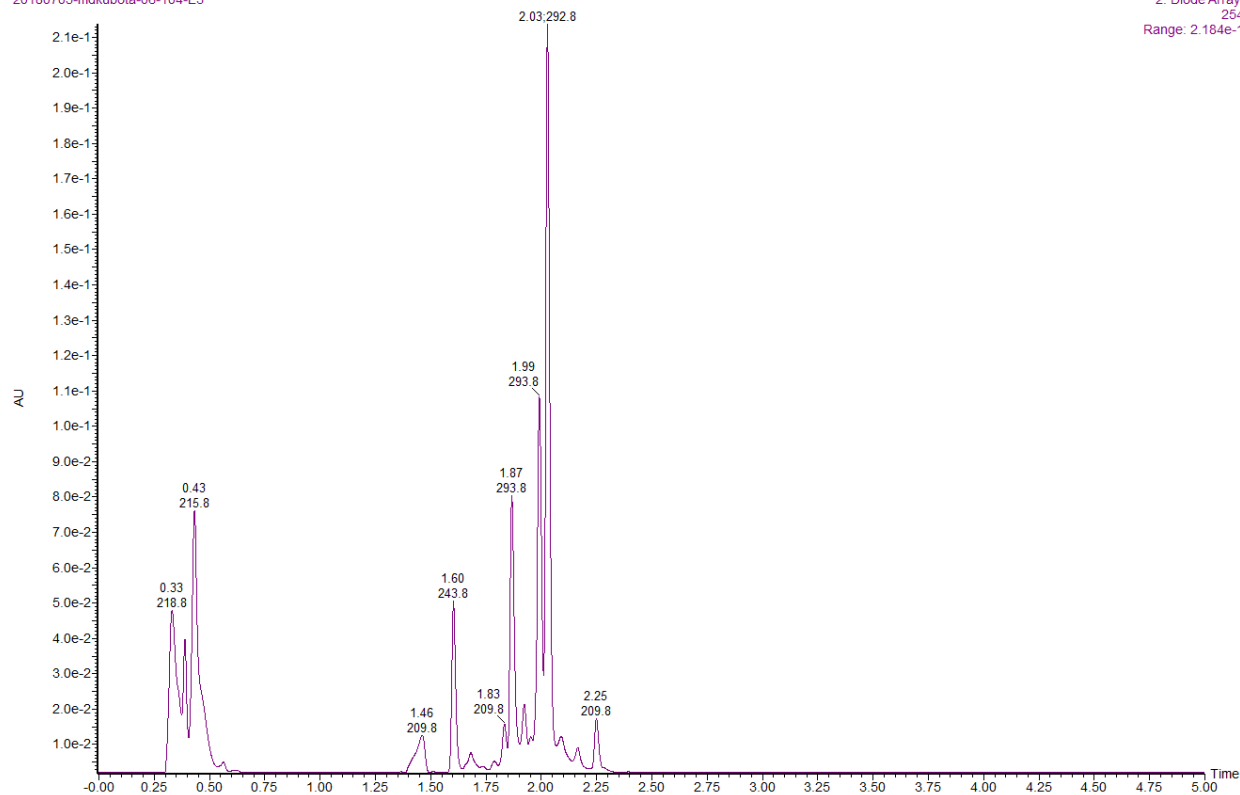
Tz-5 & 5-VU				
t	mass observed	exact mass		Product
0.69	293.09	293.07	M+Na	5-VU
1.72	685.34	685.23	M+Na	Tz-5 + 5-VU ox
1.78	663.15	663.25	M+H	Tz-5 + 5-VU ox
1.87	435.23	435.18	M+Na	hydrolysis
1.92	435.40	435.18	M+Na	hydrolysis
1.99	435.78	435.18	M+Na	hydrolysis
2.03	446.26	446.18	M+H	Tz-5

AA

sample

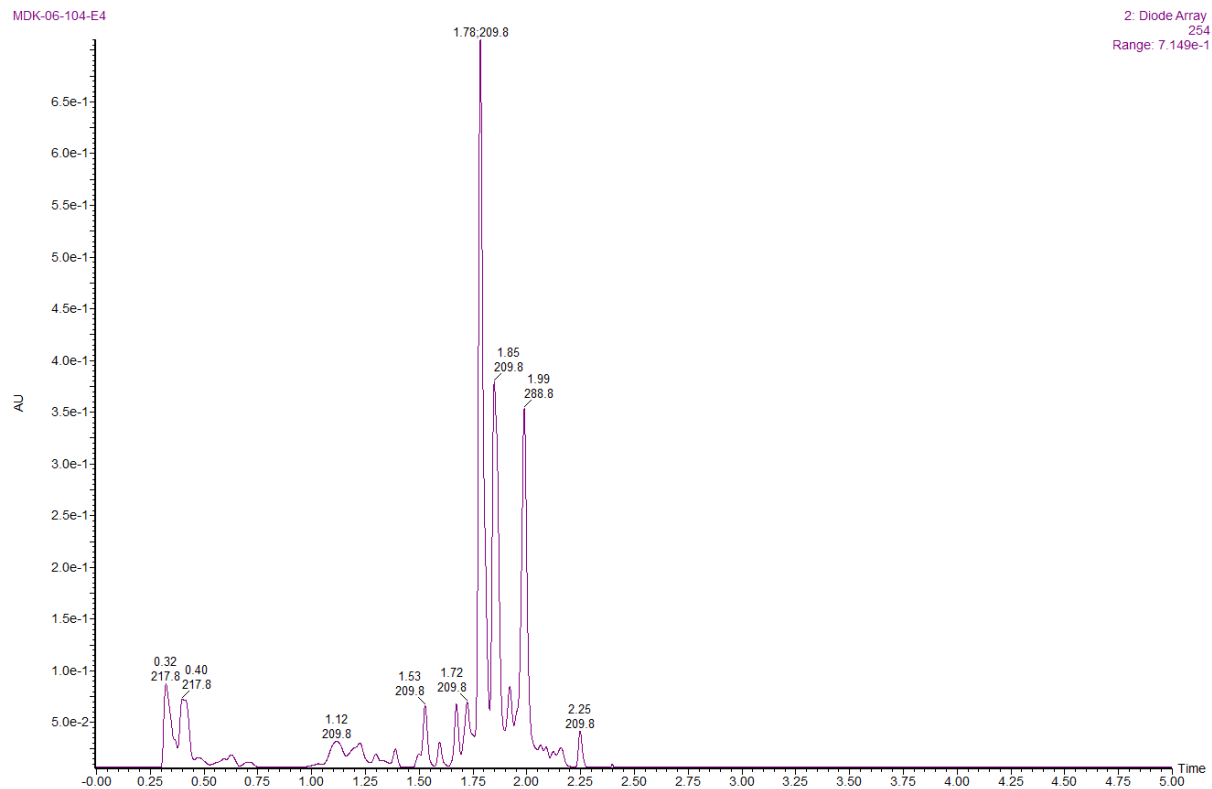
20180705-mdkubota-06-104-E3

2: Diode Array
254
Range: 2.184e-1



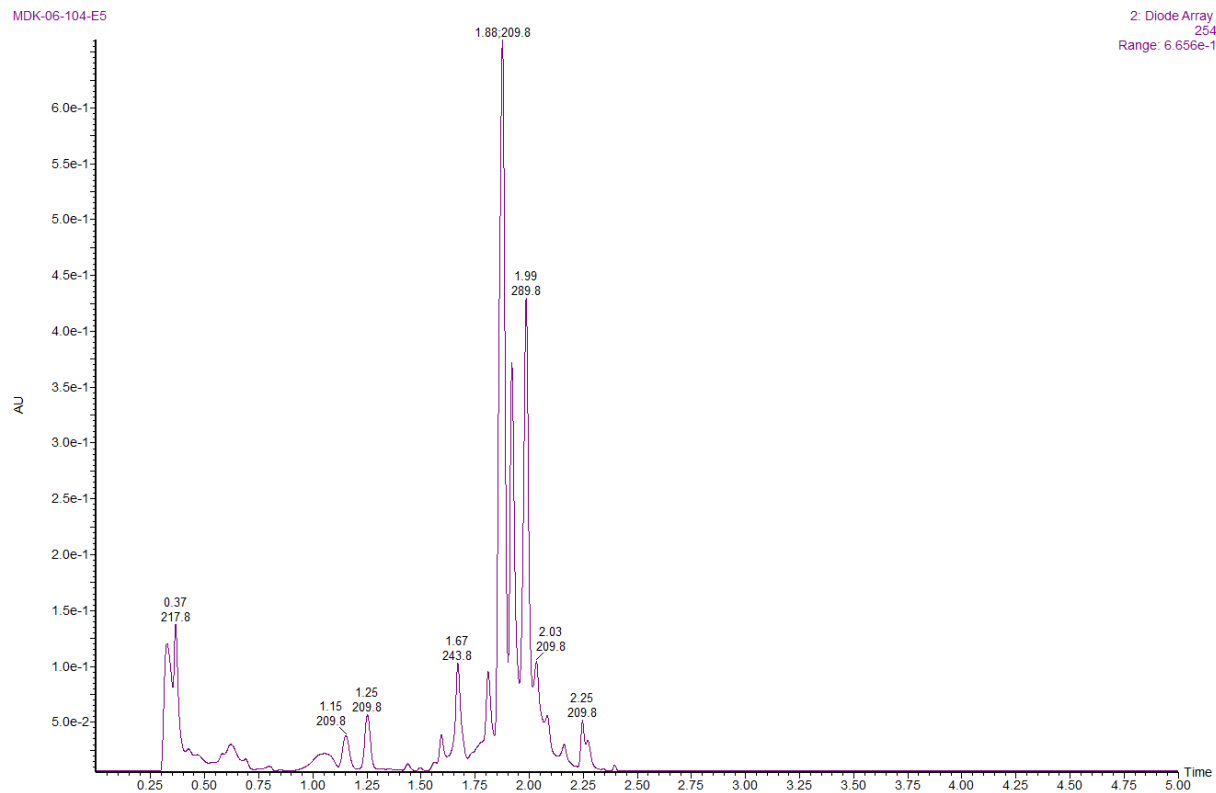
Tz-5 & 5-VC				
t	mass observed	exact mass		Product
0.43	292.07	292.09	M+Na	5-VC
1.83	686.27	686.27	M+Na	Tz-5 + 5-VC
1.87	435.53	435.18	M+Na	hydrolysis
1.99	435.32	435.18	M+Na	hydrolysis
2.03	445.30	445.17	M+Na	Tz-5

AB



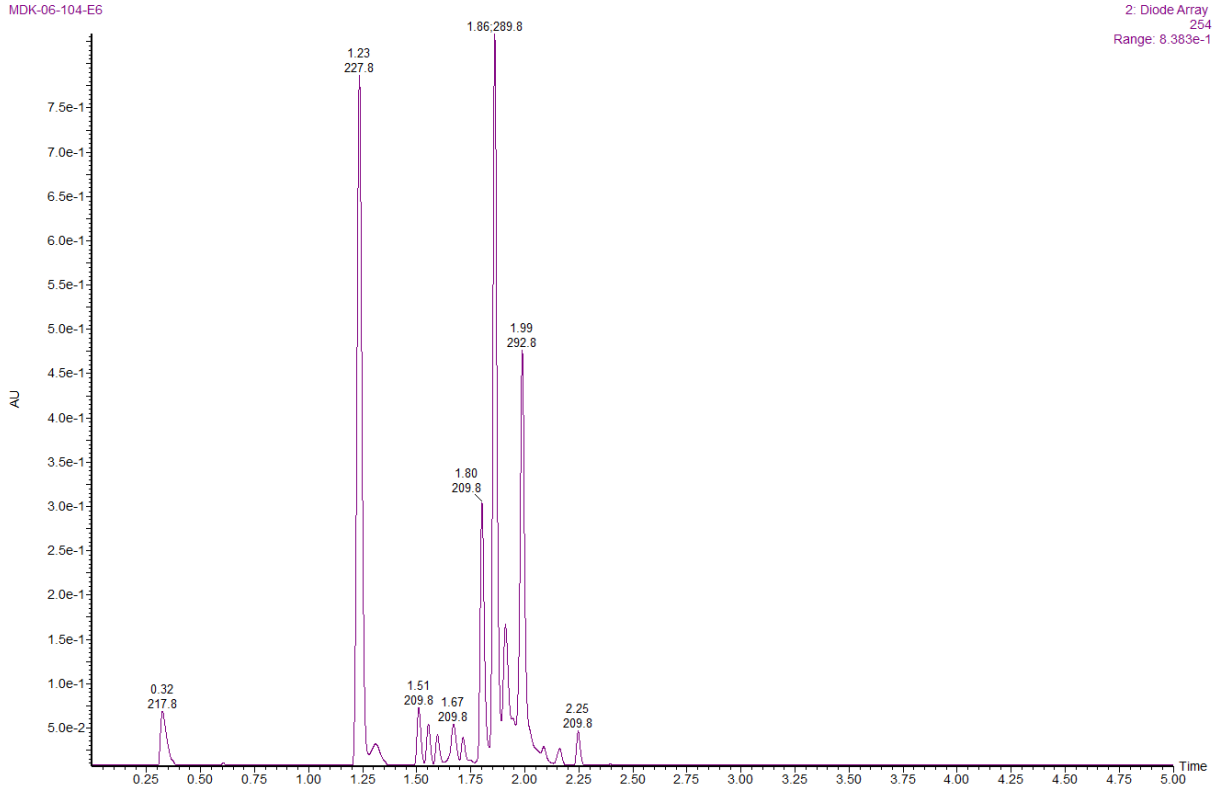
Tz-5 & 7-dVA				
t	mass observed	exact mass		Product
1.12	292.31	292.12	M	7-dVA
1.78	707.27	707.27	M+Na	Tz-5 + 7-dVA ox
1.85	707.27	707.27	M+Na	Tz-5 + 7-dVA ox
1.99	687.15	687.30	M+H	Tz-5 + 7-dVA

AC



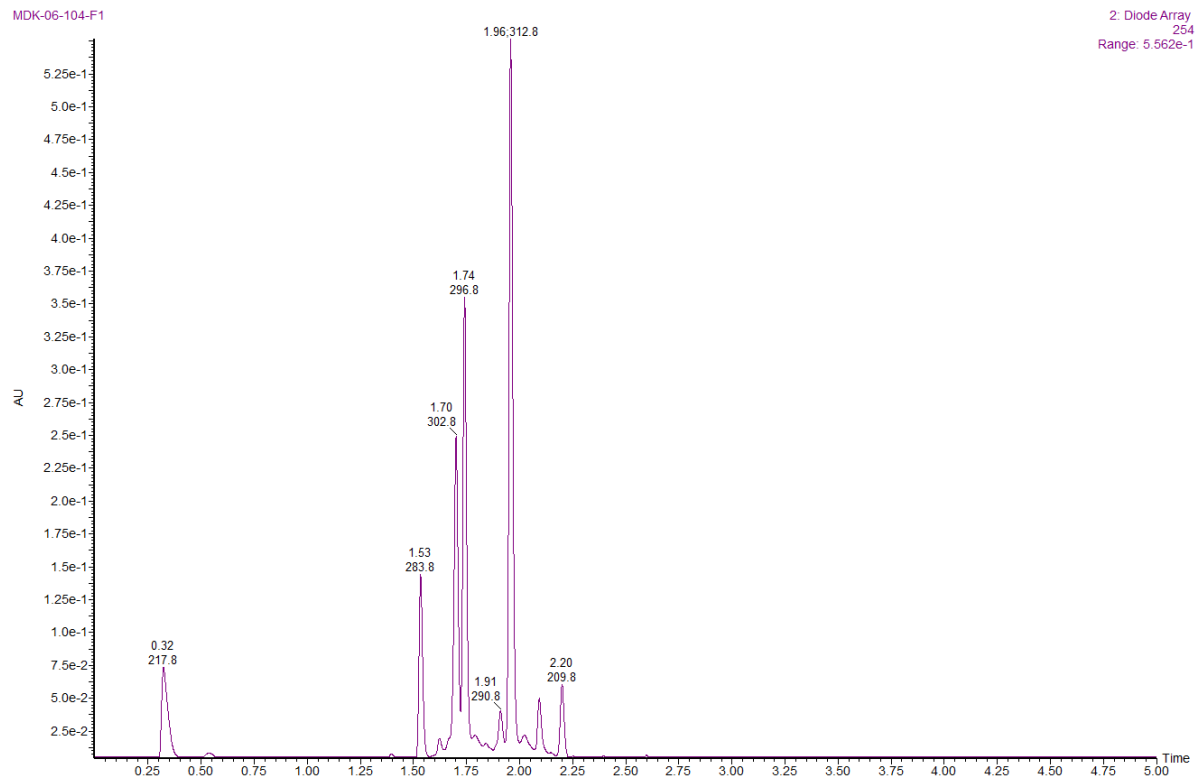
Tz-5 & 7-dVAb				
t	mass observed	exact mass		Product
1.88	435.19	435.18	M+Na	hydrolysis
1.89	555.24	555.26	M+H	Tz-5 + 7-dVAb
1.92	554.14	554.25	M	Tz-5 + 7-dVAb
2.03	445.15	445.15	M	Tz-5
2.08	553.20	553.24	M+H	Tz-5 + 7-dVAb ox

AD



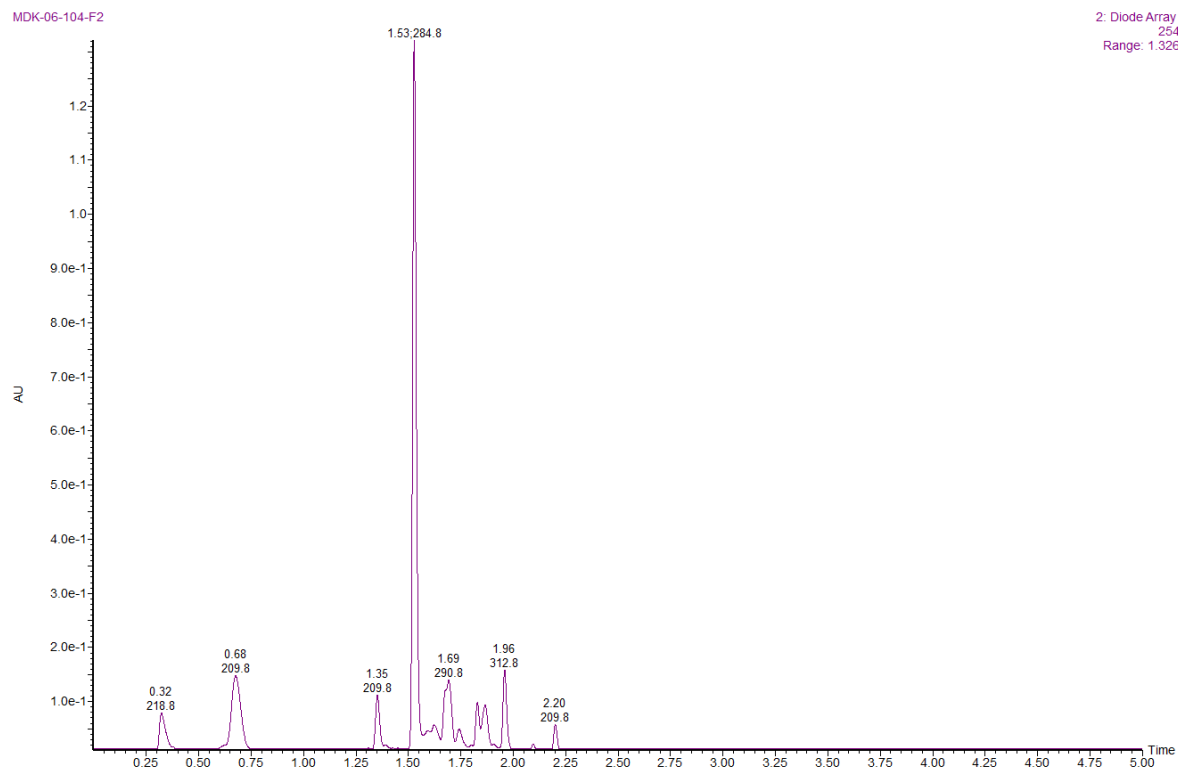
Tz-5 & 2-VA				
t	mass observed	exact mass		Product
1.23	294.14	294.14	M+H	2-VA
1.51	724.20	724.23	M+K	Tz-5 + 2-VA ox
1.80	708.16	708.26	M+Na	Tz-5 + 2-VA ox
1.86	686.18	686.28	M+H	Tz-5 + 2-VA ox
1.91	688.33	688.30	M+H	Tz-5 + 2-VA
1.99	435.23	435.18	M+Na	hydrolysis

AE



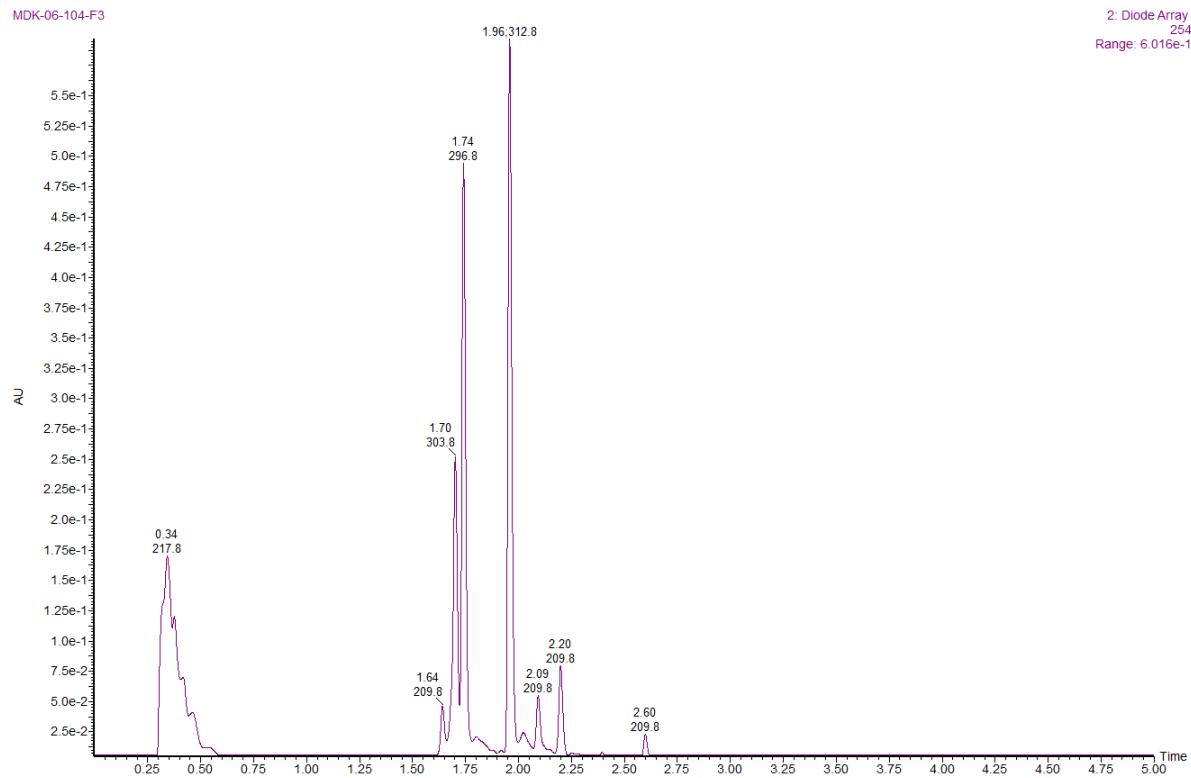
5-VUb & DP-Tz				
t	mass observed	exact mass		Product
1.53	367.18	367.09	M+Na	DP-Tz + 5-VUb ox
1.70	249.05	249.07	M+Na	hydrolysis
1.74	249.03	249.07	M+Na	hydrolysis
1.96	249.05	249.07	M+Na	hydrolysis

AF



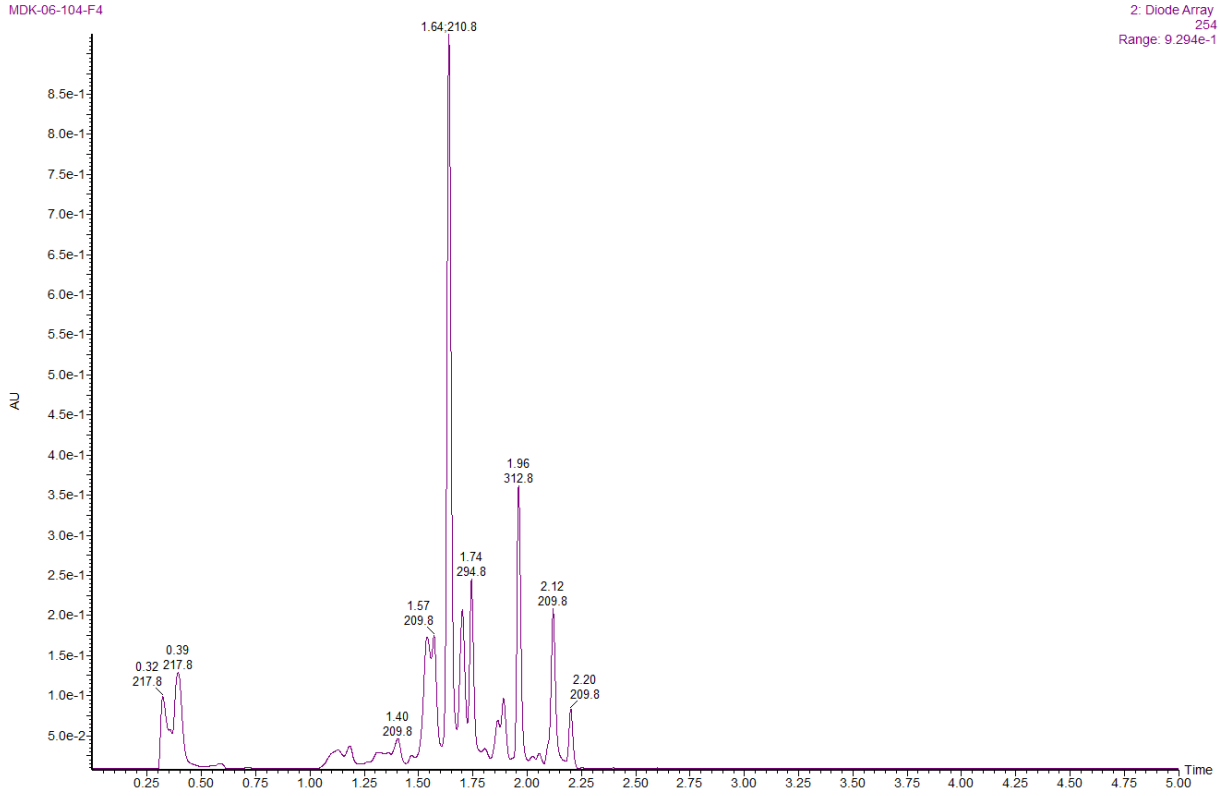
5-VU & DP-Tz				
t	mass observed	exact mass		Product
1.35	499.07	499.13	M+Na	DP-Tz + 5-VU ox
1.53	499.11	499.13	M+Na	DP-Tz + 5-VU ox
1.69	249.05	249.07	M+Na	hydrolysis
1.74	258.95	259.07	M+Na	DP-Tz
1.83	501.05	501.15	M+Na	DP-Tz + 5-VU
1.96	249.01	249.07	M+Na	hydrolysis

AG



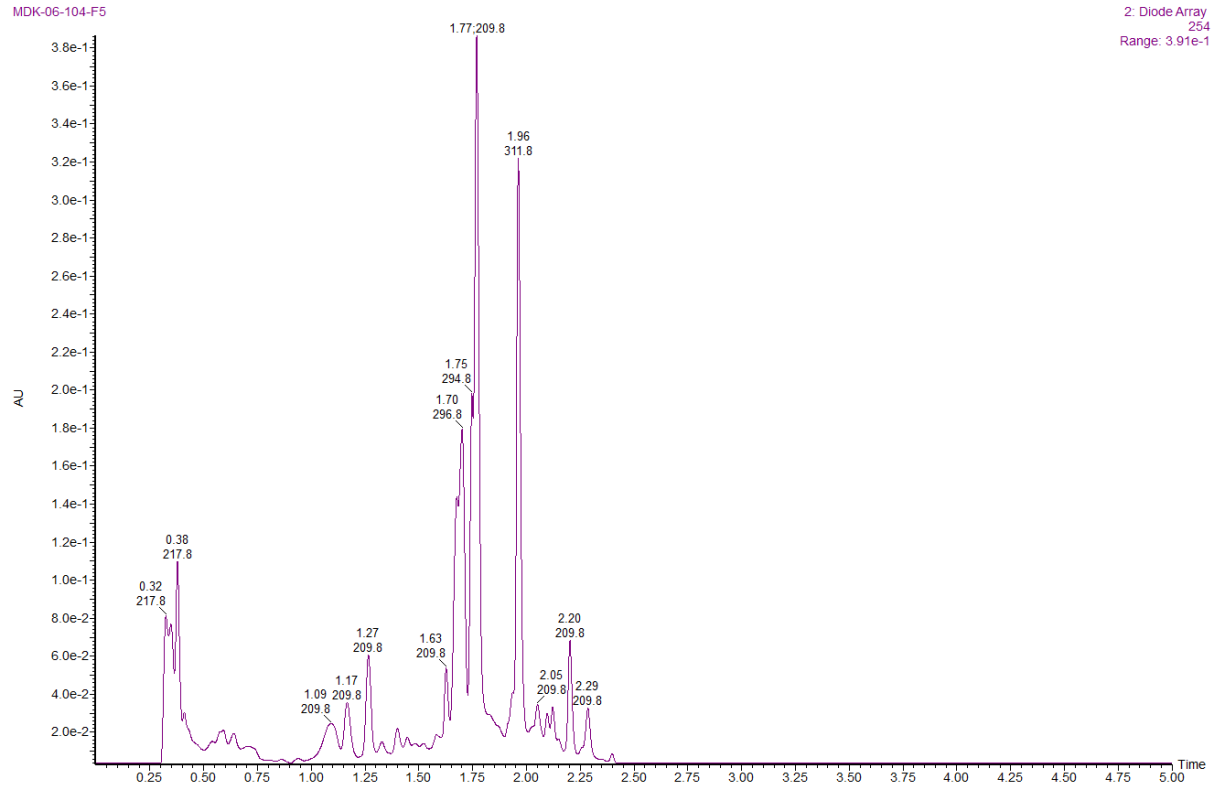
5-VC & DP-Tz				
t	mass observed	exact mass		Product
1.64	500.20	500.17	M+Na	DP-Tz + 5-VC
1.70	475.15	475.16	M+Na	DP-Tz + 5-VC ox
1.74	260.00	259.07	M+Na	DP-Tz
1.96	249.05	249.07	M+Na	hydrolysis
2.19	249.02	249.07	M+Na	hydrolysis

AH



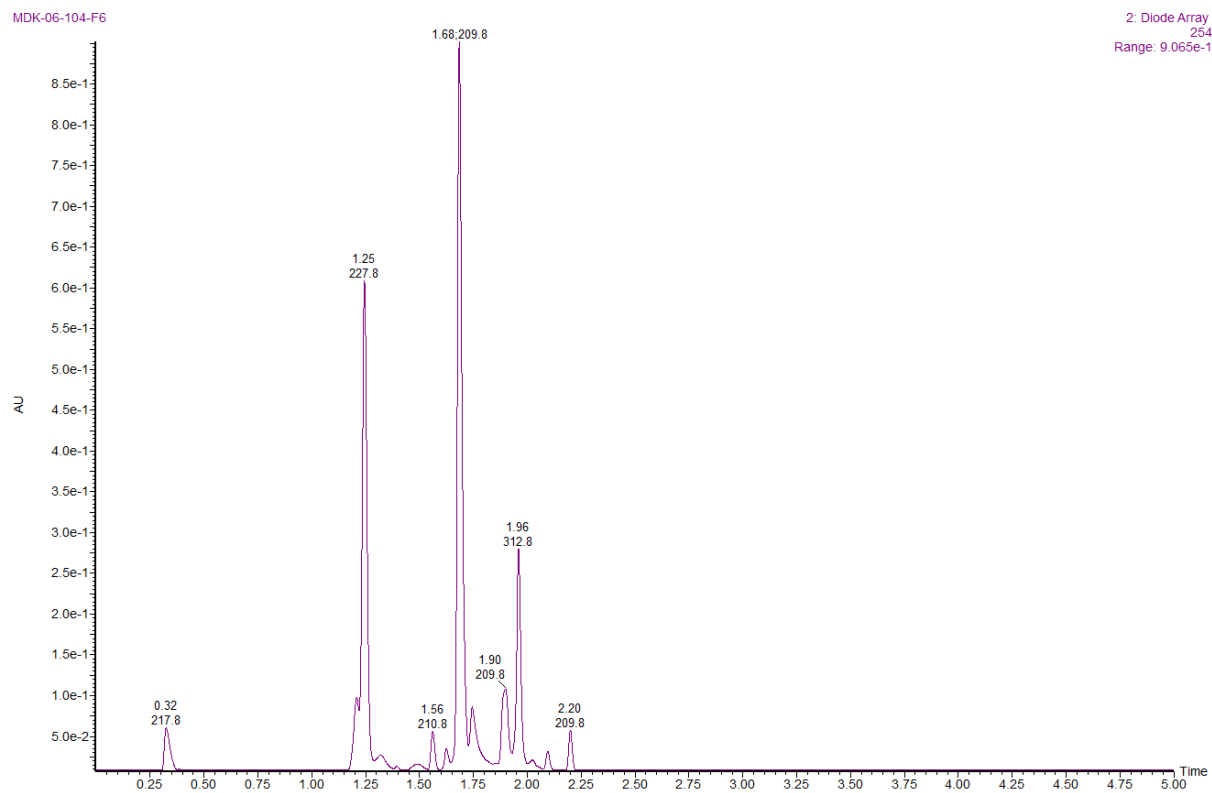
7-dVA & DP-Tz				
t	mass observed	exact mass		Product
1.57	293.06	293.03	M+H	7-dVA
1.64	521.22	521.17	M+Na	DP-Tz + 7-dVA ox
1.70	249.01	249.07	M+Na	hydrolysis
1.74	259.04	259.07	M+Na	Dp-Tz
1.89	501.38	501.20	M+H	DP-Tz + 7-dVA
1.96	249.01	249.07	M+Na	hydrolysis
2.12	501.22	501.20	M+H	DP-Tz + 7-dVA

AI



7-dVAb & DPTz				
t	mass observed	exact mass		Product
1.08	227.05	227.10	M+H	hydrolysis
1.70	249.05	249.07	M+Na	hydrolysis
1.75	259.08	259.07	M+Na	Dp-Tz
1.77	389.12	389.12	M+Na	DP-Tz + 7-dVAb ox
1.96	249.01	249.07	M+Na	hydrolysis

AJ



2-VA & DP-Tz				
t	mass observed	exact mass		Product
1.25	294.15	294.14	M+H	2-VA
1.56	502.44	502.20	M+H	DP-Tz + 2-VA
1.68	522.27	522.16	M+Na	DP-Tz + 2-VA ox
1.91	502.19	502.20	M+H	DP-Tz + 2-VA
1.96	249.10	249.07	M+Na	hydrolysis

Figure 2-S4. LC-MS analysis of reactions between tetrazines and nucleobase/nucleosides. Showing hydrolysis of tetrazines, cycloadducts between tetrazines and nucleobase/nucleosides, and oxidized products of cycloadducts. Multiple similar peaks explained by regioisomers formation. A) **Tz-1 + 5-VUb**, B) **Tz-1 + 5-VU**, C) **Tz-1 + 5-VC**, D) **Tz-1 + 7-dVA**, E) **Tz-1 + 7-dVAb**, F) **Tz-1 + 2-VA**, G) **Tz-2 + 5-VUb**, H) **Tz-2 + 5-VU**, I) **Tz-2 + 5-VC**, J) **Tz-2 + 7-dVA**, K) **Tz-2 + 7-dVAb**, L) **Tz-2 + 2-VA**, M) **Tz-3 + 5-VUb**, N) **Tz-3 + 5-VU**, O) **Tz-3 + 5-VC**, P) **Tz-3 + 7-dVA**, Q) **Tz-3 + 7-dVAb**, R) **Tz-3 + 2-VA**, S) **Tz-4 + 5-VUb**, T) **Tz-4 + 5-VU**, U) **Tz-4 + 5-VC**, V) **Tz-4 + 7-dVA**, W) **Tz-4 + 7-dVAb**, X) **Tz-4 + 2-VA**, Y) **Tz-5 + 5-VUb**, Z) **Tz-5 + 5-VU**, AA) **Tz-5 + 5-VC**, AB) **Tz-5 + 7-dVA**, AC) **Tz-5 + 7-dVAb**, AD) **Tz-5 + 2-VA**, AE) **DP-Tz + 5-VUb**, AF) **DP-Tz + 5-VU**, AG) **DP-Tz + 5-VC**, AH) **DP-Tz + 7-dVA**, AI) **DP-Tz + 7-dVAb**, AJ) **DP-Tz + 2-VA**.

Below are HOMO LUMO and Transition State Diagrams for Figure S5: Structures by Calculation

Figure 2-S5A.

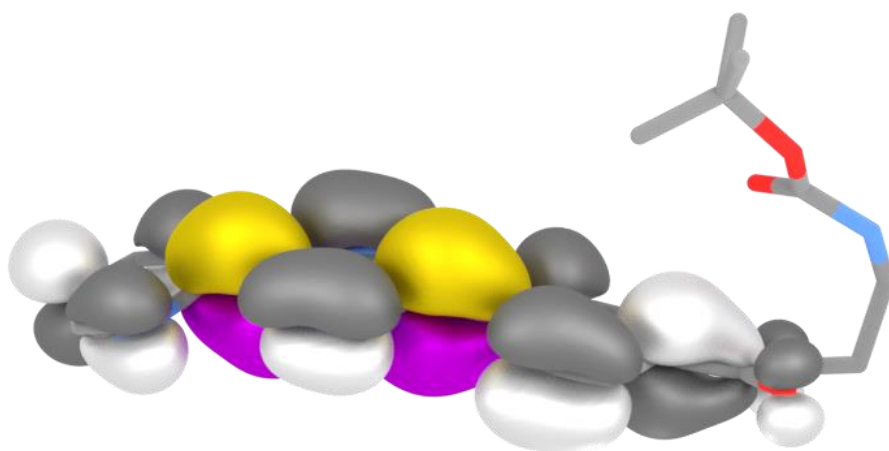
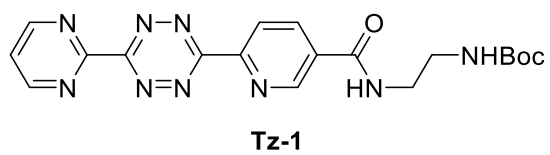


Figure 2-S5B.

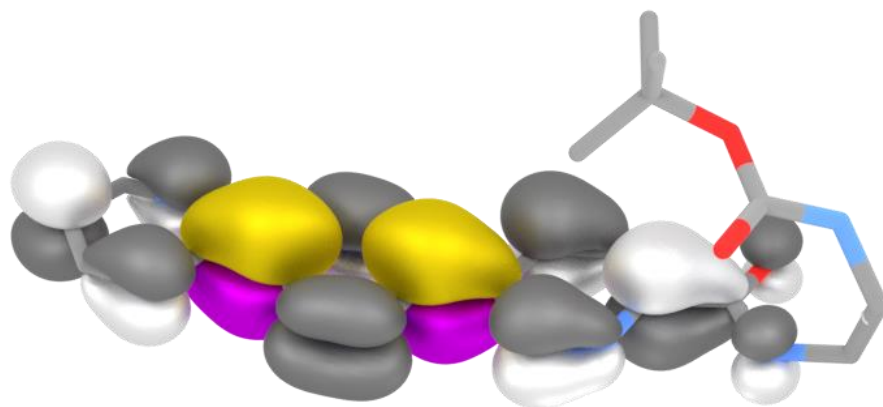
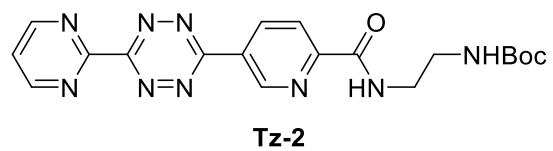


Figure 2-S5C.

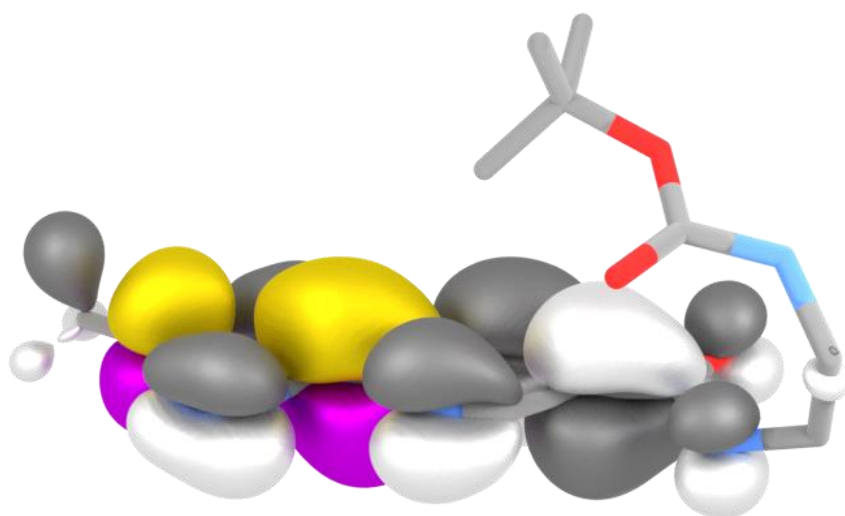
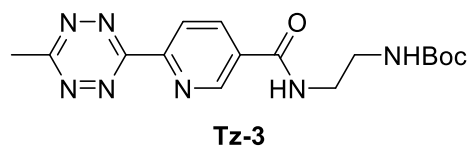


Figure 2-S5D.

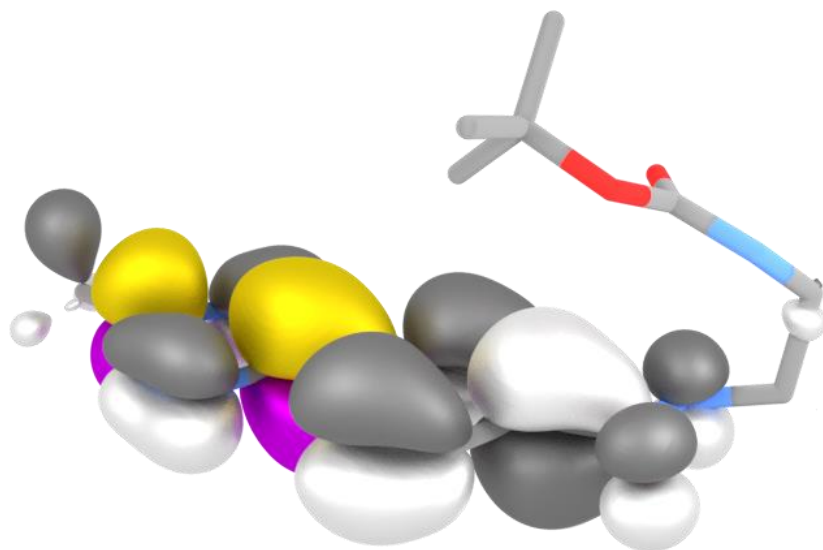
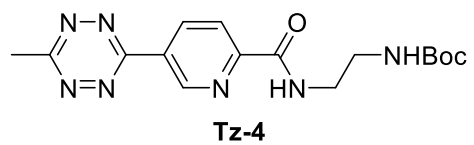


Figure 2-S5E.

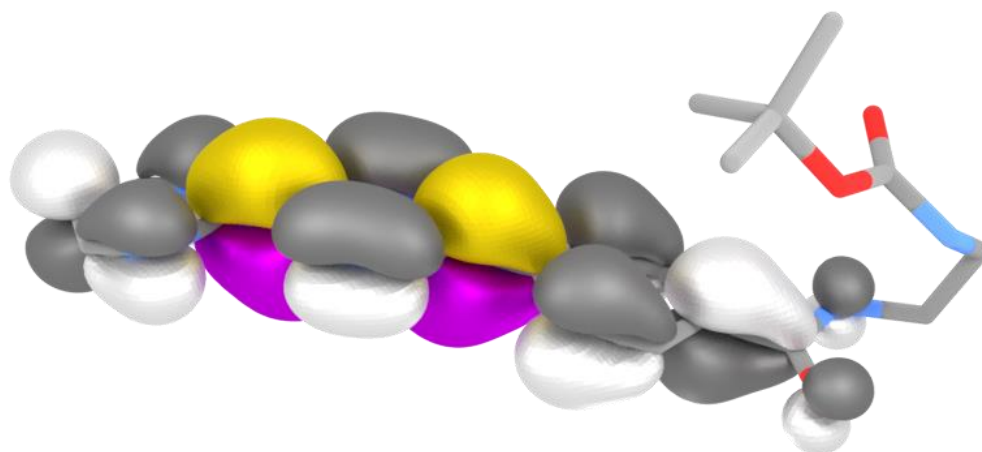
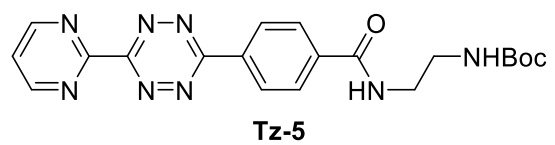


Figure 2-S5F.

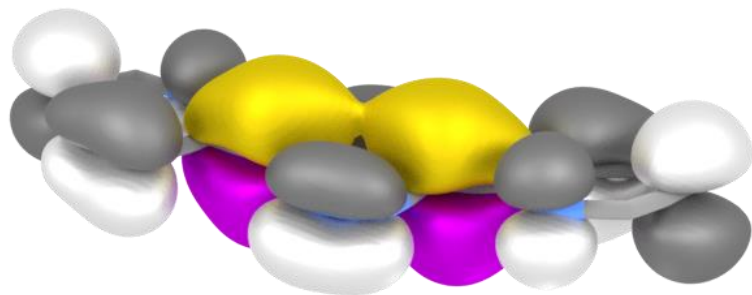
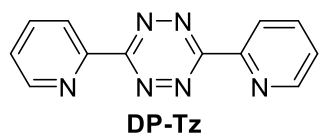


Figure 2-S5G.

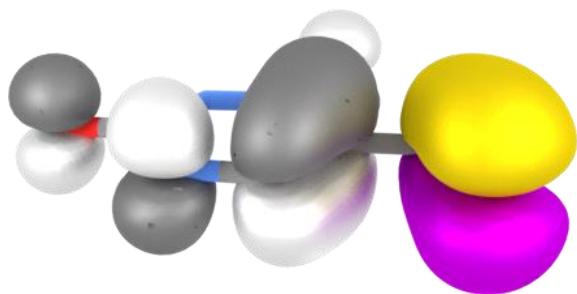
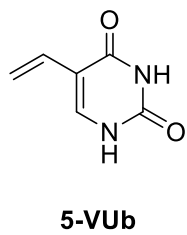


Figure 2-S5H.

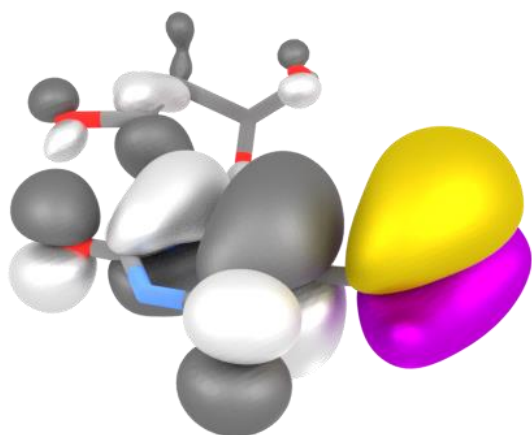
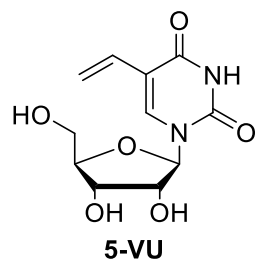


Figure 2-S5I.

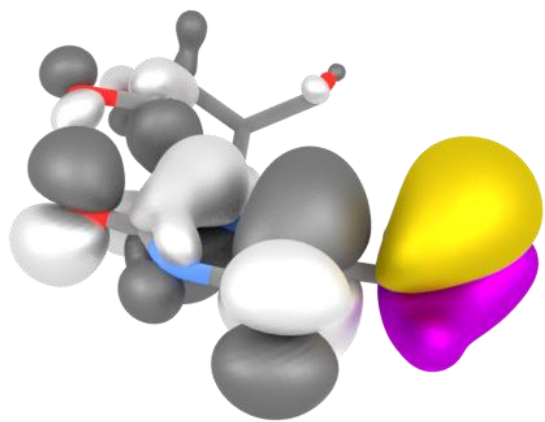
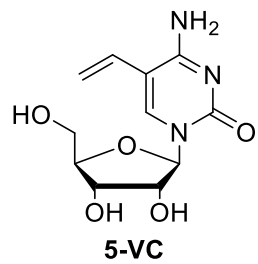


Figure 2-S5J.

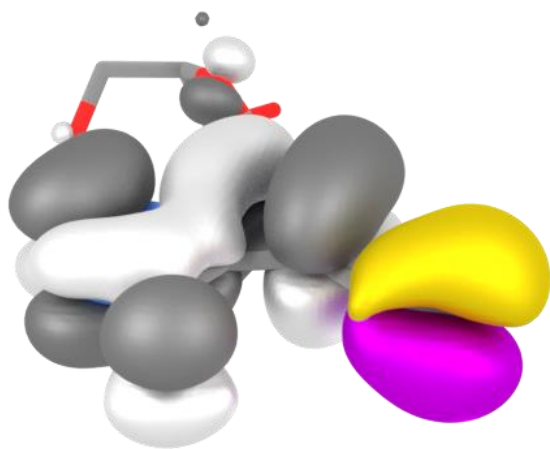
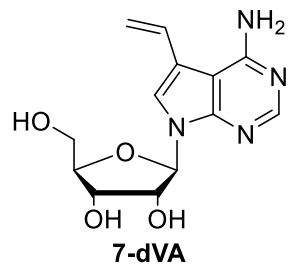
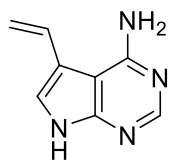


Figure 2-S5K.



7-dVAb

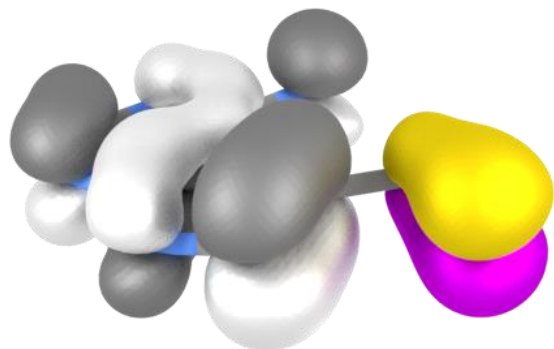
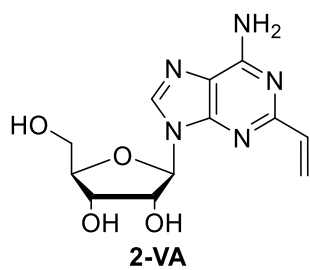
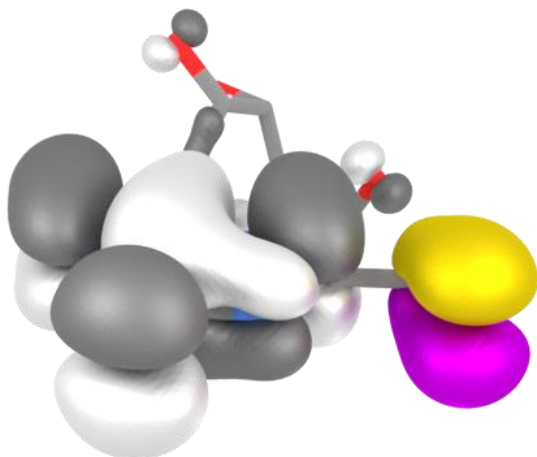


Figure 2-S5L.



2-VA



Transition States by Computation

Figure 2-S5M.

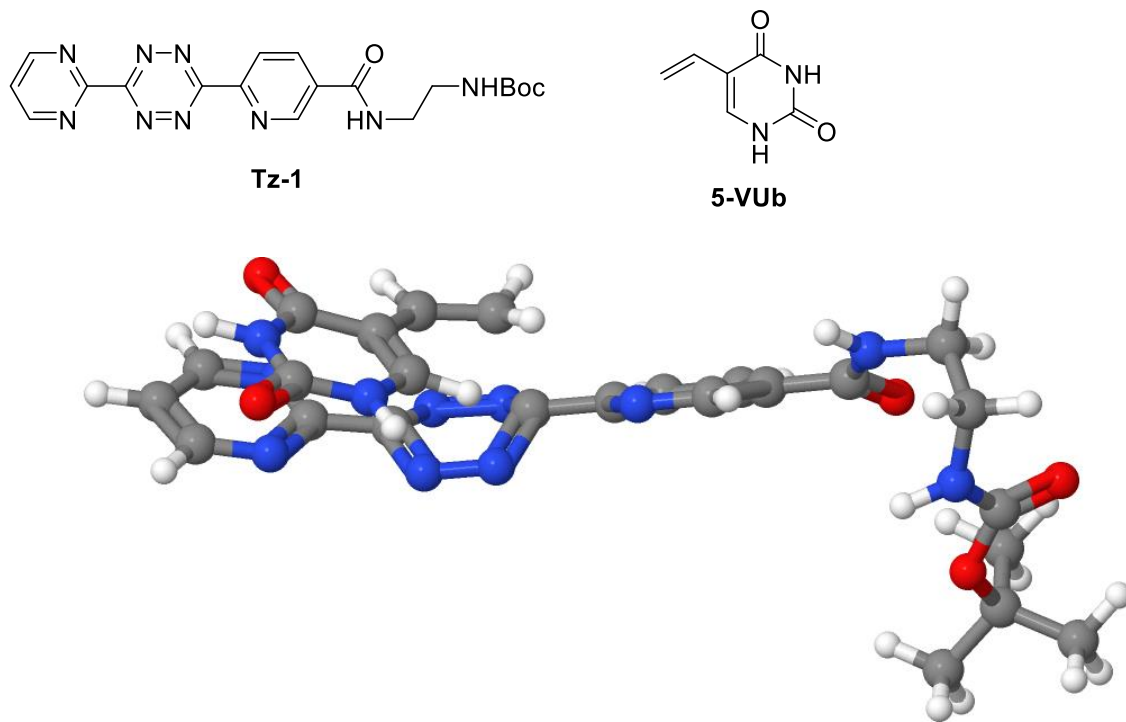


Figure 2-S5N.

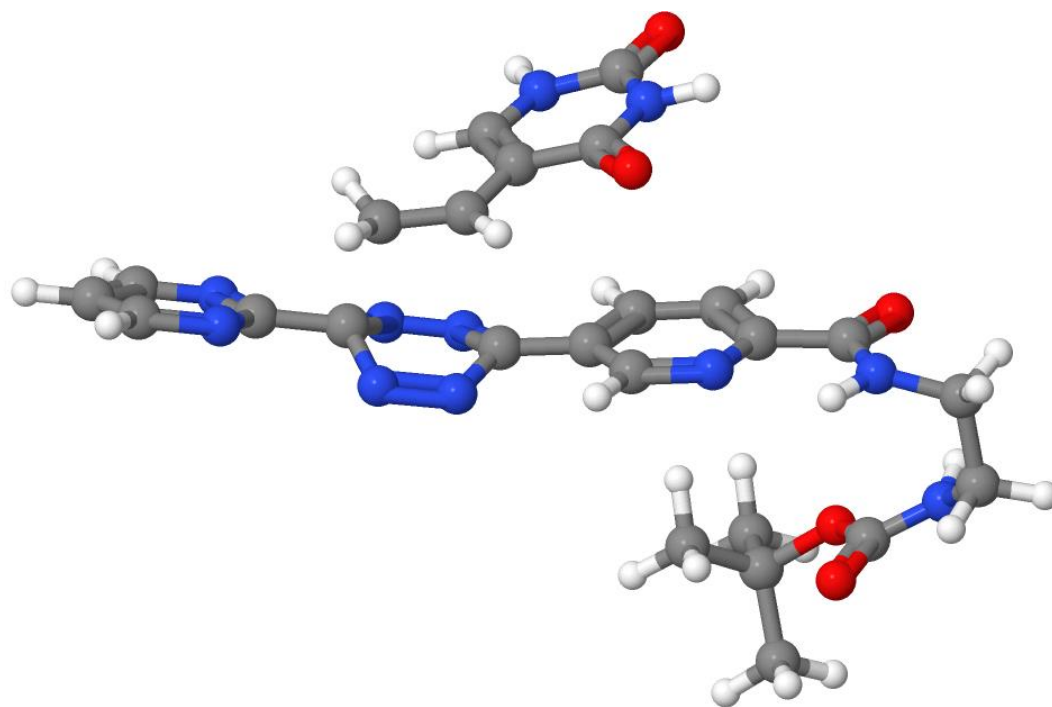
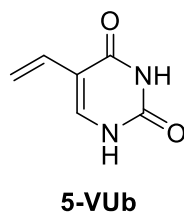
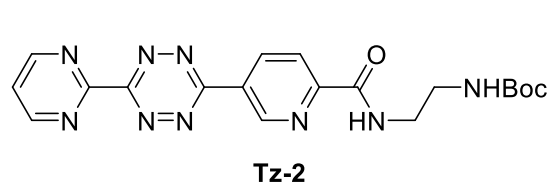
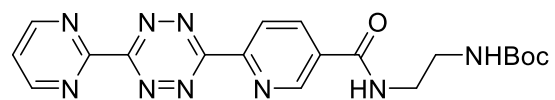
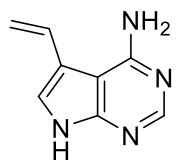


Figure 2-S50.



Tz-1



7-dVAb

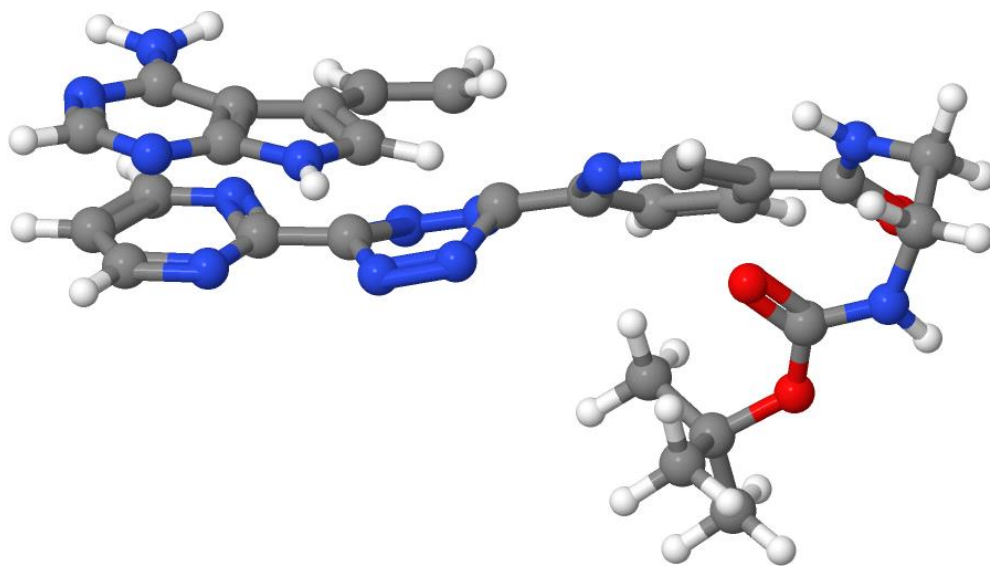


Figure 2-S5P.

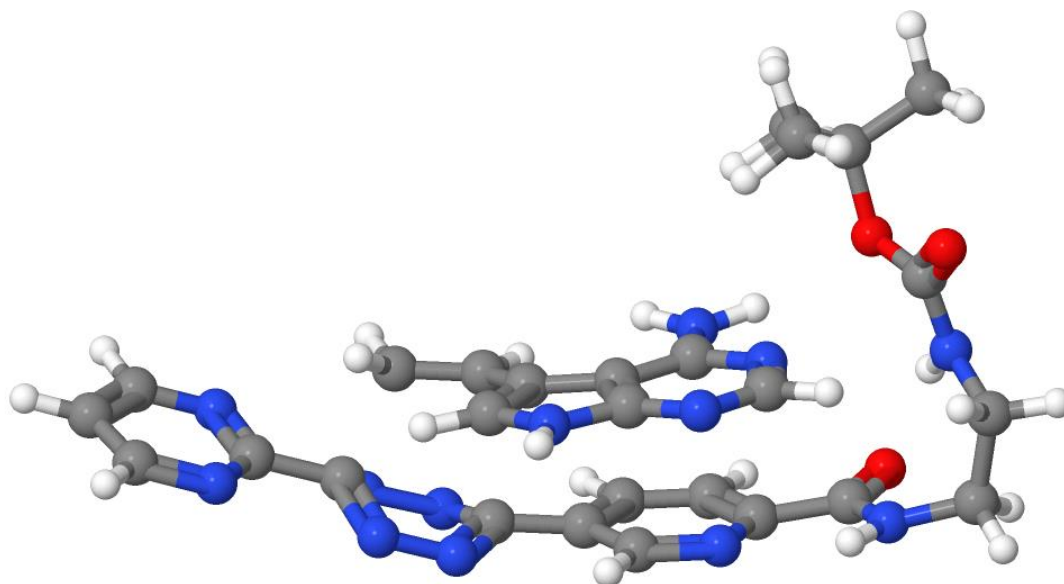
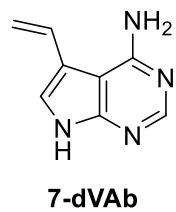
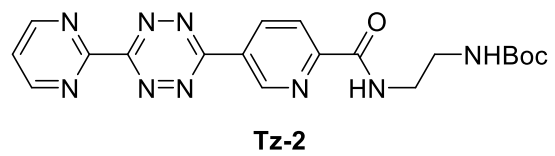
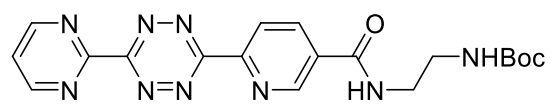
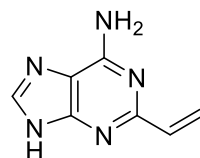


Figure 2-S5Q.



Tz-1



2-VAb

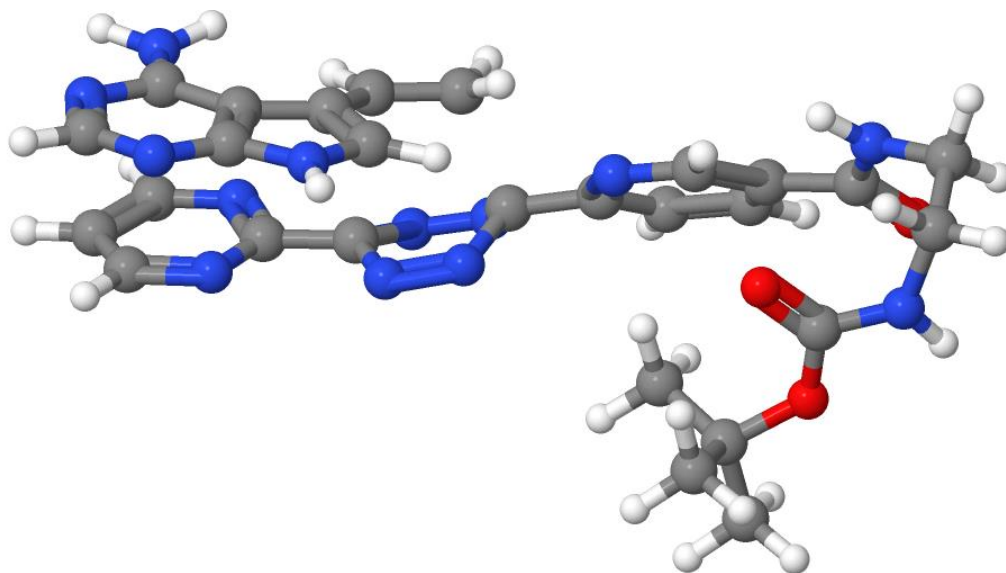


Figure 2-S5R.

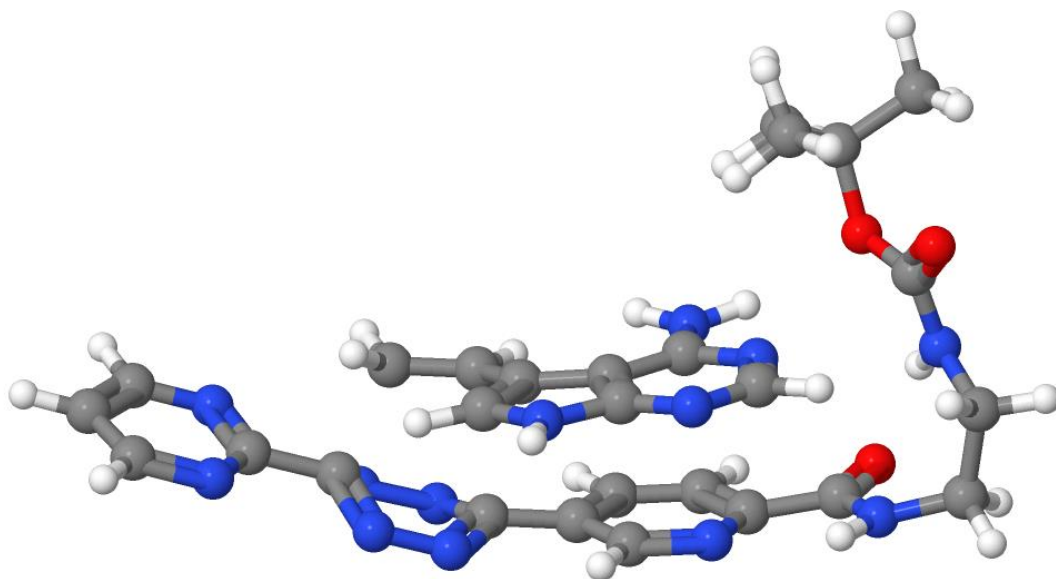
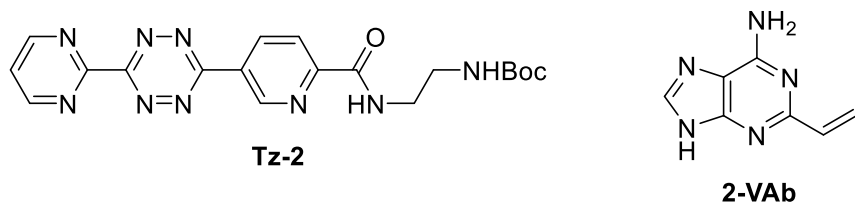


Figure 2-S5. Plot of the LUMO+1 isosurface (isovalence 0.02) of Tetrazines with positive isosurfaces colored gray (IEDDA inactive lobes) and violet (IEDDA active lobes) and negative isosurfaces colored white (IEDDA inactive lobes) and yellow (IEDDA active lobes). A) **Tz-1** B) **Tz-2** C) **Tz-3** D) **Tz-4** E) **Tz-5** F) **DP-Tz**. Plot of the HOMO isosurface (isovalence 0.02) of vinyl-nucleosides and vinyl-nucleobases with positive isosurfaces colored gray (IEDDA inactive lobes) and violet (IEDDA active lobes) and negative isosurfaces colored white (IEDDA inactive lobes) and yellow (IEDDA active lobes). G) **5-VU_b** H) **5-VU** I) **5-VC** J) **7-dVA** K) **7-dVAb** L) **2-VA** Computational analysis of transition states. M) **Tz-1 + 5-VU_b** N) **Tz-2 + 5-VU_b** O) **Tz-1 + 7-dVAb** P) **Tz-2 + 7-dVAb** Q) **Tz-1 + 2-VAb** R) **Tz-2 + 2-VAb** Transition state showing two distinct bond lengths, d_1 and d_2 S) **DP-Tz + 5-VU_b** T) Arrhenius plot comparing rate constants measured in DMSO with computed free energy barriers

Figure 2-S5S.

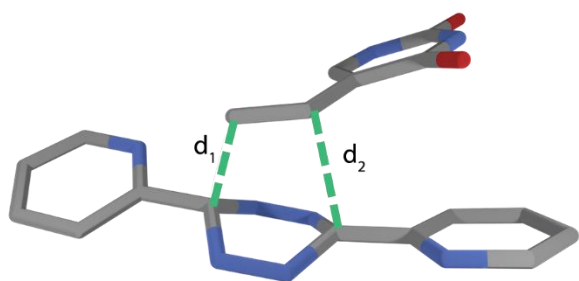


Figure 2-S5T.

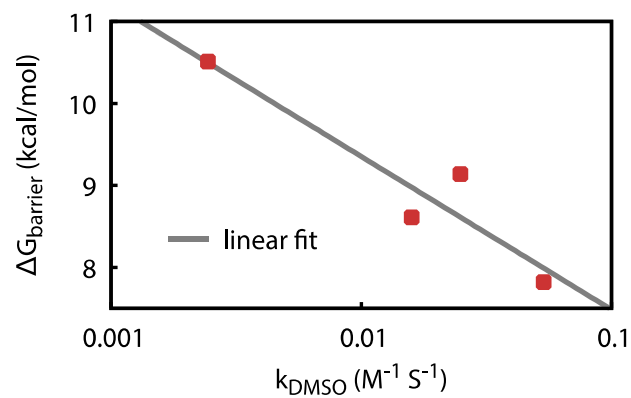


Table 2-S1.

	5-VUb	7-dVAb	2-VAb
Tz-1	9.14	7.82	10.45
Tz-2	10.51	8.61	11.68

Table 2-S21. shows the lowest free energy barrier found for each tetrazine-vinyl nucleobase pair,

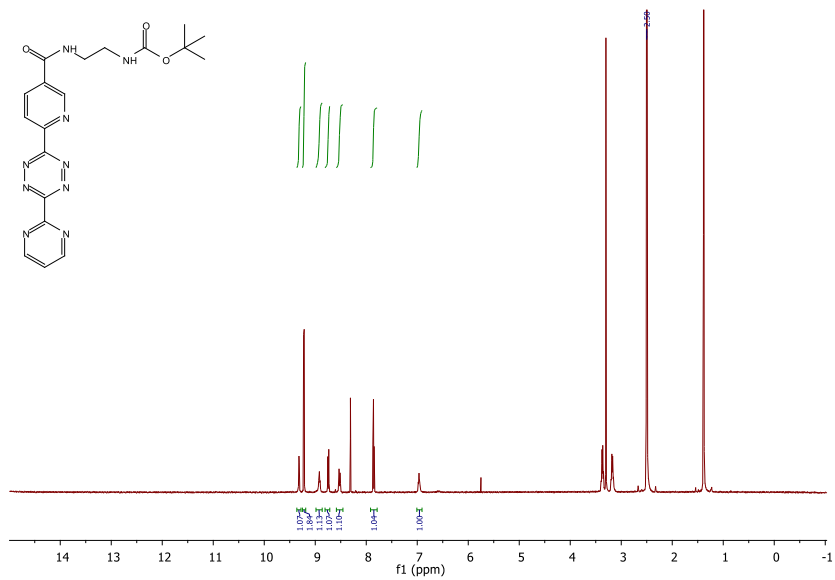
$$\Delta G_{\text{barrier}} = \Delta G_{\text{TS}} - \Delta G_{\text{complex}}$$

where ΔG_{TS} and $\Delta G_{\text{complex}}$ are the free energies of the transition state and initial complex, respectively. In contrast to the driving forces derived from the HOMO-LUMO+1 gap, the computed barriers reproduce all observed trends in reactivity, i.e., **tz1** > **tz2** and **7-dVAb** > **5-VUb**. Furthermore, the estimated relative rates of, for example, the **Tz-1-5-VUb** reaction compared to the **Tz-2-5-VUb** reaction, agree well with experiment: **Tz-1** was estimated to be faster than **Tz-2** by factors of 10.1 and 3.7 for the reactions with **5-VUb** and **7-dVAb**, respectively, compared to factors of 10 and 2.2 measured experimentally. This stands in stark contrast to the results from HOMO-LUMO+1 driving forces, in which essentially no difference in reactivity between **Tz-1** and **Tz-2** is predicted.

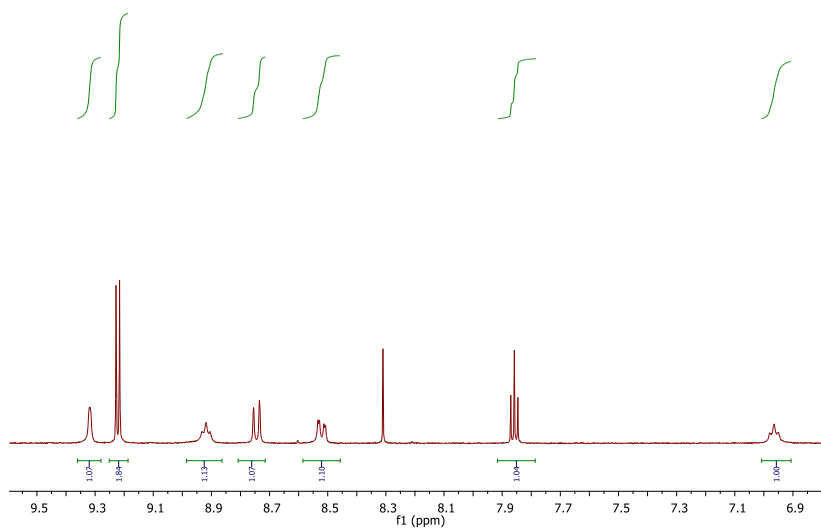
Table 2-S2. Free energy ($\Delta G_{\text{barrier}}$ in kcal/mol) of the lowest reaction barrier computed for each tetrazine-vinylnucleotide pair

Tetrazine Hydrolysis Analysis

A



B



C

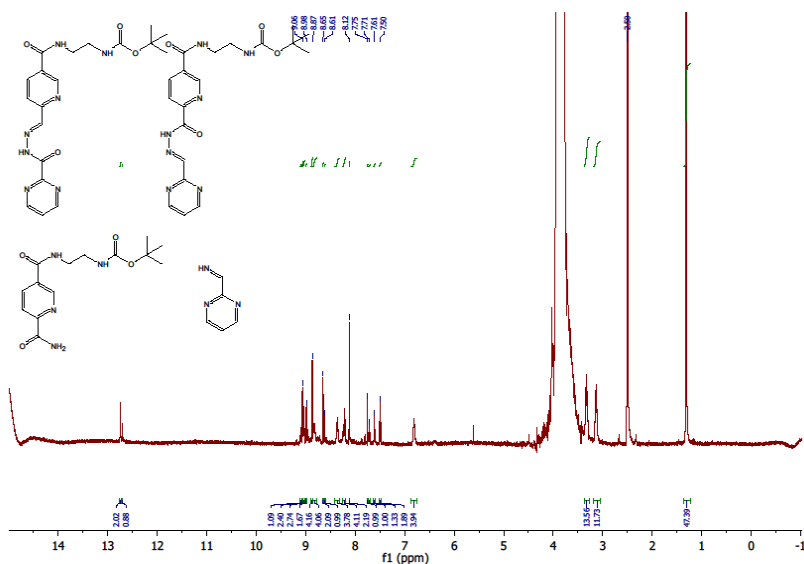


Figure 2-S6. ¹H NMR analysis of Tz-1 hydrolysis. A) initial ¹H NMR of Tz-1. B) initial ¹H NMR of Tz-1 with zoom on aromatic region. C) ¹H NMR of Tz-1 after water addition showing hydrazide regioisomers.

Trypan Blue Exclusion Assay of 5-EU and 5-VU

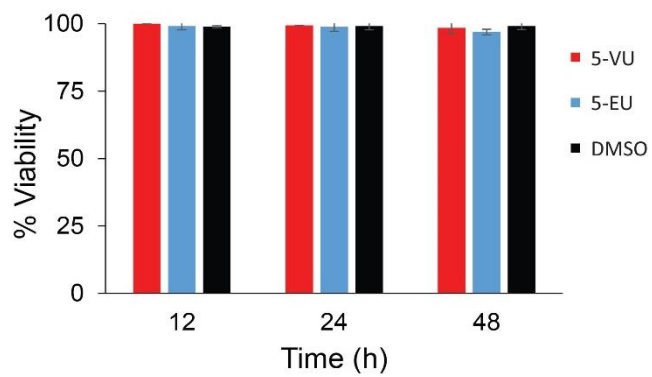


Figure 2-S7. Trypan Blue Exclusion assay cells treated with **5-VU** and **5-EU** for 12, 24, and 48 h.

MTT Assay of Vinyl-nucleosides

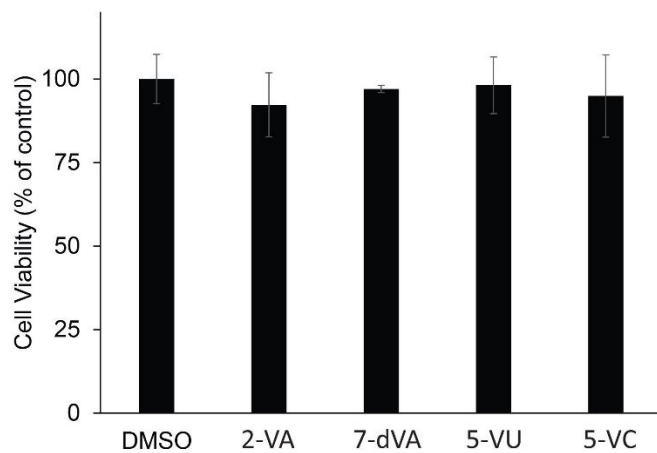
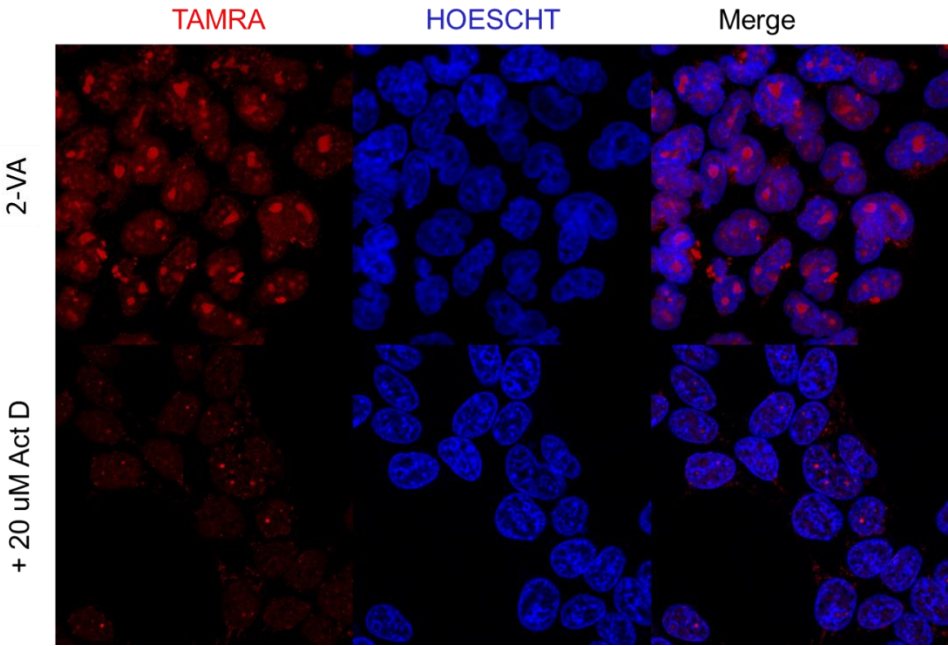


Figure 2-S8. MTT viability assay of cells treated for 12 h with 1 mM of each analog, normalized to the DMSO treated control. Vinyl-nucleosides are not cytotoxic to cells at 48 h.

Cell Imaging with 2-VA and 7-dVA

A



B

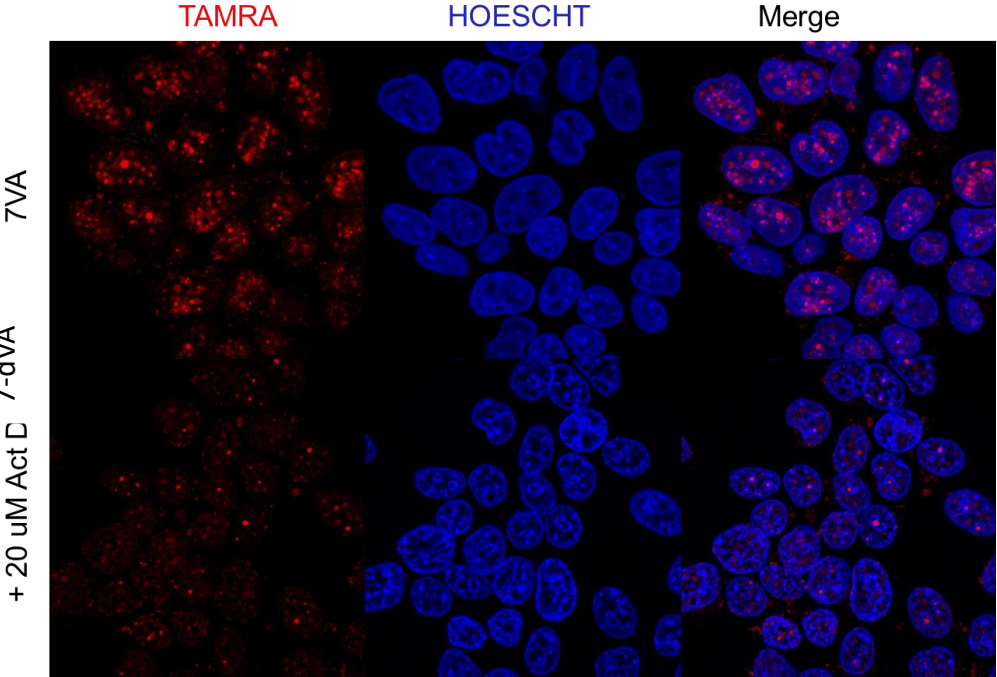


Figure 2-S9. Fluorescent imaging of **2-VA** (A) and **7-dVA** (B) in HEK293T cells. **TAMRA-Tz-3** was reacted with vinyl incorporated RNA for 2 h at 37 °C. Nucleus was stained with HOESCHT. Addition of 20 μ M actinomycin D revealed loss of fluorescent signal revealing vinyl-nucleosides are incorporated through polymerase I/II.

Mutually Orthogonal Bioorthogonal Chemistries Experiments

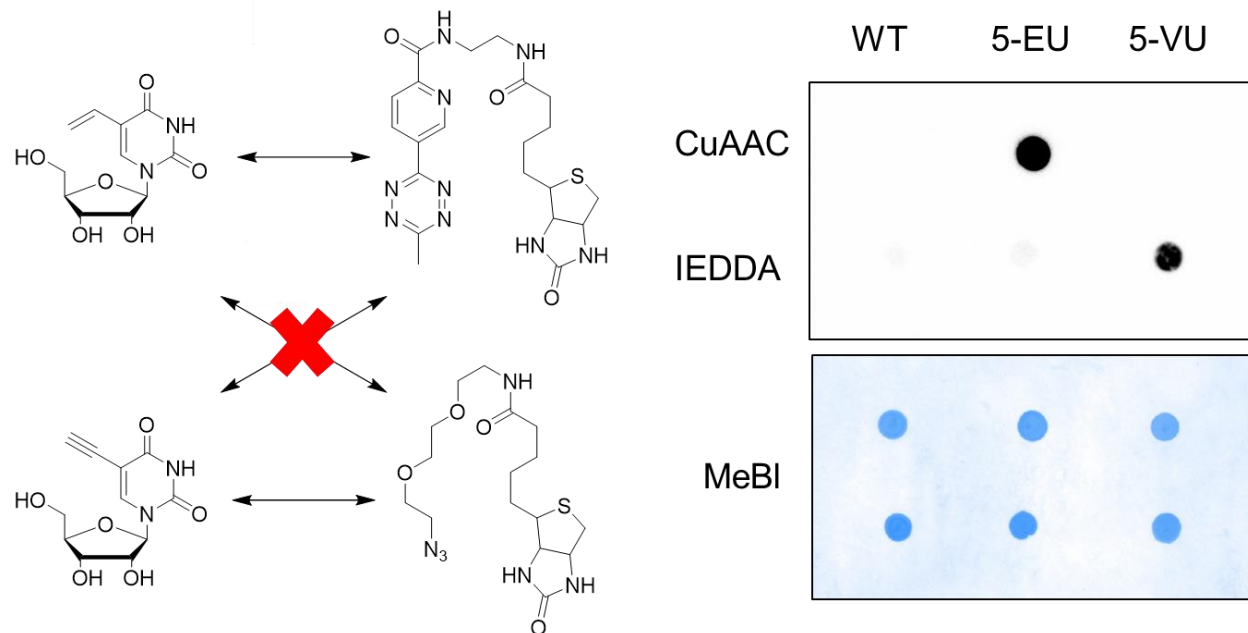
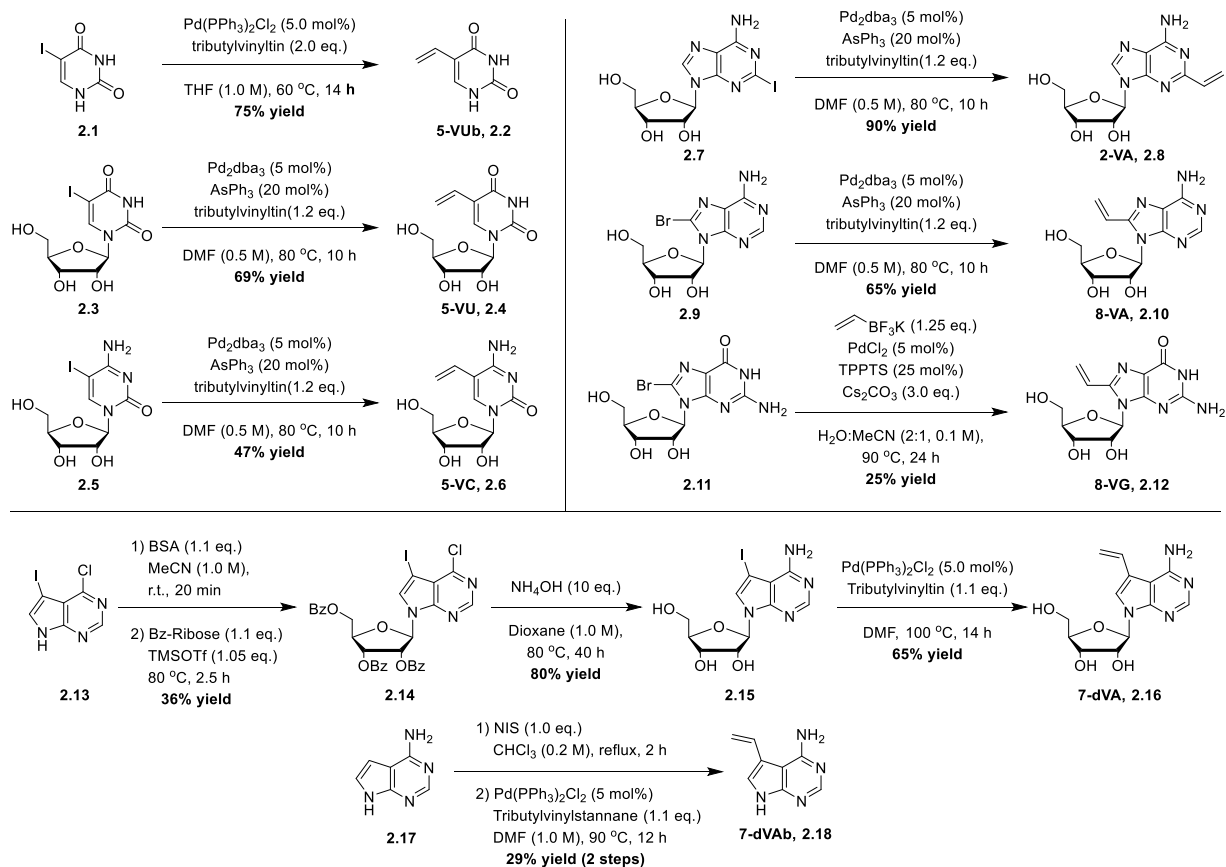


Figure 2-S10. Mutually orthogonal bioorthogonal chemistries. HEK239T cells were incubated with **5-EU** or **5-VU** and RNA was isolated. The RNA was then reacted with biotin-azide and **Biotin-Tz-4** resulting in specific reactions between CuAAC and IEDDA chemical partners as shown by dot blot analysis.

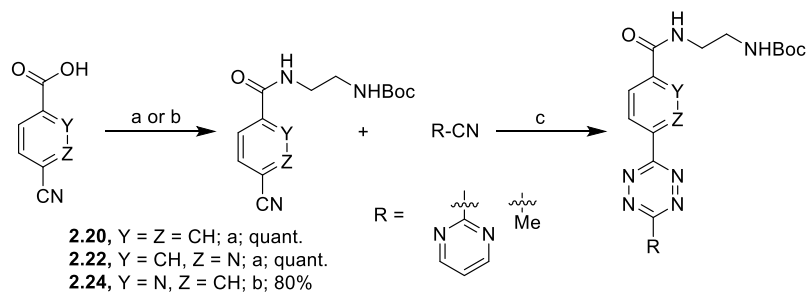
General Synthetic Methods

Compounds 2.2¹² and 2.30¹³ were synthesized as previously reported. Compounds 2.25-2.29 were synthesized following previously reported methods¹⁴⁻¹⁶. All reagents were purchased from commercial suppliers and were of analytical grade and used without further purification unless otherwise noted. Reaction progress was monitored by thin-layer chromatography on EMD 60 F254 plates, visualized with UV light. Compounds were purified via flash column chromatography using Sorbent Technologies 60 Å 230 x 400 mesh silica gel or Teledyne ISCO CombiFlash System with RediSep Rf Media. Preparative reverse-phase HPLC was performed on a Rainin Dynamax equipped with a ZORBAX SB-C18 column (Agilent) with HPLC grade acetonitrile and 18 MΩ deionized water, each containing 0.1% trifluoroacetic acid. Anhydrous solvents dichloromethane (DCM), methanol (MeOH), dimethylformamide (DMF), tetrahydrofuran (THF), toluene (PhMe) were degassed and dried over molecular sieves. All reaction vessels were flame dried prior to use. NMR spectra were acquired with Bruker Advanced spectrometers. All reactions were carried in dark unless otherwise noted. All spectra were acquired at 298 K. ¹H-NMR spectra were acquired at 400 MHz and 500 MHz. ¹³C-NMR spectra were acquired at 125 MHz. Chemical shifts are reported in ppm relative to residual non-deuterated NMR solvent, and coupling constants (J) are provided in Hz. All NMR spectra was analyzed using MestreNova software. Low and high-resolution electrospray ionization (ESI) mass were collected at the University of California-Irvine Mass Spectrometry Facility. The abbreviations used can be found in the document JOC standard Abbreviations and Acronyms, <http://pubs.acs.org/paragonplus>

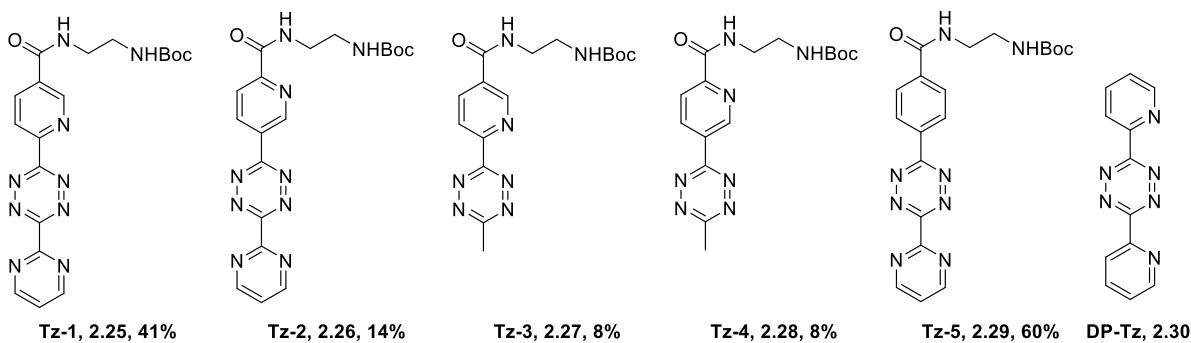
Synthetic Procedures



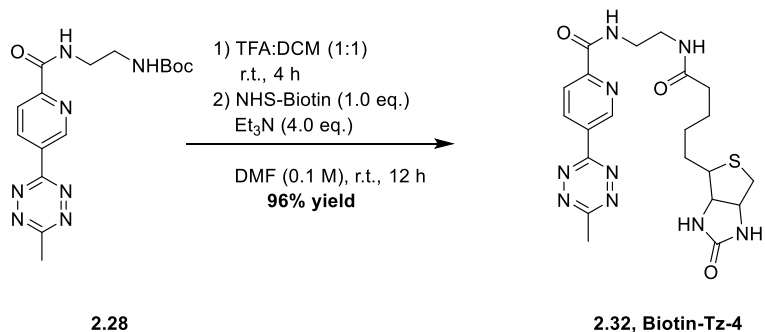
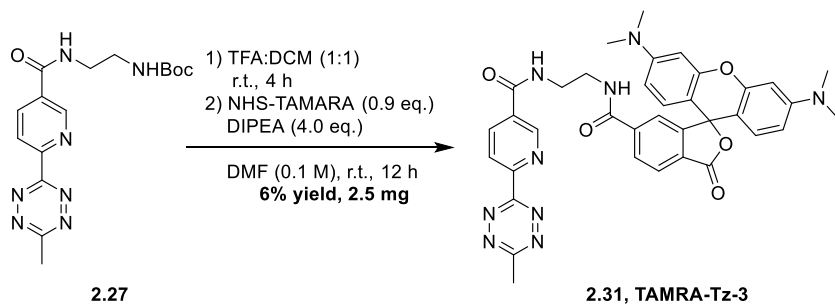
Scheme 2-1. Vinyl-Nucleoside Synthetic Scheme.



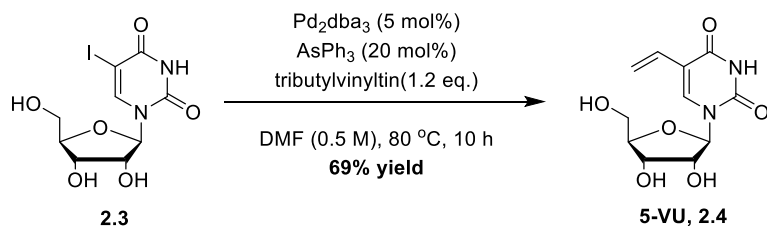
a) EDC, DMAP, N-Boc-ethylenediamine, DCM, r.t. 5 h; b) HBTU, N-Boc-ethylenediamine, DIPEA, DMF r.t. 5 h; c) i) NH_2NH_2 , $\text{Zn}(\text{OTf})_2$, EtOH, reflux, 12 h; ii) NaNO_2 , AcOH, 10 min



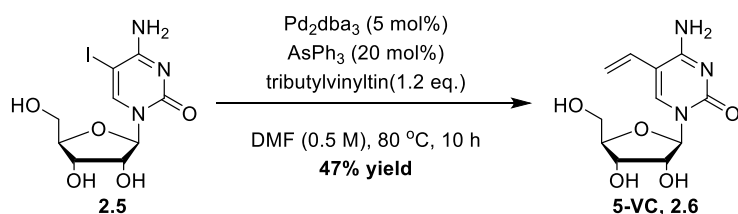
Scheme 2-2. Tetrazine Synthetic Scheme.



Scheme 2-3. Tetrazine Conjugate Synthetic Scheme.

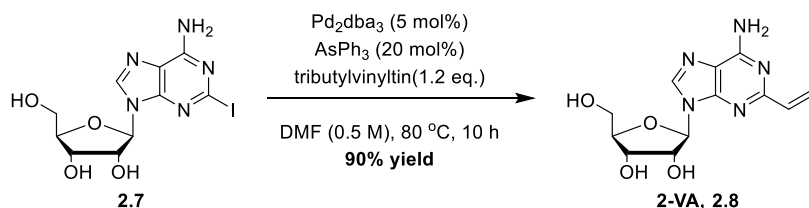


5-vinyluridine (**2.4**) was prepared according to a modified procedure by Fraina, V., *et al.*¹² 5-Iodouridine, **2.3** (0.50 g, 1.35 mmol, $\text{Pd}_2(\text{dba})_3$ (67.5 mg, 67.6 μmol), AsPh_3 (82.7 mg, 0.27 mmol) was dissolved in DMF (3 mL). tributylvinylstannane (0.47 mL, 1.62 mmol) was added to the mixture and stirred for 10 h. Upon completion, the mixture was concentrated *in vacuo* and purified by silica flash column chromatography (EtOAc followed by 0-10% MeOH/DCM) to give **5-VU, 2.4** (0.25 mg, 69%) as a white solid. HRMS Calcd for $\text{C}_{11}\text{H}_{14}\text{N}_2\text{O}_6\text{Na}$ [$\text{M}+\text{Na}^+$] 293.09, found 293.0750 [$\text{M}+\text{Na}^+$]; ^1H NMR (400 MHz, CDCl_3) δ 8.21 (s, 1H), 6.39 (dd, $J = 17.7$, 11.7 Hz, 1H), 5.88 (ddd, $J = 8.1$, 5.6, 1.6 Hz, 2H), 5.12 (dd, $J = 11.5$, 1.6 Hz, 1H), 4.19 – 4.14 (m, 2H), 4.01 – 3.97 (m, 1H), 3.89 – 3.83 (m, 1H), 3.76 – 3.70 (m, 1H); ^{13}C NMR (126 MHz, CD_3OD) δ 151.77, 139.10, 129.07, 115.31, 113.29, 90.87, 86.18, 75.96, 70.93, 61.87.

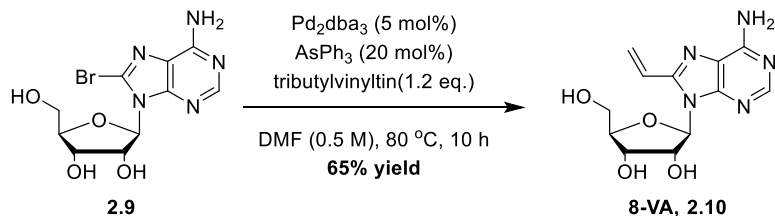


5-Iodocytidine, **2.5** (0.50 g, 1.35 mmol, $\text{Pd}_2(\text{dba})_3$ (62.0 mg, 67.7 μmol), AsPh_3 (82.9 mg, 0.27 mmol) was dissolved in DMF (3 mL). tributylvinylstannane (0.48 mL, 1.63 mmol) was added to the mixture and stirred for 10 h. Upon completion, the mixture was concentrated *in vacuo* and purified by silica flash column chromatography (EtOAc followed by 10% $\text{H}_2\text{O}/\text{MeCN}$) to give **5-VC, 2.6** (172 mg, 47%) as an off-white solid. HRMS Calcd for $\text{C}_{11}\text{H}_{16}\text{N}_3\text{O}_5$ [$\text{M}+\text{H}^+$]

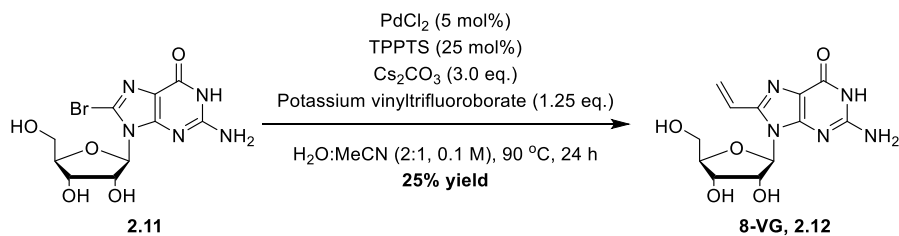
270.11, found 270.1090 [M+H⁺]; ¹H NMR (400 MHz, D₂O) δ 8.12 (s, 1H), 6.43 (dd, *J* = 17.2, 11.0 Hz, 1H), 5.89 (d, *J* = 3.0 Hz, 1H), 5.55 (d, *J* = 17.2 Hz, 1H), 5.35 (d, *J* = 11.0 Hz, 1H), 4.31 (dd, *J* = 5.1, 3.0 Hz, 1H), 4.29 – 4.24 (m, 1H), 4.19 – 4.12 (m, 1H), 4.02 (dd, *J* = 12.9, 2.6 Hz, 1H), 3.87 (dd, *J* = 12.9, 3.4 Hz, 1H); ¹³C NMR (126 MHz, D₂O) δ 164.00, 156.83, 138.23, 126.79, 126.77, 117.29, 117.27, 107.49, 90.71, 83.56, 74.50, 68.70, 60.04.



2-Iodoadenosine, **2.7** (500 mg, 1.27 mmol), Pd₂dba₃ (58.2 mg, 63.5 μmol), and AsPh₃ (77.9 mg, 0.25 mmol) was dissolved in DMF (1.3 mL) and stirred at 100 °C. Tributylvinyltin (0.45 mL, 1.53 mmol) was added to the mixture and stirred for 10 h. The reaction was then concentrated *in vacuo* and purified by silica flash column chromatography (10% MeOH/DCM) to give **2-VA, 2.8** (335 mg, 90%) as a tan foam. HRMS Calcd for C₁₂H₁₅N₅O₄Na [M+Na⁺] 316.11, found 316.1022 [M+Na⁺]; ¹H NMR (400 MHz, DMSO) δ 8.27 (s, 1H), 7.23 (s, 2H), 6.55 (dd, *J* = 17.2, 10.4 Hz, 1H), 6.31 (dd, *J* = 17.2, 1.8 Hz, 1H), 5.84 (d, *J* = 6.4 Hz, 1H), 5.54 – 5.46 (m, 1H), 5.37 (d, *J* = 6.2 Hz, 1H), 5.33 (d, *J* = 4.6 Hz, 1H), 5.13 (d, *J* = 4.2 Hz, 1H), 4.60 (dd, *J* = 11.3, 5.9 Hz, 1H), 4.11 (d, *J* = 2.5 Hz, 1H), 3.92 (d, *J* = 2.8 Hz, 1H), 3.70 – 3.58 (m, 1H), 3.56 – 3.46 (m, 1H); ¹³C NMR (126 MHz, DMSO) δ 157.80, 155.75, 149.73, 140.42, 137.10, 121.21, 118.62, 87.74, 85.98, 73.31, 70.84, 61.82.

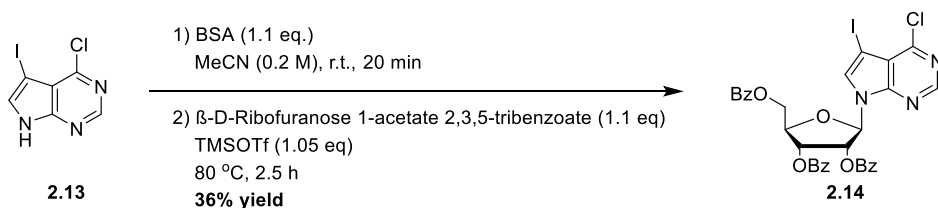


8-Bromo-adenosine, **2.9** (50 mg, 0.14 mmol), AsPh₃ (8.80 mg, 28.9 μmol) and Pd₂dba₃ (6.60 mg, 7.22 μmol) were added to a flask and dissolved in DMF (0.2 mL) and heated to 80 °C. Tributylvinyltin (51.0 μL, 173 μmol) was added to the flask and stirred for 10 h. The mixture was concentrated *in vacuo* and purified by silica flash column chromatography (EtOAc then 10% MeOH/DCM) to give **8-VA, 2.10** (21.7 mg, 65%) as a white solid. HRMS Calcd for C₁₂H₁₅N₅O₄Na [M+Na⁺] 316.11, found 316.1022 [M+Na⁺]; ¹H NMR (400 MHz, DMSO) δ 8.10 (s, *J* = 8.4 Hz, 1H), 7.39 (s, 2H), 7.08 (dd, *J* = 17.0, 11.1 Hz, 1H), 6.35 (dd, *J* = 17.0, 1.8 Hz, 1H), 5.95 (d, *J* = 7.1 Hz, 1H), 5.72 – 5.59 (m, 2H), 5.34 (d, *J* = 6.8 Hz, 1H), 5.17 (d, *J* = 4.6 Hz, 1H), 4.81 (dd, *J* = 12.5, 6.8 Hz, 1H), 4.16 (td, *J* = 5.1, 2.4 Hz, 1H), 3.98 (d, *J* = 2.6 Hz, 1H), 3.68 (dt, *J* = 12.1, 3.5 Hz, 1H), 3.56 (ddd, *J* = 11.9, 8.3, 3.5 Hz, 1H); ¹³C NMR (126 MHz, DMSO) δ 155.91, 152.02, 149.74, 147.71, 124.14, 123.02, 118.90, 87.78, 86.50, 72.21, 70.64, 61.96.



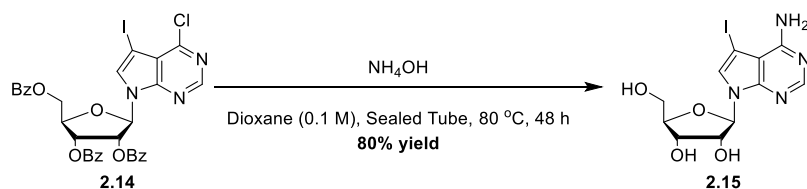
8-VG (2.12) was prepared according to a modified procedure by Zilbershtein, L. *et al.*¹⁷ PdCl₂ (12.2 mg, 0.07 mmol) and TPPTS (0.19 g, 0.35 mmol) was dissolved in a mixture of H₂O:MeCN (2:1, 14 mL) and stirred for 10 min at r.t. 8-Bromoguanosine, **2.11** (0.50 g, 1.38 mmol), Potassium vinyltrifluoroborate (0.23 g, 1.73 mmol), and Cs₂CO₃ (1.35 g, 4.14 mmol)

were added to the mixture and heated to 90 °C and stirred for 24 h. The mixture was then allowed to cool to r.t. and concentrated *in vacuo*. The crude mixture was then purified by C18 reverse phase column chromatography (5-95% MeCN/H₂O) to give **8-VG, 2.12** (0.11 g, 25% yield) as a green solid. HRMS Calcd for C₁₂H₅N₅O₅Na [M+Na⁺] 332.11, found 332.0971 [M+Na⁺]; ¹H NMR (499 MHz, DMSO) δ 10.90 (s, 1H), 6.96 (dd, *J* = 17.1, 11.1 Hz, 1H), 6.52 (s, 2H), 6.12 (dd, *J* = 17.0, 1.8 Hz, 1H), 5.80 (d, *J* = 7.1 Hz, 1H), 5.45 – 5.38 (m, 1H), 5.31 (s, 1H), 5.18 (s, 1H), 5.04 (s, 1H), 4.54 (s, 1H), 4.09 (s, 1H), 3.86 (d, *J* = 3.3 Hz, 1H), 3.65 (d, *J* = 11.3 Hz, 1H), 3.57 (d, *J* = 11.8 Hz, 1H); ¹³C NMR (126 MHz, DMSO) δ 153.66, 152.03, 144.10, 124.81, 119.33, 116.44, 86.78, 85.60, 72.05, 70.04, 61.61.

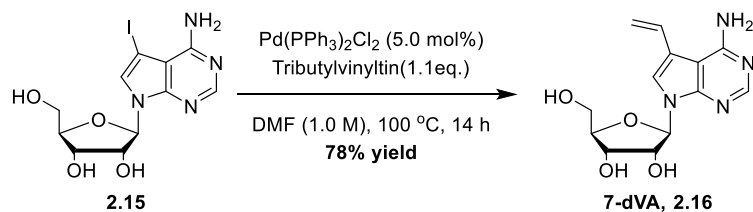


6-Chloro-7-iodo-7-deazapurine, **2.13** (2.00 g, 7.16 mmol) was suspended in MeCN (36 mL). BSA (1.93 mL, 7.87 mmol) was added to the suspension and stirred for 20 min at r.t. β-D-Ribofuranose 1-acetate 2,3,5-tribenzoate (3.97 g, 7.87 mmol) and TMSOTf (1.36 mL, 7.51 mmol) were added to the mixture and heated to 80 °C and stirred for 2.5 h. Upon completion, sat. NaHCO₃ solution (40 mL) was added to the mixture, extracted with EtOAc (3 x 50 mL), and dried of MgSO₄. The crude mixture was then concentrated *in vacuo* and purified by silica flash column chromatography (0-50% EtOAc/Hex) to give **2.14** (2.61 g, 50%) as a clear foam. HRMS Calcd for C₃₂H₂₃ClIN₃O₇Na [M+Na⁺] 746.06, found 746.0167 [M+Na⁺]; ¹H NMR (400 MHz, CDCl₃) δ 8.57 (s, 1H), 8.14 – 8.08 (m, 2H), 8.03 – 7.95 (m, 2H), 7.95 – 7.89 (m, 2H), 7.65 – 7.46 (m, 6H), 7.42 – 7.32 (m, 4H), 6.68 (d, *J* = 5.4 Hz, 1H), 6.17 (t, *J* = 5.6 Hz, 1H), 6.12 (dd, *J*

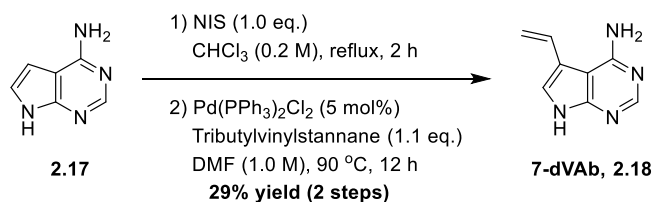
= 5.7, 4.6 Hz, 1H), 4.90 (dd, $J = 12.2, 3.1$ Hz, 1H), 4.81 (dd, $J = 7.7, 3.5$ Hz, 1H), 4.73 – 4.63 (m, 1H). ^{13}C NMR (126 MHz, CDCl_3) δ 166.16, 165.42, 165.13, 153.16, 151.30, 151.05, 133.86, 133.83, 133.63, 132.17, 129.90, 129.89, 129.77, 129.35, 128.88, 128.75, 128.63, 128.59, 128.45, 117.86, 86.92, 80.73, 74.24, 71.52, 63.56, 53.73.



2.14 (500 mg, 691 μmol) was placed in a sealed tube with a 1:1 mixture of strong NH_4OH solution and 1,4-Dioxane (12 mL). The tube was then sealed, heated to 80 $^\circ\text{C}$, and stirred for 48 h. The mixture was then cooled to r.t. and concentrated *in vacuo*. The crude material was then purified by silica flash column chromatography (0-10% MeOH/DCM/1% Et_3N) to give **2.15** (217 mg, 80%) as a white solid. HRMS Calcd for $\text{C}_{11}\text{H}_{13}\text{IN}_4\text{O}_4\text{Na}$ [$\text{M}+\text{Na}^+$] 414.99, found 414.9879 [$\text{M}+\text{Na}^+$]; ^1H NMR (400 MHz, DMSO) δ 8.10 (s, 1H), 7.67 (s, 1H), 6.66 (s, 2H), 6.02 (d, $J = 6.2$ Hz, 1H), 5.29 (d, $J = 6.4$ Hz, 1H), 5.14 (t, $J = 5.5$ Hz, 1H), 5.09 (d, $J = 4.7$ Hz, 1H), 4.35 (dd, $J = 11.6, 6.1$ Hz, 1H), 4.06 (dd, $J = 8.1, 4.9$ Hz, 1H), 3.88 (q, $J = 3.6$ Hz, 1H), 3.67 – 3.58 (m, 1H), 3.53 (ddd, $J = 11.9, 5.9, 3.9$ Hz, 1H); ^{13}C NMR (126 MHz, DMSO) δ 157.26, 151.99, 150.20, 127.18, 103.26, 86.79, 85.23, 73.91, 70.57, 61.59, 52.02.

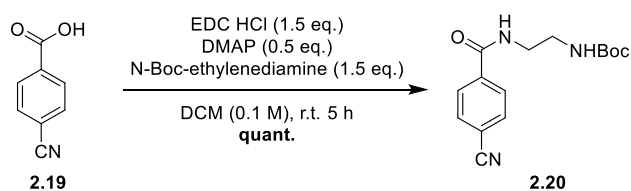


7-dVA (2.16) was synthesized following a modified procedure by Hottin, A., *et al.*¹⁸ **2.15** (206 mg, 524 μmol) and $\text{Pd}(\text{PPh}_3)_2\text{Cl}_2$ (18.4 mg, 26.2 μmol) was added to a flask and dissolved in DMF (0.5 mL) and heated to 100 $^\circ\text{C}$. Tributylvinyltin (169 μL , 577 μmol) was added to the flask and stirred for 14 h. The mixture was cooled to r.t. and concentrated *in vacuo*. The crude material was then purified by silica flash column chromatography (0-10% MeOH/DCM/1% Et₃N) and then treated with AcOH and filtered over a pad of silica (10% MeOH/DCM) to give **7-dVA, 2.16** (161 mg, 78%) as a white solid. HRMS Calcd for $\text{C}_{13}\text{H}_{16}\text{IN}_4\text{O}_4\text{Na}$ [$\text{M}+\text{Na}^+$] 315.12, found 315.1069 [$\text{M}+\text{Na}^+$]; ¹H NMR (400 MHz, DMSO) δ 8.05 (s, $J = 24.1$ Hz, 1H), 7.66 (s, 1H), 7.11 (dd, $J = 17.2, 10.9$ Hz, 1H), 6.71 (s, 2H), 6.04 (d, $J = 6.2$ Hz, 1H), 5.56 (d, $J = 17.2$ Hz, 1H), 5.24 (d, $J = 24.6$ Hz, 2H), 5.18 – 5.01 (m, 2H), 4.40 (t, $J = 5.4$ Hz, 1H), 4.08 (d, $J = 3.6$ Hz, 1H), 3.89 (d, $J = 3.4$ Hz, 1H), 3.64 (d, $J = 11.6$ Hz, 1H), 3.54 (d, $J = 11.8$ Hz, 1H); ¹³C NMR (126 MHz, DMSO) δ 157.66, 151.48, 150.72, 129.04, 119.15, 114.05, 113.01, 100.79, 87.02, 85.05, 73.68, 70.54, 61.67.

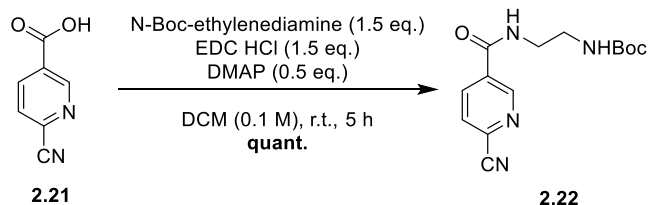


6-Amino-7-deazapurine, **2.17** (0.50 g, 3.73 mmol) and NIS (0.84 g, 3.73 mmol) was refluxed in CHCl_3 (15 mL) for 2 h. Upon completion, the mixture was cooled to r.t., filtered and washed with DCM (30 mL) and the precipitate was placed in a flask. $\text{Pd}(\text{PPh}_3)_2\text{Cl}_2$ (131 mg, 0.19 mmol), tributylvinylstannane (1.19 mL, 4.10 mmol) was added to the flask and dissolved in DMF (4 mL). The mixture was heated to 90 $^\circ\text{C}$ and stirred for 12 h. Upon completion, the reaction was allowed to cool to r.t., filtered over celite and concentrated *in vacuo*. The crude

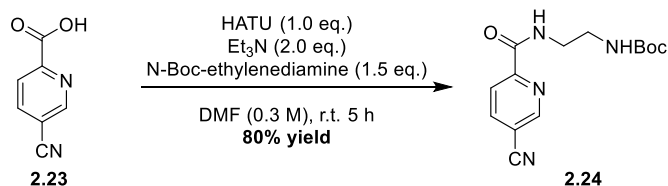
precipitate was then purified by silica flash column chromatography (5-10% MeOH/DCM) to give **7-dVAb, 2.18** (173 mg, 29%) as a cream solid. HRMS Calcd for $C_8H_9N_4$ $[M+H^+]$ 161.08, found 161.0827 $[M+H^+]$; 1H NMR (400 MHz, DMSO) δ 11.61 (s, 1H), 8.01 (s, $J = 12.1$ Hz, 1H), 7.37 (s, 1H), 7.09 (dd, $J = 17.2, 10.9$ Hz, 1H), 6.53 (s, 2H), 5.53 (d, $J = 17.2$ Hz, 1H), 5.06 (d, $J = 10.9$ Hz, 1H); ^{13}C NMR (126 MHz, DMSO) δ 157.51, 151.53, 151.35, 129.63, 118.42, 113.53, 111.95, 100.05.



N-Boc-ethylenediamine (1.61 mL, 10.2 mmol) was added to a mixture of 4-cyanobenzoic acid, **2.19** (1.00 g, 6.79 mmol) and DMAP (415 mg, 3.39 mmol) was dissolved in DCM (70 mL) and stirred for 5 min. EDC HCl (1.95 g, 10.2 mmol) was added to the mixture and stirred at r.t. for 5 h. Upon completion, 1 M citric acid (50 mL) was added to the mixture and separated. The organic layer was then washed with sat. $NaHCO_3$ solution (50 mL) and dried over $MgSO_4$. The crude organic layer was then concentrated *in vacuo* and purified by silica flash column chromatography (5% MeOH/DCM) to give **2.20** (2.04 g, quant.) as a white solid. HRMS Calcd for $C_{15}H_{19}N_3O_3Na$ $[M+Na^+]$ 312.14, found 312.1324 $[M+Na^+]$; 1H NMR (400 MHz, $CDCl_3$) δ 7.94 (d, $J = 8.3$ Hz, 2H), 7.72 (d, $J = 8.4$ Hz, 2H), 7.64 (s, 1H), 5.02 (s, 1H), 3.56 (dd, $J = 10.4, 4.8$ Hz, 2H), 3.42 (dd, $J = 10.8, 5.9$ Hz, 2H), 1.43 (s, 9H); ^{13}C NMR (101 MHz, $CDCl_3$) δ 165.83, 138.21, 132.48, 127.88, 123.32, 123.31, 118.26, 115.11, 80.57, 43.24, 39.82, 28.45.

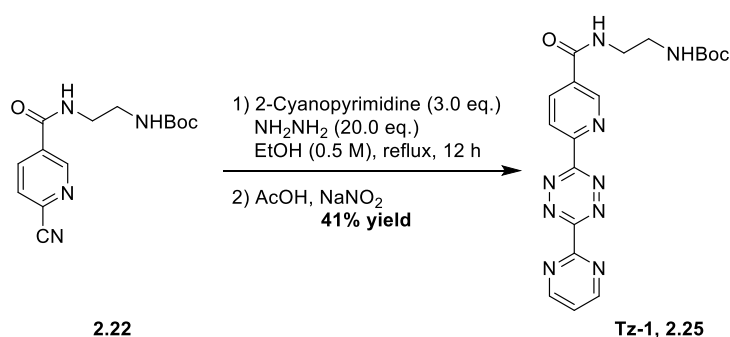


6-cyanonicotinic acid, **2.21** (1.00 g, 6.76 mmol), DMAP (0.49 g, 3.38 mmol), N-Boc-ethylenediamine (1.6 mL, 10.1 mmol) was stirred in DCM (60 mL) for 5 min. EDC HCl (1.94 g, 10.1 mmol) was added to the mixture and stirred for 5 h. The mixture was then added into 1 M citric acid (60 mL) and extracted and washed with sat. NaHCO₃ solution (60 mL). The organic layer was separated, dried over MgSO₄ and concentrated *in vacuo*. The crude product was then purified by silica flash column chromatography (5-10% MeOH/DCM) to give **2.22** (1.96 g, quantitative yield) as a white solid. HRMS Calcd for C₁₂H₁₈N₄O₃Na [M+Na⁺] 313.14, found 313.1292 [M+Na⁺]; ¹H NMR (400 MHz, CDCl₃) δ 9.15 (s, 1H), 8.30 (dd, *J* = 8.1, 2.2 Hz, 1H), 8.03 (s, 1H), 7.78 (d, *J* = 8.1 Hz, 1H), 5.03 (s, 1H), 3.58 (dd, *J* = 10.1, 4.6 Hz, 2H), 3.44 (dd, *J* = 10.6, 6.1 Hz, 2H), 1.44 (s, 9H); ¹³C NMR (126 MHz, CDCl₃) δ 149.63, 136.02, 135.77, 132.30, 128.18, 116.77, 80.86, 43.70, 39.63, 28.35.



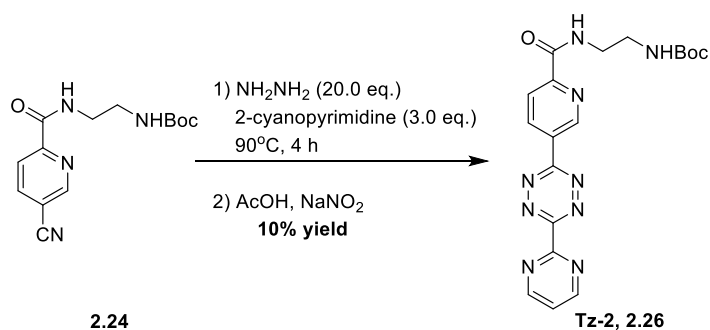
5-cyanopyridine-2-carboxylic acid, **2.23** (1.00 g, 6.75 mmol) was dissolved in DMF (23 mL). N-Boc-ethylenediamine (1.07 mL, 6.75 mmol) and Et₃N (1.88 mL, 13.5 mmol) were added to the mixture and stirred for 5 min. HATU (2.82 g, 7.43 mmol) was added to the mixture and the mixture was stirred at r.t. for 5 h. Upon completion, sat. NaHCO₃ solution (20 mL) was

added and extracted with EtOAc (40 mL). The organic layer was then washed with water (3 x 100 mL), dried over MgSO₄ and concentrated *in vacuo*. The crude material was then purified by silica flash column chromatography (50-100% EtOAc/Hex) to give **2.24** (1.56 g, 80%) as a white solid. HRMS Calcd for C₁₄H₁₈N₄O₃Na [M+Na⁺] 313.14, found 313.1277 [M+Na⁺]; ¹H NMR (400 MHz, CDCl₃) δ 8.82 (dd, *J* = 2.0, 0.9 Hz, 1H), 8.31 (dd, *J* = 8.1, 0.8 Hz, 2H), 8.13 (dd, *J* = 8.1, 2.0 Hz, 1H), 4.90 (s, 1H), 3.60 (dd, *J* = 11.7, 5.9 Hz, 2H), 3.40 (dd, *J* = 11.5, 5.8 Hz, 2H), 1.41 (s, 9H); ¹³C NMR (126 MHz, CDCl₃) δ 163.30, 156.60, 152.41, 150.98, 141.03, 122.26, 116.16, 112.32, 79.88, 40.64, 40.28, 28.43.



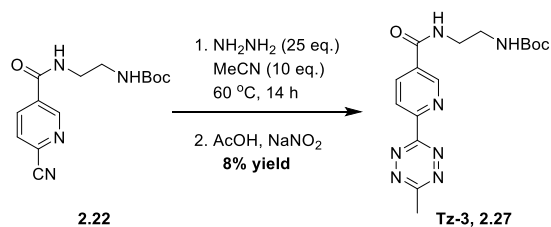
2.22 (500 mg, 1.72 mmol) and 2-cyanopyrimidine (1.10 g, 5.17 mmol) was dissolved in EtOH (3 mL). Hydrazine (1.08 mL, 34.4 mmol) was added to the mixture and refluxed for 12 h. The mixture was then allowed to cool to r.t and concentrated *in vacuo*. 1 M NaNO₂ solution (15 mL) was added to the flask and AcOH was added to the mixture slowly until a pH of 5 was reached. The mixture stirred for 20 min and then neutralized with saturated NaHCO₃ solution, extracted with DCM (3 x 25 mL), and dried over MgSO₄. The organic mixture was then concentrated *in vacuo* and purified by silica flash column chromatography (0-5% MeOH/DCM). The pink residue was then further purified with recrystallization in EtOH to give **Tz-1, 2.25** (298 mg, 41%) as magenta crystals. HRMS Calcd for C₁₉H₂₁N₉O₃Na [M+Na⁺]

446.18, found 446.1665 [M+Na⁺]; ¹H NMR (499 MHz, CDCl₃) δ 9.43 (s, 1H), 9.17 (d, *J* = 4.8 Hz, 2H), 8.87 (d, *J* = 8.2 Hz, 1H), 8.49 (dd, *J* = 8.2, 2.2 Hz, 1H), 7.98 (s, 1H), 7.62 (t, *J* = 4.9 Hz, 1H), 5.04 (s, 1H), 3.71 – 3.61 (m, 2H), 3.48 (s, 2H), 1.45 (s, *J* = 4.3 Hz, 9H); ¹³C NMR (126 MHz, CDCl₃) δ 164.80, 163.76, 163.66, 159.48, 158.65, 157.64, 151.83, 149.78, 136.76, 132.37, 124.72, 122.83, 80.63, 43.30, 39.95, 28.47.

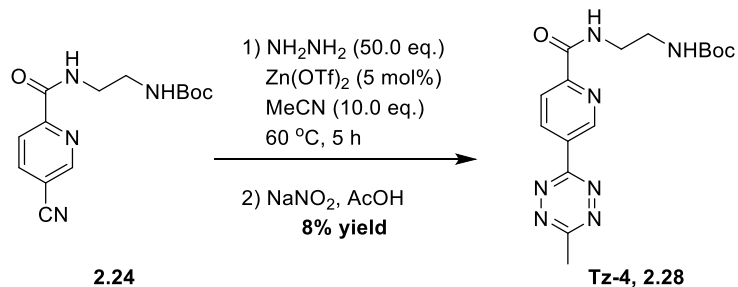


2.24 (500 mg, 2.38 mmol) and 2-cyanopyrimidine (750 mg, 7.13 mmol) was dissolved in hydrazine (1.49 mL, 47.5 mmol) and stirred at 90 °C for 4 h. The mixture was then allowed to cool to r.t. and 20 mL of 1 M NaNO₂ solution was added to the mixture. AcOH was added to the mixture slowly until a pH of 5 was reached. The mixture stirred for 10 min and then neutralized with saturated NaHCO₃ solution, extracted with DCM (3 x 25 mL), and dried over MgSO₄. The organic mixture was then concentrated *in vacuo* and purified by silica flash column chromatography (0-50% Acetone/DCM). The pink residue was then further purified with recrystallization in EtOH to give **Tz-2, 2.26** (72.9 mg, 10%) as purple crystals. HRMS Calcd for C₁₉H₂₁N₉O₃Na [M+Na⁺] 446.18, found 446.1665 [M+Na⁺]; ¹H NMR (400 MHz, CDCl₃) δ 9.84 (s, 1H), 9.19 – 9.09 (m, *J* = 5.8 Hz, 3H), 8.45 (d, *J* = 8.2 Hz, 2H), 7.62 (t, *J* = 4.8 Hz, 1H), 4.99 (s, 1H), 3.65 (m, *J* = 5.8 Hz, 2H), 3.44 (m, *J* = 5.4 Hz, 2H), 1.43 (s, 9H); ¹³C NMR (126 MHz,

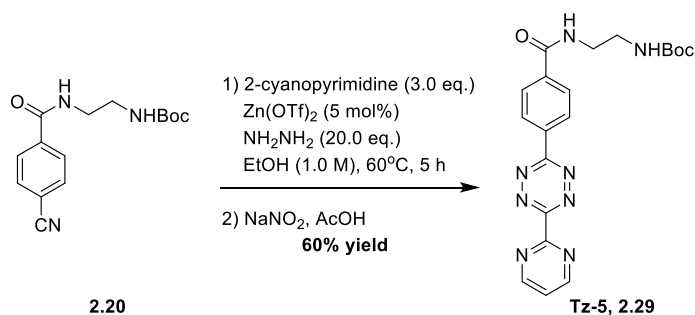
CDCl₃) δ 163.52, 163.36, 159.50, 159.29, 158.56, 153.04, 148.45, 137.34, 129.59, 122.79, 122.60, 122.36, 79.68, 40.31, 29.32, 28.39.



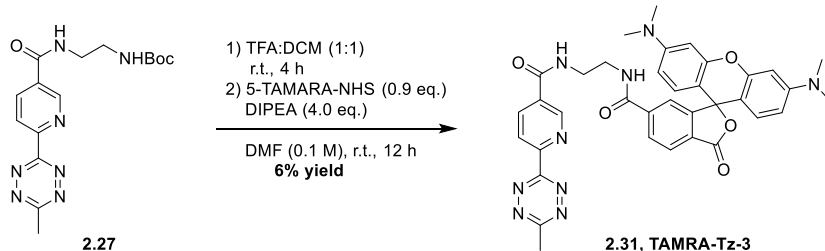
2.22 (1.14 g, 3.92 mmol) was dissolved in MeCN (2.05 mL, 39.2 mmol) and heated to 60 °C. Hydrazine (3.08 mL, 98.0 mmol) was added to the mixture and stirred for 14 h. The mixture was then allowed to cool to r.t. and AcOH (4 mL) was added to the mixture. A 3 M NaNO₂ solution (30 mL) was added slowly to the mixture. The pH was adjusted to 5 using AcOH and stirred until bubbles ceased. The mixture was then diluted with DCM (40 mL) and washed with sat. NaHCO₃ solution. The organic layer was separated, dried over MgSO₄, and concentrated *in vacuo*. The impure residue was then purified by silica flash column chromatography (0-40% Acetone/DCM) give **Tz-3, 2.27** (0.11 g, 8% yield) as a pink solid. HRMS Calcd for C₁₆H₂₂N₇O₃ [M+H⁺] 360.18, found 360.1798 [M+H⁺]; ¹H NMR (400 MHz, CDCl₃) δ 9.36 (s, 1H), 8.72 (d, *J* = 8.2 Hz, 1H), 8.44 (dd, *J* = 8.2, 2.1 Hz, 1H), 7.91 (s, 1H), 5.02 (s, 1H), 3.63 (dd, *J* = 10.1, 4.7 Hz, 2H), 3.51 – 3.41 (m, 2H), 3.18 (s, 3H), 1.45 (s, 9H); ¹³C NMR (126 MHz, CDCl₃) δ 173.67, 172.25, 168.34, 163.32, 149.42, 136.55, 134.25, 131.88, 123.54, 80.62, 53.46, 39.85, 28.38, 21.45.



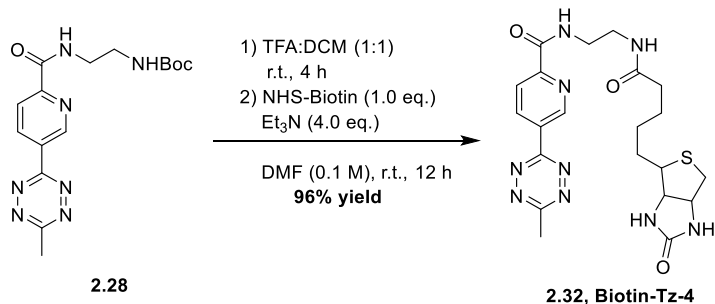
2.24 (500 mg, 1.72 mmol), $\text{Zn}(\text{OTf})_2$ (31.8 mg, 86.1 μmol) were dissolved in MeCN (0.89 mL, 17.2 mmol) and heated to 60 °C. Hydrazine (2.70 mL, 86.1 mmol) was added to the mixture and stirred for 5 h. The mixture was then allowed to cool to r.t. and 40 mL of 1 M NaNO_2 solution was added to the mixture. AcOH was added to the mixture slowly until a pH of 5 was reached. The mixture stirred for 10 min and was then neutralized with saturated NaHCO_3 solution, extracted with DCM (3 x 40 mL), and dried over MgSO_4 . The organic mixture was then concentrated *in vacuo* and purified by silica flash column chromatography (50-80% EtOAc/Hex) to give **Tz-4, 2.28** (33.7 mg, 8%) as a pink solid. HRMS Calcd for $\text{C}_{16}\text{H}_{21}\text{N}_7\text{O}_3\text{Na}$ [$\text{M}+\text{Na}^+$] 383.17, found 382.1604 [$\text{M}+\text{Na}^+$]; ^1H NMR (400 MHz, CDCl_3) δ 9.72 (d, $J = 2.1$ Hz, 1H), 9.01 (dd, $J = 8.2, 2.1$ Hz, 1H), 8.41 (d, $J = 8.2$ Hz, 1H), 4.94 (s, 1H), 3.64 (dd, $J = 11.5, 5.8$ Hz, 3H), 3.44 (dd, $J = 11.1, 5.6$ Hz, 3H), 3.16 (s, 3H), 1.43 (s, 9H); ^{13}C NMR (151 MHz, CDCl_3) δ 168.30, 164.38, 162.86, 156.50, 152.63, 147.81, 136.66, 130.17, 122.60, 79.80, 40.62, 40.37, 28.49, 21.50.



2.20 (500 mg, 1.73 mmol), 2-cyanopyrimidine (545 mg, 5.18 mmol), Zn(OTf)₂ (31.4 mg, 0.09 mmol) were dissolved in EtOH (1.7 mL). Hydrazine (1.09 mL, 34.6 mmol) was added to the mixture and heated to 60 °C and stirred for 5 h. The mixture was then allowed to cool to r.t. and 15 mL of 1 M NaNO₂ solution was added to the mixture. AcOH was added to the mixture slowly until a pH of 5 was reached. The mixture stirred for 10 min and then neutralized with saturated NaHCO₃ solution, extracted with DCM (3 x 20 mL), and dried over MgSO₄. The organic mixture was then concentrated *in vacuo* and purified by silica flash column chromatography (0-5% MeOH/DCM) to give **Tz-5, 2.29** (0.44 g, 60%) as a purple solid. HRMS Calcd for C₂₀H₂₂N₈O₃Na [M+Na⁺] 445.18, found 445.1713 [M+Na⁺]; ¹H NMR (400 MHz, CDCl₃) δ 9.14 (d, *J* = 4.9 Hz, 2H), 8.79 (d, *J* = 8.6 Hz, 2H), 8.09 (d, *J* = 8.4 Hz, 2H), 7.59 (t, *J* = 4.9 Hz, 1H), 5.08 (s, *J* = 10.7 Hz, 1H), 3.61 (dd, *J* = 10.6, 4.9 Hz, 2H), 3.46 (d, *J* = 4.7 Hz, 2H), 1.44 (s, *J* = 5.8 Hz, 9H); ¹³C NMR (126 MHz, CDCl₃) δ 166.80, 164.23, 163.33, 159.63, 158.58, 158.03, 138.56, 133.95, 129.05, 128.18, 122.70, 80.42, 42.86, 39.95, 28.49.



Tz-3, 2.27 (25.0 mg, 69.6 μmol) was dissolved in a 1:1 TFA:DCM solution (1 mL) and stirred at r.t., for 4 h. The mixture was then concentrated *in vacuo*. 5-TAMARA-NHS ester (66.0 mg, 62.6 μmol) was dissolved in DMF (0.6 mL) and stirred at r.t. DIPEA (48.5 μL , 27.8 μmol) was added to the mixture and stirred for 12 h. The mixture was concentrated *in vacuo* and the crude product was purified by reverse phase C18 column chromatography (30-70% MeCN/H₂O with 0.1% TFA) to give **2.31, TAMRA-Tz-3** (2.5 mg, 6% yield) as a red solid. HRMS Calcd for C₃₆H₃₄N₉O₅ [M+H⁺] 672.27, found 672.2689 [M+H⁺]; ¹H NMR (400 MHz, CD₃OD) δ 9.23 (s, 1H), 9.00 (s, 1H), 8.76 (s, 1H), 8.74 (s, 1H), 8.50 (dd, *J* = 8.3, 2.2 Hz, 1H), 8.25 (dd, *J* = 7.9, 1.8 Hz, 1H), 7.51 (d, *J* = 8.0 Hz, 1H), 7.12 (d, *J* = 9.5 Hz, 2H), 7.05 (dd, *J* = 9.5, 2.4 Hz, 2H), 6.97 (d, *J* = 2.4 Hz, 2H), 3.80 – 3.71 (m, 4H), 3.10 (s, 3H); ¹³C NMR (126 MHz, CD₃OD) δ 169.96, 168.73, 167.76, 164.19, 160.67, 159.08, 159.01, 153.64, 150.31, 138.25, 138.15, 137.72, 133.90, 132.97, 132.33, 131.93, 131.37, 124.65, 115.59, 114.74, 97.45, 40.93, 21.31.



Tz-4, 2.28 (19 mg, 52.9 μmol) was dissolved in TFA:DCM (1:1, 1 mL) and stirred at r.t. for 4 h. The mixture was then concentrated *in vacuo*. NHS-Biotin (18 mg, 52.9 μmol) was added to the flask and dissolved in DMF (0.5 mL). Et₃N (30 μL , 0.21 mmol) was added to the mixture and stirred at r.t. for 12 h. The mixture was then concentrated *in vacuo* and purified by C18 reverse phase column chromatography (0-50% MeCN/H₂O with 0.1% TFA) to give **2.32, Biotin-Tz-4** (24.7 mg, 96% yield) as a pink solid. HRMS Calcd for C₂₁H₂₇N₉O₃SNa [M+Na⁺] 508.18, found 508.1850 [M+Na⁺]; ¹H NMR (400 MHz, CD₃OD) δ 9.68 (s, 1H), 9.00 (d, *J* = 8.2 Hz, 1H), 8.30 (s, 1H), 7.25 (d, *J* = 8.9 Hz, 1H), 6.84 (d, *J* = 8.9 Hz, 1H), 4.42 (dd, *J* = 7.7, 4.7 Hz, 2H), 4.22 (dd, *J* = 7.8, 4.5 Hz, 2H), 3.56 (s, 2H), 3.45 (d, *J* = 5.2 Hz, 2H), 3.09 (s, 1H), 3.06 (s, 3H), 2.89 – 2.80 (m, 1H), 2.63 (d, *J* = 12.7 Hz, 1H), 2.19 (t, *J* = 7.3 Hz, 2H), 1.73 – 1.43 (m, 6H), 1.37 (dd, *J* = 15.1, 7.3 Hz, 3H); ¹³C NMR (126 MHz, CD₃OD) δ 169.58, 158.80, 127.17, 119.44, 117.18, 115.62, 115.43, 115.14, 114.92, 112.65, 63.28, 61.62, 56.88, 41.01, 39.87, 36.79, 31.95, 29.61, 29.44, 26.80, 21.26.

2.6 References

1. Novikova, I. V.; Hennelly, S. P.; Tung, C. S.; Sanbonmatsu, K. Y., Rise of the RNA machines: exploring the structure of long non-coding RNAs. *J Mol Biol* 2013, 425 (19), 3731-46.
2. Morris, K. V.; Mattick, J. S., The rise of regulatory RNA. *Nat. Rev. Genet.* 2014, 15 (6), 423-37.
3. Prescher, J. A.; Bertozzi, C. R., Chemistry in living systems. *Nat. Chem. Biol.* 2005, 1 (1), 13-21.
4. Miller, M. R.; Robinson, K. J.; Cleary, M. D.; Doe, C. Q., TU-tagging: cell type-specific RNA isolation from intact complex tissues. *Nat Methods* 2009, 6 (6), 439-U57.
5. Zheng, Y.; Beal, P. A., Synthesis and evaluation of an alkyne-modified ATP analog for enzymatic incorporation into RNA. *Bioorg Med Chem Lett* 2016, 26 (7), 1799-802.
6. Jao, C. Y.; Salic, A., Exploring RNA transcription and turnover in vivo by using click chemistry. *Proc. Natl. Acad. Sci. U. S. A.* 2008, 105 (41), 15779-84.
7. Curanovic, D.; Cohen, M.; Singh, I.; Slagle, C. E.; Leslie, C. S.; Jaffrey, S. R., Global profiling of stimulus-induced polyadenylation in cells using a poly(A) trap. *Nat. Chem. Biol.* 2013, 9 (11), 671-3.
8. Nainar, S.; Beasley, S.; Fazio, M.; Kubota, M.; Dai, N.; Correa, I. R., Jr.; Spitale, R. C., Metabolic Incorporation of Azide Functionality into Cellular RNA. *ChemBioChem* 2016, 17 (22), 2149-2152.
9. Nainar, S.; Kubota, M.; McNitt, C.; Tran, C.; Popik, V. V.; Spitale, R. C., Temporal Labeling of Nascent RNA Using Photoclick Chemistry in Live Cells. *J. Am. Chem. Soc.* 2017, 139 (24), 8090-8093.

10. Duffy, E. E.; Rutenberg-Schoenberg, M.; Stark, C. D.; Kitchen, R. R.; Gerstein, M. B.; Simon, M. D., Tracking Distinct RNA Populations Using Efficient and Reversible Covalent Chemistry. *Molecular Cell* 2015, 59 (5), 858-866.
11. Paredes, E.; Das, S. R., Click chemistry for rapid labeling and ligation of RNA. *ChemBioChem* 2011, 12 (1), 125-31.
12. Winz, M. L.; Samanta, A.; Benzinger, D.; Jaschke, A., Site-specific terminal and internal labeling of RNA by poly(A) polymerase tailing and copper-catalyzed or copper-free strain-promoted click chemistry. *Nucleic Acids Research* 2012, 40 (10).
13. Feng, H. J.; Zhang, X. G.; Zhang, C. L., mRIN for direct assessment of genome-wide and gene-specific mRNA integrity from large-scale RNA-sequencing data. *Nature Communications* 2015, 6.
14. Maeda, T.; Date, A.; Watanabe, M.; Hidaka, Y.; Iwatani, Y.; Takano, T., Optimization of Recovery and Analysis of RNA in Sorted Cells in mRNA Quantification After Fluorescence-activated Cell Sorting. *Ann Clin Lab Sci* 2016, 46 (6), 571-577.
15. Nilsson, H.; Krawczyk, K. M.; Johansson, M. E., High salt buffer improves integrity of RNA after fluorescence-activated cell sorting of intracellular labeled cells. *J Biotechnol* 2014, 192, 62-65.
16. Nguyen, K.; Fazio, M.; Kubota, M.; Nainar, S.; Feng, C.; Li, X.; Atwood, S. X.; Bredy, T. W.; Spitale, R. C., Cell-Selective Bioorthogonal Metabolic Labeling of RNA. *J. Am. Chem. Soc.* 2017, 139 (6), 2148-2151.
17. Wu, H. X.; Devaraj, N. K., Inverse Electron-Demand Diels-Alder Bioorthogonal Reactions. *Topics Curr Chem* 2016, 374 (1).

18. Brachet, E.; Belmont, P., Inverse Electron Demand Diels-Alder (IEDDA) Reactions: Synthesis of Heterocycles and Natural Products Along with Bioorthogonal and Material Sciences Applications. *Curr Org Chem* 2016, 20 (21), 2136-2160.
19. Lang, K.; Davis, L.; Wallace, S.; Mahesh, M.; Cox, D. J.; Blackman, M. L.; Fox, J. M.; Chin, J. W., Genetic Encoding of Bicyclononynes and trans-Cyclooctenes for Site-Specific Protein Labeling in Vitro and in Live Mammalian Cells via Rapid Fluorogenic Diels–Alder Reactions. *J. Am. Chem. Soc.* 2012, 134 (25), 10317-10320.
20. Patterson, D. M.; Nazarova, L. A.; Xie, B.; Kamber, D. N.; Prescher, J. A., Functionalized Cyclopropenes As Bioorthogonal Chemical Reporters. *J. Am. Chem. Soc.* 2012, 134 (45), 18638-18643.
21. Lang, K.; Davis, L.; Torres-Kolbus, J.; Chou, C.; Deiters, A.; Chin, J. W., Genetically encoded norbornene directs site-specific cellular protein labelling via a rapid bioorthogonal reaction. *Nature Chem.* 2012, 4, 298.
22. Rossin, R.; van den Bosch, S. M.; ten Hoeve, W.; Carvelli, M.; Versteegen, R. M.; Lub, J.; Robillard, M. S., Highly Reactive trans-Cyclooctene Tags with Improved Stability for Diels–Alder Chemistry in Living Systems. *Bioconjugate Chem.* 2013, 24 (7), 1210-1217.
23. Busskamp, H.; Batroff, E.; Niederwieser, A.; Abdel-Rahman, O. S.; Winter, R. F.; Wittmann, V.; Marx, A., Efficient labelling of enzymatically synthesized vinyl-modified DNA by an inverse-electron-demand Diels-Alder reaction. *Chem Commun* 2014, 50 (74), 10827-10829.
24. George, J. T.; Srivatsan, S. G., Vinyluridine as a Versatile Chemoselective Handle for the Post-transcriptional Chemical Functionalization of RNA. *Bioconjugate Chem.* 2017, 28 (5), 1529-1536.

25. Lutz, S.; Liu, L. F.; Liu, Y. C., Engineering Kinases to Phosphorylate Nucleoside Analogs for Antiviral and Cancer Therapy. *Chimia* 2009, 63 (11), 737-744.
26. Mathews, I. I.; Erion, M. D.; Ealick, S. E., Structure of human adenosine kinase at 1.5 angstrom resolution. *Biochemistry* 1998, 37 (45), 15607-15620.
27. Suzuki, N. N.; Koizumi, K.; Fukushima, M.; Matsuda, A.; Inagaki, F., Structural basis for the specificity, catalysis, and regulation of human uridine-cytidine kinase. *Structure* 2004, 12 (5), 751-764.
28. Curanovic, D.; Cohen, M.; Singh, I.; Slagle, C. E.; Leslie, C. S.; Jaffrey, S. R., Global profiling of stimulus-induced polyadenylation in cells using a poly(A) trap. *Nature Chemical Biology* 2013, 9 (11), 671-+.
29. Zheng, Y. X.; Beal, P. A., Synthesis and evaluation of an alkyne-modified ATP analog for enzymatic incorporation into RNA. *Bioorganic & Medicinal Chemistry Letters* 2016, 26 (7), 1799-1802.
30. Grammel, M.; Hang, H.; Conrad, N. K., Chemical Reporters for Monitoring RNA Synthesis and Poly(A) Tail Dynamics. *ChemBioChem* 2012, 13 (8), 1112-1115.
31. Dudycz, L.; Stolarski, R.; Pless, R.; Shugar, D., H-1-Nmr Study of the Syn-Anti Dynamic Equilibrium in Adenine Nucleosides and Nucleotides with the Aid of Some Synthetic Model Analogs with Fixed Conformations. *Z Naturforsch C* 1979, 34 (5-6), 359-373.
32. Rosemeyer, H.; Toth, G.; Golankiewicz, B.; Kazimierczuk, Z.; Bourgeois, W.; Kretschmer, U.; Muth, H. P.; Seela, F., Syn Anti-Conformational Analysis of Regular and Modified Nucleosides by 1d H-1 Noe Difference Spectroscopy - a Simple Graphical-Method Based on Conformationally Rigid Molecules. *Journal of Organic Chemistry* 1990, 55 (22), 5784-5790.

33. Lang, K.; Davis, L.; Torres-Kolbus, J.; Chou, C. J.; Deiters, A.; Chin, J. W., Genetically encoded norbornene directs site-specific cellular protein labelling via a rapid bioorthogonal reaction. *Nat Chem* 2012, 4 (4), 298-304.
34. Li, Z. Q.; Wang, D. Y.; Li, L.; Pan, S. J.; Na, Z. K.; Tan, C. Y. J.; Yao, S. Q., "Minimalist" Cyclopropene-Containing Photo-Cross-Linkers Suitable for Live-Cell Imaging and Affinity-Based Protein Labeling. *Journal of the American Chemical Society* 2014, 136 (28), 9990-9998.
35. Horner, S.; Uth, C.; Avrutina, O.; Frauendorf, H.; Wiessler, M.; Kolmar, H., Combination of inverse electron-demand Diels-Alder reaction with highly efficient oxime ligation expands the toolbox of site-selective peptide conjugations (vol 51, pg 11130, 2015). *Chem Commun* 2015, 51 (58), 11727-11727.
36. Knall, A. C.; Hollauf, M.; Slugovc, C., Kinetic studies of inverse electron demand Diels-Alder reactions (iEDDA) of norbornenes and 3,6-dipyridin-2-yl-1,2,4,5-tetrazine. *Tetrahedron Lett* 2014, 55 (34), 4763-4766.
37. Bickelhaupt, F. M.; Houk, K. N., Analyzing Reaction Rates with the Distortion/Interaction-Activation Strain Model. *Angew Chem Int Edit* 2017, 56 (34), 10070-10086.
38. Blizzard, R. J.; Backus, D. R.; Brown, W.; Bazewicz, C. G.; Li, Y.; Mehl, R. A., Ideal Bioorthogonal Reactions Using A Site-Specifically Encoded Tetrazine Amino Acid. *Journal of the American Chemical Society* 2015, 137 (32), 10044-10047.
39. An, R.; Jia, Y.; Wan, B. H.; Zhang, Y. F.; Dong, P.; Li, J.; Liang, X. G., Non-Enzymatic Depurination of Nucleic Acids: Factors and Mechanisms. *Plos One* 2014, 9 (12).

40. Burger, K.; Muhl, B.; Kellner, M.; Rohrmoser, M.; Gruber-Eber, A.; Windhager, L.; Friedel, C. C.; Dolken, L.; Eick, D., 4-thiouridine inhibits rRNA synthesis and causes a nucleolar stress response. *Rna Biol* 2013, 10 (10), 1623-1630.
41. Triemer, T.; Messikommer, A.; Glasauer, S. M. K.; Alzeer, J.; Paulisch, M. H.; Luedtke, N. W., Superresolution imaging of individual replication forks reveals unexpected prodrug resistance mechanism. *P Natl Acad Sci USA* 2018, 115 (7), E1366-E1373.

Chapter 3

Conclusion & Future Perspectives

3.1 Conclusion & Future Perspectives

The research accomplishments presented in this thesis have described the development of bioorthogonally functionalized nucleosides, the development of their complementary reacting partner, and their use to study RNA biology. These compounds advance the chemical toolbox available for RNA chemical biology and becomes comparable to the chemical toolbox for other biomacromolecules. Use of these methods developed offer a greater understanding of RNA biology.

In chapter 1, azido modification of the 2' position on the ribose sugar was explored on pyrimidine nucleosides and their incorporation into RNA transcripts. Synthetic challenges from this work stemmed from the scalability of the synthesis. Upon examination of the synthesis, the least efficient and the most hazardous reaction in the synthetic pathway was determined to be the azidation of 2,2'-anhydrouridine to 2'-azidouridine. Initially this reaction was accomplished by refluxing 2,2'-anhydrouridine in DMF with NaN_3 in excess. This reaction on the milligram scale still has the possibility of explosion but can be managed. Initially this reaction was poor yielding, but through optimization a yield of 55% was achieved. In the scale up of this reaction, a different azidation method was pursued to minimize the possibility of explosion. To accomplish this, reaction conditions lowered the amount of azide content into the reaction and lowered the temperature of the reaction. The reaction utilized a "naked" azide ion in the reaction through the use of TMS-N_3 with LiF in a TMEDA:DMF mixture. While this reaction took a longer time to go to completion, the reaction

was able to produce grams of material needed for biological tests. 2'-Azidocytidine revealed to be readily incorporated into RNA transcripts through dot blot analysis. 2'-Azidouridine was shown not to be incorporated into RNA. In conclusion, we demonstrated the availability and utility of 2'-azido functionality for the study of RNA.

In chapter 2, vinyl functionalization on nucleobases and nucleosides for metabolic incorporation was explored. Due to the introduction of a poor dienophile for inverse electron demand Diels-Alder (IEDDA), the exploration of finding a reactive tetrazine was pursued to maintain fast kinetics. Positional functionalization of the nucleobases was determined by analysis of the initial kinase crystal structures involved in the metabolic pathway for incorporation. Vinyl-nucleosides and vinyl-nucleobases were synthesized using Stille coupling and Suzuki coupling. DFT calculations were used to determine the lowest LUMO+1 energies of tetrazines. A variety of tetrazines were synthesized and a kinetic analysis was performed to determine the fastest tetrazine-vinyl-nucleoside pair. While trying to correlate the HOMO-LUMO+1 gap with the kinetics, discrepancies were found. From this analysis, it was determined that the frontier orbital picture was incomplete and does not take into account the long-range noncovalent interactions. The fastest tetrazine was observed to undergo rapid hydrolysis. It was determined that the addition of AcOH (lowered pH) to the reaction mixture stabilized the hydrolysis of the tetrazine and still maintains RNA integrity. This offers the possibility to perform this reaction in acidic environments. With the vinyl-nucleosides in hand, they were tested for metabolic incorporation, imaging, and toxicity. Only 5-vinyluridine, 2-vinyladenosine, and 7-deazavinyladenosine were incorporated into transcripts by dot blot analysis. 5-vinyluridine was also found to be nontoxic to cells unlike the popularly used 5-ethynyluridine. With the vinyl functionality being incorporated into

RNA transcripts, this offers another set of chemistry that can be used to study RNA. It was then demonstrated that the use of IEDDA and copper catalyzed alkyne azide cycloadditions could be used to simultaneously without cross reactivity between the two chemistries. In conclusion, we demonstrated the utility of vinyl-nucleosides for the study of RNA.

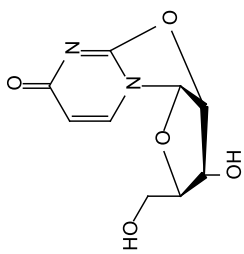
Current progress in the use of these nucleosides and reacting partners offers the user the ability to perform bioorthogonal reactions on RNA. Use RNA biochemical methods supplemented with these reactions offers advancement of such biochemical methods and unveils RNA biology. A lacking area for these chemistries stems from the ability to perform reactions in a spatiotemporal manner. This can be made possible by the use of photodibo.¹ However, the availability of photodibo is scarce. A possible method to get around this is to utilize the vinyl ether-phenanthrenequinone photoclick reaction created by Li, J. *et al.*² The synthesis for such nucleosides could be pursued through a similar synthesis for 2'-azidouridine but with TMS-vinylether. Or possibly through a modified synthesis similar to the synthesis of 2'-vinyletherthymine by Gallagher, W. *et al.*³ In conclusion, the use of small unnatural functionalities on nucleosides offers the utility of new chemistries that can advance RNA biochemical methods.

3.2 References

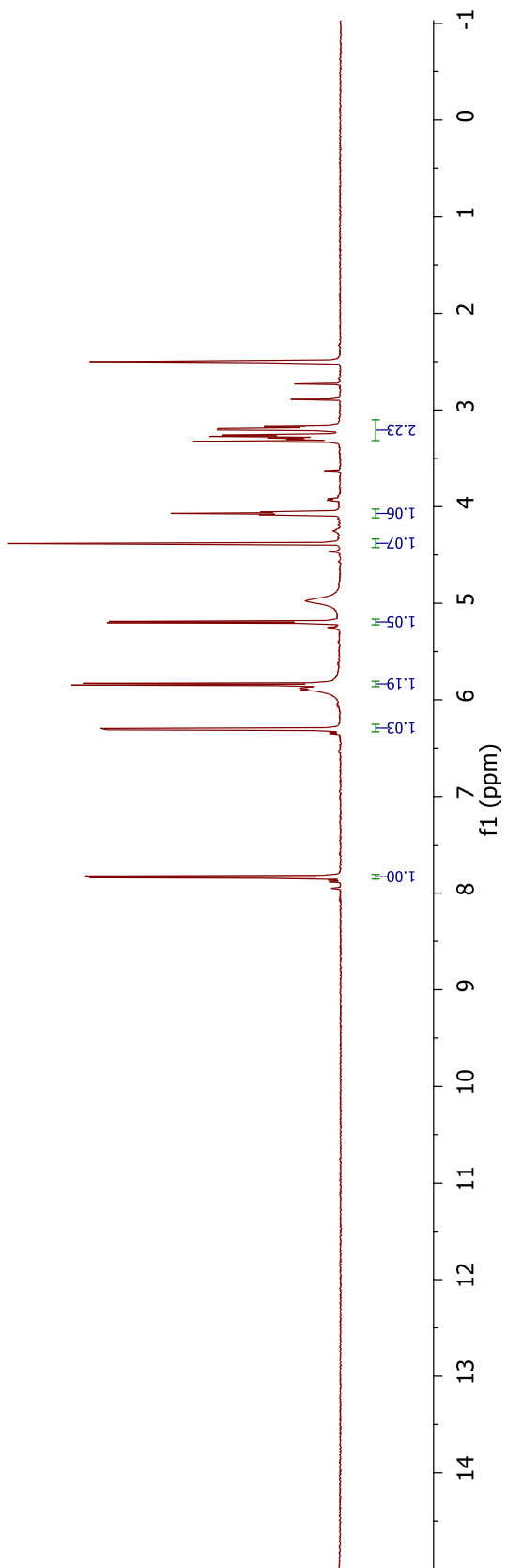
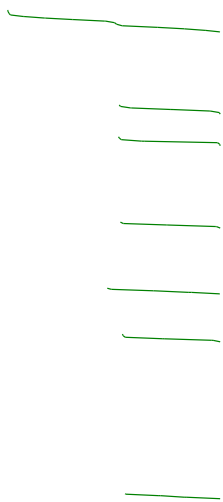
1. Nainar, S.; Kubota, M.; McNitt, C.; Tran, C.; Popik, V. V.; Spitale, R. C., *Journal of the American Chemical Society* **2017**, *139*, 8090-8093.
2. Li, J.; Kong, H.; Huang, L.; Cheng, B.; Qin, K.; Zheng, M.; Yan, Z.; Zhang, Y., *Journal of the American Chemical Society* **2018**, *140*, 14542-14546.
3. Gallagher, W. P.; Deshpande, P. P.; Li, J.; Katipally, K.; Sausker, J., *Organic Letters* **2015**, *17*, 14-17.

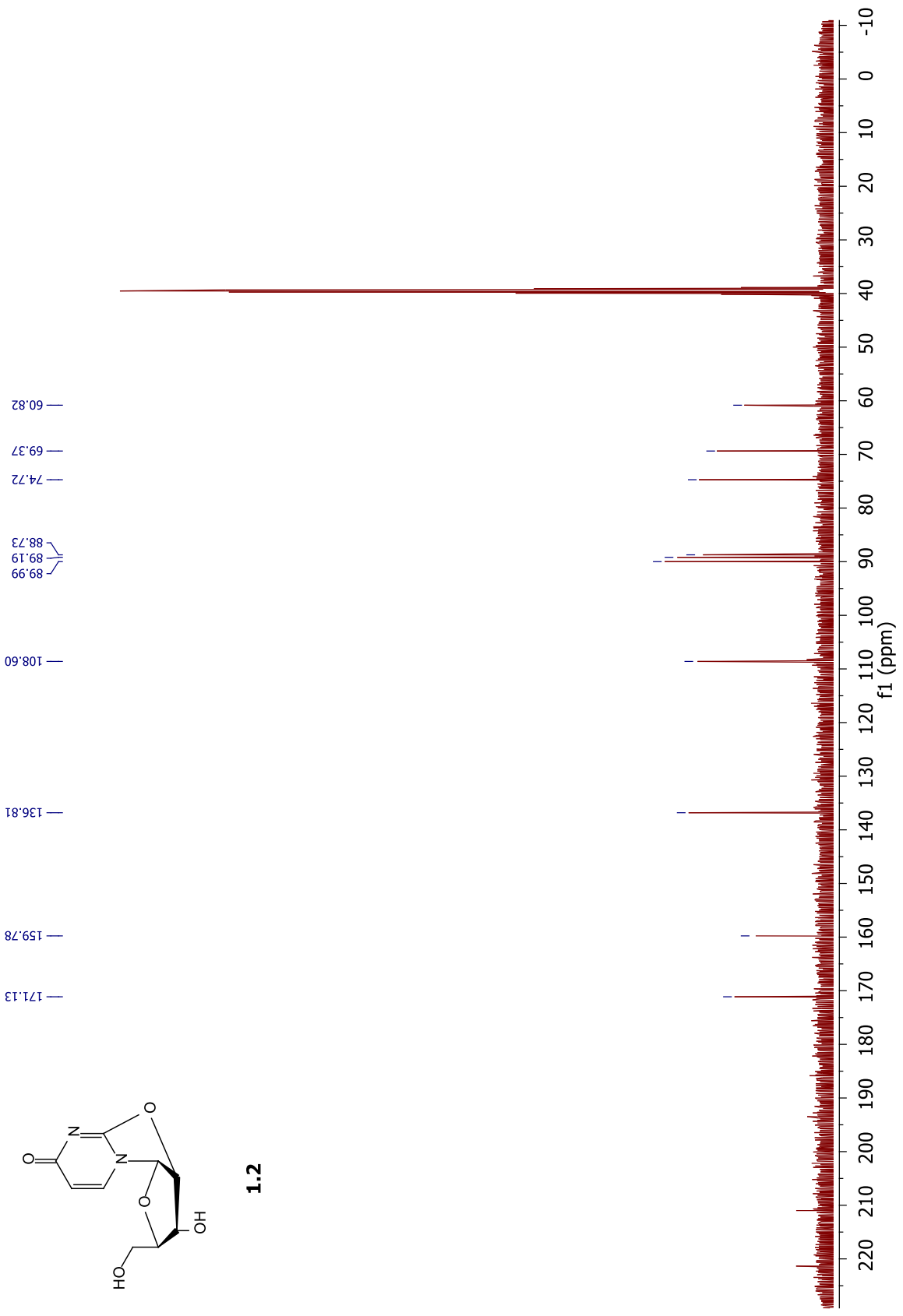
Appendix A

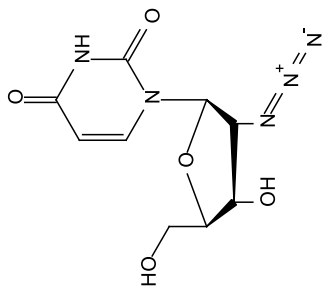
Supplemental NMR Spectra



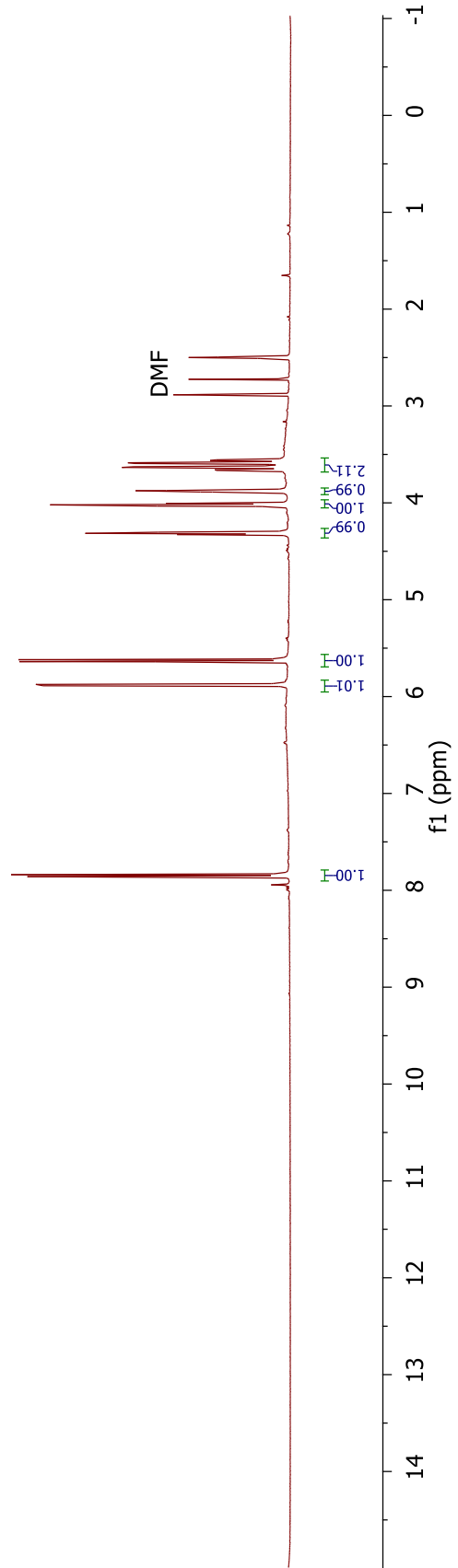
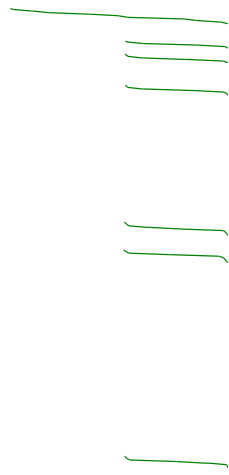
1.2

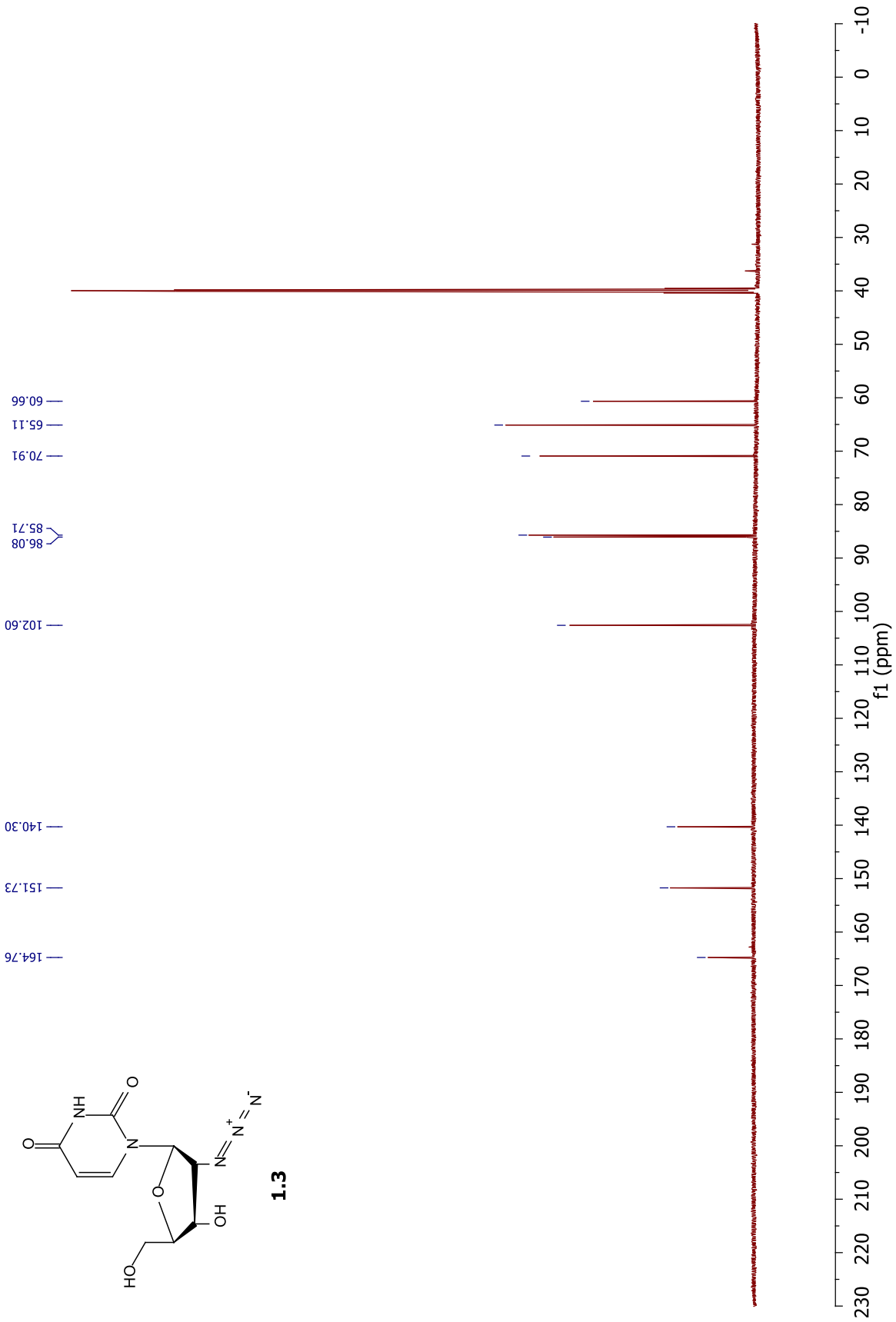
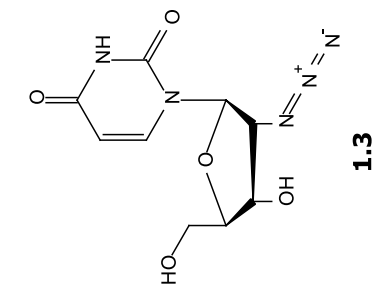


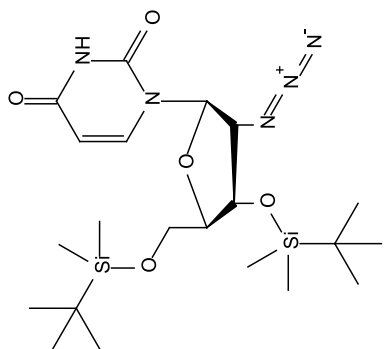




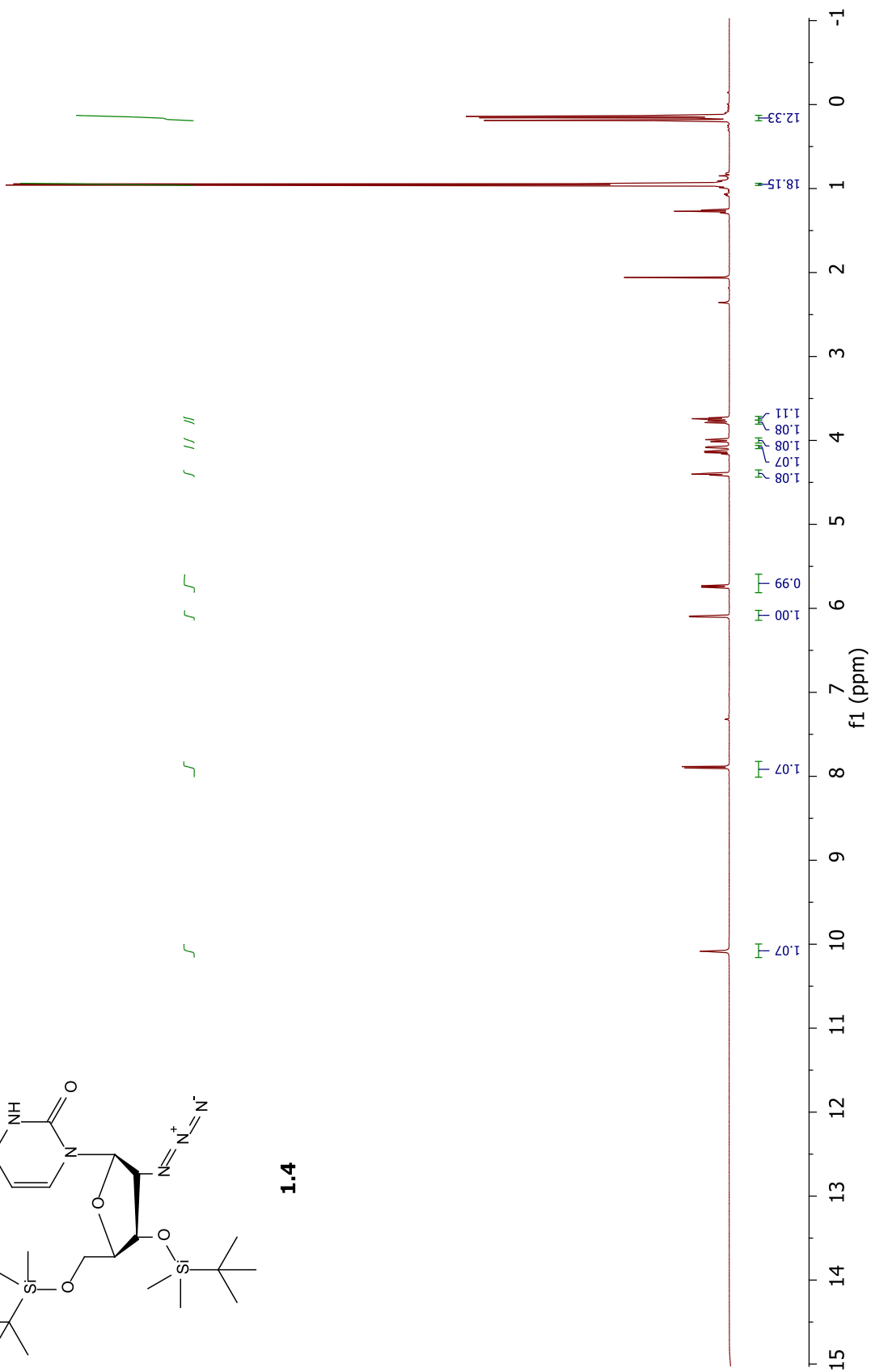
1.3

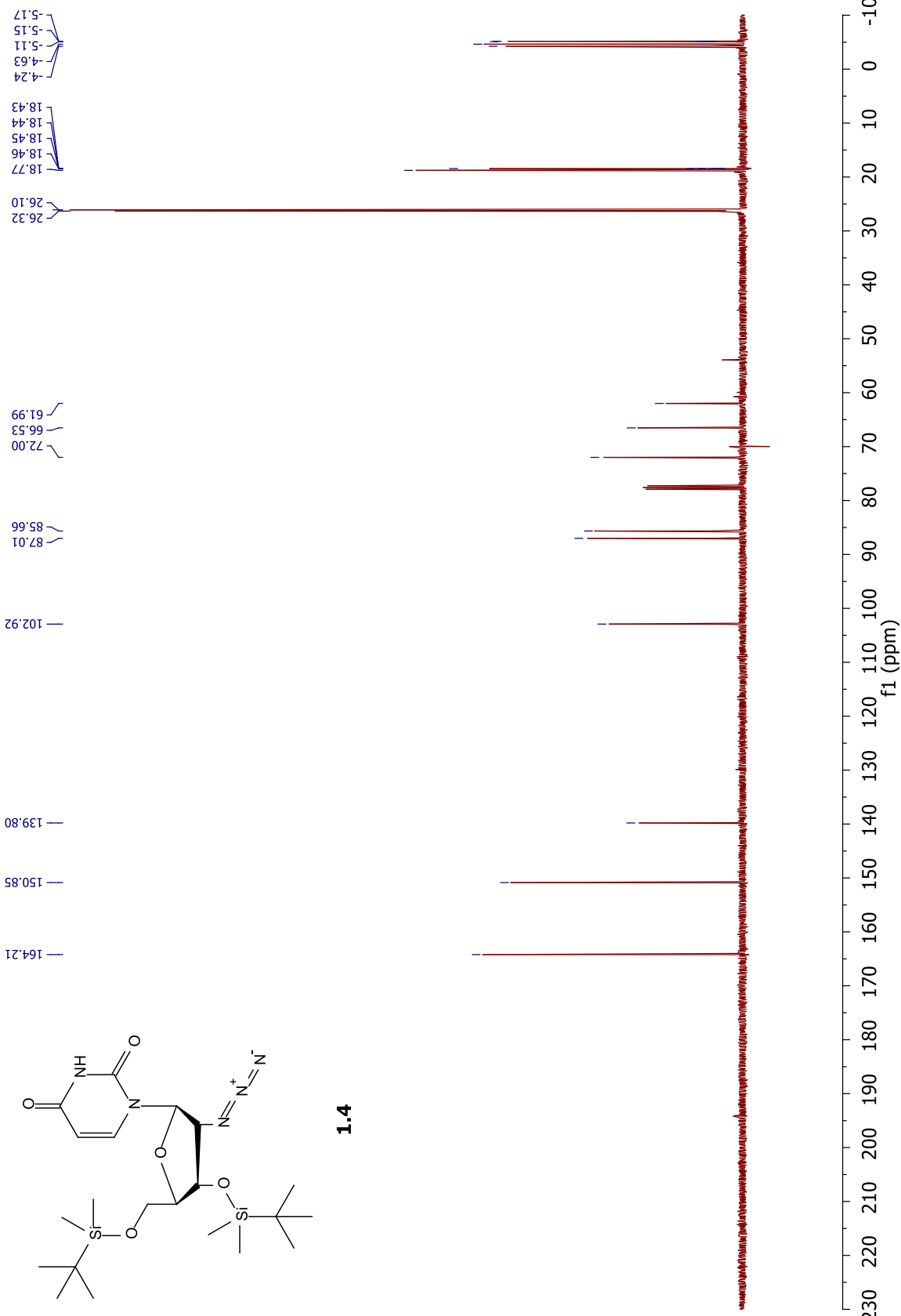




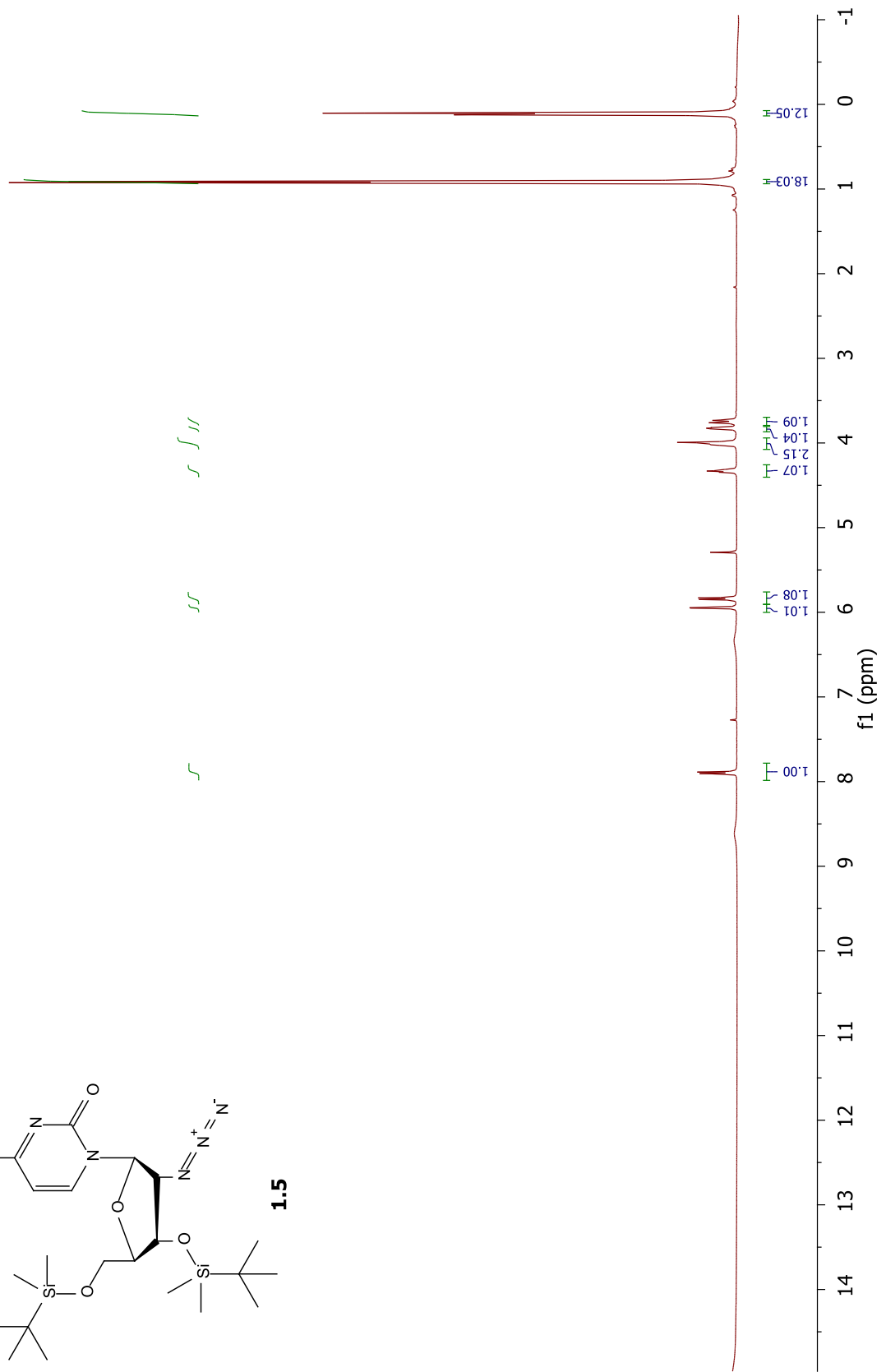
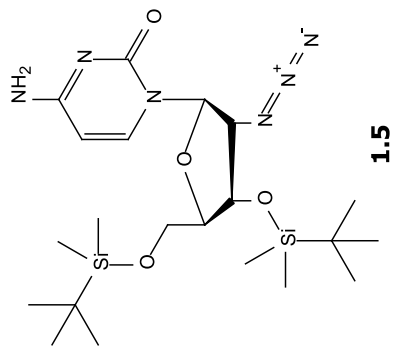


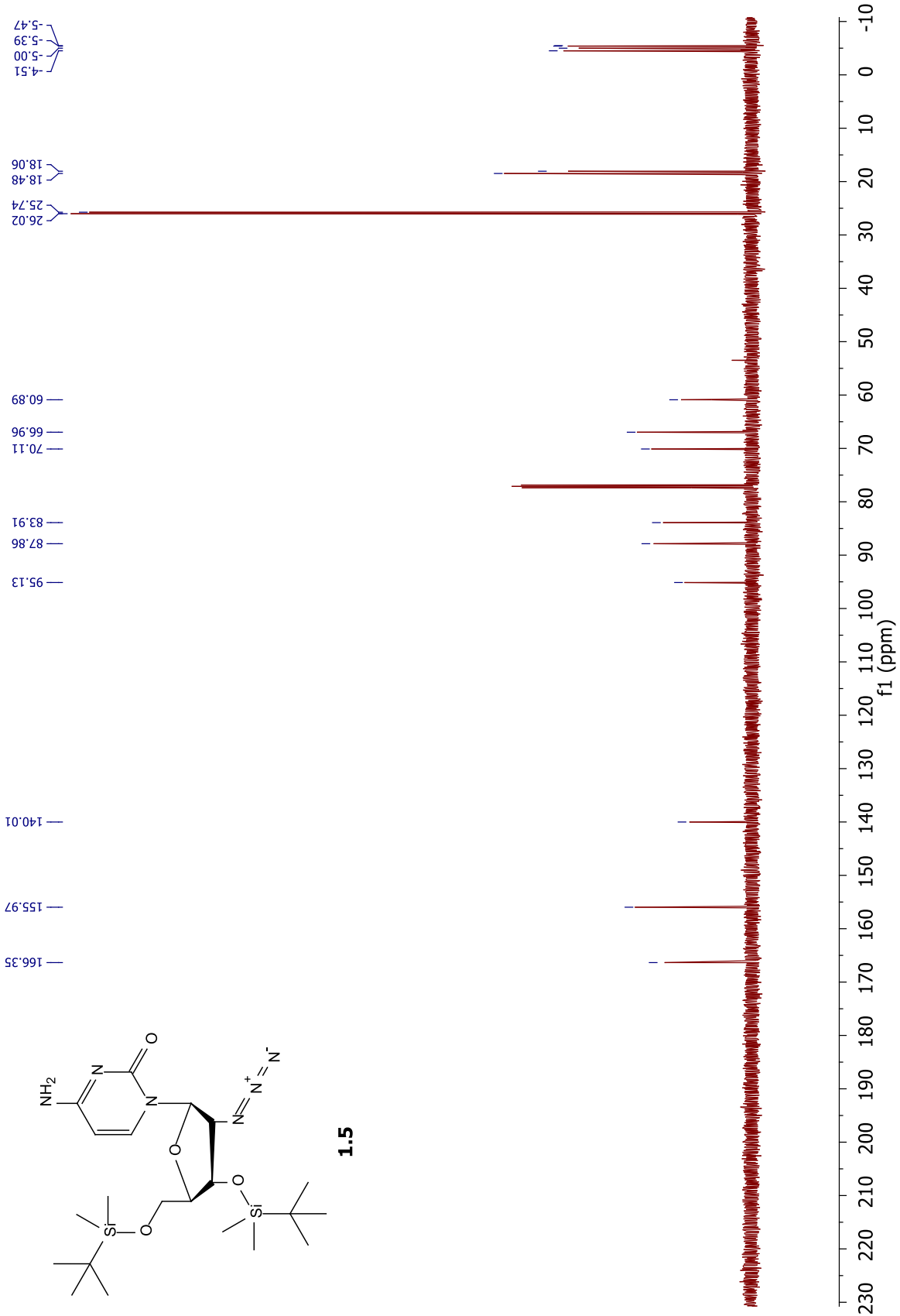
1.4

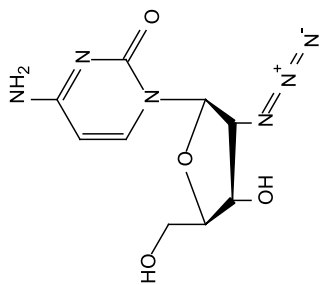




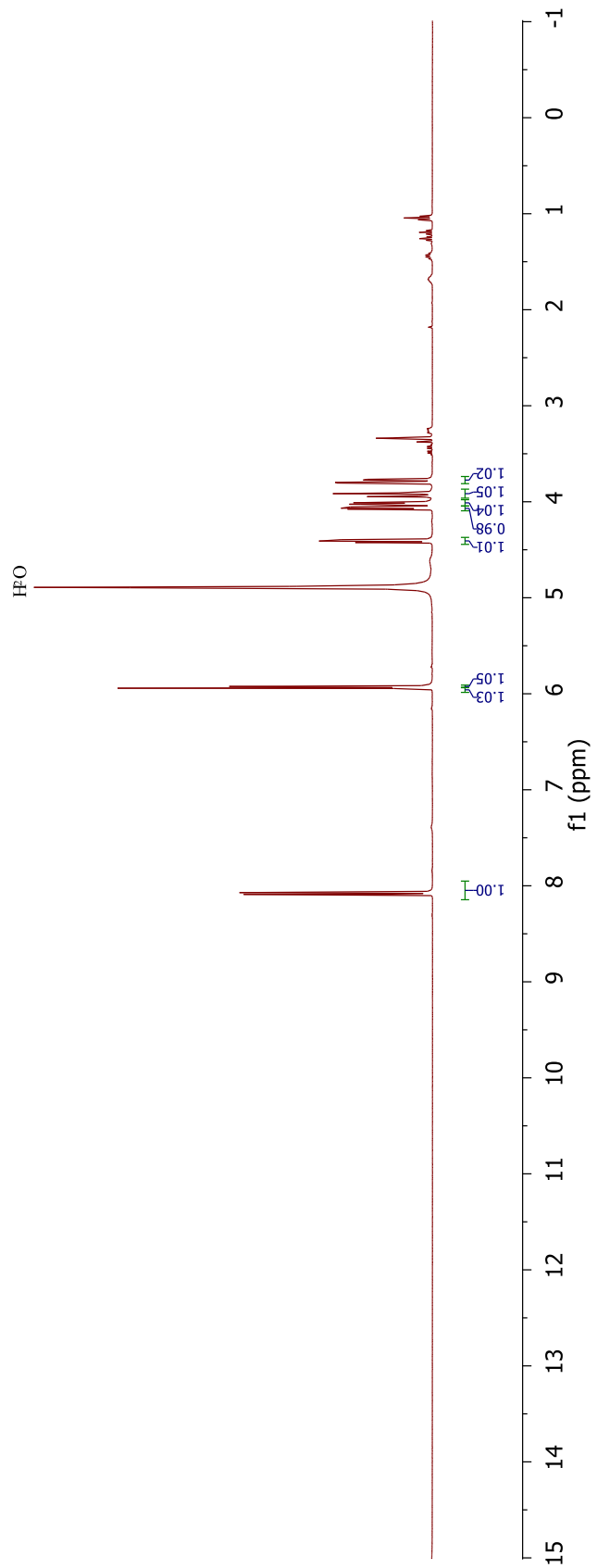
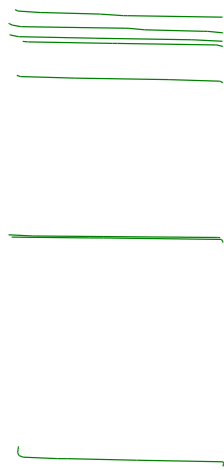
1.4

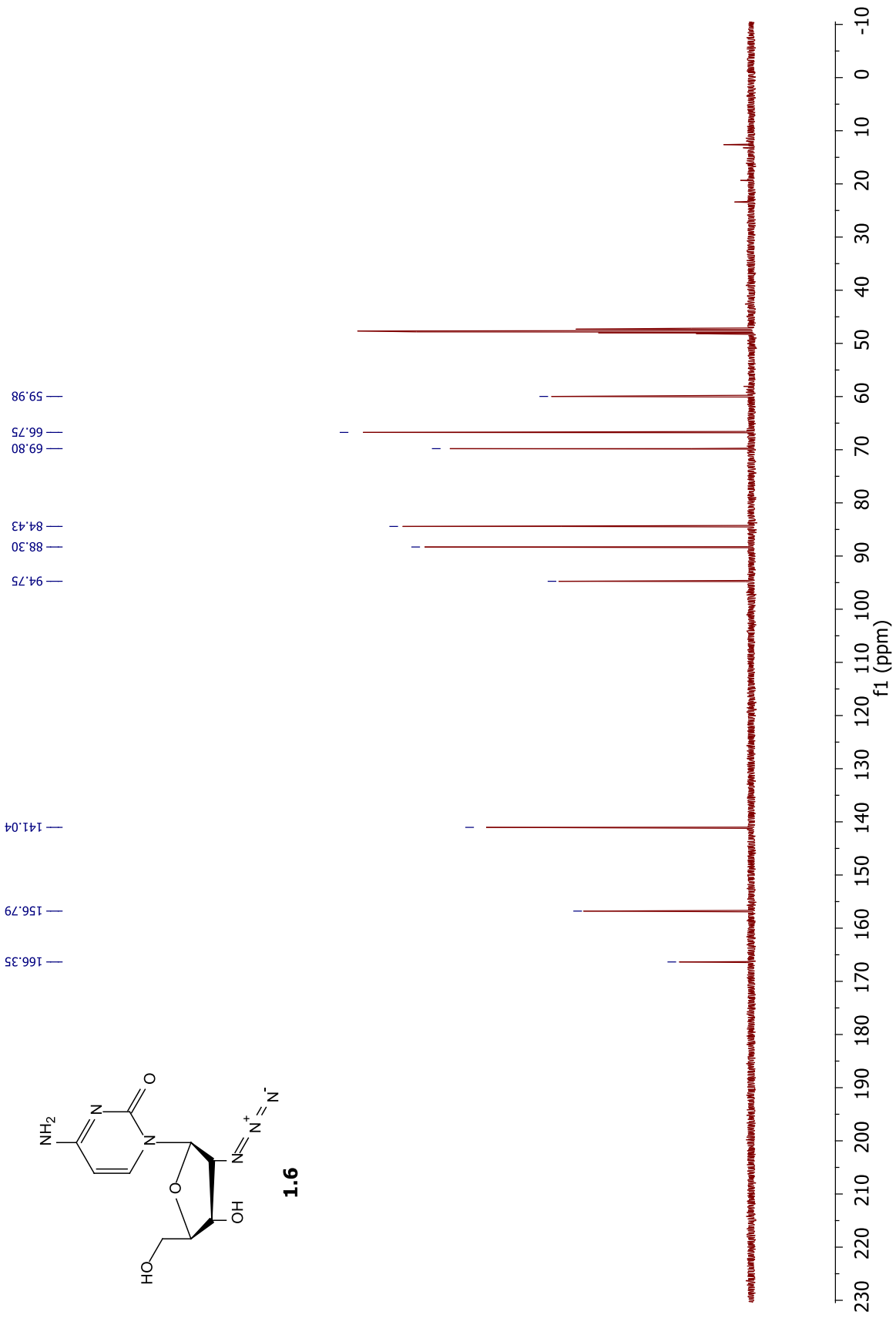


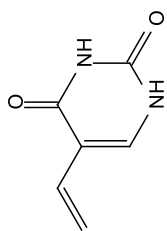




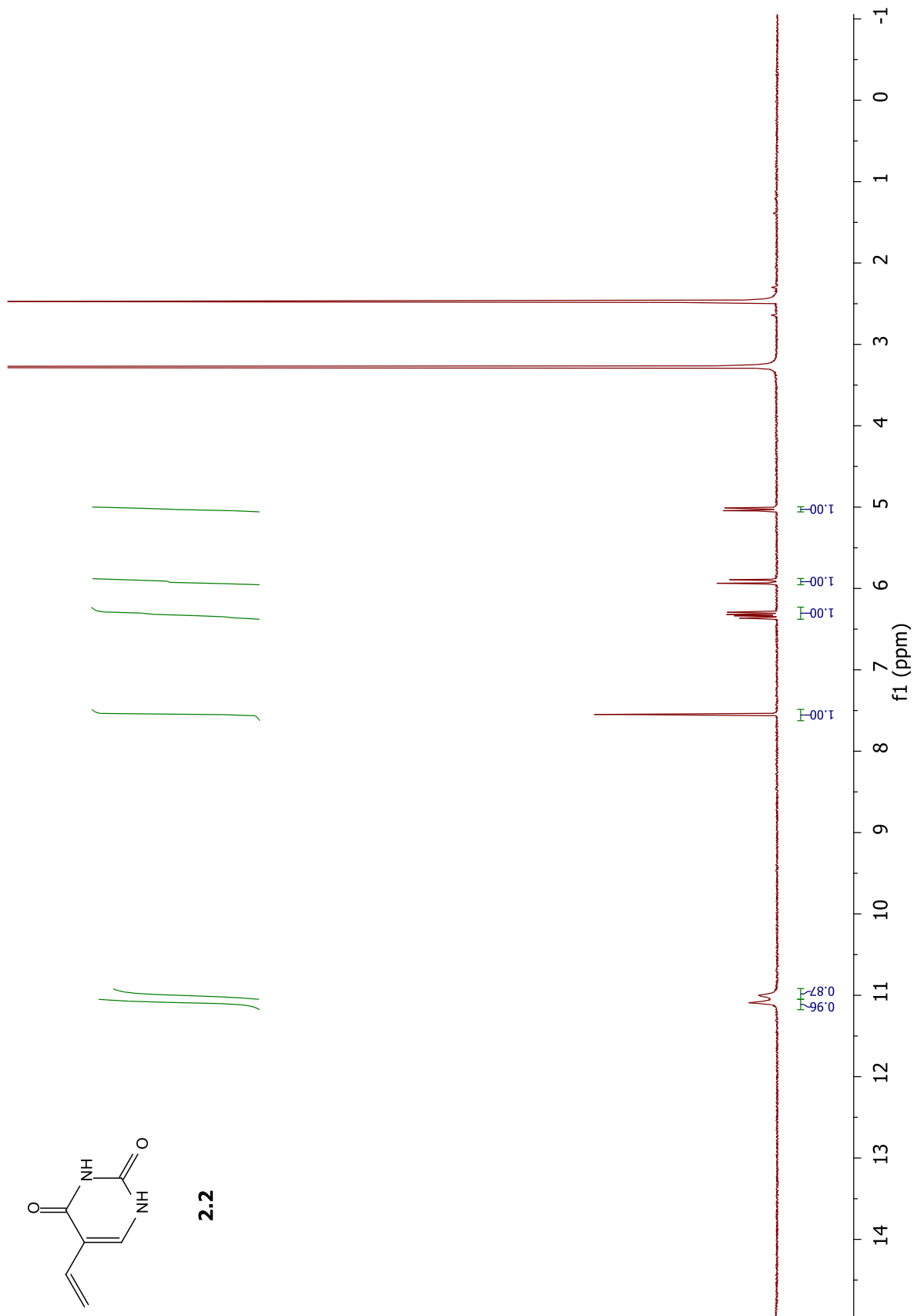
1.6

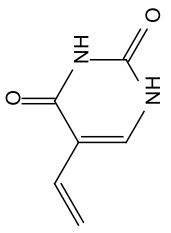
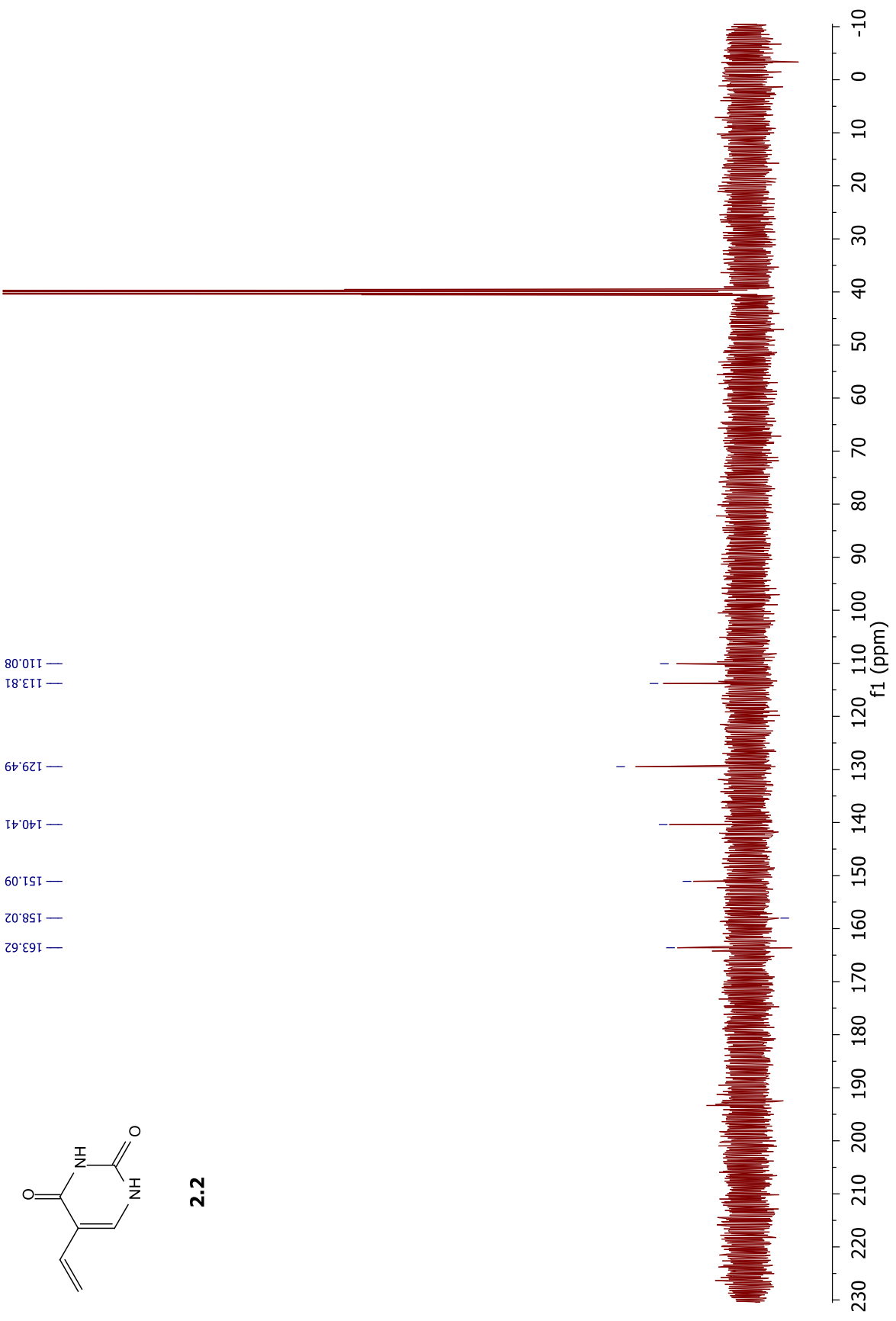




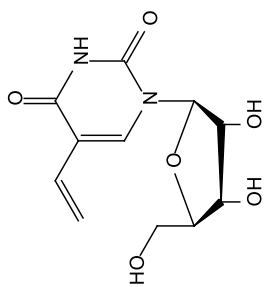


2.2

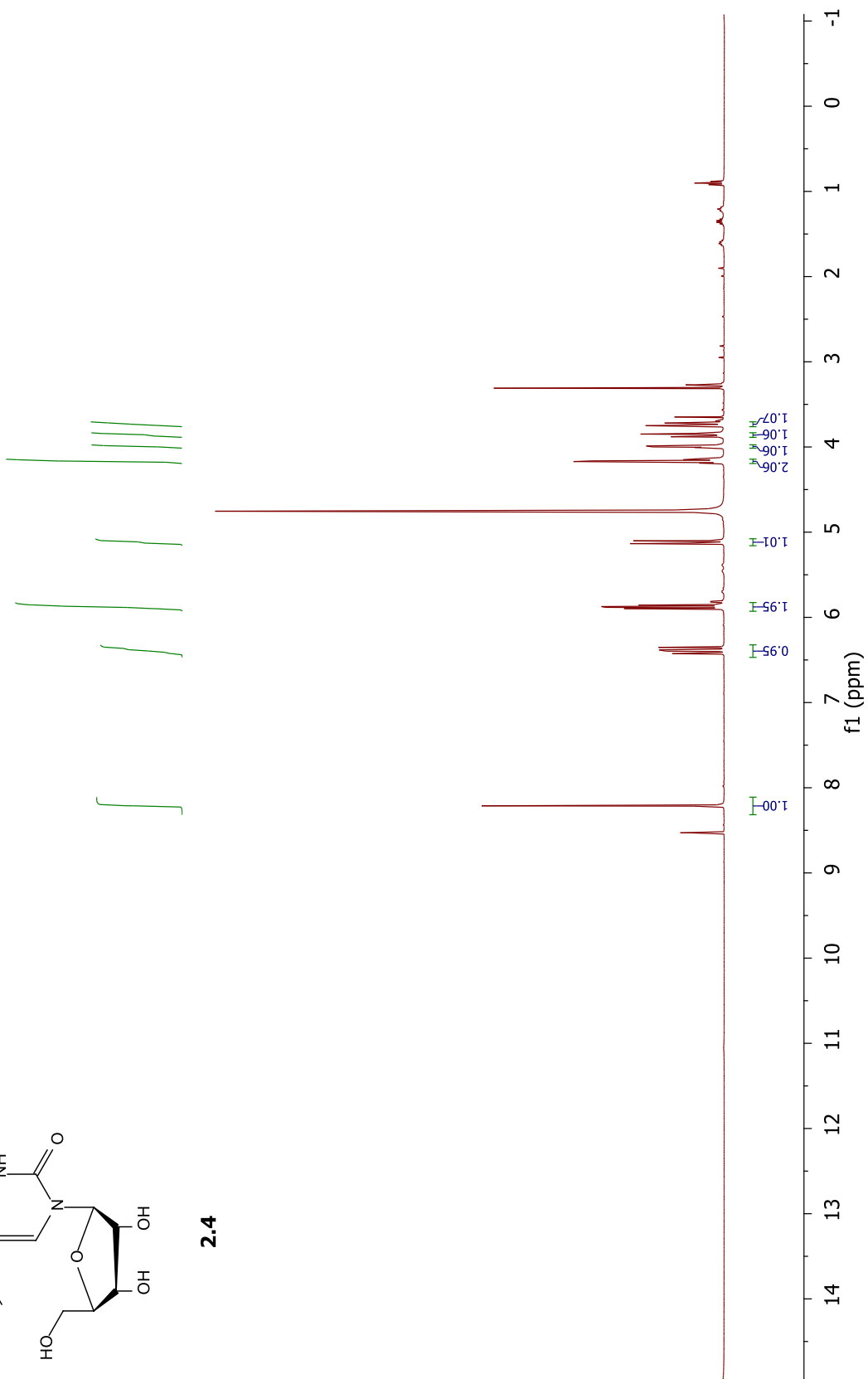


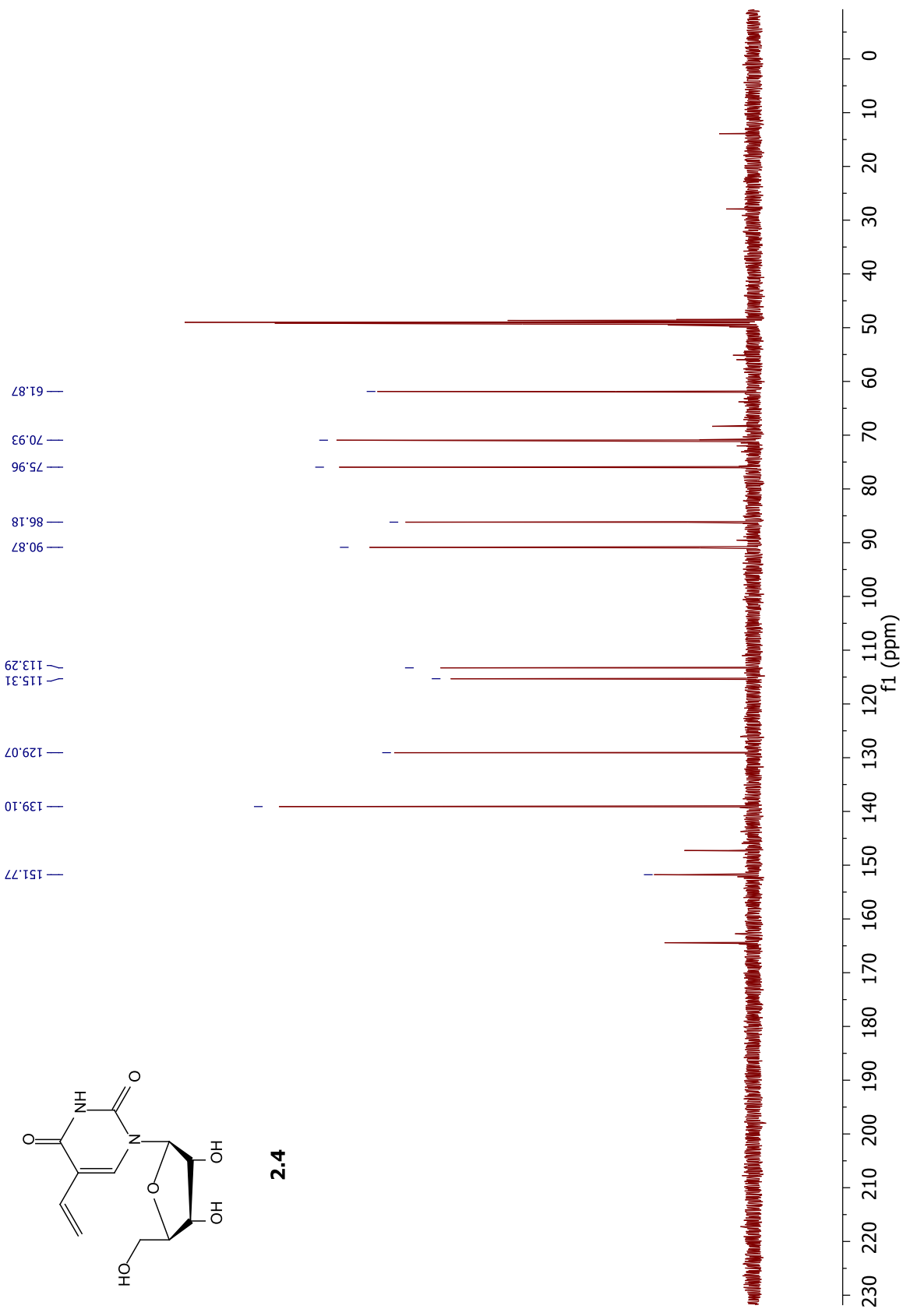


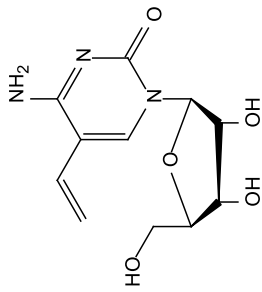
2.2



2.4

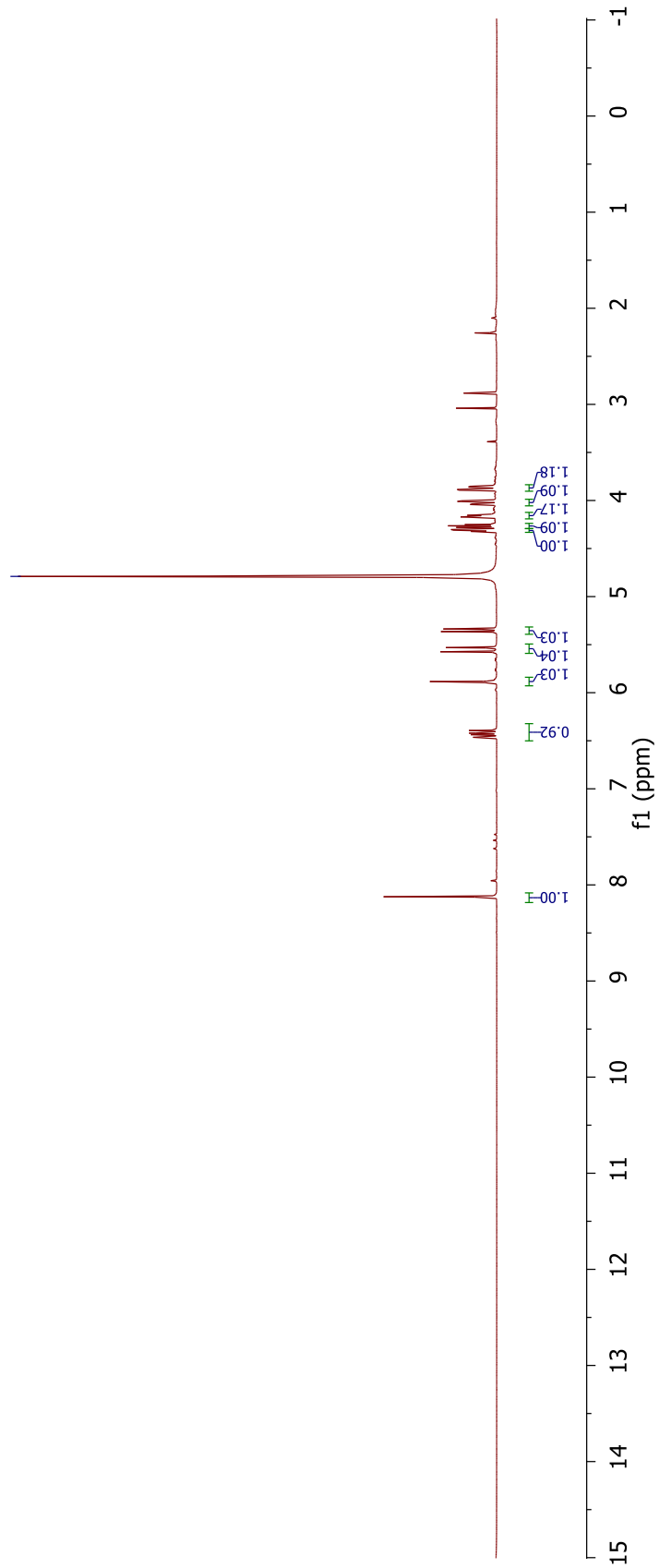
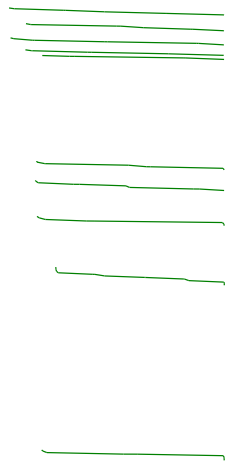


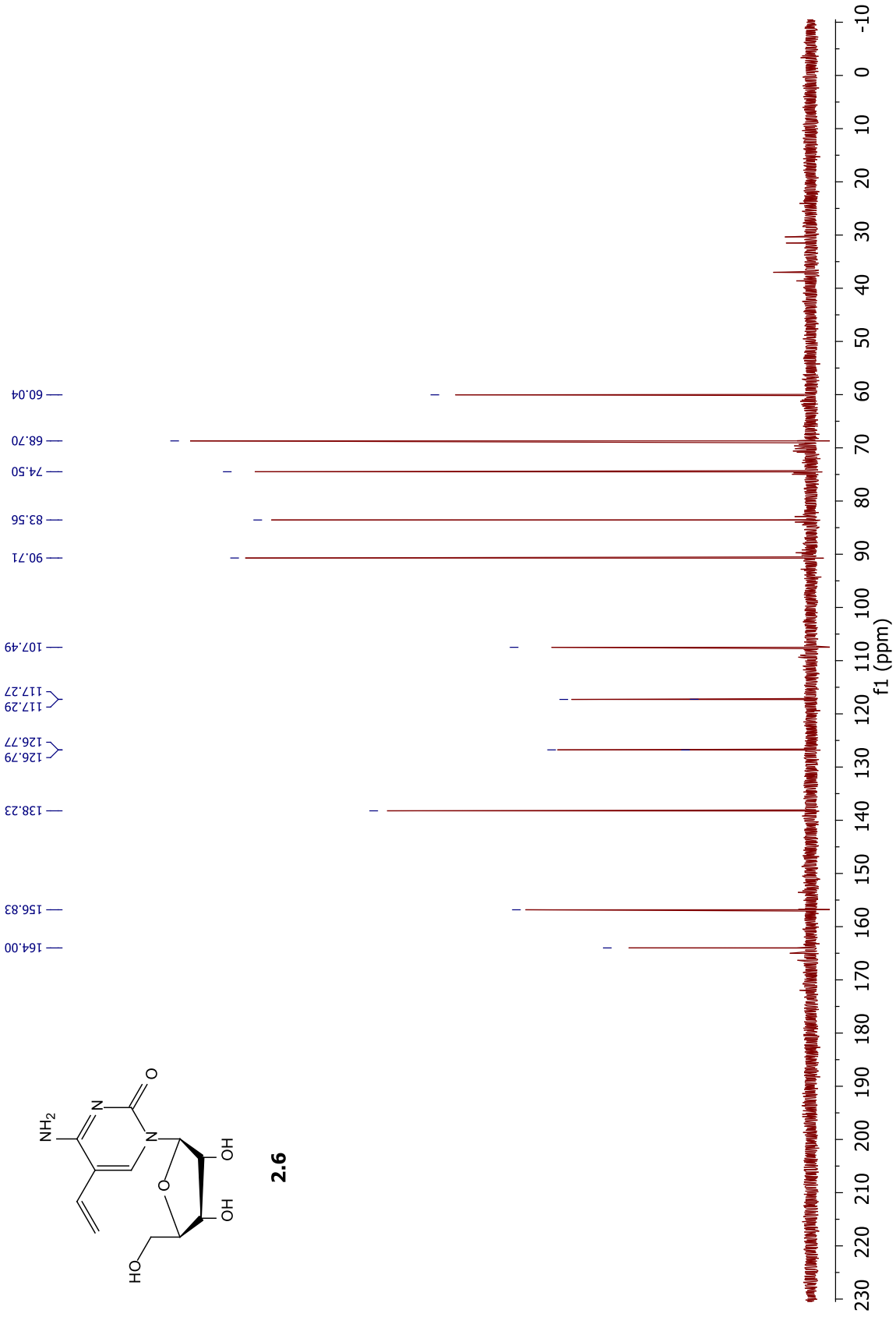


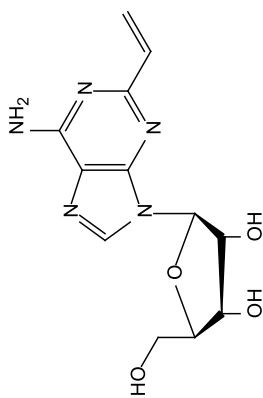


2.6

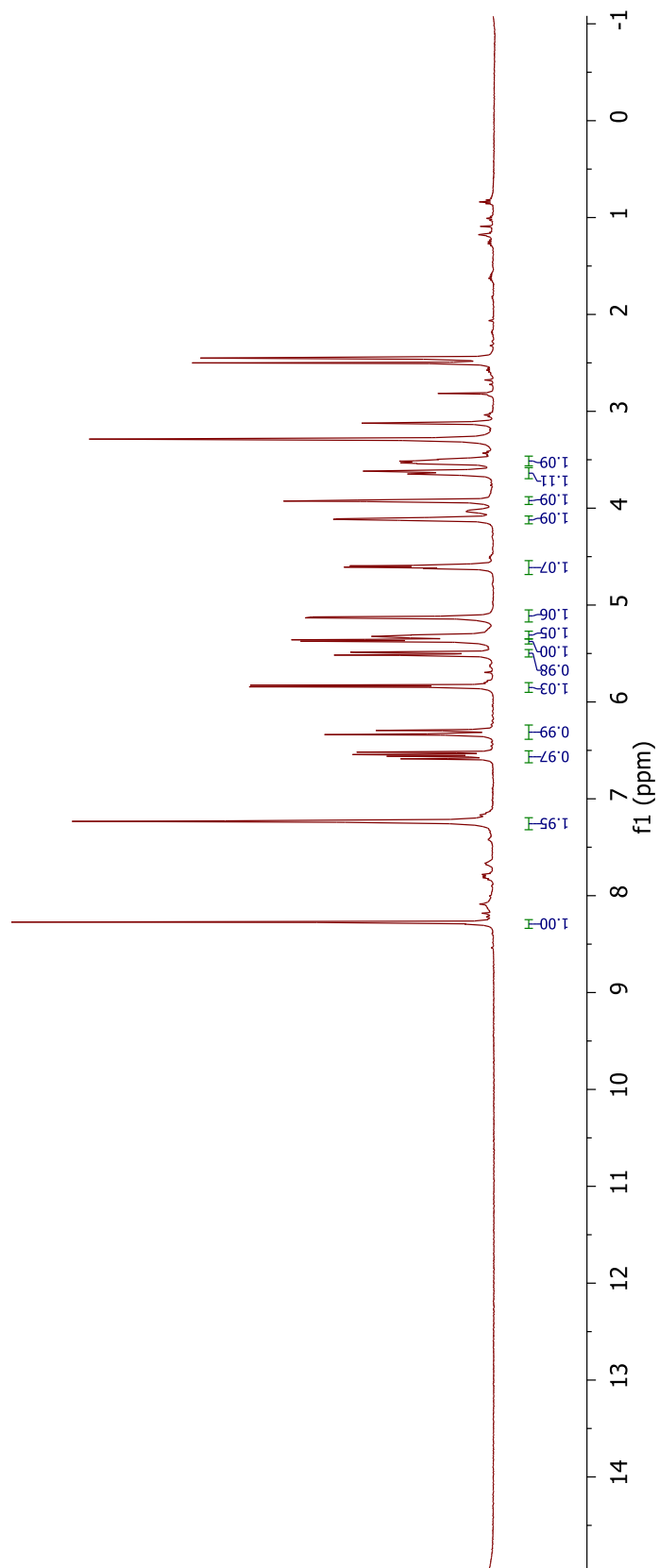
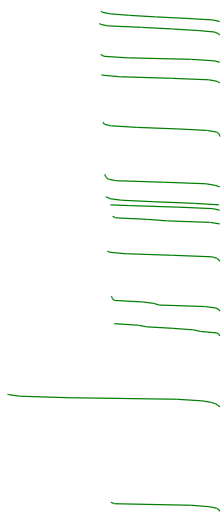
4.79

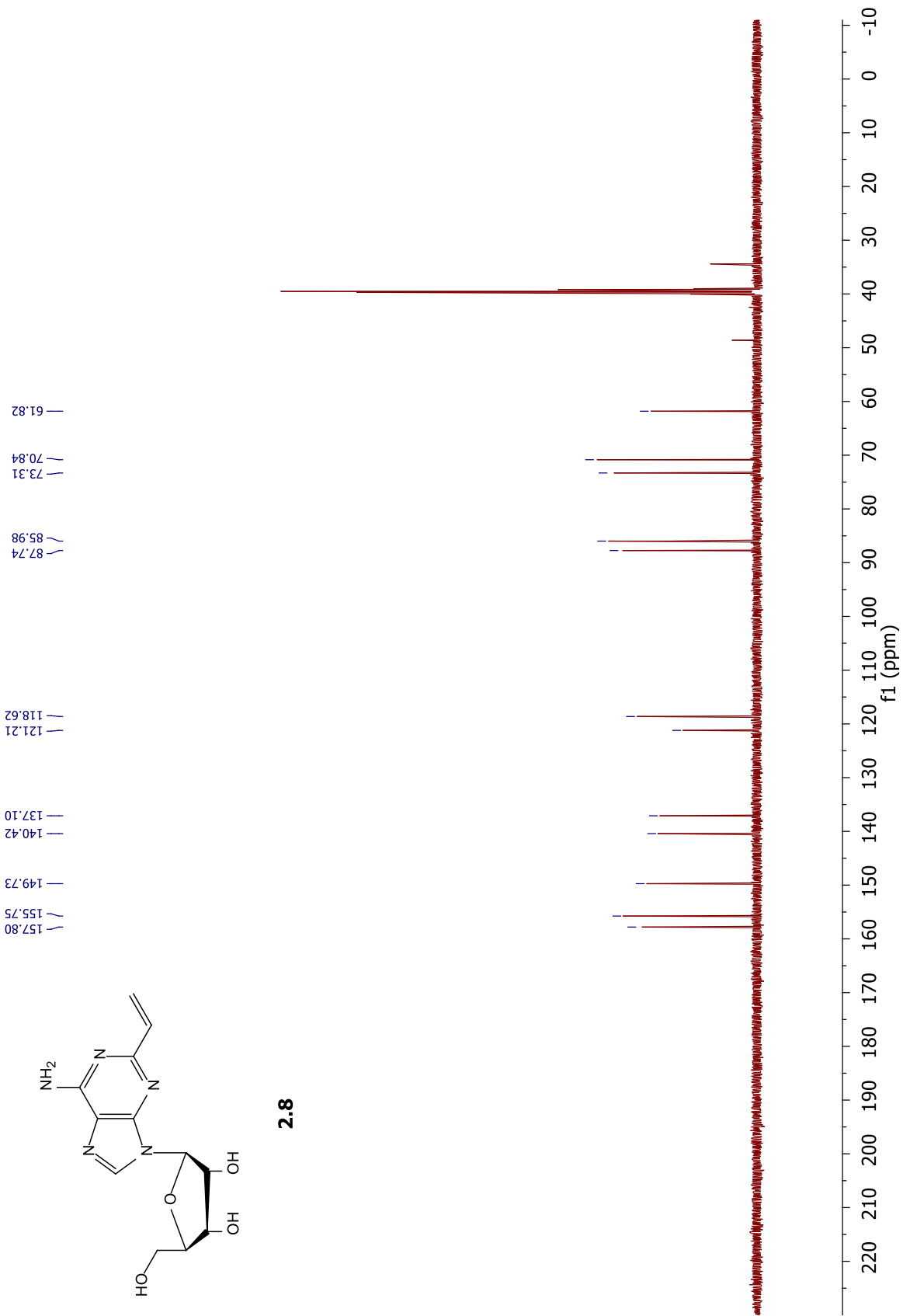


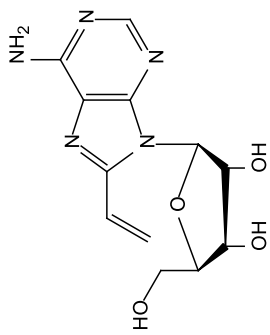




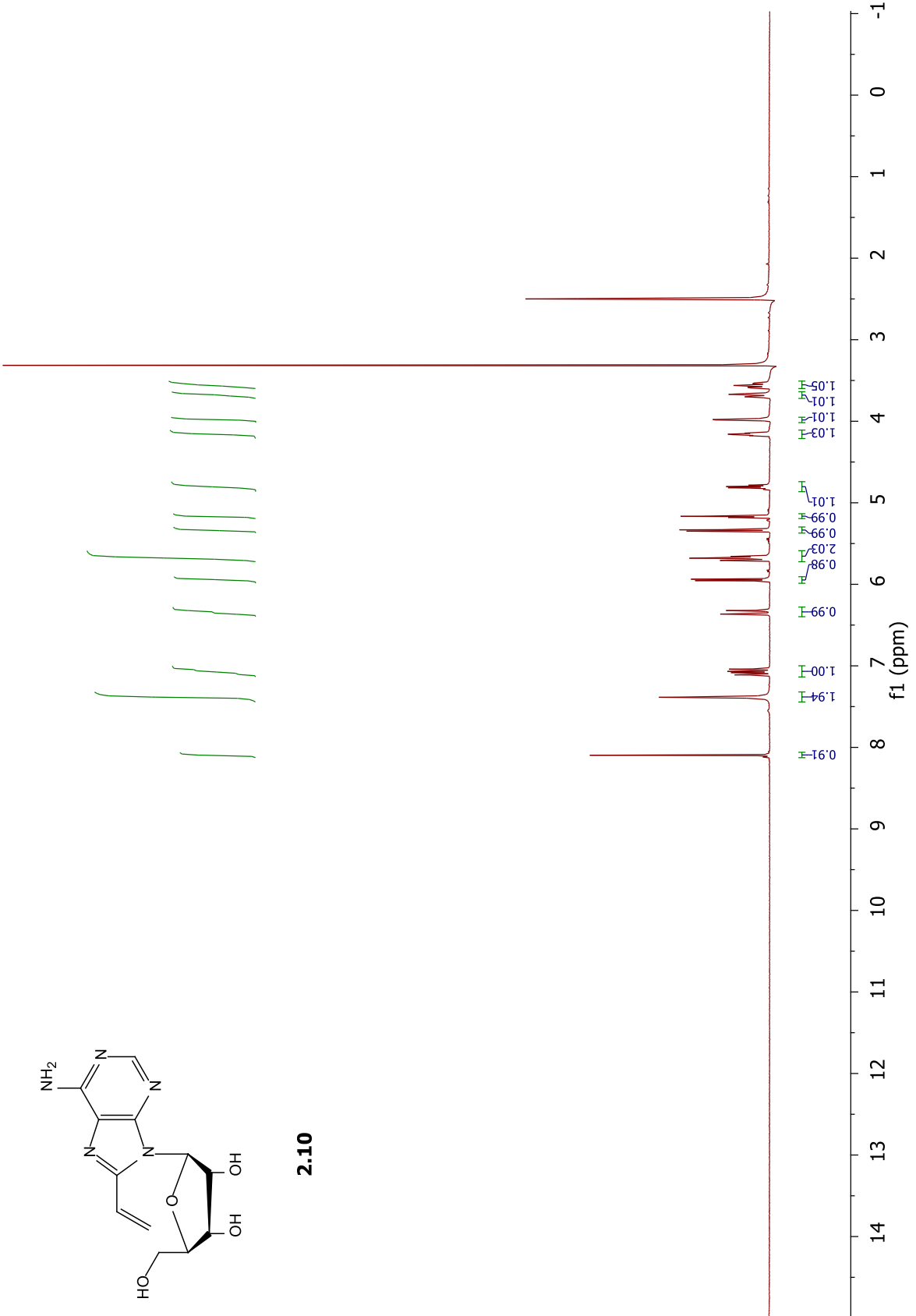
2.8

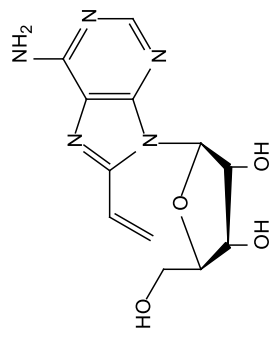
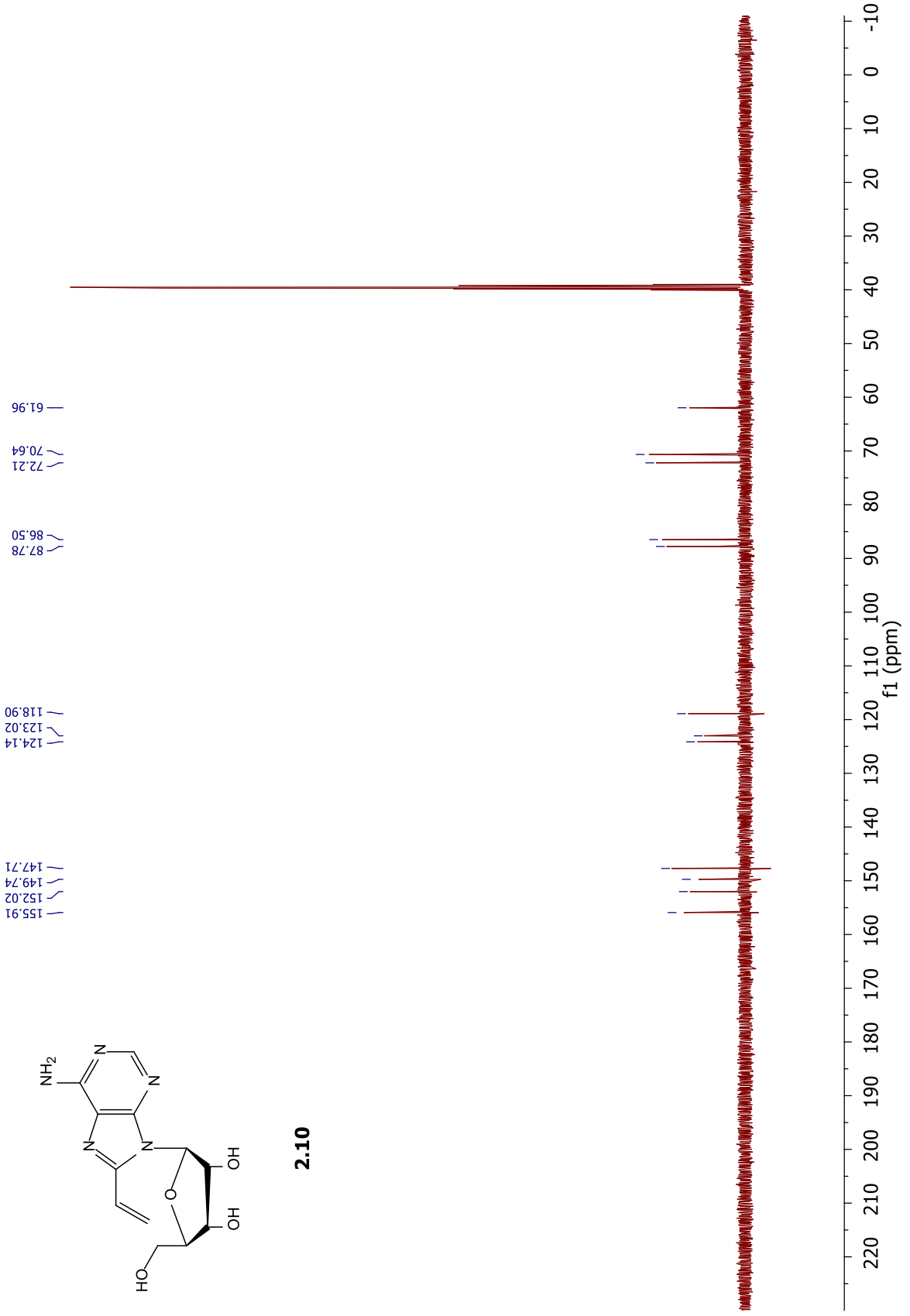




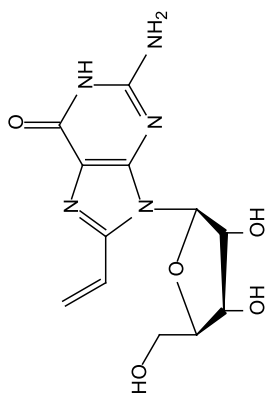


2.10

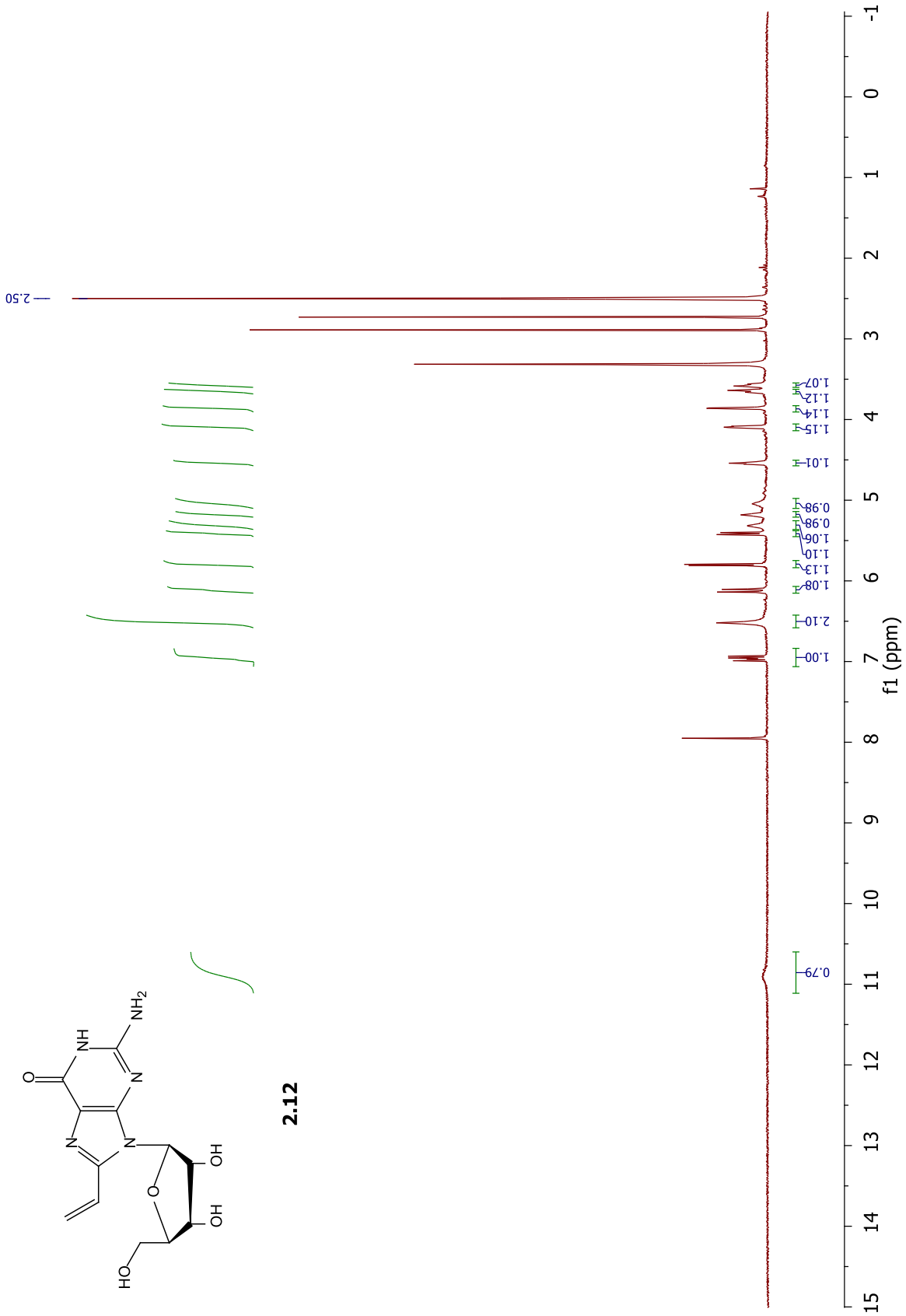


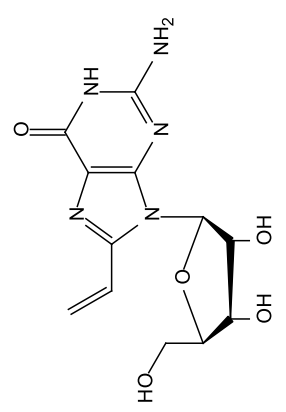
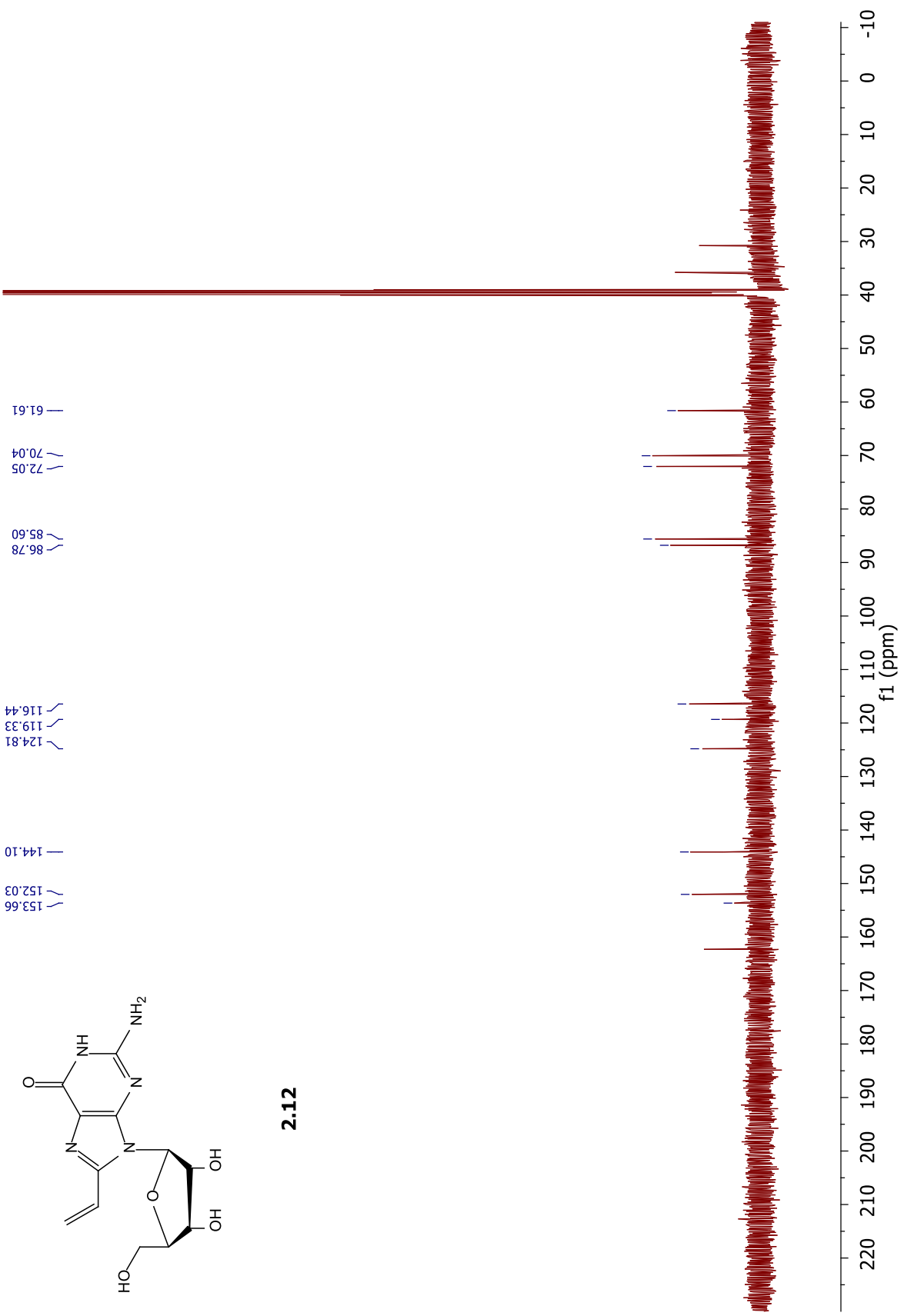


2.10

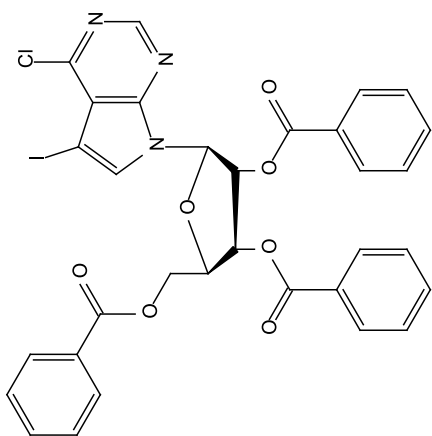


2.12

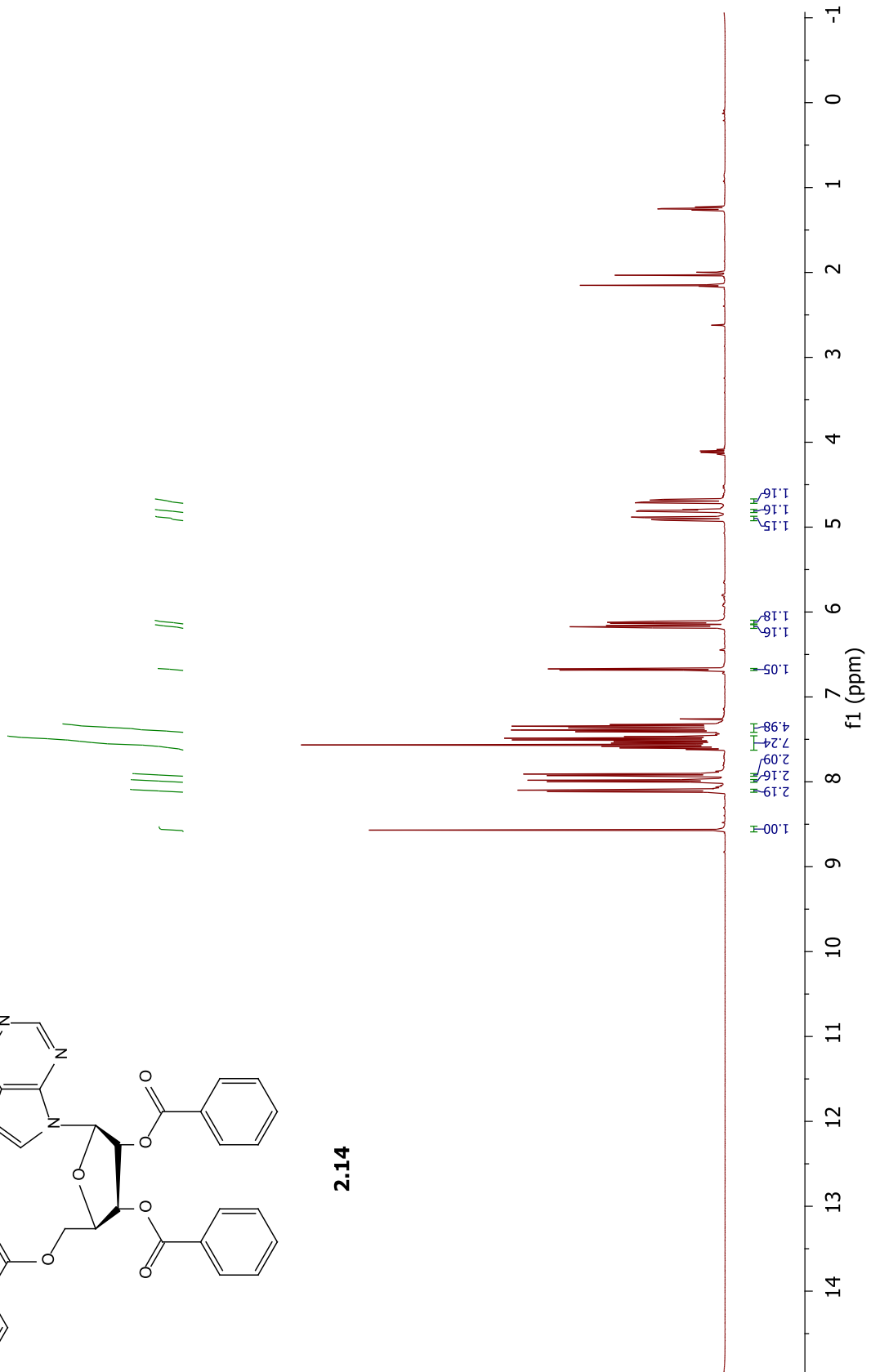


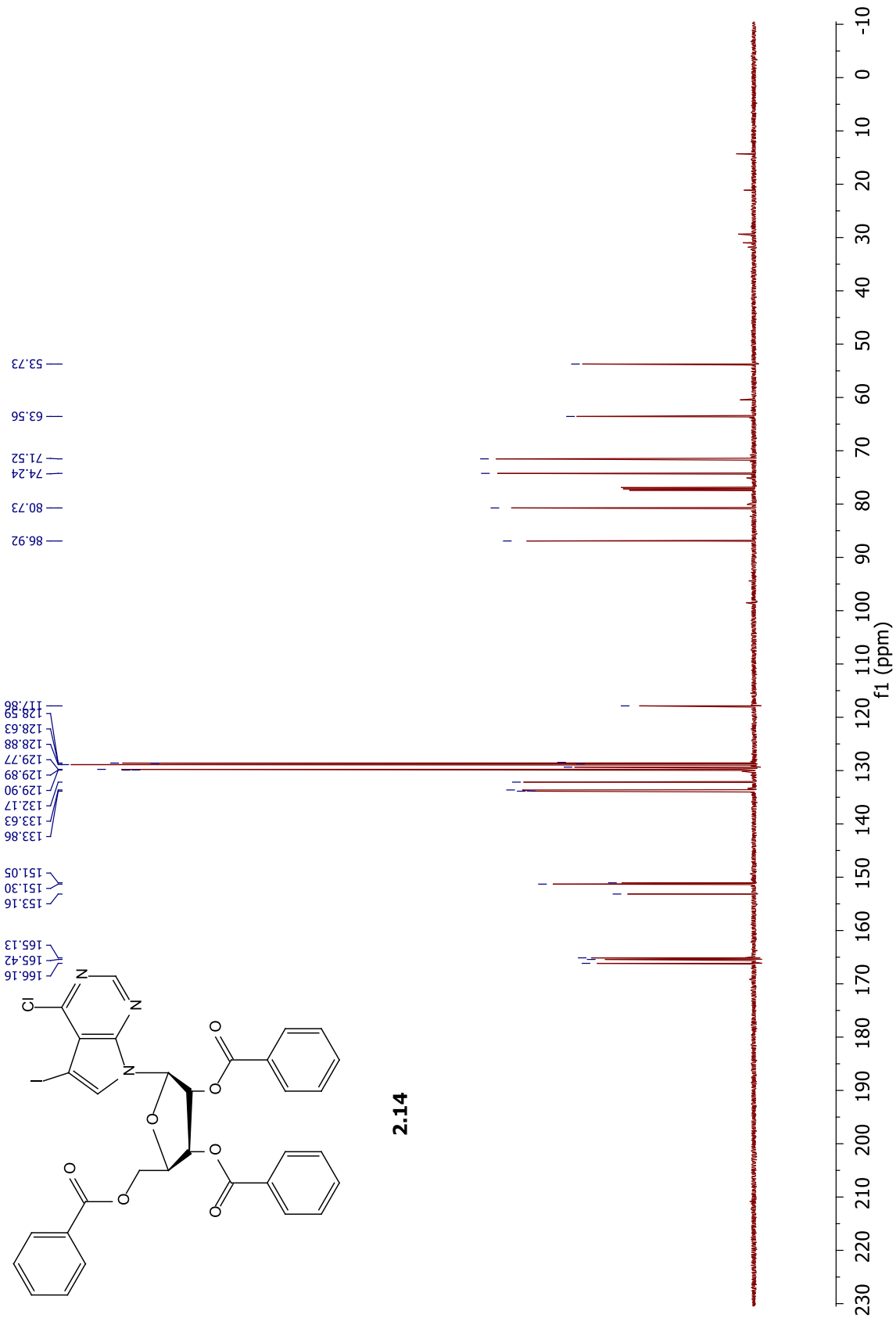


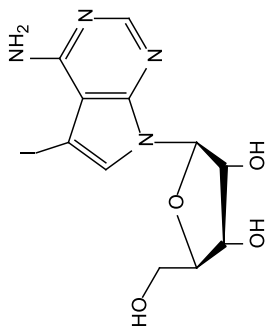
2.12



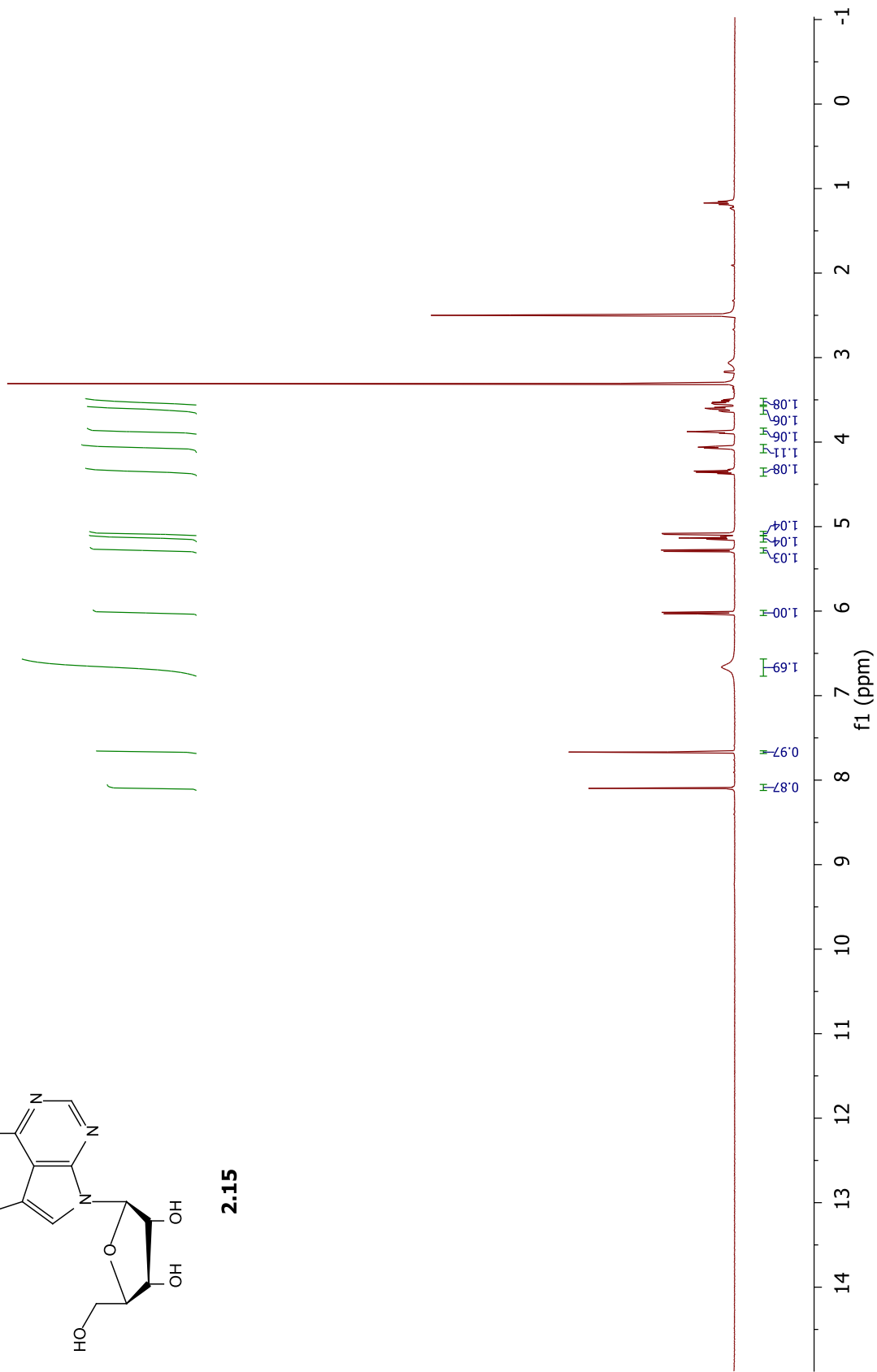
2.14

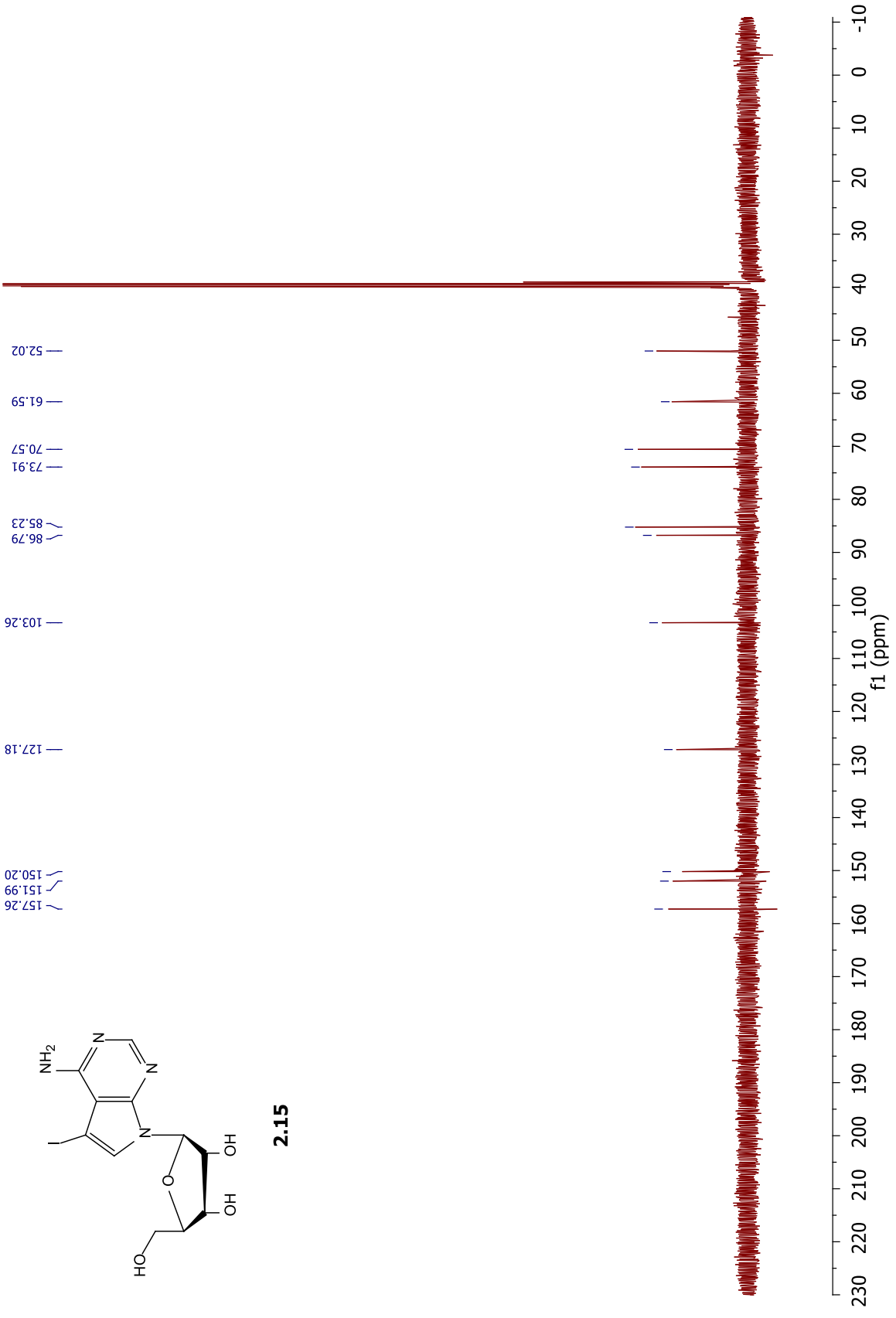


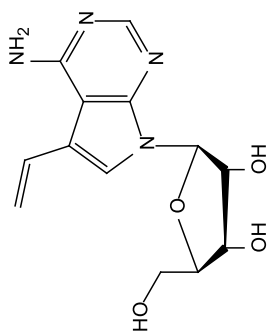




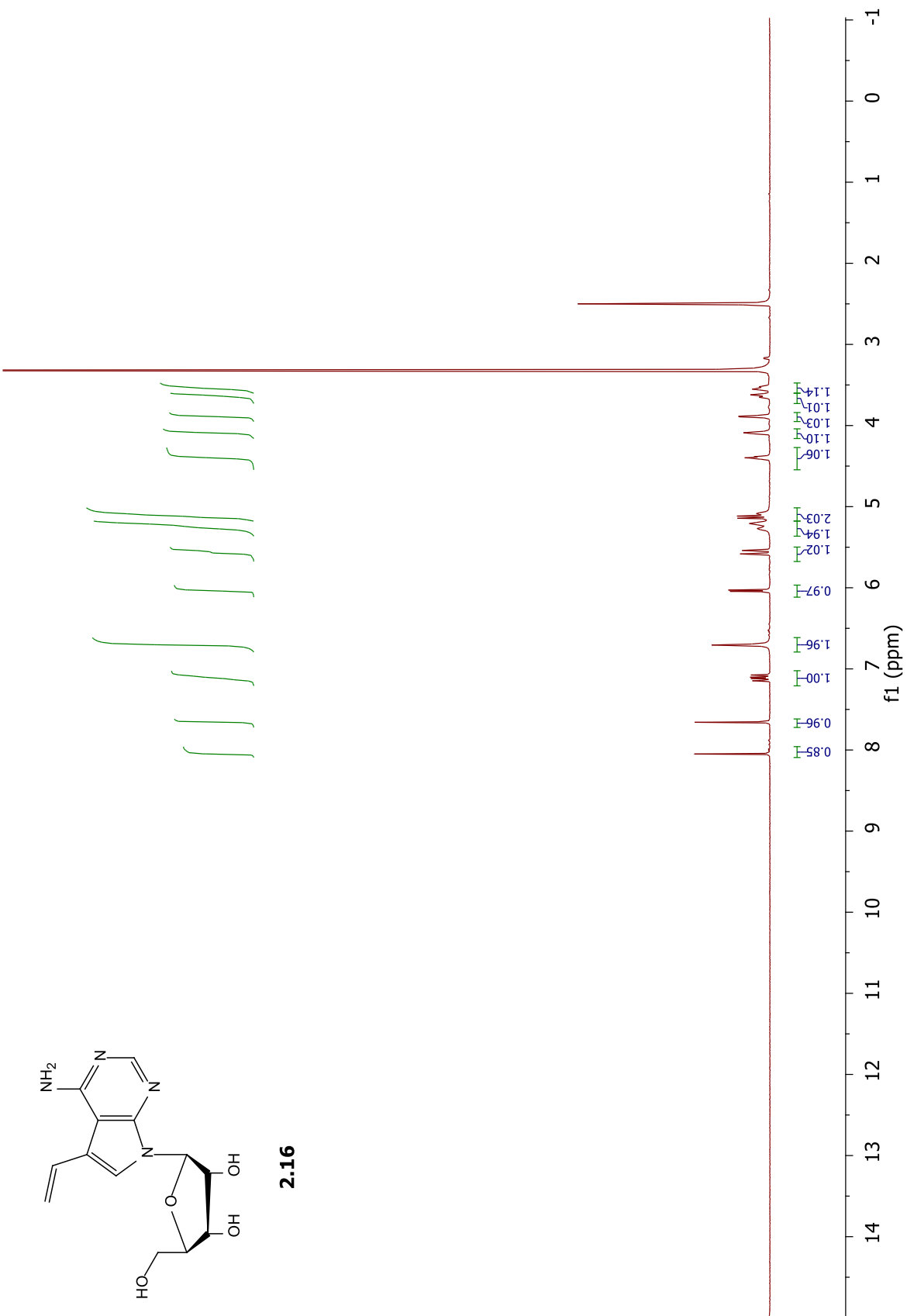
2.15

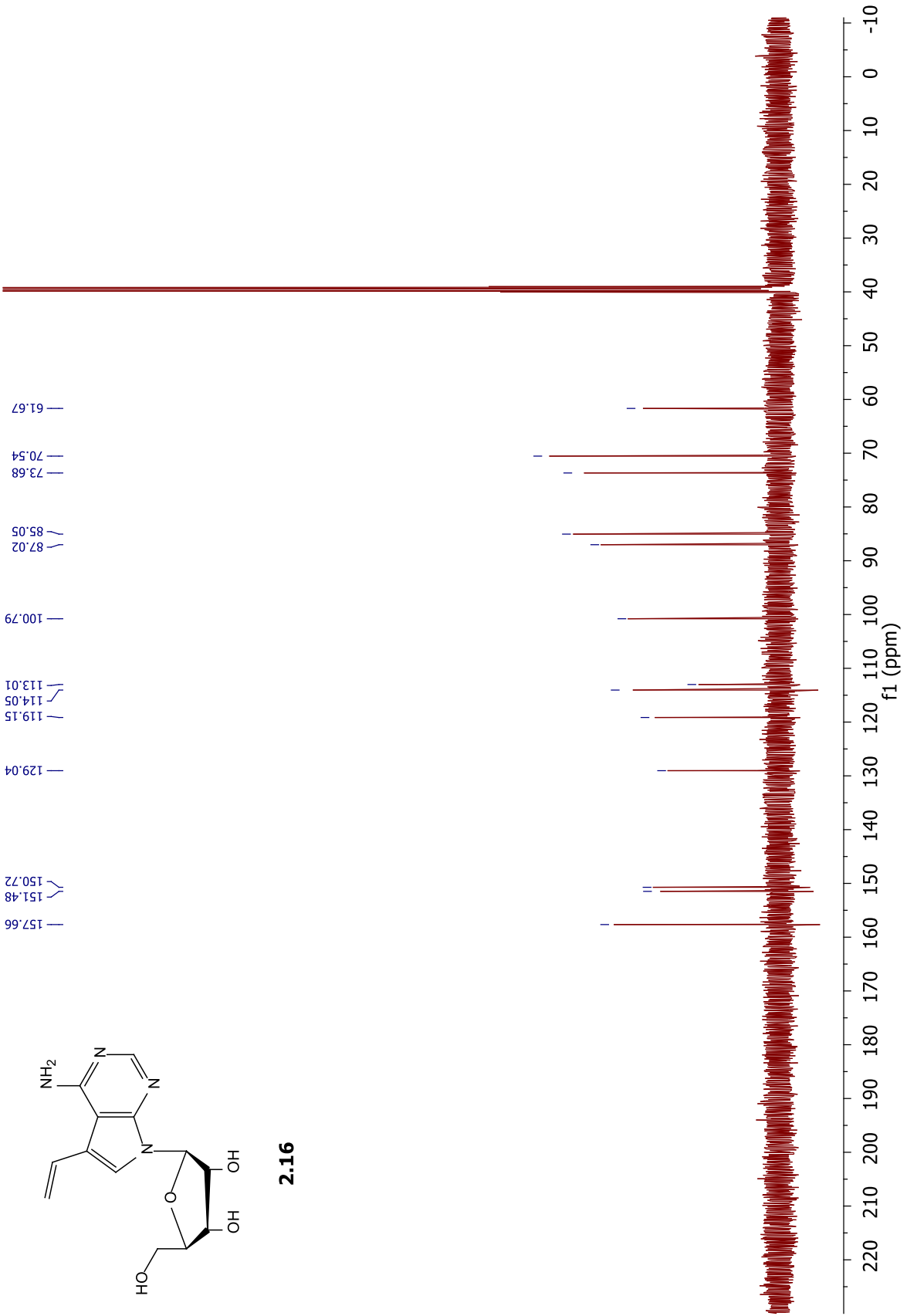


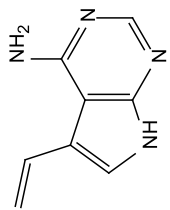




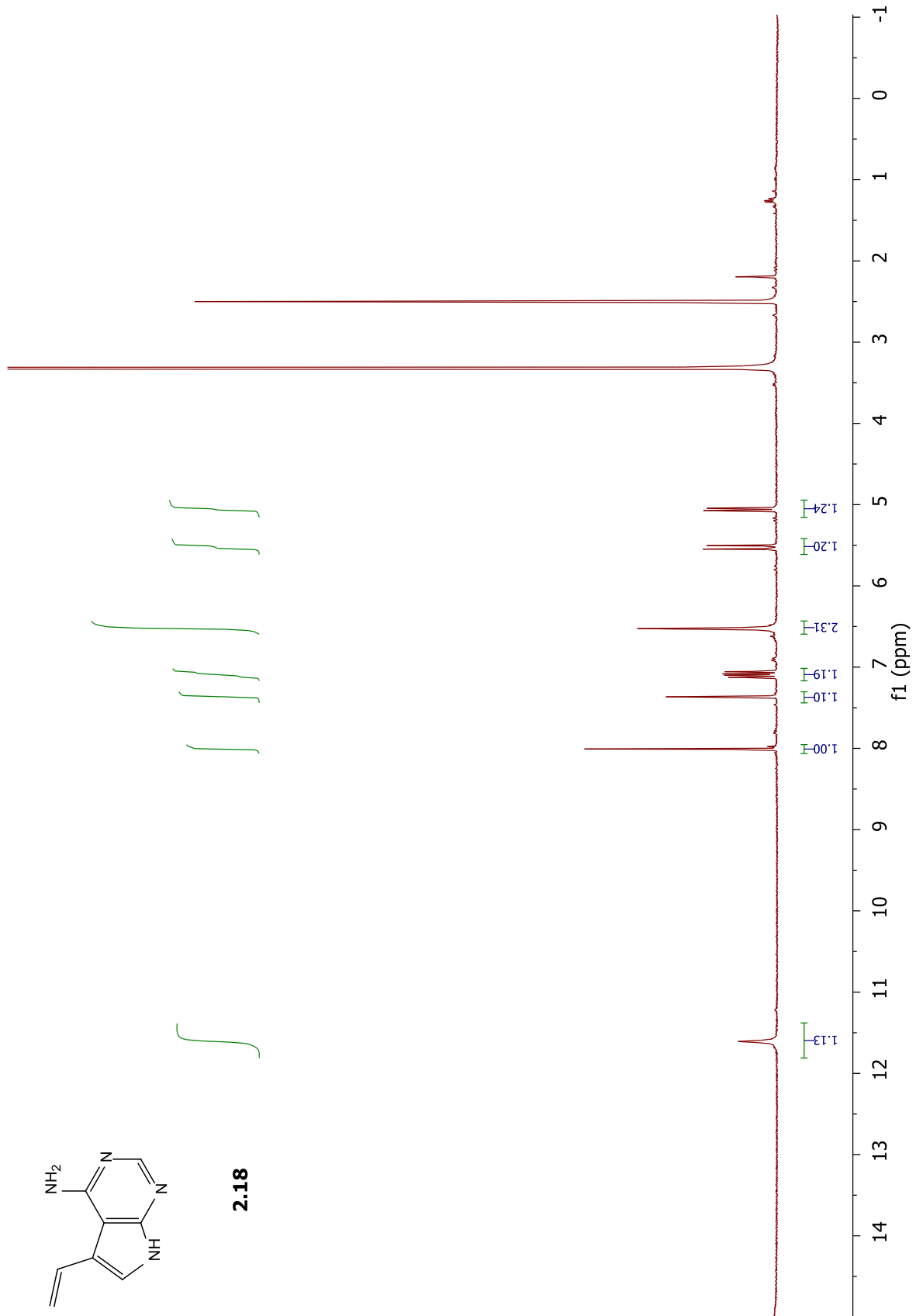
2.16

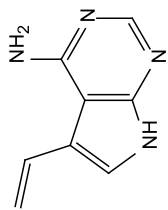




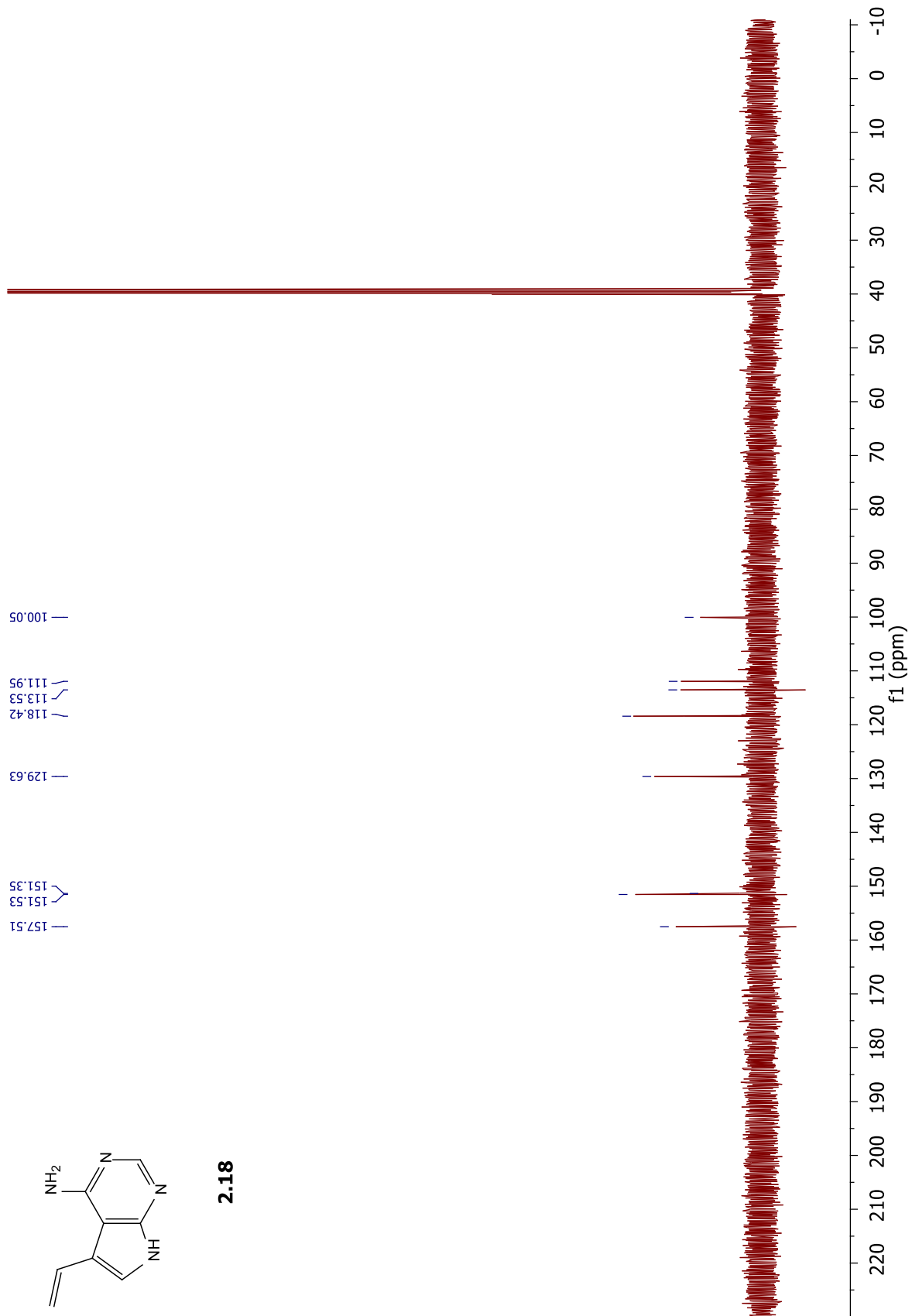


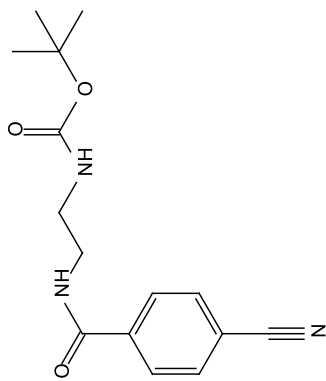
2.18



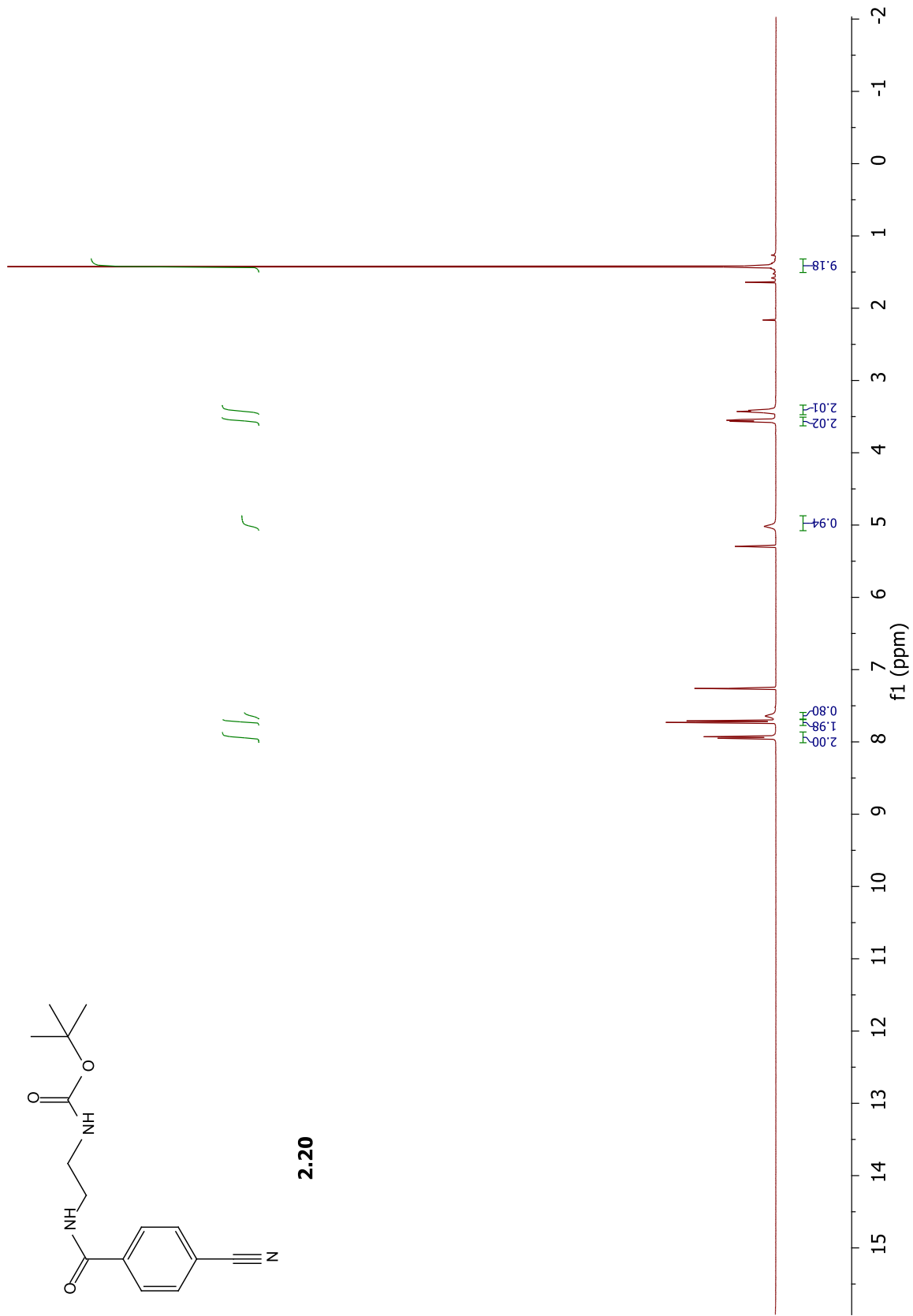


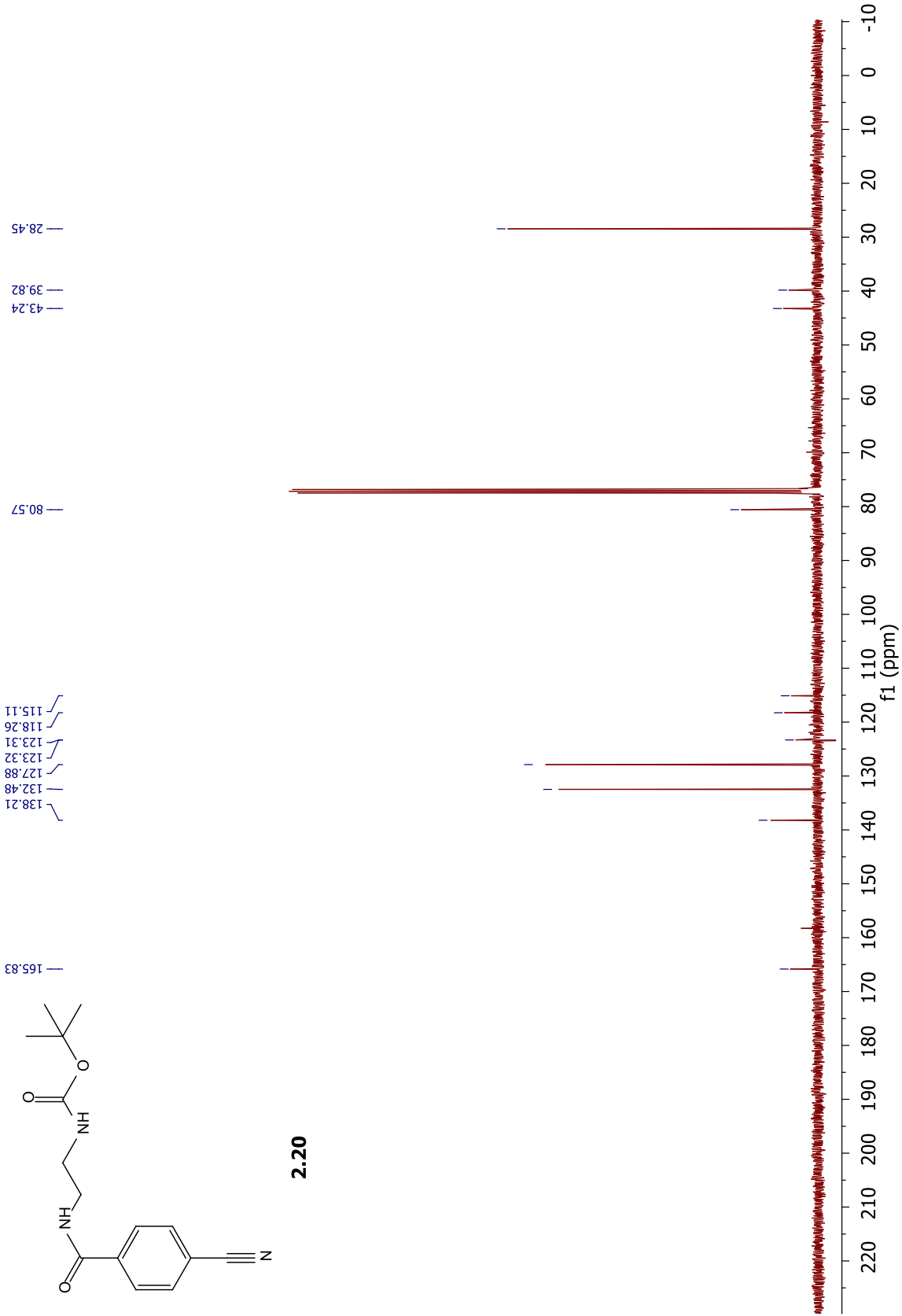
2.18

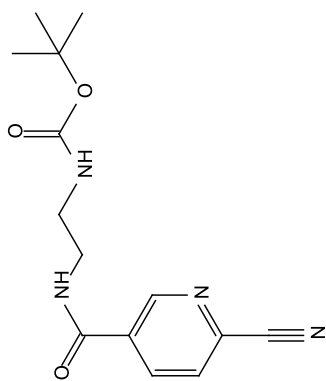




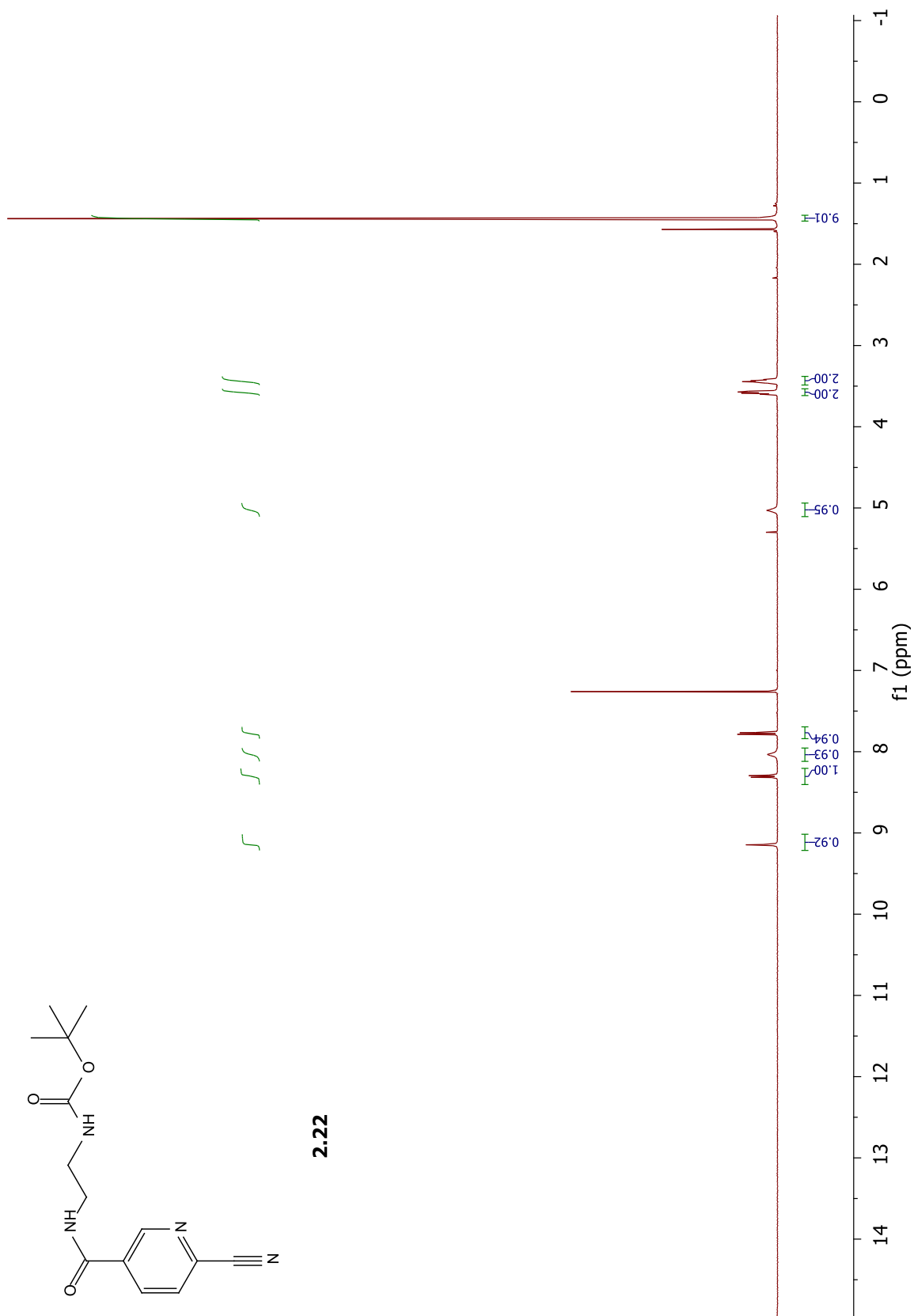
2.20

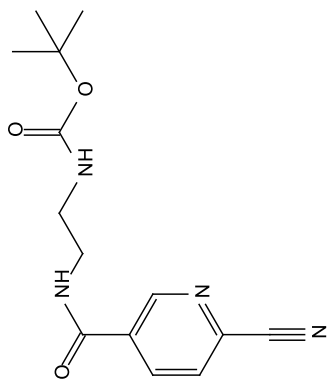




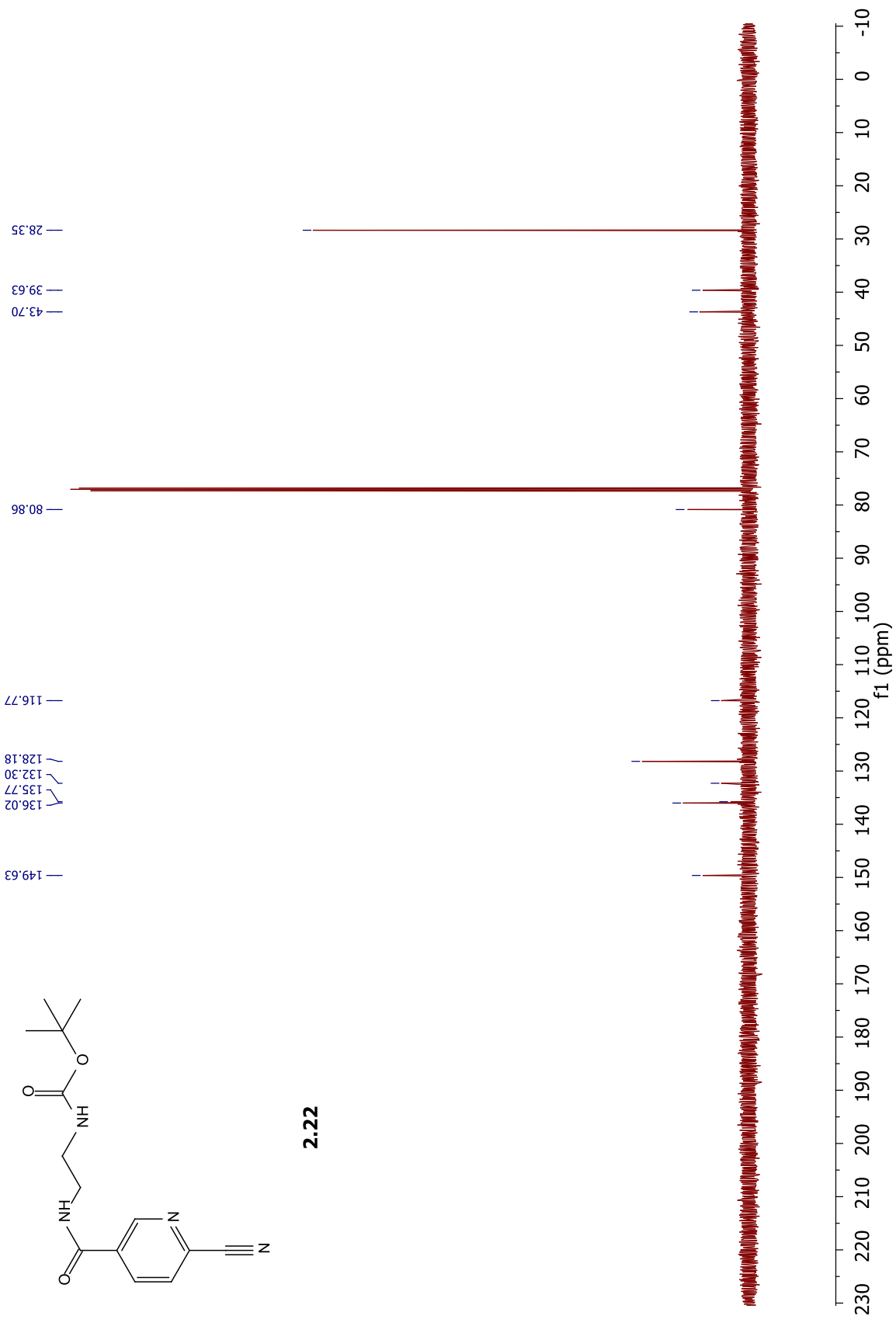


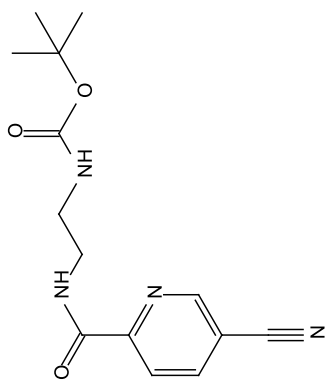
2.22



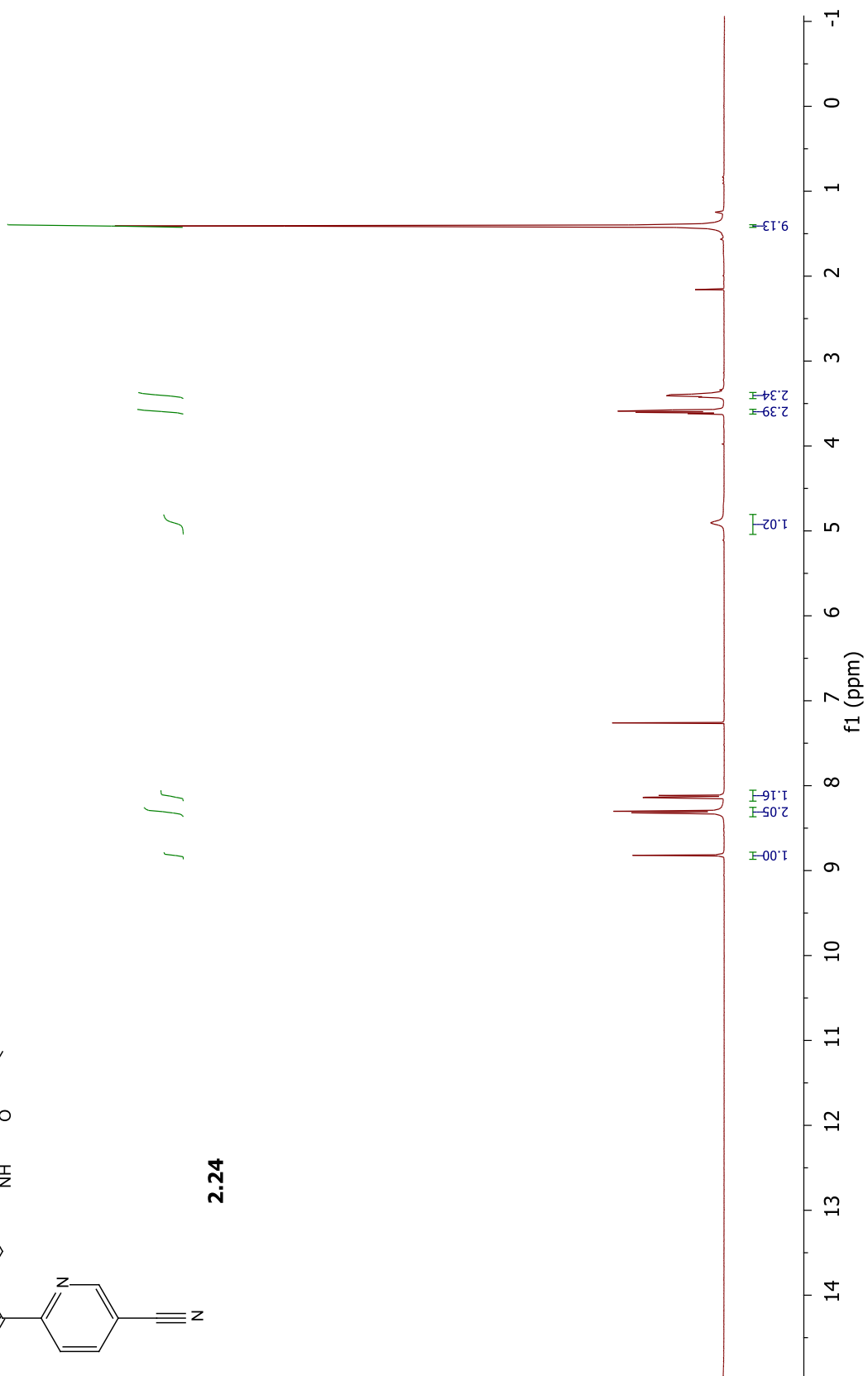


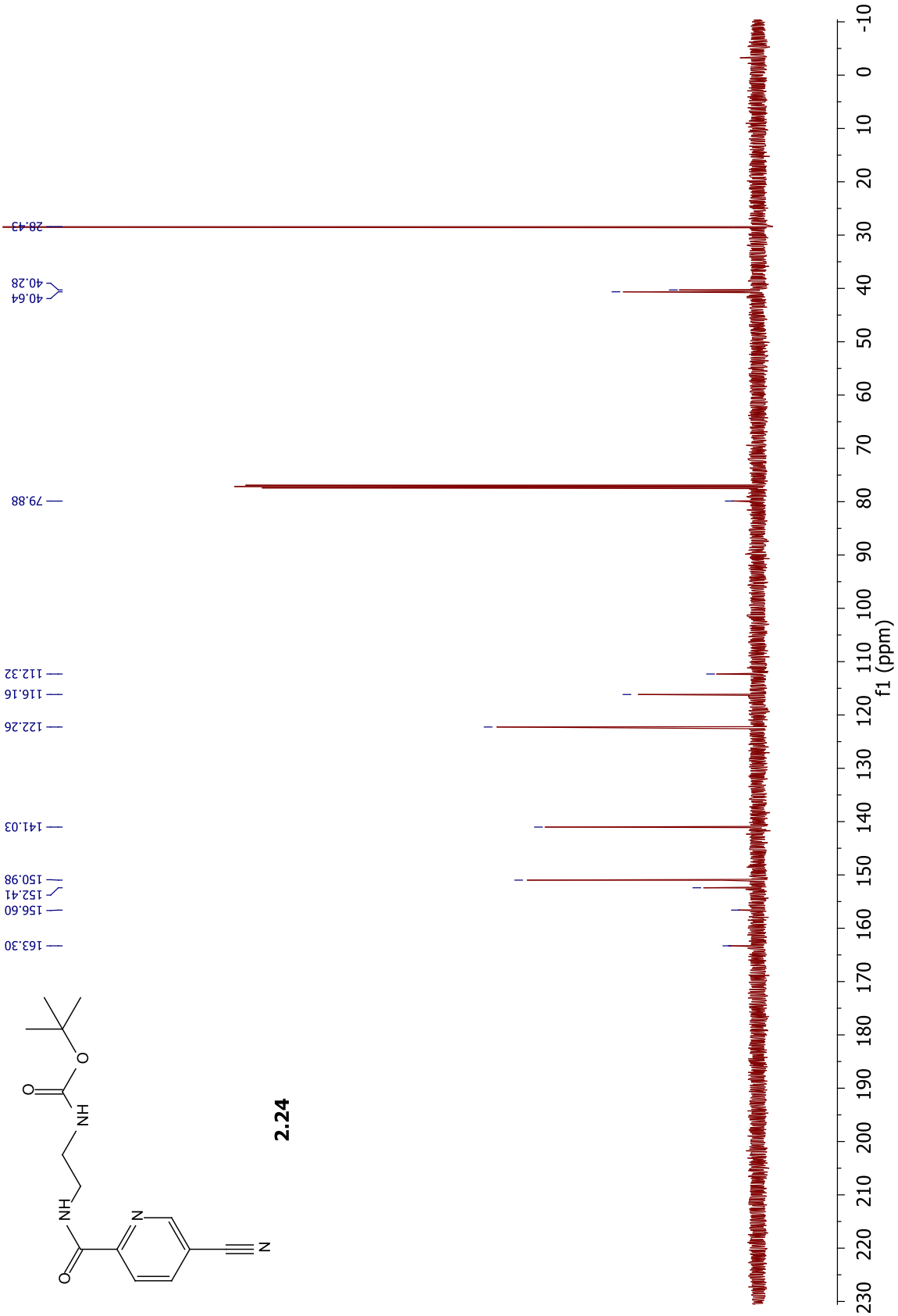
2.22

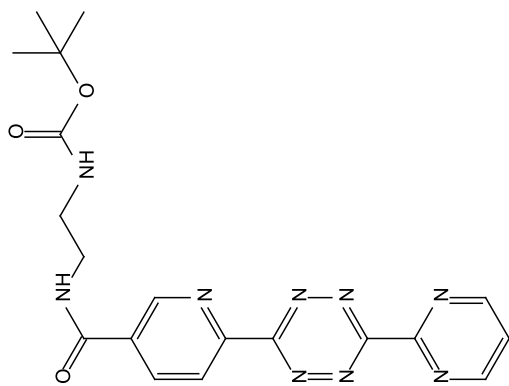




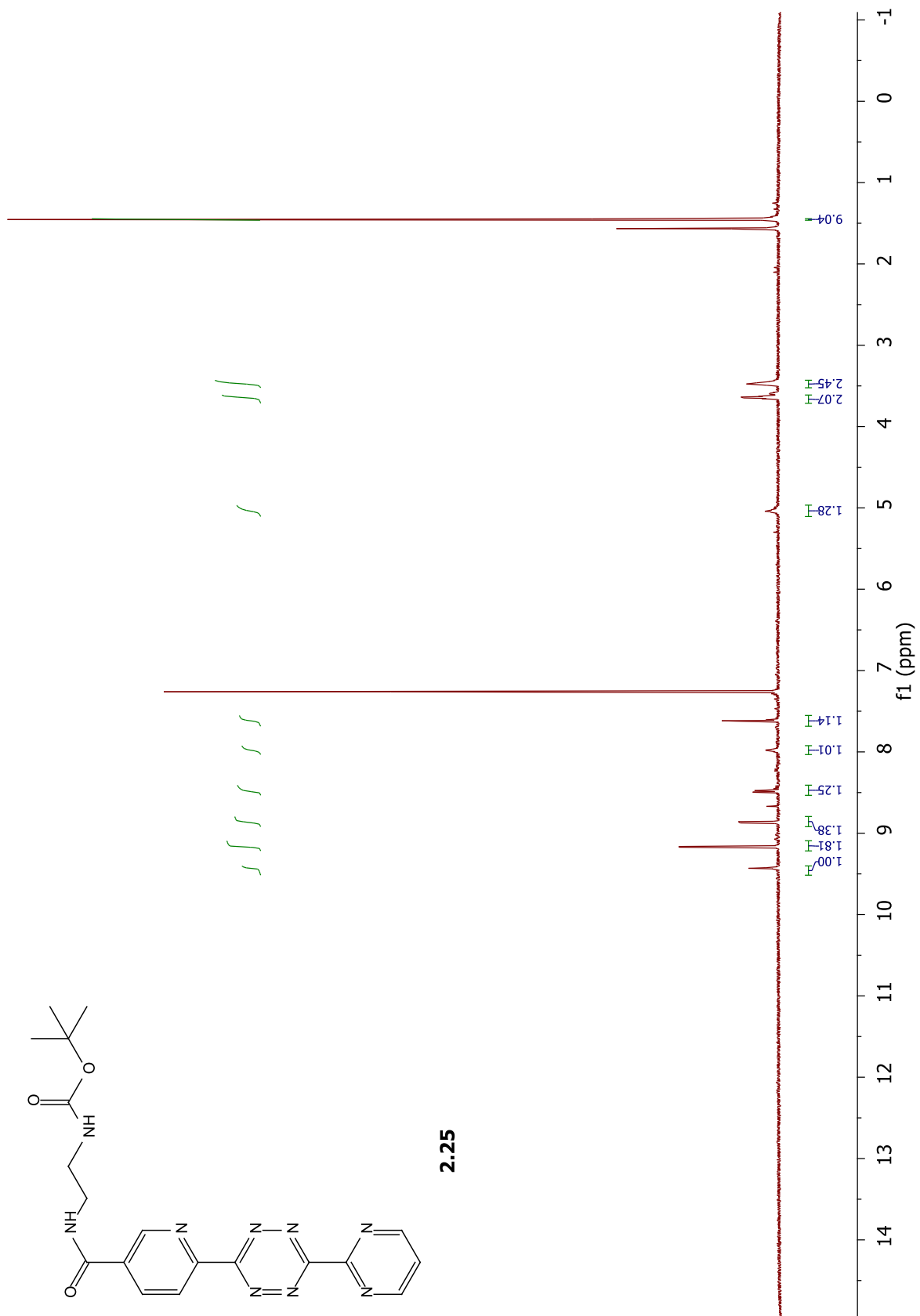
2.24

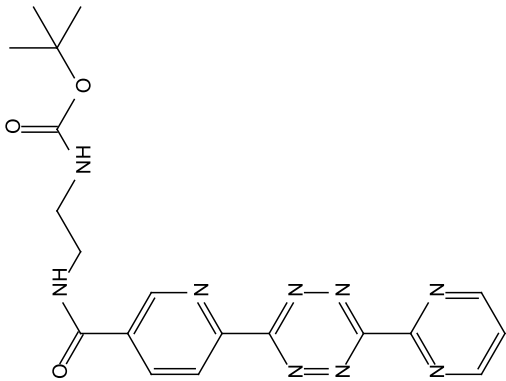
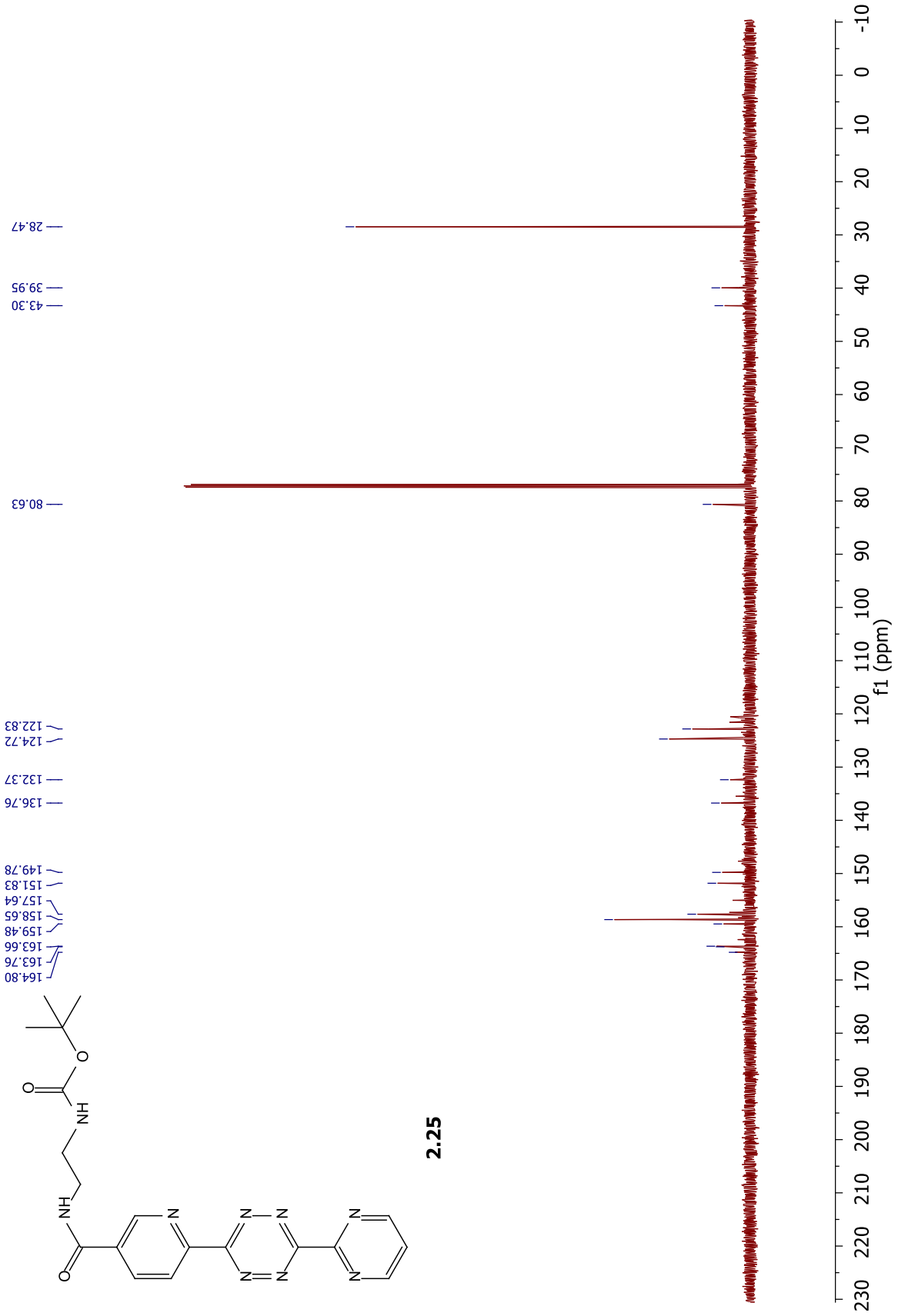




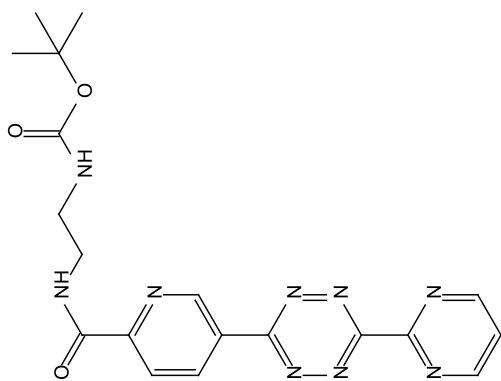


2.25

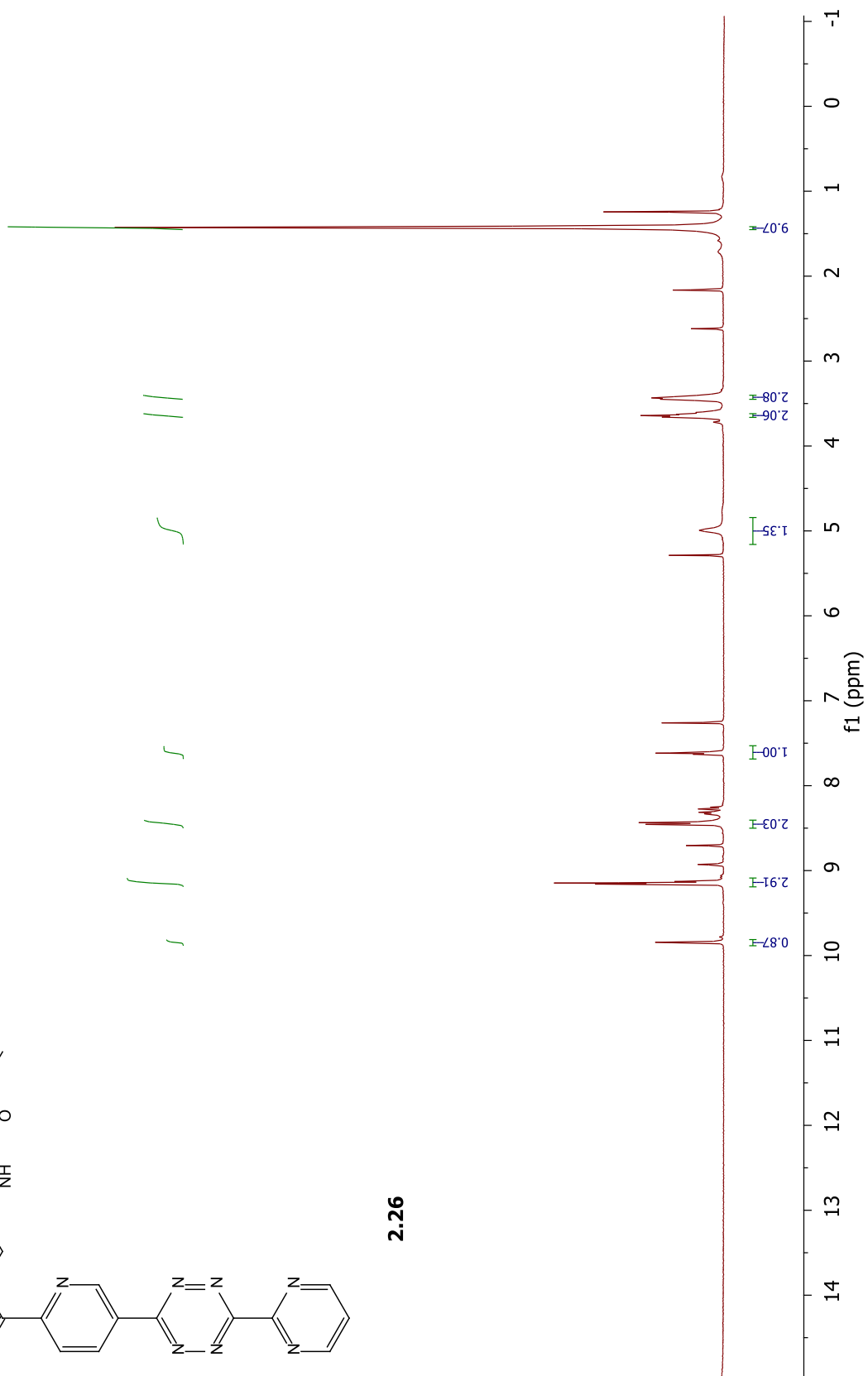


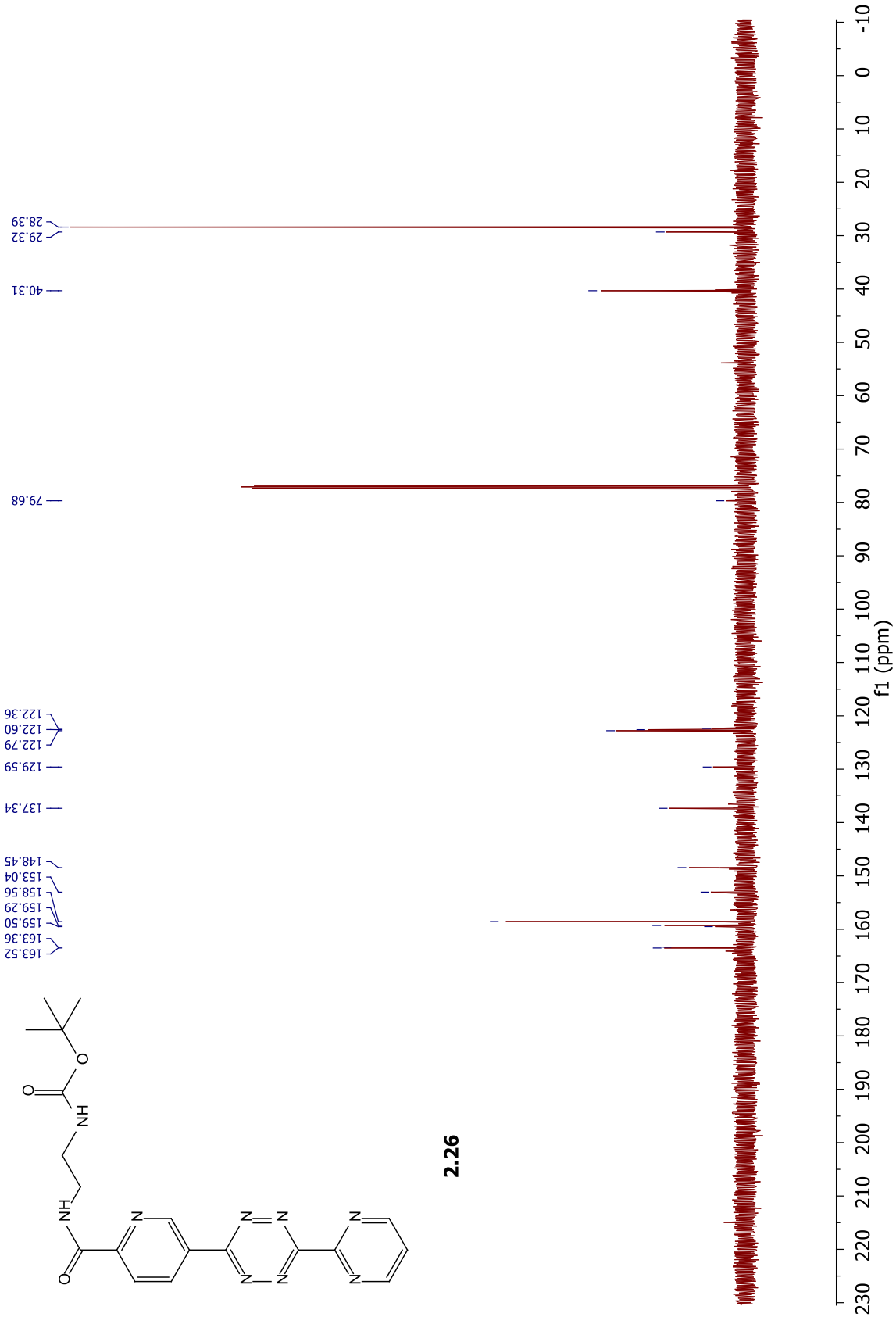


2.25



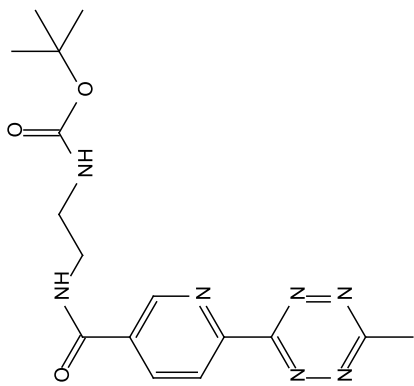
2.26



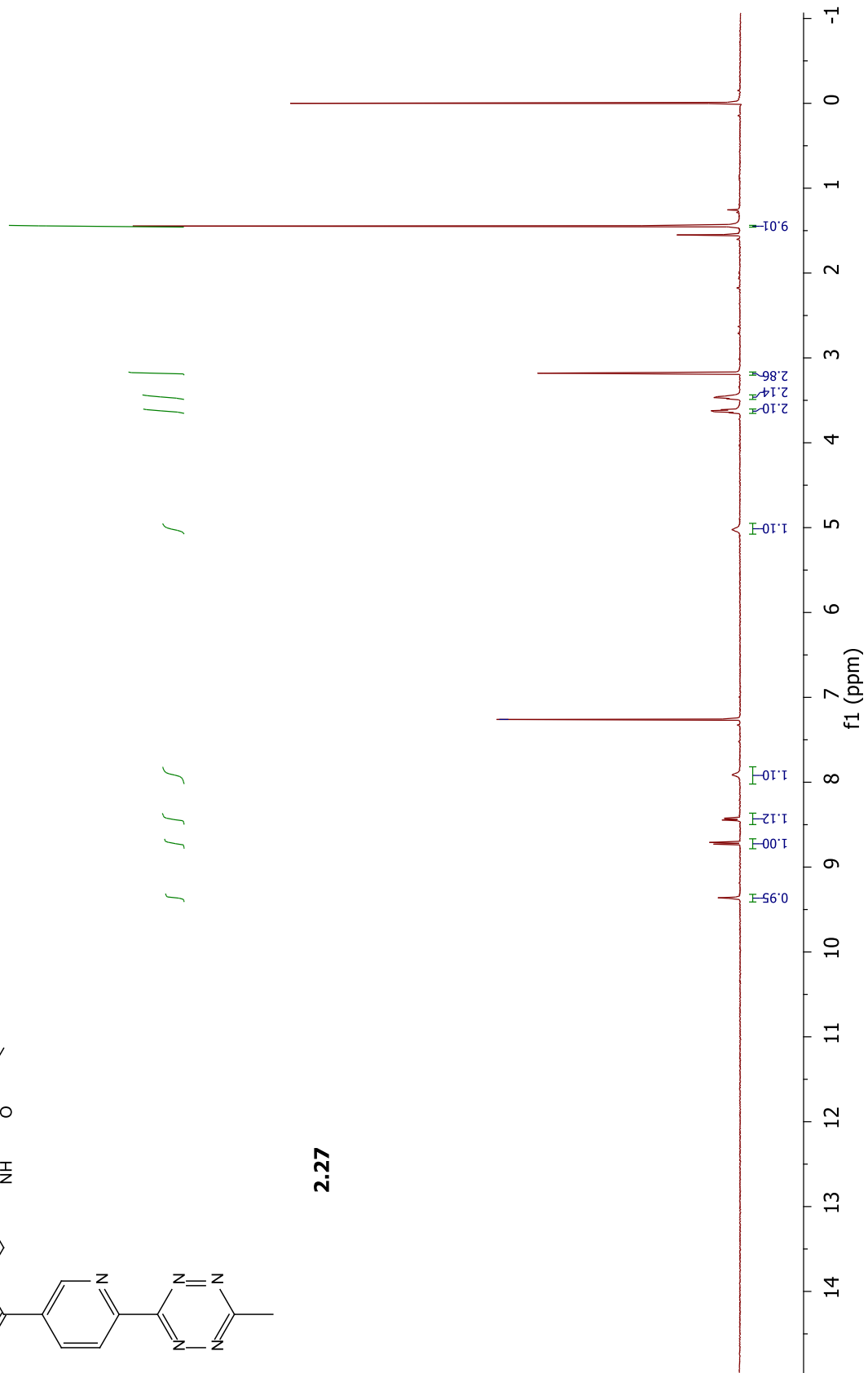


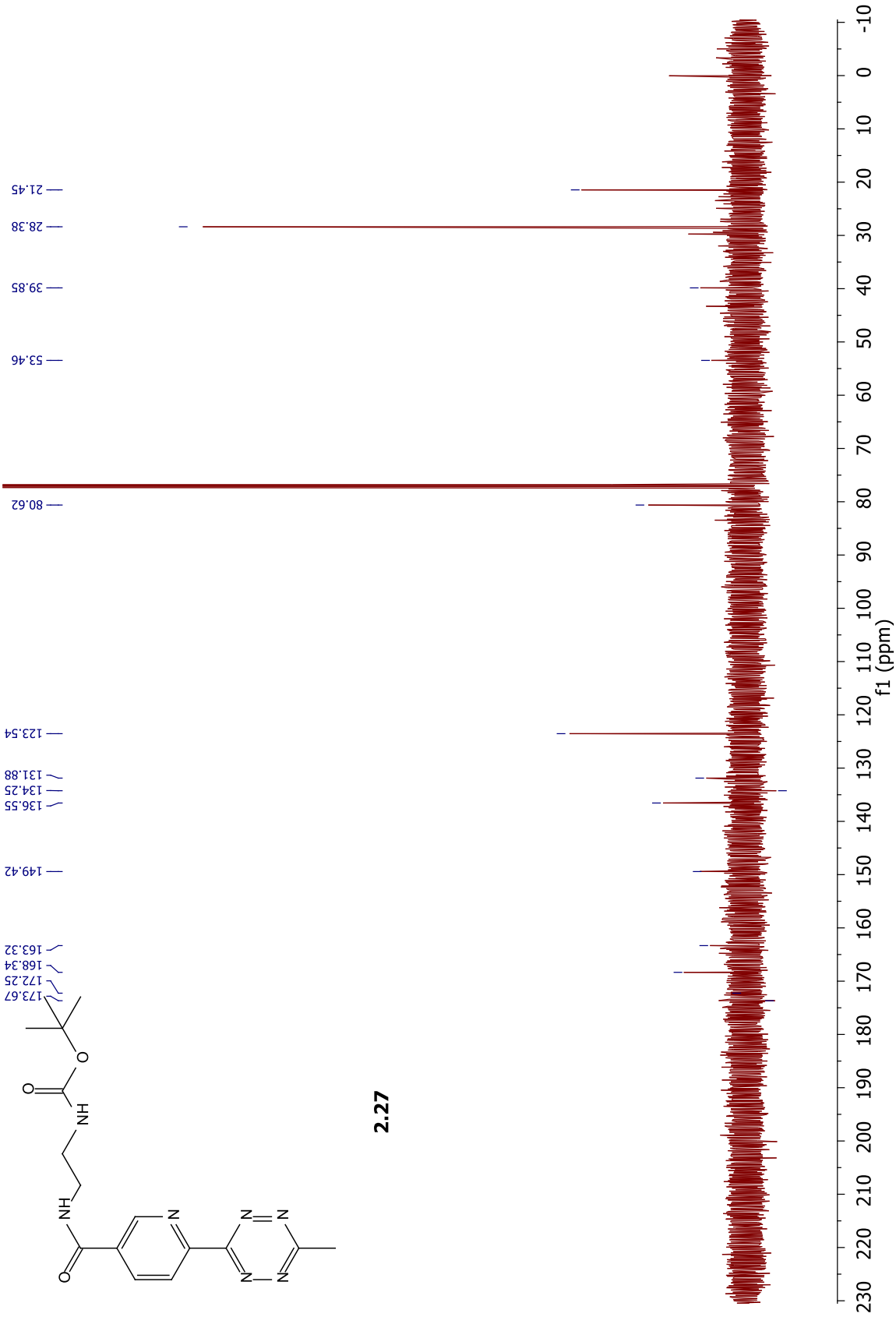
2.26

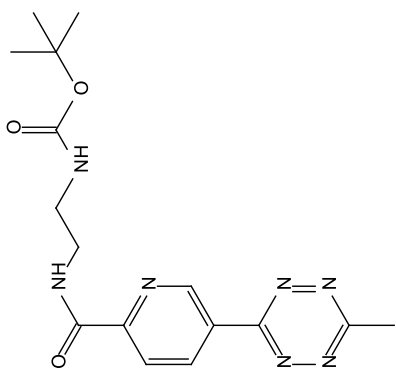
— 7.26



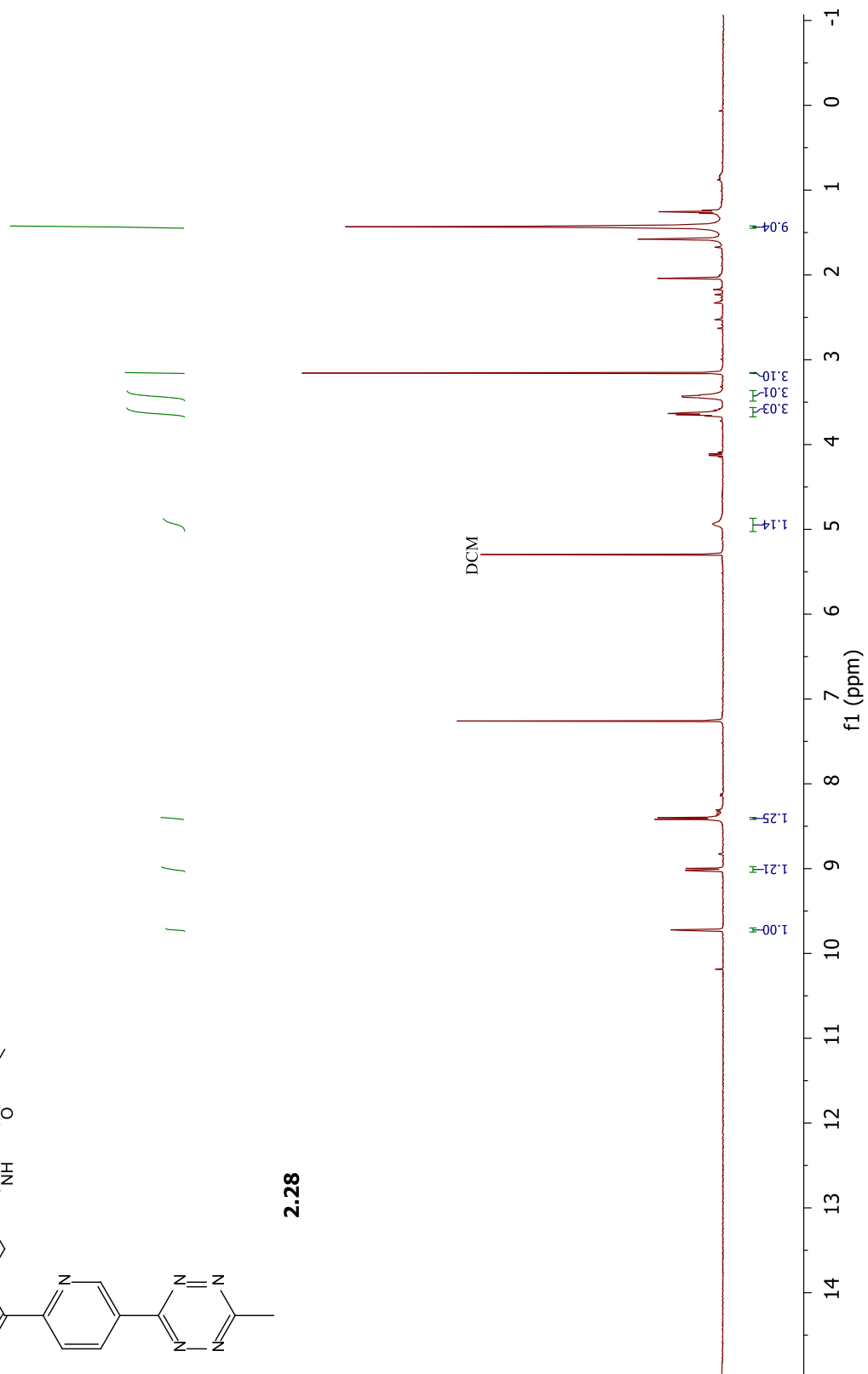
2.27

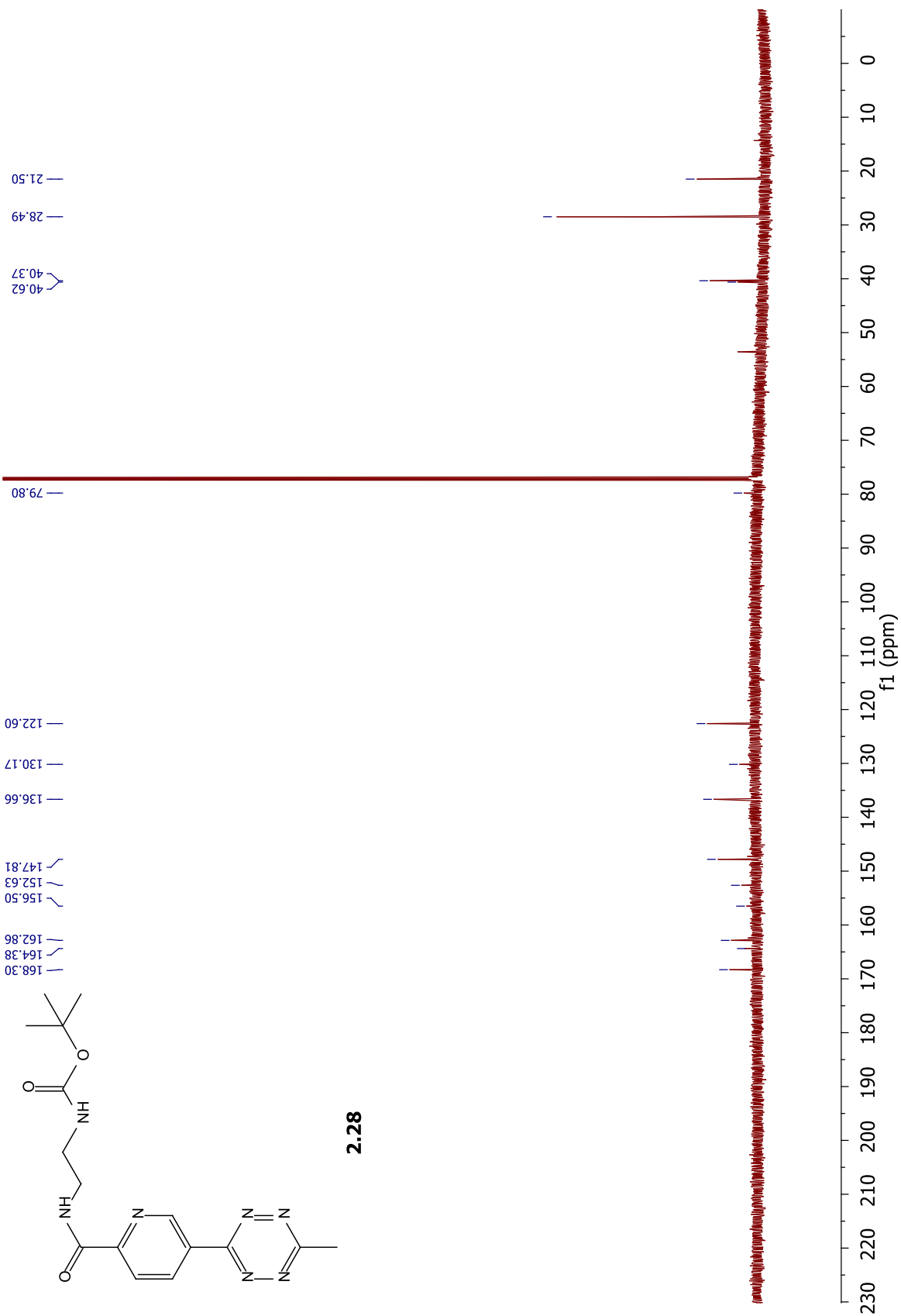


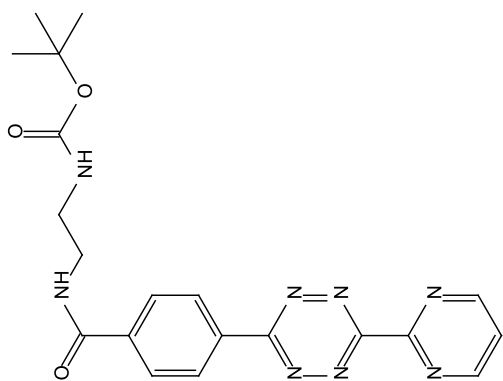




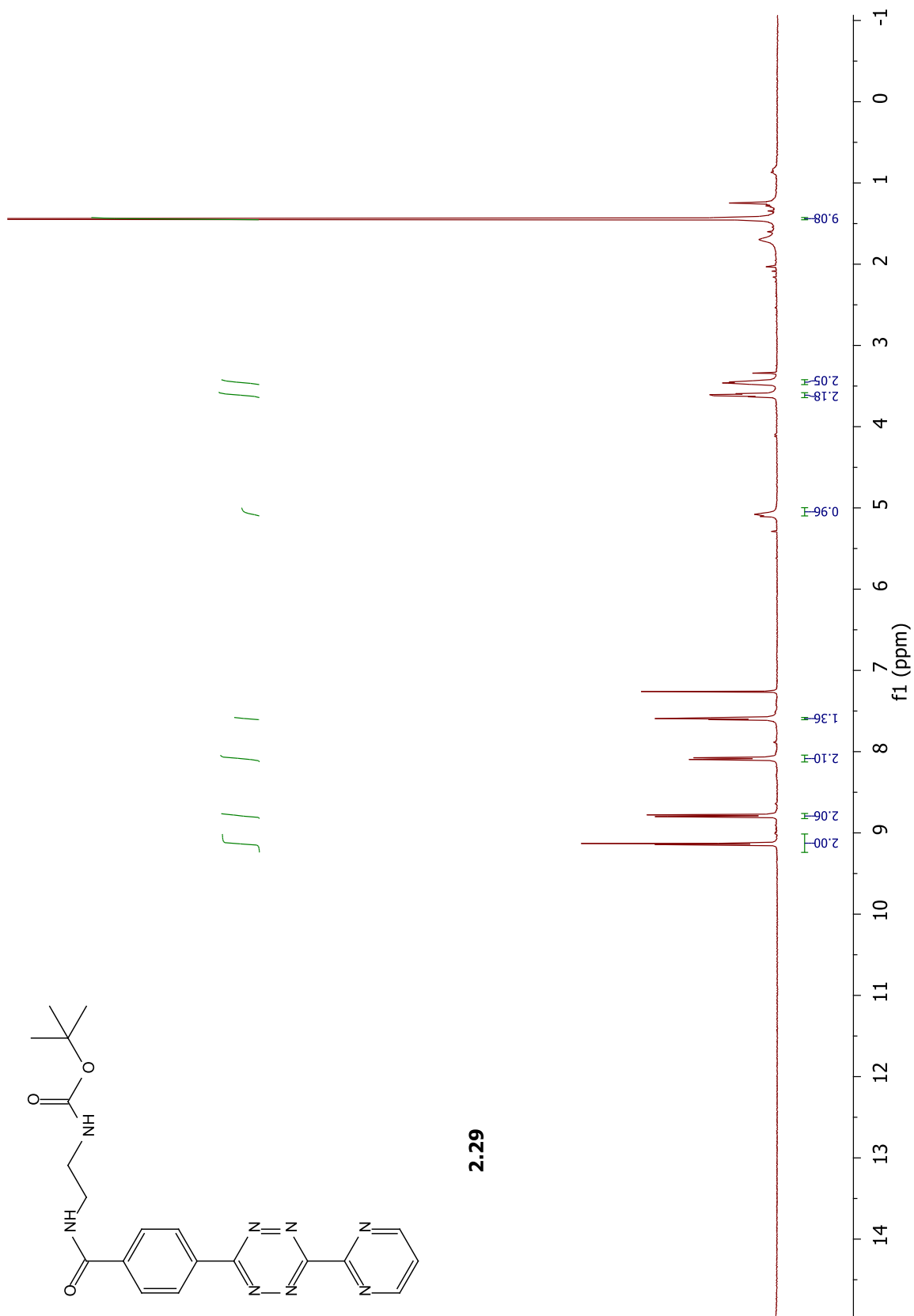
2.28

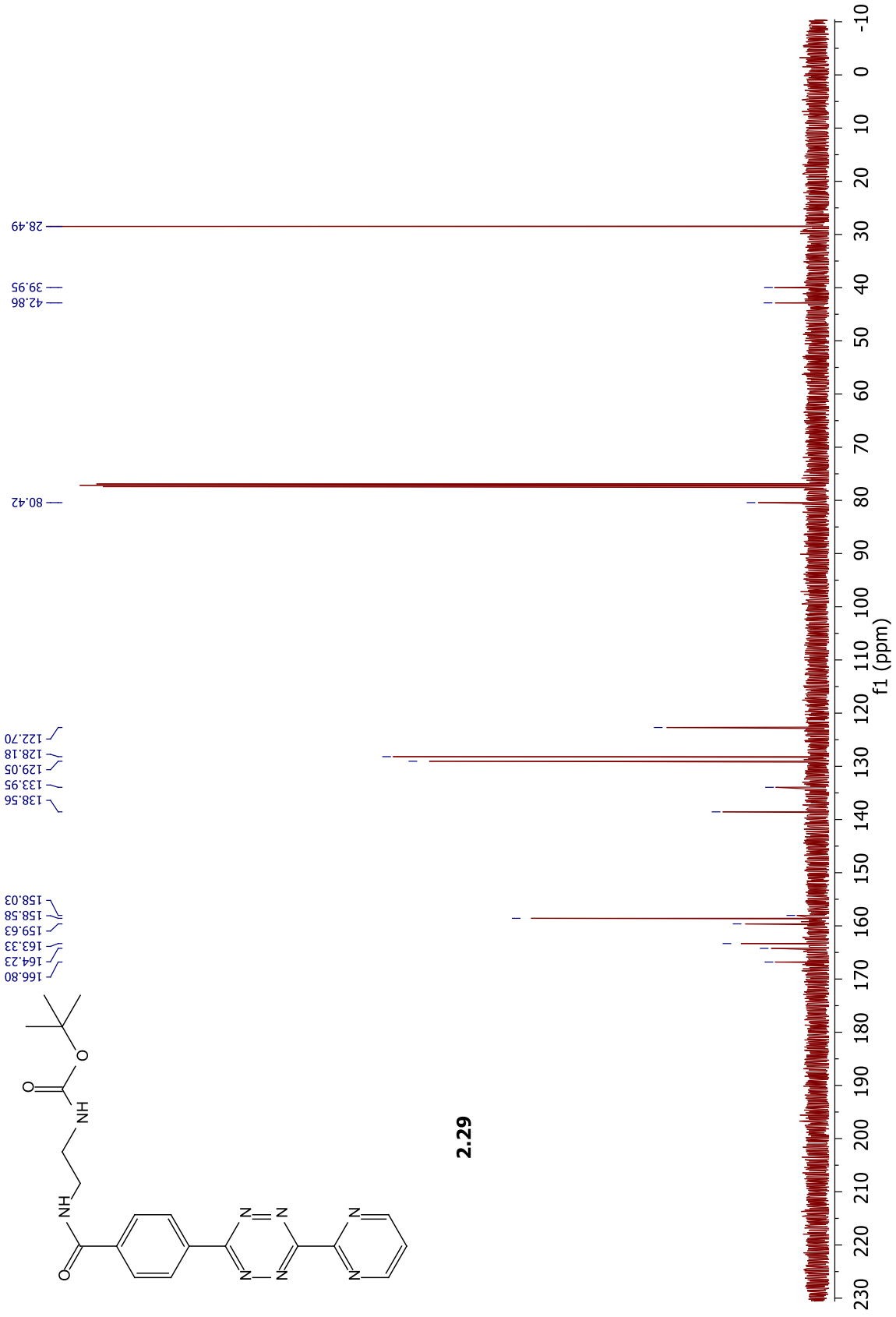




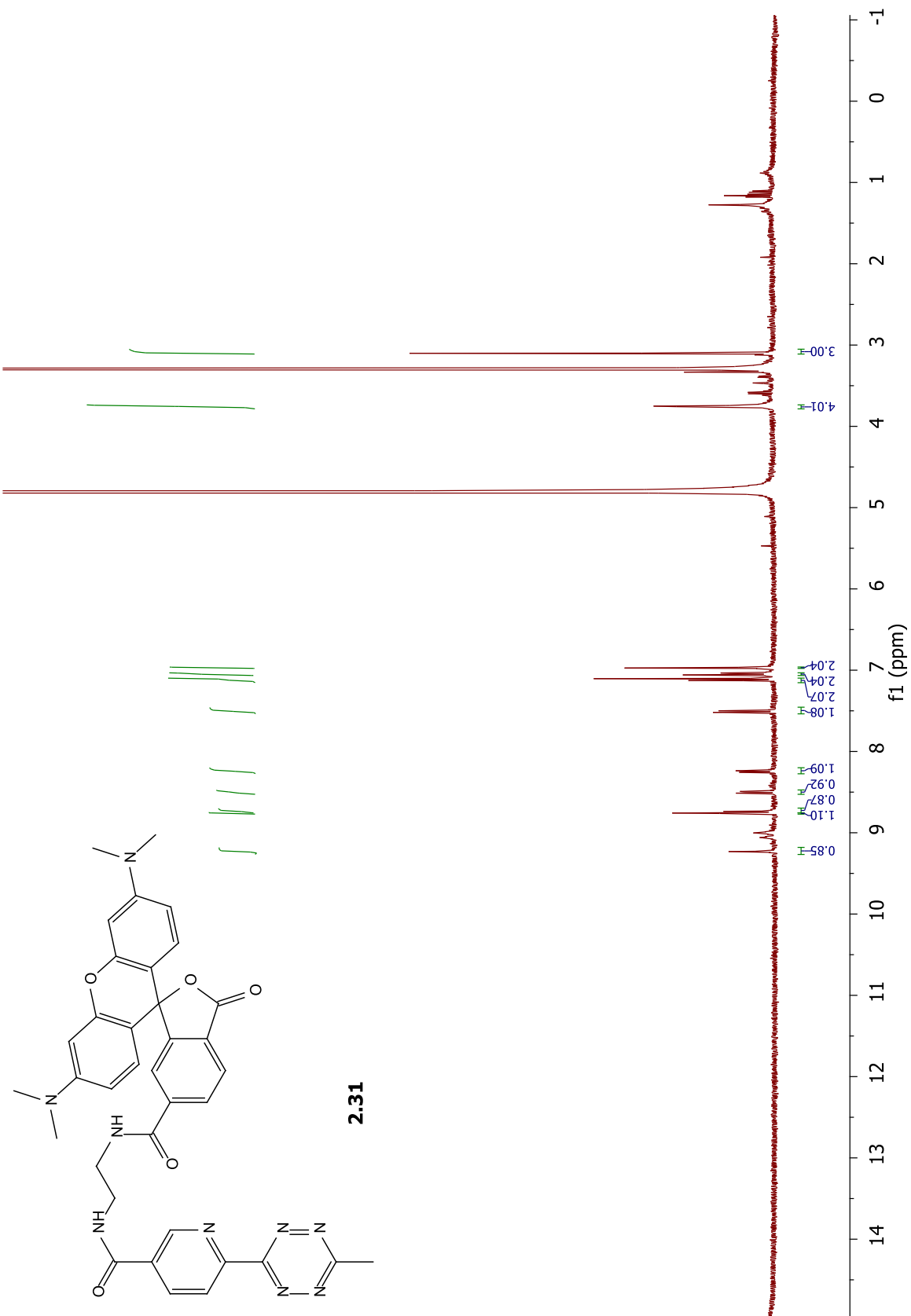


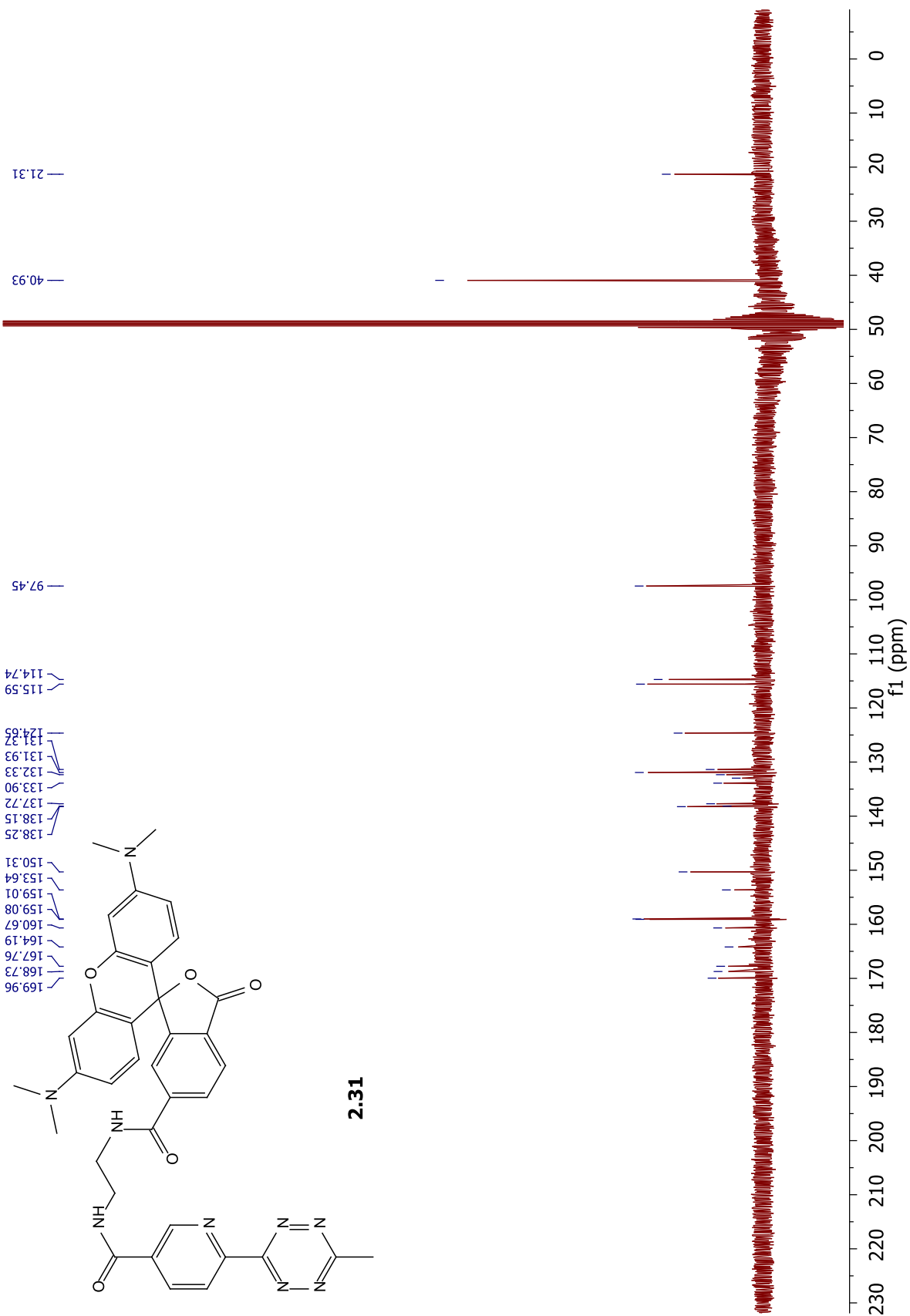
2.29

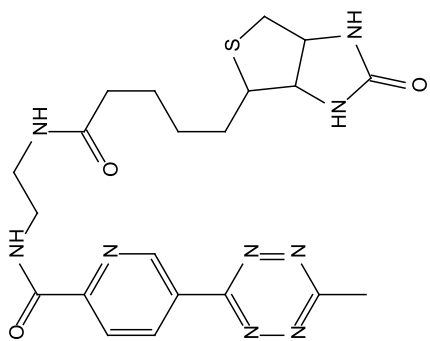




2.29







2.32

